The University Of Sheffield.

Gas turbines for carbon capture

By:

Jean-Michel John Alexandre Bellas

A thesis submitted in partial fulfilment of the requirements for the degree of Doctor of Philosophy

The University of Sheffield
Energy 2050
Faculty of Engineering
Department of Mechanical Engineering

November 2018

Declaration of authorship

The candidate confirms that:

1. This work was done wholly while in candidature for a research degree at this University;

2. Where I have consulted the published work of others, this is always clearly attributed;

3. Where I have quoted from the work of others, the source is always given. With the exception of such quotations, this thesis is entirely my own work;

4. I have acknowledged all main sources of help;

5. Where the thesis is based on work done by myself jointly with others, I have made clear exactly what was done by others and what I have contributed myself;

6. Either none of this work has been published before submission, or parts of this work have been published as:

Journal publications

Chapter 2 is associated with the following publication where this study was conceived by all of the authors named:

- Diego, M.E., Akram, M., Bellas, JM.. Finney, K. N. and Pourkashanian, M. 2017. Making gas-CCS a commercial reality: The challenges of scaling up. Greenhouse Gases Science and Technology, Vol. 7, 778-801. DOI: https://doi.org/10.1002/ghg.1695.

The author of this thesis has written the sections that include exhaust gas recirculation and selective exhaust gas recirculation of the above named publication.

Chapter 4 is associated with a manuscript currently under peer-review for the International Journal of Greenhouse Gas Control where this study was conceived by all of the authors named:

- Bellas, JM., Finney, K. N., Diego, M.E., Ingham, D. and Pourkashanian, M. Experimental investigation of the impacts of selective exhaust gas recirculation on a micro gas turbine. International Journal of Greenhouse Gas Control. Under peer-review.

The author of this thesis has conducted the experimental work and written the full manuscript under consideration.

Chapter 6 is associated with the following two publications where this study was conceived by all of the authors named:

- Diego, M.E., Bellas, J.-M., Pourkashanian, M., 2018. Techno-economic analysis of a hybrid CO_2 capture system for natural gas combined cycles with selective exhaust gas recirculation. Appl. Energy 215, 778–791. https://doi.org/10.1016/j.apenergy.2018.02.066.
- Diego, M.E., Bellas, J.-M., Pourkashanian, M., 2017. Process Analysis of Selective Exhaust Gas Recirculation for CO_2 Capture in Natural Gas Combined Cycle Power Plants Using Amines. J. Eng. Gas Turbines Power 139, 121701. https://doi.org/10.1115/1.4037323.

The author of this thesis has conducted and written the economic analysis associated with the two above named publications.

Conference proceedings and presentations

- Bellas, JM., Finney, K. N., Diego, M.E., Ingham, D. and Pourkashanian, M. Experimental investigation of the impacts of selective exhaust gas recirculation on a micro gas turbine. IEAGHG, GHGT14, Melbourne, Australia, 21-26 October 2018. *Oral presentation.*
- Bellas, J., Akram, M.,Diego, M, E., Finney, K, N., Ingham, D. and Pourkashanian. 2017. Gas turbines for carbon capture. [Poster]. Exhibited at: UKCCSRC Autumn 2017 Biannual Conference, Sheffield, UK. 12th September 2017. 59.4 x 84.1 cm.

- Bellas, J., Akram, M.,Diego, M, E., Finney, K, N., Ingham, D. and Pourkashanian. 2017. Gas turbines for carbon capture. [Poster]. Exhibited at: Department of Mechanical Engineering annual PhD poster day. The University of Sheffield, UK. 15th May 2017. 59.4 x 84.1 cm.
- Diego, M.E., Bellas, J.-M., Pourkashanian, M., 2017. Process Analysis of Selective Exhaust Gas Recirculation for CO_2 Capture in Natural Gas Combined Cycle Power Plants Using Amines. ASME Turbo Expo 2017: Turbomachinery Technical Conference and Exposition, in: Volume 3: Coal, Biomass and Alternative Fuels; Cycle Innovations; Electric Power; Industrial and Cogeneration Applications; Organic Rankine Cycle Power Systems. ASME, p. V003T06A025. https://doi.org/10.1115/GT2017-64387. Charlotte, North Carolina, USA, 26–30 June 2017. *Conference proceedings.*
- Diego, M.E., Bellas, J.-M., Pourkashanian, M., 2017. Investigation of CO_2 capture in natural gas combined cycles with selective exhaust gas recirculation. 9th Trondheim Conference on Carbon Capture, Transport and Storage. Trondheim, Norway. 12-14 June 2017. *Oral presentation.*

Acknowledgements

This thesis was undertaken thanks to funding from the UK Engineering and Physical Sciences Research Council (SELECT EP/M001482/1). The author would also like to acknowledge the UKCCSRC for making the PACT Core Facilities available for research; the UKCCSRC is funded by the EPSRC, as part of the Research Council UK Energy Programme.

I would like to thank Professor Mohamed Pourkashanian and Professor Derek Ingham for giving me the opportunity to complete the research associated with this thesis, and the University of Sheffield for my PhD scholarship award.

I wish to acknowledge and pay special thanks to the supervisory team Dr Karen N Finney, Dr Maria Elena Diego, Dr Muhammad Akram, Professor Derek Ingham and Professor Mohamed Pourkashanian for their guidance and support throughout the PhD.

Karen, Marlen, Akram, Derek and Mohamed, your continued encouragement, structure and guidance, constructive feedback, patience and in-depth knowledge, and valuable input has been instrumental in the completion of this research work.

I also would like to thank the team at the PACT Research Centre, for their technical support and guidance.

Thank you to all my colleagues within the Energy 2050 group for making my experience memorable.

Finally, I am grateful to my family and friends for their ongoing support, encouragement, enthusiasm and patience throughout this project. The continued faith and belief has driven me to keep going and follow my dreams.

Abstract

The objective of this research was to investigate the influence of selective exhaust gas recirculation (S-EGR) applied to gas-fired systems and determine if energy and economic savings can be realised.

The gas turbine experimental campaigns evaluated the performance of a micro gas turbine (mGT) under S-EGR conditions, simulated by injecting CO_2 into the compressor inlet. The mGT performance was affected under these conditions in terms of efficiency, compressor operation and emissions, however, this was more prominent at part loads. The flue gas CO_2 concentrations increased by up to 6 times (up to 10.1 vol% at 60 kW_e) with respect to the reference case without S-EGR, which can be beneficial to improve the downstream amine capture plant (ACP) performance, as demonstrated by subsequent experimental campaigns. The first assessed ACP performance with flue gas CO_2 concentrations of 5.2-9.0 vol%. The results showed that the specific reboiler duty reduced by 21% and the liquid-to-gas ratio increased from 2.59 to 4.22 between the lowest and highest flue gas CO_2 concentrations tested. The plant performance was also analysed at varying reboiler temperatures (124-127°C), using a flue gas with 9.0 vol% CO_2 concentration. The results indicated that the overall specific reboiler duty and CO_2 capture efficiencies reduced at lower reboiler temperatures. Overall, the results indicate that S-EGR operation in the gas turbine could be beneficial since it can lead to reductions in overall energy costs.

The economic analysis evaluated the application of two S-EGR configurations (parallel and hybrid) in combined cycle gas turbine (CCGT) power plants, with the cost of electricity ranging from $82-90 and $82-93 per MWh_e, respectively. The cost of CO_2 avoided for the parallel and hybrid schemes varied from $80-105 and $83-119 per tonne of CO_2 avoided. The sensitivity analysis performed also demonstrated the economic competitiveness of S-EGR against ACP and EGR.

Table of contents

List of figures

List of tables

Abbreviations

AMP	2-Amino-2-methyl-1-propanol
ACP	Amine capture plant
BEC	Bare erected costs
CAPEX	Capital expenditure
CCS	Carbon capture and storage
CCU	Carbon capture and utilisation
CCUS	Carbon capture, utilisation and storage
CRU	Climatic Research Unit
CCGT	Combined cycle gas turbine
COMB	Combustor
COMP	Compressor
CFD	Computational fluid dynamics
COP	Conference of the Parties
COA	Cost of CO_2 avoided
COE	Cost of Electricity
DEA	Diethanolamine
DMAE	Dimethylaminoethanol
DLN	Dry low NOx
EGR	Exhaust gas recirculation
F-gases	Fluorinated gases
FTIR	Fourier Transform Infrared

gpu	Gas permeation unit
GT	Gas turbine
GEN	Generator
GWP	Global warming potential
GISS	Goddard Institute for Space Studies
GHG	Greenhouse gases
HRSG	Heat recovery steam generator
HHV	Higher heating value
HFCs	Hydrofluorocarbons
IPCC	Intergovernmental Panel on Climate Change
IEA	International Energy Association
kW	Kilowatt
kWh	Kilowatt hour of electricity
L/G	Liquid-to-gas ratio
LVH	Lower heating value
MJ	Megajoules
MOC	Minimum oxygen concentration
kW_e	Net electrical power output
NOx	Nitrogen oxides
SOx	Sulphur oxides
TOC	Total overnight costs

Nomenclature

A_M	Membrane area
$\alpha_{f,p}$	Permeability ratio
BEC	Bare erected costs
CH_4	Methane
c_i	Concentration
$c_{i,f}$	Feed concentration
$c_{i,p}$	Permeate concentration
CO	Carbon monoxide
CO_2	Carbon dioxide
$CO_{2,CR}$	CO_2 capture rate
C_p	Specific heat capacity at constant pressure
C_{SKID}	Skid cost
∂c	Concentration gradient over the membrane
D_i	Diffusion coefficient
$D_{i,f}/D_{i,p}$	Diffusion coefficient ratio at feed and permeate
∂x	Position represented by length
$EINOx$	NO_x emissions index
EXP	Scaling exponent
FOM	Fixed operating and maintenance costs
$GtCO_2$-eq/yr	Gigatonne of CO_2 equivalent per year

h_1	Compressor inlet enthalpy
h_2	Combustor inlet enthalpy
h_3	Combustor outlet enthalpy
h_4	Turbine outlet enthalpy
H_2	Hydrogen
H_2O	Water
HCO_3	Bicarbonate
HR	Heat rate
$\varphi_{i,wet}$	Wet gas species concentration
J_i	Gas flux through membrane
kg CO_2 per MWh	Kilogram of CO_2 per megawatt hour of electricity
kt CO_2 / yr	Kilo tonnes of CO_2 per year
l	Membrane thickness
$\dot{m}_a$	Inlet air mass flowrate
$\dot{m}_f$	Fuel mass flowrate
$\dot{m}_t$	Total mass flowrate
MJ/kg CO_2	Megajoule per kilogram of CO_2
Mt CO_2/yr	Mega tonnes of CO_2 per year
MW	Molecular weight
N_2	Nitrogen
N_2O	Nitrous oxide

$nCO_{2Abs_{in}}$	CO_2 molar flowrate entering the absorber
$nCO_{2Abs_{out}}$	CO_2 molar flowrate leaving the absorber
η_{el}	Electrical efficiency
NF_3	Nitrogen trifluoride
n_{FG}	Molar flue gas flowrate
NH	Nitrogen monohydride
NH_2	Amidoge (Amino radical)
NH_2COOH	Carbamate acid
NH_3	Ammonia
O_2	Oxygen
O_3	Ozone
P_1	Compressor inlet pressure
P_2	Compressor outlet pressure
P_3	Turbine inlet pressure
P_4	Turbine outlet pressure
P_e	Net power output
ρ_f	Density of the fuel
PHW_f	Pressurised hot water flowrate
p_i	Partial pressure
P_i	Permeability
$p_{i,f}$	Feed partial pressure
$p_{i,p}$	Permeate partial pressure

Q_{f1}	Thermal input
R	Ideal gas constant
RC	Reference cost
RD	Reboiler duty
RP	Reference parameter
SF_6	Sulphur hexafluoride
S_i	Solubility coefficient
$S_{i,f}/S_{i,p}$	Solubility coefficient ratio at feed and permeate
SO_2	Sulphur dioxide
SP	Scaling parameter
TOC	Total overnight costs
$T\&SC$	Transport and storage costs
T_1	Compressor inlet temperature
T_2	Compressor outlet temperature
T_3	Recuperator air-side outlet temperature
T_4	Combustor outlet temperature
T_5	Turbine outlet temperature
$vol\ \%_{\cdot H2O}$	Water vapour volume concentration
VOM	Variable operating and maintenance costs

1 Introduction

1.1 Background

The consequences of climate change on social, economic and environmental factors will largely depend on how mitigation strategies are implemented and adapted based on future climate change scenarios (Moss et al., 2010). Greenhouse gas (GHG) emissions reduction and mitigation is imperative to limit the effects of climate change. Carbon dioxide (CO_2) is the most abundant anthropogenic GHG, where atmospheric concentrations since the pre-industrial era (280 parts per million (ppm) – c. 1750 to 1850) have significantly increased (IEA, 2017a). The rapid growth in CO_2 emissions is evident from Figure 1.1, which illustrates that CO_2 emissions increased from 315.7 ppm in 1958 to 411.3 ppm in 2018, an average rise of 1.57 ppm per year.

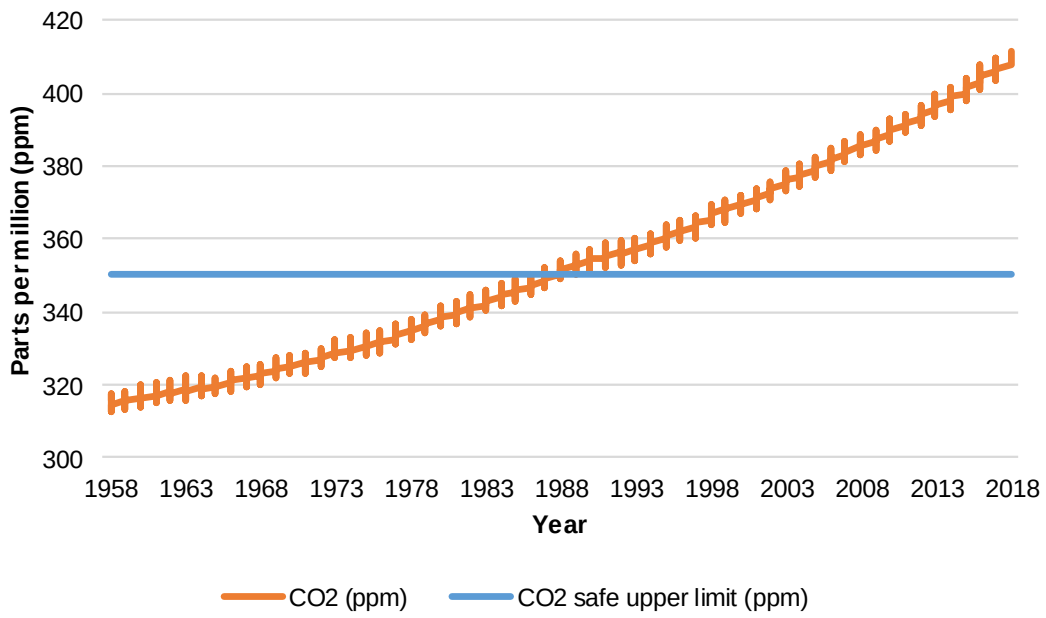

Figure 1.1. Globally averaged CO_2 data from 1958 to 2018

(NASA, 2018).

This continued rapid rise of CO_2 has and will continue to influence the climate and result in detrimental impacts, including sea level rise, extreme weather events (e.g. flooding and droughts), species extinction, and poor air quality. These impacts will have a global negative consequence on social, economic and environmental factors, hence, it is important to mitigate and reduce these emissions to abate climate change. Firstly, it is necessary to understand the trends in global CO_2 emissions to provide effective solutions to assist with climate change mitigation. In

2016, global CO_2 emissions totalled ~36 Gt increasing by ~0.4 Gt/year from 1970 to 2016. However, the annual increase in global CO_2 emissions slowed from 2012 to 2015. In the period 2012 to 2013, CO_2 emissions increased by 1.8%, and in 2013 to 2014 a rise of 0.8% was reported. Interestingly in the period 2014 to 2015, CO_2 emissions decreased by 0.2%, whereas, the 2015 to 2016 period reported a 0.5% increase in emissions (Janssens-Maenhout et al., 2017). These values indicate the annual increase of CO_2 emissions compared to preceding years has slowed. This is likely due to changes in the energy mix, e.g. increased used of renewables, reduced use of fossil fuels for electricity production, improved efficiency and the impact of the financial crisis on the global economy. Karmellos et al. (2016) add that changes to China's economic structure and improvements to how we use energy are the principle factors leading to this observed slowdown in CO_2 emissions. As shown in Figure 1.2, coal, oil, and natural gas remain the dominant fuels for electricity generation. This is important, as these fuels are responsible for the greatest concentrations of CO_2 due to their use for electricity, heat generation and transportation. Therefore, to reduce CO_2 emissions, the development and implementation of low carbon technologies are required.

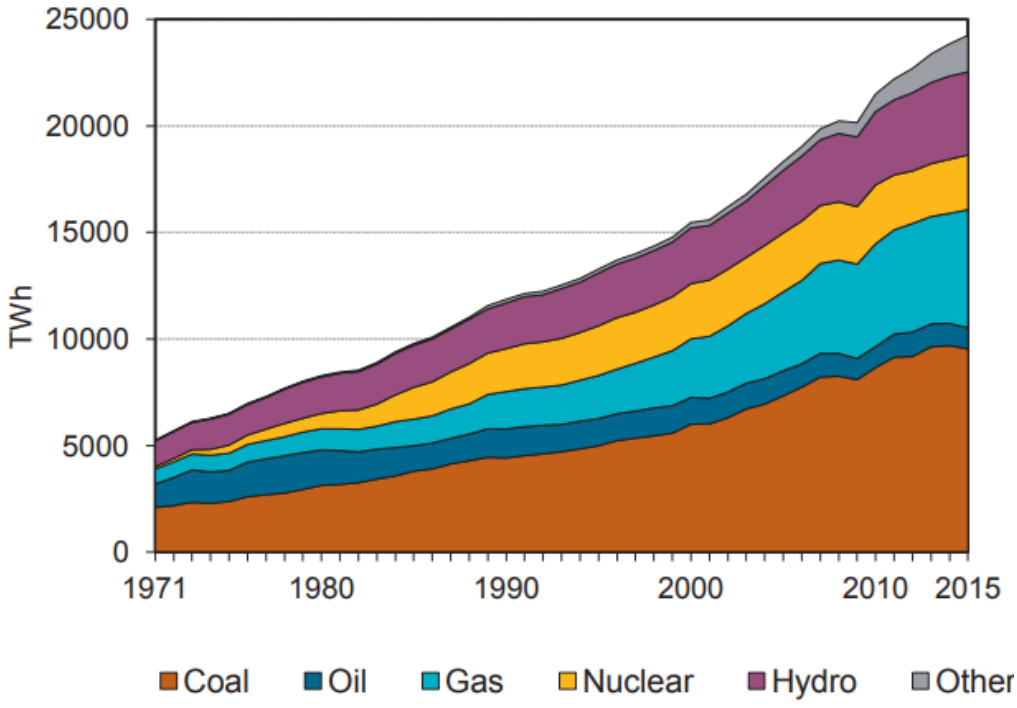

Figure 1.2. World electricity generation by fuel from 1971 to 2015

(IEA, 2017a).

As shown in Table 1.1 (p.3), the progress of low carbon technologies is evident, indicated by the growth of renewable energy from 2014 to 2017. This 52% increase

demonstrates the growth of low carbon technologies (e.g. solar, wind, tidal and geothermal), compared to coal which decreased ~3%, with oil and natural gas consumption increasing ~5% and ~8%, respectively, during the same period. As shown in Figure 1.2 (p.2), oil, coal and natural gas remain the dominant fuels for electricity generation. This is also reflected in Figure 1.3 with oil, coal and natural gas representing ~34%, ~28%, and ~23% of global primary energy share for 2017 (BP, 2018).

Table 1.1. Primary world fuel consumption 2014 and 2017

Fuel	Fuel consumption (Mtoe)			
	2014	*2015*	*2016*	*2017*
Coal	3862	3765	3706	3732
Natural gas	2922	2987	3073	3156
Oil	4395	4476	4557	4622
Nuclear energy	575	583	591	596
Hydroelectricity	880	881	913	919
Renewables	320	369	417	487

(BP, 2018).

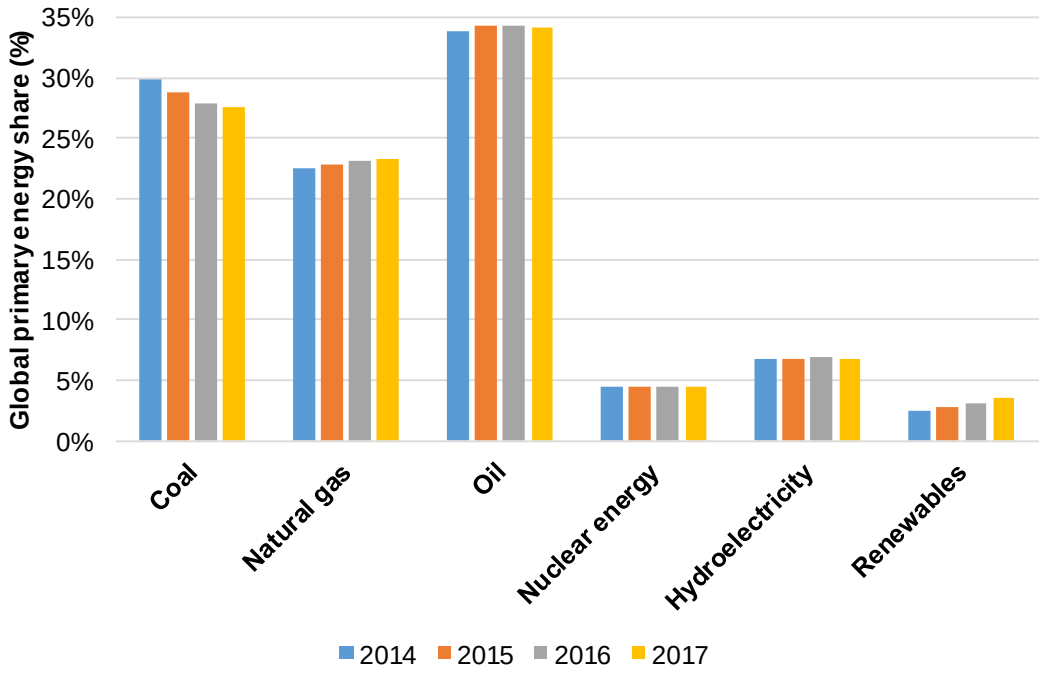

Figure 1.3. Comparison of world primary energy share 2014 to 2017

(BP, 2018).

The increased use of low carbon technologies within the energy mix is promising as coal, oil and natural gas combustion account for the highest amount of CO_2 emissions compared to other fuel sources as indicated by Figure 1.4 (p. 4).

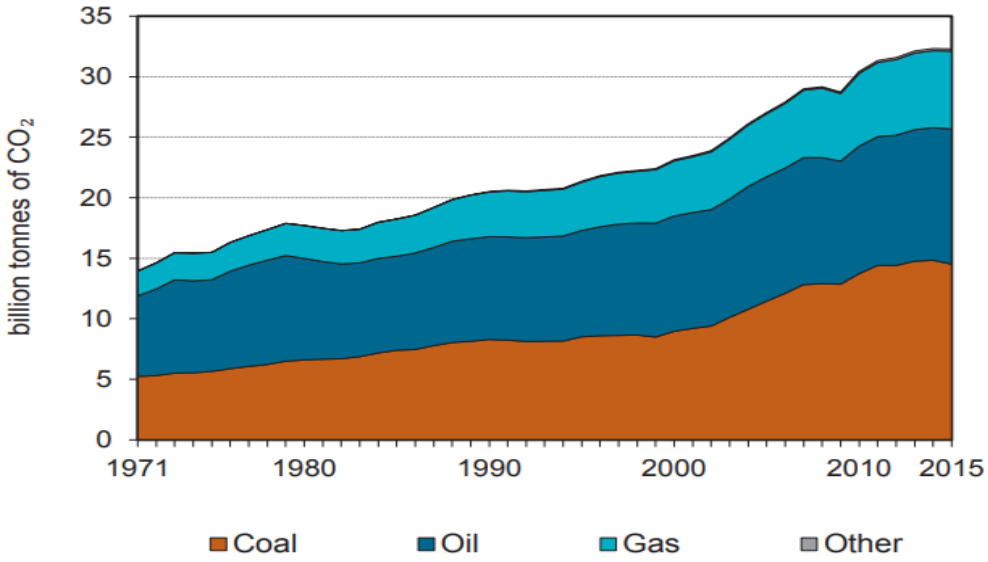

Figure 1.4. CO_2 emissions share from fossil fuels from 1971 to 2015

(IEA, 2017a).

Nonetheless, electricity and heat generation remains one of the primary sources of global CO_2 emissions (47% in 2015) (IEA, 2017a). In the 2040 energy future scenarios, natural gas demand from the power generation sector is expected to increase to 36% by 2040 becoming the main fossil fuel in the energy mix (IEA, 2017b). Despite the increasing use of low carbon energy options for electricity generation, fossil fuels will still be used and CO_2 emissions from these systems require mitigation

Globally, nations are acting and working towards emissions reduction through international conventions. At the 21st United Nations Framework Convention on Climate Change (UNFCCC) Conference of the Parties (COP), member states agreed on a new climate change protocol including legislative mechanisms to maintain the rise in worldwide average temperatures "*below 2°C above pre–industrial levels and pursuing efforts to limit the temperature increase to 1.5°C above pre–industrial levels*" (UNFCCC, 2015). This international agreement demonstrates that nations are taking climate change seriously. In the European Union, this is evident, with action areas to combat climate change including a 40% reduction in GHG emissions compared to 1990 levels, an increase of 27% in renewable energy and 27% improvement in energy efficiency by 2030 (EC, 2018). The EU have also published the Energy 2050 roadmap outlining scenarios to achieve energy decarbonisation and transition to a low carbon energy system by 2050 (EC, 2012). These scenarios require collective action from all industries e.g. agriculture, power generation, forestry and transportation. In 2016, power

generation accounted for 54% of all EU GHG emissions (EEA 2018). Therefore, reducing GHG emissions, notably CO_2 emissions from power generation is fundamental towards achieving climate change targets. This is of vital importance in the UK, where transport and power generation accounted for 27% and 24%, respectively, of total UK GHG emissions in 2017 (BEIS, 2019). To contribute towards achieving the EU emission targets, the UK government has set out its own targets via the implementation of legislative measures including the Climate Change Act 2008 (UKGov, 2019). The target outlined in the Climate Change Act is to ensure the net UK carbon account for the year 2050 is at least 80% lower than the 1990 baseline (UKGov, 2019). To achieve this target, the power generation sector needs to reduce the carbon intensity to 50 gCO_2/kWh by 2050 (CCC, 2015). To deliver a decarbonised low carbon energy system requires the implementation of low carbon power generation including biomass, wind, solar and fossil fuel combustion coupled with carbon capture and storage (CCS). In the European context, particularly in the UK and other Northern European countries e.g. Norway, CCS is recognised as a key enabling zero emission technology to assist in the reduction of CO_2 emissions from large stationary combustion plants and other heavy industries e.g. steel and cement production. It is anticipated that without CCS, meeting the 2050 climate change targets set out by the UK government will significantly increase the abatement cost, as more expensive mitigation options would be required (ETI 2015; CCC 2016; Oxburgh, 2016). To enable CCS as a key UK climate change mitigation strategy will require investment in low carbon electricity (40 GW of new installed capacity) by 2030 (CCC, 2015). This new capacity is to facilitate the anticipated increase in electricity demand and to replace plants at the end of their life cycle. The UK governments' electricity market reform delivery plan predicts that ~13 GW of this new capacity will come from power plants coupled with CCS (DECC, 2015). As the UK moves towards low carbon power generation, the shift from coal-fired power to natural-gas power generation is expected. By 2020, it is anticipated that up to 30 GW of new combined-cycle gas turbine (CCGT) power plants will be installed in the UK (CCC, 2015). Increasing the use of natural gas in the energy mix, will provide flexibility to meet shortfalls in the demanded electricity, and compensate for gaps in renewable and nuclear power to the grid. Furthermore, using unabated natural gas instead of coal, provides further benefits, notably the lower carbon intensity which is ~350-400 gCO_2/kWh, that can assist with reducing CO_2 emissions in the short term (IEAGHG, 2012a). However, to contribute toward CO_2 emission targets and deliver low carbon electricity generation, CCS will require integration with CCGT power plants.

1.2 Carbon capture, utilisation and storage

To mitigate emissions from power generation and industrial systems carbon capture, utilisation and storage (CCUS) is considered as a fundamental option to meet the 2°C or below Paris agreement emission target (IEA, 2017b). In CCS, the captured CO_2 is pressurised to approximately 100 to 150 bar and transferred to a storage location, e.g. geological storage, where it can remain for millions of years (Boot-Handford et al., 2014). In CCU, the captured CO_2 is utilised to add value to the power generation lifecycle by creating a commercial product from a waste gas. There is a range of applications for CCU such as enhanced oil and coal-bed methane recovery, conversion into chemicals and fuel, and mineral carbonation (Cuéllar-Franca and Azapagic, 2015). The options for CO_2 capture include pre-combustion, post-combustion and oxy-fuel combustion. Pre-combustion CO_2 capture involves the integrated gasification or reforming of a solid or gaseous fuel, respectively, where it is converted to synthesis gas (mainly comprises of hydrogen (H_2) and CO although some CO_2 can be present) at high temperature and pressure, in the presence of steam (H_2O) and oxygen (O_2) (see Figure 1.5). The syngas is then subject to the water gas shift reaction (Dimitriou et al., 2015), involving the oxidation of CO which produces CO_2 and H_2. Following this, the CO_2 is captured and then processed for storage or use, and the H_2 is used to generate electricity.

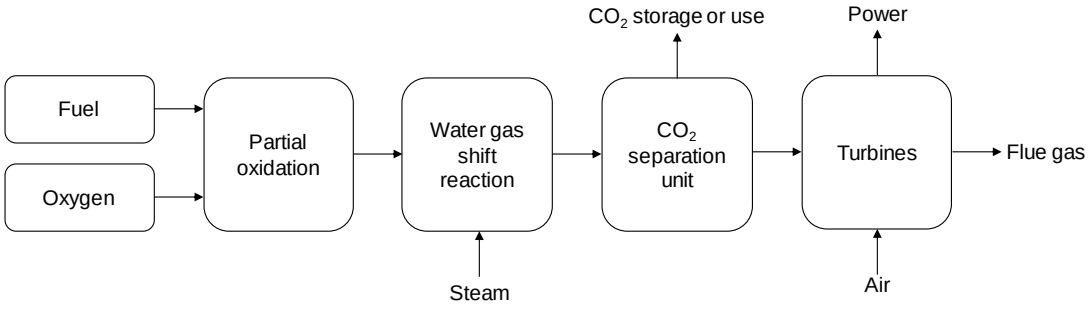

Figure 1.5. Schematic of the process for pre–combustion capture.

Oxy-fuel combustion (see Figure 1.6, p.7) requires the modification of the combustion process, where the fuel is burnt in the presence of a highly rich O_2 stream (> 95%) mixed with recycled CO_2. The system will operate at typical 30-35 vol% O_2 in total within the combustor, although higher O_2 concentrations are being explored (Arias et al., 2018; Black et al., 2013). This highly-concentrated O_2 stream is usually supplied from a cryogenic air separation unit, where low-temperature condensation (< -182°C) splits the O_2 from the nitrogen (N_2). The combustion of the fuel within this highly enriched O_2 stream results in much higher furnace temperatures, therefore, it is necessary to recycle the CO_2-concentrated flue gas

(RFG) to act as a diluent and regulate flame temperature similar to conventional air firing (Wall et al., 2009). Following the combustion process, CO_2 and water vapour are the main products in the exhaust gas stream. Condensation removes the water vapour and the CO_2 stream is subject to purification and dehydration prior to being transported for storage or utilisation.

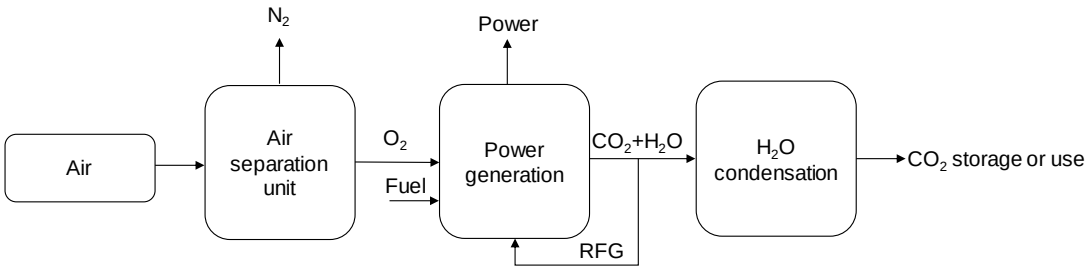

Figure 1.6. Schematic of the process for oxy-fuel combustion capture.

Post-combustion CO_2 capture (PCC) captures CO_2 in the flue gas generated after combustion, and then it is processed for compression, transportation and storage or use (see Figure 1.7). The most advanced PCC CO_2 capture technology is amine absorption, which has already achieved commercial scale (NRG Energy, 2017; SaskPower, 2017). Post-combustion CO_2 capture is the mostly widely used because it is the most developed option compared to pre-combustion and oxy-fuel CO_2 capture. Wet scrubbing using monoethanolamine (MEA) is a developed technology used in gas sweetening and the chemical industry, which is the mostly widely used solvent for gas scrubbing technology.

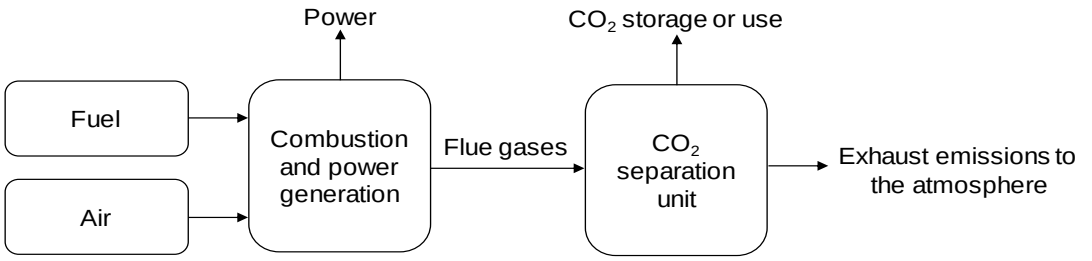

Figure 1.7. Schematic of the process for post-combustion capture.

The CO_2 is absorbed by a solvent (typically MEA) in an absorption column separating it from the remaining flue gases. Following this, CO_2 is removed from the solvent in a stripper column and processed for storage or use. The solvent is recirculated within the system and reused. Other technologies proposed for PCC include the use of solid sorbents in high-temperature looping cycles, membranes, adsorption and cryogenic separation. These processes are at different phases of research and development, requiring further optimisation before being considered for commercial deployment (Boot-Handford et al., 2014; Mondal et al., 2012).

1.2.1 Current status of CCUS

There are currently only two operational commercial-scale PCC plants that use amines. These include SaskPower Boundary Dam CCS project near Estevan, Saskatchewan, Canada and Petra Nova, Texas, USA. The Boundary Dam project was the world's first full scale operational CCS plant where 1 million tonnes a year of CO_2 can be captured (Stéphenne, 2014). This 139 MW thermal coal–fired power plant was retrofitted with an ACP and has a capture efficiency of 90% using the Shell Cansolv process (Stéphenne, 2014). Since January 2017, Petra Nova has become the largest operational CCS plant (NRG Energy, 2017). This facility captures up to 1.4 million tonnes a year of CO_2 at a 90% capture efficiency, using the KS-1 amine solvent created by Mitsubishi Heavy Industries (NRG Energy, 2017). The knowledge gained from the development of these two commercial scale CCS plants and early pilot and demonstration scale plants provide valuable information to reduce the uncertainty associated with cost, design, construction and operation of future CCS schemes. This will be important in building confidence with investors and stakeholders that CCS is a cost-effective zero emission technology that can be delivered at scale. It is anticipated that the lesson learnt from Boundary Dam alone will decrease CCS costs by ~30% (GCCSI, 2015). However, a large proportion of CCS projects are focused on coal-fired power generation, not natural gas, principally because these plants produce higher CO_2 emissions compared to CCGT's. Nonetheless, CCS from commercial scale CCGT plants (gas-CCS) is also required to meet emission targets. The deployment of gas-CCS will also assist in reducing costs associated with CCS and make this technology a competitive mitigation option. In the UK, the CCS commercialisation programme was cancelled in 2015, which offered £1 billion of funding to develop CCS. This front end engineering and design (FEED) study proposed to apply CCS to a 385 MW_e CCGT power plant located in Peterhead, Scotland (Herraiz, 2016). However, smaller pilot scale projects have continued to develop gas-CCS, including the CO_2 Technology Centre Mongstad in Norway (Thimsen et al. 2014; Hamborg et al. 2014) and the Pilot-Scale Advanced Capture (PACT) facilities in the UK (Best et al. 2016). The application of gas-CCS poses challenges, notably due to the lower flue gas CO_2 and higher O_2 concentrations compared to coal fired plants. Gas turbines also operate with high excess air, principally to control oxides of nitrogen (NOx) emissions and for cooling down the metallurgy, resulting in large volumetric flue gas flowrates. To treat these large flowrates requires larger absorber columns and auxiliary equipment, thus leading to greater costs for gas-CCS.

1.2.2 Challenges of combined cycle gas turbines coupled with PCC

As noted previously, the use of natural gas for electricity generation is likely to rise in the coming decades as nations move towards cleaner energy production (IEA, 2017b). Coal-fired plants have higher CO_2 concentrations (~13 vol%) and lower O_2 levels of ~3 vol% compared to natural gas combustion. As the emission targets become stricter and nations move towards a carbon-free society, coal combustion is likely to decline. In addition, energy flexibility will become imperative to future energy scenarios. As gas turbine combustion systems can offer flexibility and lower CO_2 emissions compared to coal, the use of natural gas for electricity generation purposes is expected to rise. This means CCS is essential to mitigate CO_2 emissions from CCGT power stations (IEA, 2017b). Natural gas systems have the lowest flue gas CO_2 concentrations compared to other fossil fuels, ~4 vol% CO_2, which equates to ~300-400 kg CO_2 per MWh in CCGT power stations (IEAGHG, 2012a). Coupling CCS with natural gas combustion processes (gas-CCS) is difficult due to the high excess air requirements of the combustor leading to greater exhaust flowrates, higher remaining oxygen and lower CO_2 concentrations (Bolland and Mathieu, 1998; Li et al., 2011a; Lugo-Leyte et al., 2010). The higher excess air is required to decrease the turbine inlet temperature to levels the turbine blades can tolerate due to limits in metallurgy, hence, safeguarding the turbomachinery (Martínez et al., 2011). Furthermore, the high excess air in gas turbines is needed to control NOx emissions, by decreasing the flame temperature to limit NOx formation (Davis and Black, 2000). Modern heavy-duty gas turbines utilise lean pre-mixed Dry Low NOx combustors, which have been designed to operate at low NOx concentrations. The air used in the combustor is controlled to ensure optimal air fuel ratios, where part of the outlet compressor air is mixed with the fuel and combusted (Davis and Black, 2000). The remaining air is used for flame quenching and combustor wall cooling which aids in the control of NOx formation, as the flame temperatures are reduced (Davis and Black, 2000). The higher air flowrates require the capture plant, especially the absorber columns to be greater in size to accommodate these flowrates (Akram et al., 2016; Biliyok and Yeung, 2013; Bolland and Sæther, 1992; Merkel et al., 2013).

McGlade et al. (2016) also identify that using natural gas as a bridging fuel (instead of coal or oil) to develop a low carbon energy system is unsustainable beyond 2020 without CCS technology in place. Therefore, the implementation of CCS is required today to create the low carbon economy of tomorrow. However, the technological and economic challenges noted above need to be resolved before governments will

consider deploying CCUS. In the UK, this is evident, with the government withdrawing £1 billion of funding to develop CCS (LSE, 2015). The recently published Clean Growth Strategy (BEIS, 2017) indicates that the UK government is willing to reconsider CCUS for our energy future. However, to deploy CCUS at scale, cost reductions are required. This combined with international collaboration e.g. Mission Innovation (Mission Innovation, 2017) and addressing issues such as liability, safety, and long-term CO_2 storage will encourage nations to commit to the deployment of CCUS (Figueroa et al., 2008). By deploying this technology at scale, a 14% reduction in CO_2 emissions is expected by the middle of the century (IEA, 2013). Therefore, the optimisation of gas-CCS is required to ensure we can deliver a long-term and low-cost mitigation strategy for the future. Understanding the operational performance and costs of gas-CCS will be imperative in the development of this technology. This is already being undertaken, where researchers are developing techniques to increase the CO_2 concentration in the exhaust gas from gas turbine systems (e.g. Akram et al., 2016; Best et al., 2016; Bolland and Mathieu, 1998; Li et al., 2011b) and proposing novel configurations (e.g. Merkel et al., 2013a, 2010) to develop CCS for commercial application. There are other strategies for increasing the CO_2 concentrations in the flue gases of gas-fired systems including humidified cycles, supplementary firing and exhaust gas recirculation (EGR) (Diego et al., 2017a), but this work will focus on selective exhaust gas recirculation (S-EGR). Merkel et al. (2013a, 2010) initially proposed S-EGR to increase the CO_2 content in the flue gases from gas fired power plants to make gas-CCS an attractive option. However, research has principally focused on modelling studies, with limited experience of investigating S-EGR experimentally, or developing appropriate costing methodologies to determine if this technology can be competitive compared to other proposed solutions, e,g EGR. Thus, this thesis will focus on these areas.

1.3 Research hypothesis

Selective exhaust gas recirculation will increase the CO_2 flue gas concentration in CCGT power plants and reduce the costs associated with the downstream CO_2 capture plant.

1.4 Research objectives

As highlighted in the introductory section, gas-CCS is seen as a promising option to contribute towards reducing CO_2 emissions. The deployment of gas-CCS requires the development of different CCS options to make it commercially attractive for

implementation in low carbon energy systems. Full-scale deployment of gas-CCS requires solutions to be developed to increase the flue gas CO_2 concentration in CCGT's whilst making the downstream CO_2 capture plant cost effective. As briefly mentioned in the introduction, S-EGR is one of the proposed options to do this, however, no pilot-scale experimental work has investigated the impacts of S-EGR on gas turbine or CO_2 capture plant performance. In addition, no works have developed suitable costing methodology to evaluate if this option is cost effective on a commercial scale. In this context, the purpose of this research project is to continue the development of S-EGR systems in CCGT power stations.

To achieve this, the following objectives are identified:

Experimental

1. Assess how different S–EGR ratios influence CO_2 concentrations in the exhaust gas stream of a Turbec T100 Series 3 micro gas turbine (mGT) at the PACT national research facilities.
2. Analyse the behaviour of O_2, NOx, CO and UHC under S–EGR conditions, following mGT combustion tests.
3. Evaluate how various S–EGR ratios influence the mGT performance.
4. Assess and evaluate how S–EGR influences the PACT ACP plant in terms of overall performance, CO_2 capture rate and specific reboiler duty using a 40wt% MEA solvent.

Economics

5. Perform an economic analysis of parallel and hybrid S-EGR configurations in commercial scale CCGT systems.

1.5 Research novelty

The research novelty of this thesis, which is considered as an original contribution to knowledge, includes:

1. Pilot plant study investigating the performance of a micro gas turbine under S–EGR conditions.
2. Pilot plant study investigating the performance of post-combustion CO_2 capture under S–EGR conditions.
3. Economic analysis of parallel and hybrid S-EGR configurations implemented into CCGT power generation cycles.

1.6 Thesis overview

This thesis comprises of seven chapters (including this one) where the contents of the subsequent six are outlined below.

- Chapter 2 provides a comprehensive literature review that outlines the knowledge gaps associated with gas-CCS options. Notably, this chapter critically evaluates methods to increase CO_2 exhaust gas concentrations in natural gas systems.
- Chapter 3 initially outlines a technical overview of gas turbines. Following this, the thermodynamic cycles associated with gas turbines are explained. In addition, the fundamentals associated with membranes and amine chemistry are also presented.
- Chapter 4 outlines the experimental methodology used for the mGT baseline and S-EGR CO_2 enhancement experimental campaigns. The results are then presented with analysis, discussion and conclusions.
- Chapter 5 outlines the experimental methodology used for the ACP experimental campaign with S-EGR. Subsequently, the results are presented with analysis, discussion and conclusions.
- Chapter 6 presents the economic analysis of parallel and hybrid S-EGR configurations implemented into CCGT's.
- Chapter 7 presents the conclusions and recommendations for future work.

2 Literature review of gas-CCS

2.1 Introduction

As highlighted in section 1.2.2, the application of CCS to gas-fired systems requires economic and energy cost reductions before it is applied to commercial-scale CCGT power stations. To achieve this, increases in flue gas CO_2 concentrations and optimisation of the downstream capture system is required. Studies that have investigated different approaches to augment the flue gas CO_2 concentration from gas-fired systems include

- humidified cycles (Heppenstall, 1998; Jonsson and Yan, 2005; Li et al., 2011a);
- supplementary firing (Biliyok and Yeung, 2013; González Díaz et al., 2016; Koornneef et al., 2012; Li et al., 2011a, 2012);
- EGR (Akram et al., 2016; Ali et al., 2017; Best et al., 2016; Bolland and Sæther, 1992; Li et al., 2011a); and
- S-EGR (Baker et al., 2017; Darabkhani et al., 2018; Diego et al., 2018, 2017b; Herraiz et al., 2018; Merkel et al., 2013).

This chapter critically analyses the above options, including recent developments of ACP for gas-fired systems.

2.2 Humidified gas turbines

Humidified gas turbine cycles are being investigated to optimise the electrical efficiency of CCGT's by introducing moisture into the system (Chiesa, 2012; Heppenstall, 1998; Rao, 2014). This process works with a modified working fluid that comprises of up to 20 vol% H_2O and the remaining fluid being air (Chiesa, 2012; Gabrielsson and Torisson, 2003; Jonsson and Yan, 2005; Li et al., 2011a). These cycles are recuperative because available heat is recovered and utilised again to produce steam, thus, replacing a proportion of the excess air (Chiesa, 2012; Heppenstall, 1998; Rao, 2014). The benefit of humidified cycles includes high efficiencies and lower economic costs compared to that of CCGT's and open cycles (Jonsson and Yan, 2005). Because of the higher specific work output and thermal efficiency, humidified cycles offer greater performance than traditional gas turbine systems (Chiesa, 2012; Gabrielsson and Torisson, 2003; Jonsson and Yan, 2005; Li et al., 2011a). In addition, the benefit of using humidified cycles is that NOx emissions are lower because of decreased flame temperatures due to H_2O addition

(Chiesa, 2012; Gabrielsson and Torisson, 2003; Jonsson and Yan, 2005; Li et al., 2011a). Furthermore, the CO_2 concentrations are increased as the flue gas volume is smaller when water vapour is removed from this stream. This is beneficial for the downstream CO_2 capture plant as higher CO_2 concentrations and reduced flue gas flowrates enable energy and cost savings to be realised (Gabrielsson and Torisson, 2003; Jonsson and Yan, 2005; Li et al., 2011a; Wei and Zang, 2012). Additionally, humidified cycles offer improved operational flexibility in terms of part-load behaviour and varying ambient conditions (notably temperature and pressure) (Chiesa, 2012; Jonsson and Yan, 2005). However, technical issues, such as complex cycle configurations, high water consumption, water demineralisation to avoid deposition and corrosion and greater financial costs, are some of the associated challenges of these systems (Saravanamuttoo et al., 2009). Humidified gas turbines inject either water or steam into the cycle, with a range of methods and schemes proposed (Chiesa, 2012; Jonsson and Yan, 2005; Rao, 2014). The two configurations which are applicable to gas-CCS include humid air or steam injection turbines (Chiesa, 2012; Jonsson and Yan, 2005; Rao, 2014). Recuperative water injection and top humid air cycles are other configurations considered in the literature, however, due to the limited efficiency gains and increases in CO_2 concentrations, these cycles are not considered suitable for CCS (Chiesa, 2012; Traverso and Massardo, 2002). Therefore, these two configurations are not discussed herein.

2.2.1 Humid air turbines

Humid air turbine cycles, see Figure 2.1 (p. 15), encompass either a saturator or humidification column where intercoolers and economizers are used to recover thermal energy from the gas turbine compressor and flue gases (Abdallah and Harvey, 2001; Chiesa, 2012; Gabrielsson and Torisson, 2003; Poullikkas, 2005; Rao, 2014). This recovered energy is used to heat up and then evaporate water in the saturator or humidification column which imbues the exiting air from the compressor, thus leading to a single-phase working fluid (Jonsson and Yan, 2005). Because the working fluid flowrate passing through the cycle is higher and additional work increases (due to the extra turbine work), the overall system efficiencies increase (Chiesa, 2012; Gabrielsson and Torisson, 2003; Rao, 2014). A key drawback of humid air turbine cycles is the high water usage which increases the costs of these systems (Horlock, 2003). To negate these issues, the water in the system can be condensed and reused, however, water treatment is required to eliminate any contaminants or impurities (Jonsson and Yan, 2005).

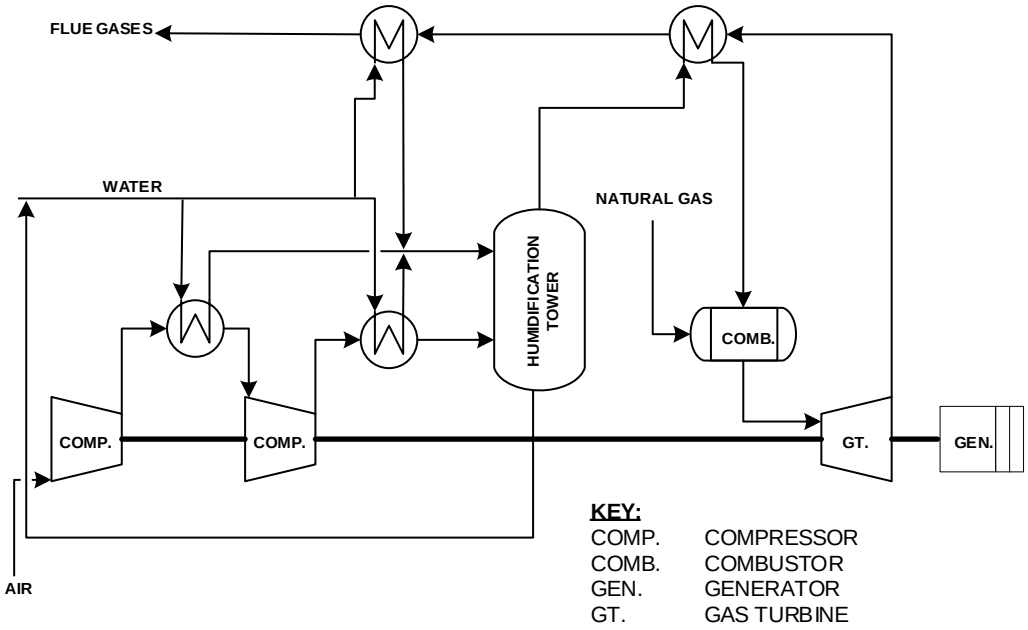

Figure 2.1. Schematic of the humid air turbine process.

Furthermore, incomplete combustion, leading to higher CO and UHC emissions, is more prominent at higher water fuel ratios (Saravanamuttoo et al., 2009). These systems are also at an early stage of development and the necessary technological advancements in turbomachinery are required to apply these cycles to commercial operations (Chiesa, 2012; Rao, 2014). The majority of experimental studies centre on saturator and humidification column performance rather than the gas turbine or CO_2 capture plant performance (Pedemonte et al., 2008a, 2008b; Traverso, 2010; Wang et al., 2007a, 2007b). Only limited works have evaluated the entire system or process optimisation to benefit gas-CCS (Li et al., 2011a; Wei and Zang, 2012). To attain the maximum efficiency and specific work, the humidity and compressor pressure ratios are typically higher in these systems (Wei and Zang, 2012). In humid air turbine cycles, the reported efficiencies are ~50% compared to simple gas turbine cycles with efficiencies of ~25-40% (Gallo, 1997; Manfrida, 1999). In the work by Li et al. (2009) they reported an electrical efficiency of ~52% at an optimal 0.14 water-air ratio without CCS. These authors also identified that the electrical efficiency reduces to ~42% with a ~0.12 water-air ratio when coupling the cycle to a CO_2 capture plant using MEA 30 wt% solvent (Li et al., 2009). The electrical efficiency in conventional CCGT systems is ~58% and with CCS ~48% indicating one of the drawbacks of humid air gas turbine cycles (Li et al., 2011a). In addition to this, CO_2 concentrations of ~5 vol% are achievable compared to conventional CCGT's (3-4 vol%), although the increased flue gas water content has the potential to diminish the solvent make up in the CO_2 capture plant, which increases the

energy penalty (Li et al., 2011a). Thus, the application of humid air gas turbine cycles for commercial gas-CCS is generally accepted as being economically unsustainable at present (Parsons et al., 2002).

2.2.2 Steam injection turbines

In this cycle, steam is added directly into the combustor independently, instead of combined with the oxidant stream (Abdallah and Harvey, 2001; Chiesa, 2012; Jonsson and Yan, 2005; Penning and de Lange, 1996; Rao, 2014). As illustrated in Figure 2.2, the evaporation process occurring in the Heat Recovery Steam Generator (HRSG) arises as a result of the heat transfer from the flue gases exiting the turbine (Chiesa, 2012; Jonsson and Yan, 2005; Rao, 2014).

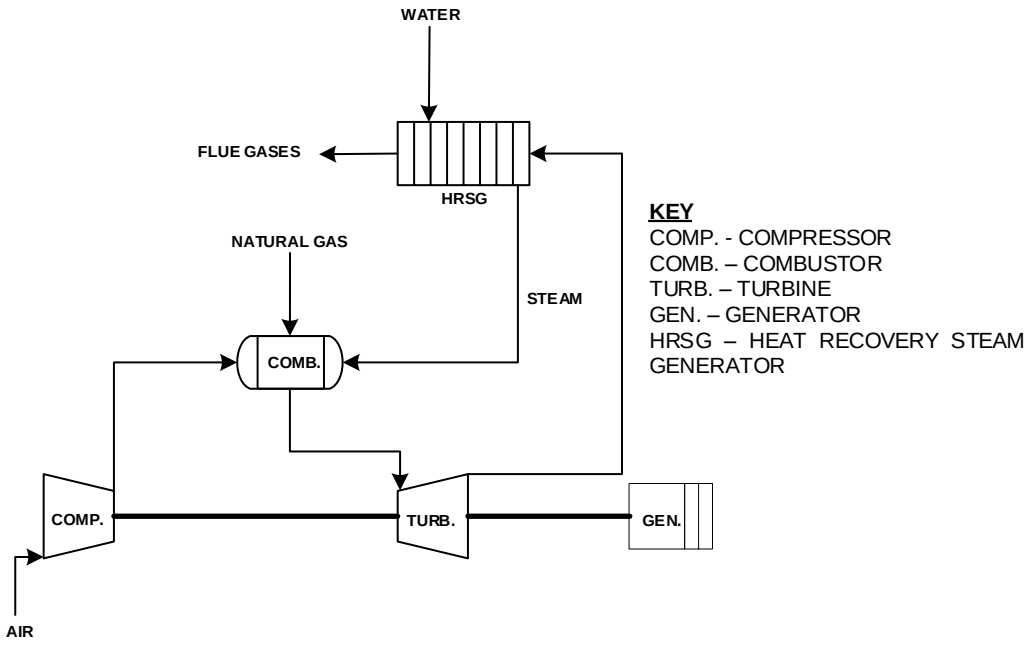

Figure 2.2. Schematic of the steam injection turbine process.

The gas turbine operability is maintained when adding steam straight into the combustor. This means that the system efficiency can be improved in comparison to cycles without this configuration due to the larger flowrate through the turbine and consistent compressor work (Chiesa, 2012; Jonsson and Yan, 2005; Rao, 2014). In terms of capital costs, this is often reduced compared to CCGTs typically <50MW as steam turbines are normally not required in steam injected cycles (Rao, 2014). However, the high water usage of these cycles often mean process losses and corrosion issues are problematic, and flowrate instabilities occur between the compressor and turbine because of this steam injection (Chiesa, 2012; Heppenstall, 1998; Poullikkas, 2005; Rao, 2014). To overcome this, much greater compressor pressure ratios are needed which restricts the quantity of steam which can be

added to the system. In addition, the turbine performance may be hindered due to a modified working fluid and its different thermodynamic properties (Chiesa, 2012; Rao, 2014). The maximum rate of steam injection in these systems is ~19% of the air mass flowrate (to the compressor inlet), where efficiencies are higher than those of simple cycles ~38-48% (Carapellucci and Milazzo, 2007; Chiesa, 2012; Ghazikhani et al., 2011). The development of these systems has also demonstrated that in steam injected combined cycles the efficiencies can exceed 60% (Carapellucci and Milazzo, 2007; Ghazikhani et al., 2011). Commercially available steam injection cycles currently use turbines developed for conventional air firing which limits the maximum steam injection rate and reduces the efficiency to 37-41% (Rao, 2014). However, by introducing intercooled compression, the efficiency can be increased to ~50% (Chiesa, 2012; Rao, 2014). Coupling steam injection cycles with CCS is therefore not beneficial because of these lower efficiencies and the technical and economic limitations of combined cycle steam injection systems in comparison to CCGTs (Chiesa, 2012; Rao, 2014).

2.3 Supplementary firing

Supplementary firing, see Figure 2.3 (p. 18), involves the combustion of extra fuel in a secondary combustor located prior to/inside the HRSG (duct burner) to increase the power output from the CCGT. In this process the flue gas temperature is increased by burning additional fuel with the excess oxygen remaining in the flue gas (Biliyok et al., 2015; Biliyok and Yeung, 2013; Carapellucci et al., 2015; González Díaz et al., 2016; Li et al., 2011a, 2012). Because of this secondary combustor, the CO_2 concentration in the flue gas stream can be increased, which aids the driving force in the absorber and reduces the stripper heat demand (Li et al., 2011a, 2012). Furthermore, the lower O_2 content (11-12 vol%) curtails the rate of solvent degradation (Gouedard et al., 2014; Herraiz, 2016). In the work by Li et al. (2012) they identified that the use of supplementary firing results in decreased NOx emissions, which would be beneficial to meet emission regulations.

Studies promoting biomass combustion, instead of fossil fuel combustion, in supplementary firing configurations would also be beneficial to mitigate CO_2 emissions. This is because of the lower carbon intensity of biomass compared to fossil fuels which might lead to zero or potentially net negative emissions if coupled with CCS (Bhattacharya and Datta, 2013; Datta et al., 2008; Gnanapragasam et al., 2009).

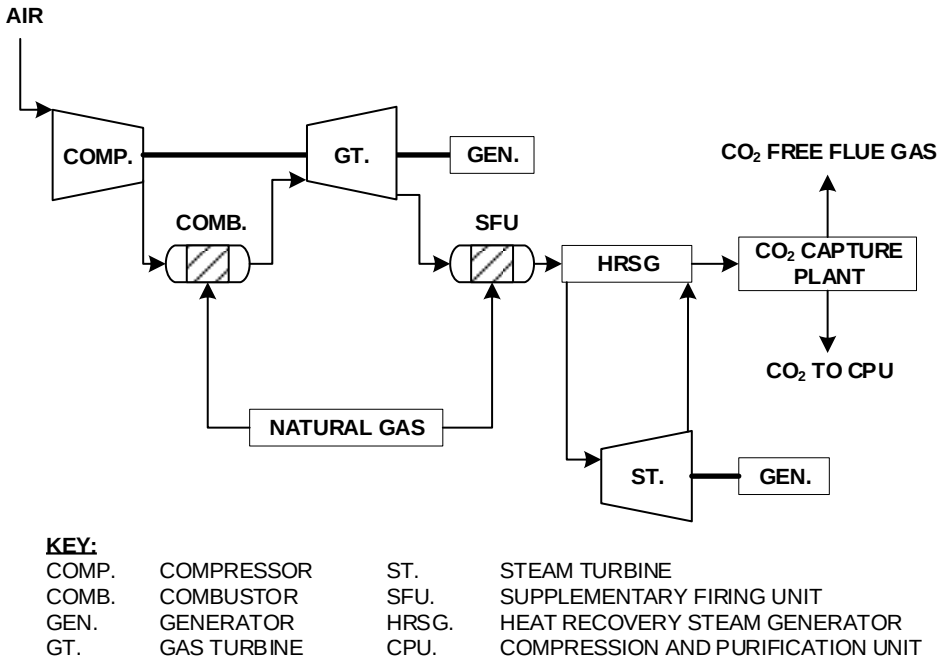

Figure 2.3. Schematic of the supplementary firing process.

The overall system efficiencies in supplementary firing cycles with ACP's is ~43-48% compared to ~50% efficiencies in CCGT power stations coupled with ACP's (DOE/NETL, 2013b; González Díaz et al., 2016; Li et al., 2011b, 2012). The application of supercritical HRSG has also been considered to overcome these reduced efficiencies (González Díaz et al., 2016; Li et al., 2012). However, supercritical HRSG's will lead to increased costs and limit operational flexibility with advancement also required to withstand higher flue gas temperatures >630°C (Li et al., 2012; Zhang et al., 2012). This means that the materials used, e.g. alloys, need to be developed to accommodate such high temperature (Zhang et al., 2012). Despite this, supplementary firing systems are designed to operate with smaller flue gas flowrates compared to CCGT configurations (if supplementary firing is working continuously), which would be beneficial to decrease the economic costs associated with the downstream CO_2 capture plant (González Díaz et al., 2016). The initial concept of supplementary firing configurations was suggested to provide extra power at peak electricity demand (Arrieta and Lora, 2005; Diego et al., 2017a). In addition, they can provide additional power when CCGT's operate at higher ambient temperatures (Arrieta and Lora, 2005; Diego et al., 2017a). A number of technical issues arise when considering supplementary firing for CCGT's with post-combustion CO_2 capture. These include the HRSG material constraints which limit the flue gas temperature to a maximum of ~800°C (Biliyok et al., 2015; González Díaz et al., 2016). If insulated casings or water-cooled furnaces are implemented,

the maximum temperature is limited to ~900-1300 (Ganapathy, 1996). This temperature limitation restricts the quantity of CO_2 which can be augmented in the exhaust gases. Researchers have identified that the CO_2 concentration can be increased up to 8.4 vol% with a ~1330°C combustion temperature (Li et al., 2011a, 2012). In addition, it has been found that at firing temperatures of ~1970°C the CO_2 concentration increases to ~11 vol% at the stoichiometric oxygen limit (Li et al., 2011a, 2012). To overcome the issues associated with the combustion temperature and to maintain high CO_2 concentrations in the flue gases, sequential supplementary firing has been proposed in CCGT's coupled with ACP's. This process involves fuel combustion across a number of stages within the HRSG, thus allowing for increased supplementary fuel combustion with reasonable flue gas temperature increases to ~800-900°C (González Díaz et al., 2016). This removes the need for any HRSG modifications, and because of the lower temperature difference compared to conventional supplementary firing, the system efficiency is enhanced (González Díaz et al., 2016). In this advanced configuration, CO_2 concentrations increase to ~11 vol% where the HRSG temperature is ~820°C with up to ~60% of the fuel combusted (González Díaz et al., 2016). Although this is at the expense of reduced O_2 concentrations of ~1 vol% in the final combustion stage of the process, where elevated combustion temperatures can overcome this issue (González Díaz et al., 2016; Li et al., 2011a). The effects mentioned above require further investigation before this advanced process is considered for application to commercial systems. Li et al. (2012) have also considered different supplementary firing options focusing on optimising system performance and efficiency in CCGT power stations. These include integrated supplementary firing systems with exhaust gas reheating, exhaust gas recirculation or an amalgamation of both with supercritical HRSG (Li et al., 2012). Other researchers have also considered advanced configurations with CCGT's coupled with CO_2 capture plants (e.g. Biliyok et al., 2015; Biliyok and Yeung, 2013b; Carapellucci et al., 2015). To apply these processes to CCGT's will require further analysis due to the complexity and economic costs, thus, research investigating the techno-economic performance would assist in identifying the benefits compared to other options considered in this chapter.

2.4 Exhaust gas recirculation

Exhaust gas recirculation (EGR) was initially used as a method to decrease NOx concentrations, where thermal NOx formation was lower due to the reduced firing temperatures (lower fuel to air ratio) under EGR (Pavri and Moore, 2001). In

addition, to decrease NO, CO and or other minor species concentrations via the reburning mechanism in the combustor (Ditaranto et al. 2011).

The principle of EGR, see Figure 2.4 (p. 21), is to recycle a certain amount of the CCGT flue gases to the compressor inlet which is combined with the oxidant stream, following the cooling and condensing stages (Bolland and Sæther, 1992). This EGR stream which enters the compressor inlet displaces a proportion of the combustion air that flows through the gas turbine cycle. This reduces the volumetric flowrate and increases the CO_2 concentration of the flue gas stream sent to the downstream CO_2 capture plant. The implementation of EGR to gas-fired systems will be beneficial to the economic and energy costs of the ACP, notably, lower specific reboiler duty and smaller equipment sizes (Akram et al., 2016; Ali et al., 2017; Bolland and Sæther, 1992; ElKady et al., 2009; González-Salazar, 2015; Li et al., 2011b). The increased CO_2 concentration can be determined by the EGR recirculation ratio. This is defined as the ratio (before cooling and condensing) between the recirculated flowrate and total flue gas flowrate. The application of EGR at commercial scale for gas-CCS is currently restricted by a number of technical challenges. The oxygen availability for combustion will reduce at higher EGR recirculation ratios. However, if the oxygen content is too low, then issues such as flame instability and incomplete combustion will occur resulting in the increase of gaseous emissions such as CO and UHC (Evulet et al., 2009). In gas-fired systems the working fluid in the combustor is subject to high flame velocities and lower residence times which will be affected under EGR operation (Li et al., 2011a). A number of studies have investigated the influence of EGR and its effects on O_2 concentration. Ditaranto et al. (2009) found that the O_2 levels of ~14 vol% in the oxidizer allow for stable combustion under EGR, with elevated CO and UHC emission levels being reported. An experimental investigation of EGR using GE's dry low NOx (DLN) system identified stable combustion with combustor outlet O_2 concentrations of ~4 vol% (ElKady et al., 2009). These authors also demonstrate that high CO and UHC levels are associated with O_2 starvation and propose operating at a higher pressure to decrease these emissions (ElKady et al., 2009). The higher CO emission levels are due to inadequate O_2 availability for the oxidation reaction to form CO_2 (ElKady et al., 2009; Evulet et al., 2009; Li et al., 2011b). Furthermore, because CO_2 has a larger specific heat capacity, the working fluid properties change leading to lower flame temperatures and speeds (ElKady et al., 2009; Evulet et al., 2009; Li et al., 2011b).

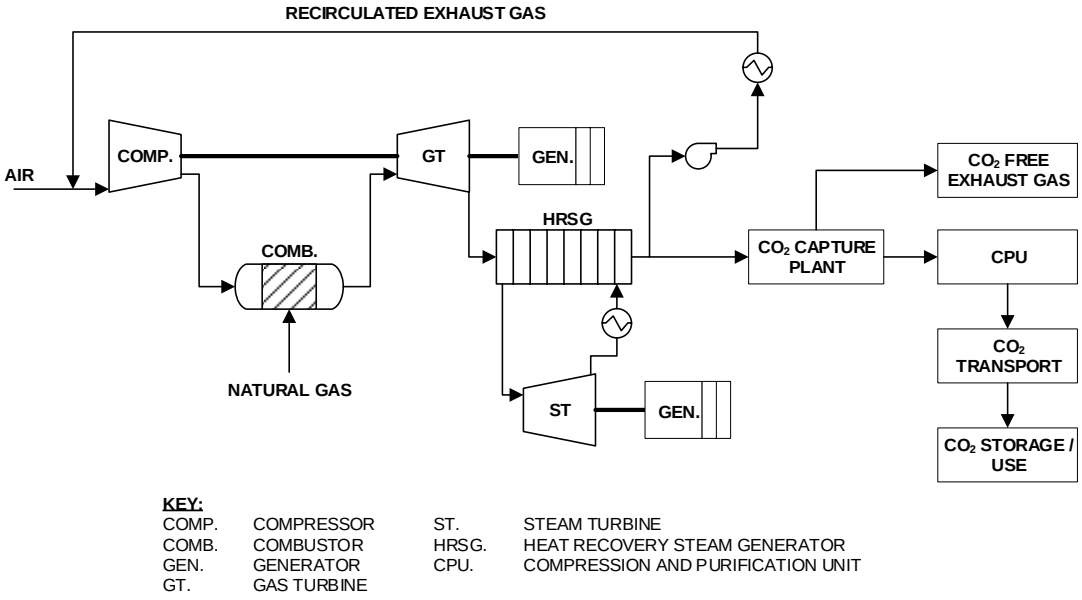

Figure 2.4. Schematic of the exhaust gas recirculation process.

In lean premixed combustors used in gas turbines, the flame velocity is dependent on the O_2 concentration in the combustion air, where for example in EGR systems the O_2 content reduces because of the changes in the working fluid properties (Pourkashanian et al., 1989). Røkke and Hustad (2005) investigated the impacts of EGR on the combustion performance of a 65 kW burner demonstrating lean flame blowout occurs below 14 vol% O_2. However, the majority of studies agree that the minimum oxygen concentration (MOC) in the oxidizer required to ensure flame stability and good combustion performance under EGR is ~16 vol% (Akram et al., 2016; Bolland and Mathieu, 1998; ElKady et al., 2009; Li et al., 2011a). This means that the EGR ratio is limited to ~40% with current combustors which results in a ~6.5 vol% flue gas CO_2 concentration (Li et al., 2011a). In order to achieve higher EGR ratios and accommodate lower O_2 concentrations, combustor optimisation is required (ElKady et al., 2009; Li et al., 2011a, 2011b). To optimise current combustors, modifications such as: operating at higher pressures, changing flame premixedness and improvement of pilots, would be required to operate beyond the 40% EGR ratio, adhering to emission regulations and to maintain lean blowout limits (ElKady et al., 2009). As mentioned previously in this section, the application of EGR promotes efficiency improvements of the downstream CO_2 capture plant. This is because of the increased concentration of CO_2 in the flue gas which decreases the energy penalties in contrast to CO_2 capture plants without EGR. In the work conducted by the National Energy Technology Laboratory, the implementation of EGR has led to reported net efficiencies of ~51% (DOE/NETL, 2013b; Li et al., 2011b). This equates to a net efficiency penalty of ~7% and ~0.5% in comparison to

a CCGT power station without and with a CO_2 capture plant, respectively (DOE/NETL, 2013b; Li et al., 2011b). In addition, it was reported that the application of EGR, coupled with an ACP to CCGT power plants would provide the lowest financial and energy cost for gas-CCS systems (DOE/NETL, 2013b). This is in comparison to CCGT power plants coupled with only ACP. Ali et al. (2017) showed that the specific reboiler duty under EGR reduces by ~21% with a 55% EGR ratio, and a negligible impact on the mGT performance. It is important to note that the EGR ratio investigated by Ali et al. (2017) is specific for a mGT, hence this might be substantially different in a commercial gas turbine. In pilot scale experimental work, Best et al. (2016) demonstrated minimal impacts on the turbomachinery with increased CO_2 concentrations of ~6.3 vol%. Mansouri Majoumerd et al. (2014) indicate at a 40% EGR, the CO_2 content increases to ~3.4 vol% within minor impacts to the turbomachinery. These works, including other studies (e.g. Akram et al., 2016; Bolland and Sæther, 1992; ElKady et al., 2009; Li et al., 2011a) and patent applications (e.g. Finkenrath et al., 2011) highlight the advancement of EGR in terms of its application for CCS systems. However, the commercial application of EGR to gas-CCS remains a challenge. The development of EGR via demonstration plant studies and optimised combustor designs, can assist in addressing the issues with this process leading to the advancement of gas-CCS.

2.5 Selective exhaust gas recirculation

In the recent work by Merkel et al. (2013), S-EGR has been recommended as a different option to augment the flue gas CO_2 concentration beyond those levels achieved in EGR whilst operating above the MOC for stable combustion. In this process, CO_2 is removed from the flue gas stream via a selective membrane separator which favours CO_2 permeation over N_2 and O_2 into an air sweep stream which returns to the compressor inlet of the gas turbine. As other gaseous species (e.g H_2O and N_2) are not recirculated as with the EGR process, the O_2 in air is less diluted, with the MOC remaining above 16 vol% O_2 (Merkel et al., 2013). This also means that the CO_2 concentration in the oxidant stream is higher due to the negligible concentrations of N_2 and H_2O. Merkel et al. (2013) state that the CO_2 separation from the flue gas into the air sweep stream can be carried out at close to atmospheric pressure due to a greater partial pressure difference. As a result, compressors or vacuums are not required, as per conventional membrane systems, hence, only blowers to feed the sweep air+CO_2 stream back to the compressor inlet are needed which is beneficial for decreasing energy consumption and costs. Merkel et al. (2013) proposed two separate S-EGR configurations, parallel and

series, as illustrated in Figures 2.5 (a) and (b) respectively. The parallel S-EGR configuration splits the flue gas stream into two separate flows after the HRSG. One stream is sent to the ACP and the subsequent stream is sent to the selective membrane. This leads to a reduction in the flue gas flowrate sent to the downstream CO_2 capture plant which contains increased CO_2 concentrations, and therefore means that the equipment size and processed costs can be reduced (Diego et al., 2017a). However, to maintain an overall CO_2 capture efficiency ~90%, a high CO_2 separation rate is required in both the selective membrane and post-combustion CO_2 capture plant, typically ≥95% (Diego et al., 2017b; Herraiz et al., 2018; Merkel et al., 2013).

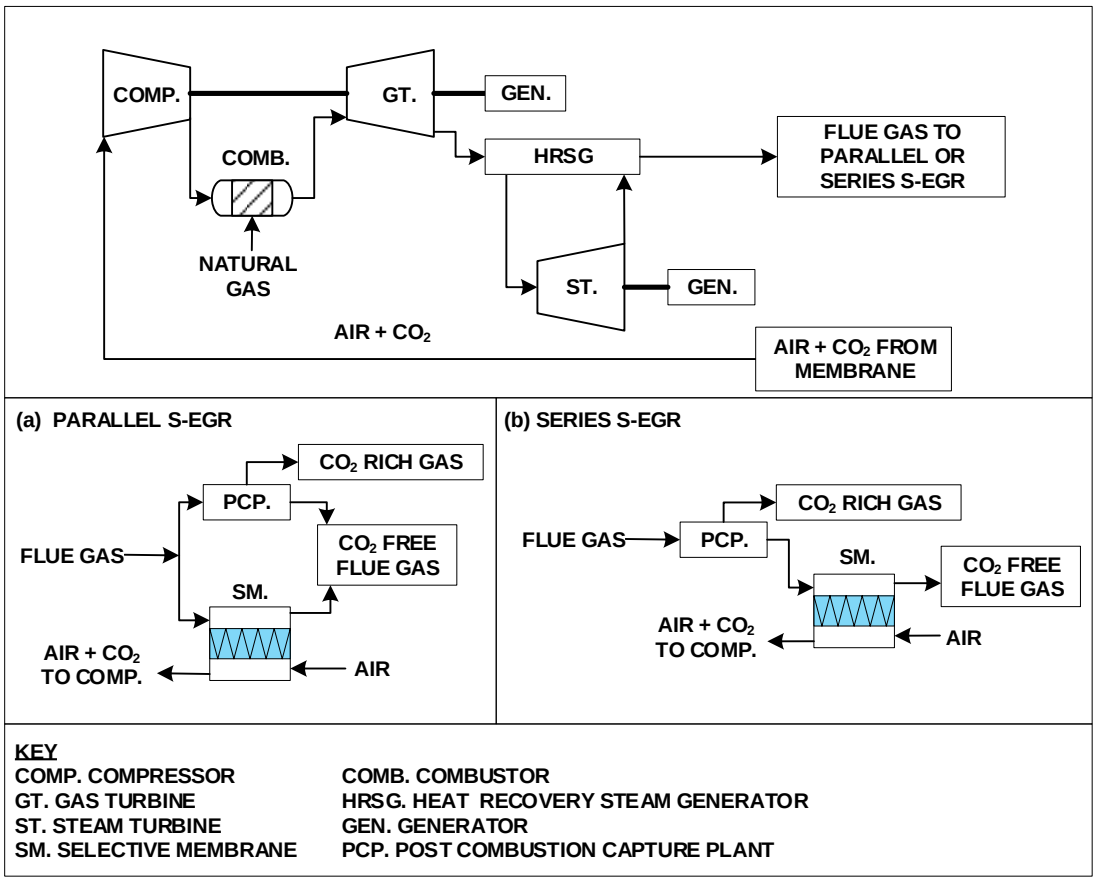

Figure 2.5. Schematic of the (a) parallel and (b) series selective exhaust gas recirculation process.

In the Series S-EGR configuration, the flue gas stream is initially treated in the CO_2 capture plant and thereafter processed in the selective membrane. In this scheme, only a proportion of the CO_2 is separated in the capture plant. The remaining CO_2 is separated via the selective membrane into the air sweep stream back to the compressor inlet. Merkel et al. (2013) highlights that this is advantageous as the selective membrane acts a pre-purification system for the CO_2 which permeates

through into the air sweep stream. Furthermore, the CO_2 capture rate in the ACP can be lower because the selective membranes separate any remaining CO_2, thus, providing greater operational flexibility (Merkel et al., 2013). For example, Herraiz et al. (2018) found that the CO_2 capture rate to be 30-58% in the S-EGR configurations investigated in their work. To quantify the S-EGR ratio, the flue gas flowrate sent to the selective membrane is divided by the total flue gas flowrate exiting the gas turbine prior to cooling and condensation. Merkel et al. (2013) use a Polaris membrane for both the parallel and series S-EGR configuration. In the parallel scheme, a 77% S-EGR ratio is used to maintain an overall 90% CO_2 capture efficiency (Merkel et al., 2013). This equates to a ~98% and ~97% CO_2 capture and separation efficiency in the ACP and selective membrane, respectively. In contrast, for the series S-EGR configuration these values are 30% and 96% for the ACP and selective membrane, resulting in an overall 91% CO_2 capture efficiency (Merkel et al., 2013).

These authors indicate that S-EGR has the potential to decrease the theoretical energy needed to liberate CO_2 from the flue gas by up to ~40%, thus achieving CO_2 concentrations of ~14 vol% (series) and ~19 vol% (parallel) in the flue gas whilst ensuring the 16 vol% MOC at the inlet of the gas turbine combustor for stable combustion (Akram et al., 2016; Bolland and Mathieu, 1998; ElKady et al., 2009; Li et al., 2011a; Merkel et al., 2013). Herraiz et al. (2018) recently investigated both S-EGR configurations in CCGT systems with an ACP using 30 wt% MEA. In both configurations, the overall CO_2 capture efficiency is 90%. In the parallel configuration, a 70% S-EGR ratio is used, with a 97% and 96% membrane separation and ACP CO_2 capture efficiency (Herraiz et al., 2018). The results show a 46% and 5% decrease in packing volume and specific reboiler duty, respectively, compared to CCGT power stations coupled with ACP systems (Herraiz et al., 2018). However, in the series configuration, the packing volume and specific reboiler duty decreased by 64% and 7%, respectively (Herraiz et al., 2018). This is using a 95% and 32% ACP CO_2 capture and membrane separation efficiency. Herraiz et al. (2018) also demonstrate the advantages of S-EGR compared to EGR in terms of packing volume and specific reboiler duty. These authors show that the packing volume decreases by 40 and 10%, and the specific reboiler duty reduces by 4 and 2% for the series and parallel configurations, respectively, with respect to the corresponding EGR configuration (Herraiz et al., 2018). Herraiz (2016) has also proposed the use of a rotary wheel using physical absorption for CO_2 selective separation instead of the selective membrane proposed by Merkel et al. (2013),

using 30 wt% MEA in the ACP. Two different solid sorbents were investigated for use in the rotary wheel including Zeolite X13 and Activated Carbon. Herraiz (2016) investigated one parallel configuration using a 70% S-EGR ratio, with a 97% (rotary wheel) and 96% (ACP) separation and CO_2 capture efficiency, respectively. Two series configurations were also investigated with 95% (rotary wheel) and 31% (ACP), and 90% (rotary wheel) and 48% (ACP) separation and CO_2 capture efficiencies, respectively. In these configurations, CO_2 concentrations in the flue gas reached ~15 vol% (parallel 97/96%), ~10 vol% (series 95/31%) and ~5 vol% (series 90/48%), respectively. Diego et al. (2017b) investigated the techno-economic performance of CCGT systems with parallel S-EGR using 30 wt% MEA in the ACP. The CO_2 capture and separation efficiencies for the ACP and selective membrane were 95% to maintain an overall 90% capture efficiency. The results show a maximum 58% S-EGR ratio, with an 8 vol% flue gas CO_2 concentration and ~20 vol% O_2 concentration at the combustor inlet (Diego et al., 2017b). Further, the economic performance of parallel S-EGR compared to CCGT power plants coupled with ACP or EGR is dependent on auxiliary consumption and selective membrane costs (Diego et al., 2017b). These same authors recently investigated the techno-economic performance of a novel hybrid S-EGR configuration (Diego et al., 2018), combining the benefits of both parallel and series S-EGR configurations. In this novel scheme, see Figure 2.6 (p. 26), a proportion of the flue gas is treated in the ACP and the remaining flue gases are sent to the first stage selective membrane, operating with a CO_2 lean air flow (Diego et al., 2018). This results in a CO_2 rich air stream that is sent to the compressor inlet, whereas, the remaining flue gas stream contains a reduced CO_2 concentration. The flue gas stream which leaves the first stage membrane is subsequently mixed with the flue gas stream exiting the absorber that still contains CO_2 (Diego et al., 2018). To avert CO_2 dilution, the flue gas streams contain equal CO_2 concentrations mixing prior to entering the second stage selective membrane. This secondary stream is then sent to the second stage membrane where any remaining CO_2 is separated into the air sweep stream, flowing through the first stage membrane back to the compressor inlet. Diego et al. (2018) show that this novel configuration augments the CO_2 content to 18 vol% which results in a 6% and 77% reduction in specific reboiler duty and flue gas flowrate sent to the ACP. This novel scheme has the advantage that the absorber CO_2 capture efficiency is lower than the parallel S-EGR configuration because the secondary membrane removes any remaining CO_2 from the flue gas stream exiting the ACP (Diego et al., 2018).

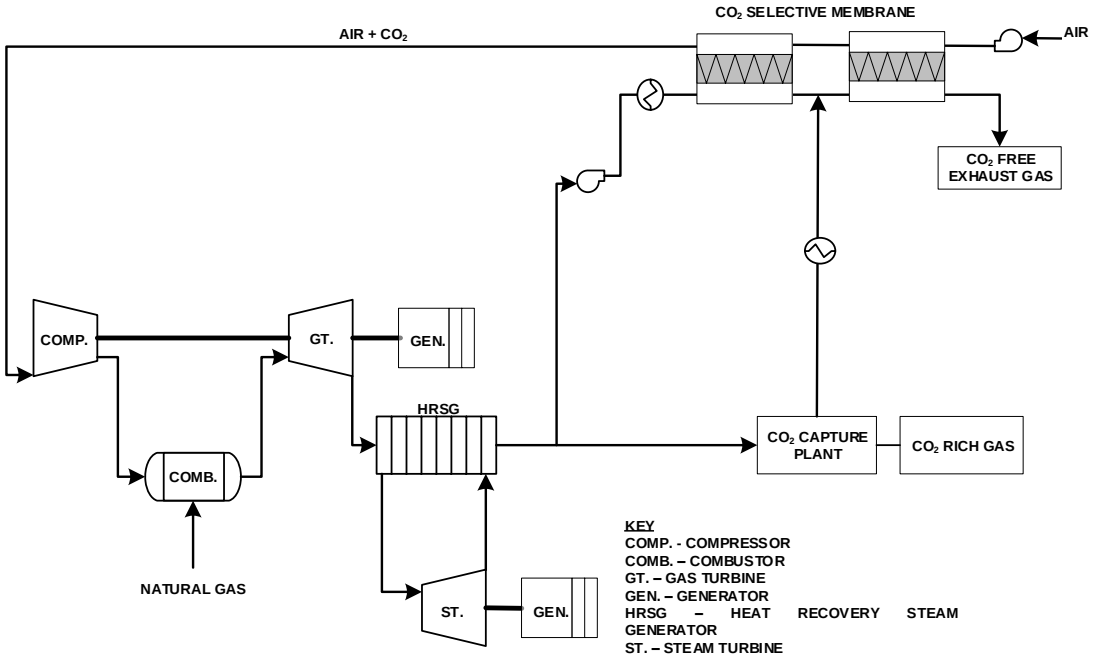

Figure 2.6. Schematic of the hybrid selective exhaust gas recirculation process.

In addition, the membrane area will be smaller compared to that of the series S-EGR configuration operating at similar conditions, which would reduce the membrane system footprint, thus, lowering costs (Diego et al., 2018). As the first membrane removes only a proportion of the flue gas with higher CO_2 content compared to the second membrane, the area needed for the membrane system reduces (Diego et al., 2018). These authors also identify that the membrane system significantly affects capital costs, and decreasing the membrane costs is essential to make S-EGR commercially attractive. Turi et al. (2017) and Merkel et al. (2013) have also investigated series S-EGR considering only CO_2 selective membranes. These studies show that the CO_2 concentrations can be increased to ~28 and ~22 vol% at compressor inlet O_2 concentrations of ~14 and ~16 vol%, respectively (Merkel et al., 2013; Turi et al., 2017). In addition, the economic evaluations show that there are cases where membrane only CO_2 separation can be competitive in comparison to a CCGT power station coupled with an ACP (Merkel et al., 2013; Turi et al., 2017). Baker et al. (2017) investigated combined S-EGR and EGR configurations to assist in addressing the challenge of large membrane areas in conventional S-EGR schemes (parallel or series). These authors highlighted that an optimised integrated scheme which uses a 20% EGR ratio, flue gas pressure of 2 bar and permeate pressure of 0.2 bar leads to a reduction of 93% in membrane area when compared to an S-EGR configuration without combined EGR (Baker et al., 2017). Despite the marginal increase in net power consumption from 335 to 347 kW_e per tonne of CO_2 (4% increase) with operating costs equating to ~$44 per

tonne of CO_2, this integrated design demonstrates the large saving which can be realised with S-EGR (Baker et al., 2017). However, this may require gas turbine modifications to accommodate these integrated systems for CO_2 mitigation. Despite these process simulation and economic studies, limited work has investigated S-EGR experimentally. Russo et al. (2018) investigated the permeability performance of a polydimethylsiloxane (PDMS) membrane system at bench scale for its use in S-EGR. Their work considered CO_2 concentrations up to 20 vol% in the retentate stream, and indicated good permeability across the membrane, although this is affected by the feed pressure used (Russo et al., 2018). Darabkhani et al. (2018) investigated the performance of a pilot scale 100 kW combustor using the PDMS membrane system in Russo et al. (2018) work. In their experimental work, CO_2 concentrations of ~7 vol% were achieved in initial combustion tests under S-EGR, with a ~11% membrane separation efficiency (Darabkhani et al., 2018). However, process simulation models indicate subsequent experimental tests can lead to increased flue gas CO_2 concentrations of up to ~10 vol% with a ~13% membrane separation efficiency. The influence of S-EGR on gas turbine combustion performance has only been investigated in a few studies. Marsh et al. (2017, 2016) investigated the impact of S-EGR on the combustor performance of a swirl burner at up to 2.2 bara. The results identify that the flame temperature and combustion kinetics are reduced with increased CO_2 concentrations in the oxidant stream (Marsh et al., 2017, 2016). As illustrated in the discussion, the development of S-EGR for gas-CCS is ongoing. However, limited studies have experimentally investigated the effects of S-EGR on gas turbine performance in terms of turbomachinery and emissions. In addition, the effects of S-EGR on the downstream CO_2 capture plant is also required. To address these gaps in the knowledge it is recommended pilot-scale studies investigating S-EGR are conducted with subsequent understanding of overall economic costs.

2.6 Post-combustion CO_2 capture processes

There are a number of studies which have evaluated the application of post-combustion CO_2 processes coupled with coal-fired power stations, though these are less prominent for gas-fired systems. As noted in section 1.2.2, the use natural gas for electricity generation is anticipated to increase by 2040. This has led to a more recent focus of applying CCS to gas fired systems. CO_2 capture using MEA has been the interest for many studies with attention also focusing on additional processes for gas-CCS (González-Salazar, 2015; IEAGHG, 2012a). These include the chilled ammonia process, calcium looping, molten carbonate fuel cells and

cryogenic separation (Chiesa et al., 2011; Hu and Ahn, 2017; IEAGHG, 2009a; Sreenivasulu et al., 2015). CO_2 capture using amines is the most developed of all the above-mentioned processes, with this technology currently operating commercially (NRG Energy, 2017; Stéphenne, 2014). As amine scrubbing is the most widely applied, the following section evaluates the key issues which need to be addressed to apply this technology to commercial scale gas-CCS.

2.6.1 Amine capture plant processes

As mentioned above, post-combustion CO_2 capture using amines (typically MEA 30 wt%) is the most advanced process for removing CO_2 from fossil fuel combustion flue gases. This process, see Figure 2.7, cools the flue gases via a direct contact cooler to ~40°C, where they enter the bottom of the absorption column and the aqueous–MEA solvent enters into the top of the absorption column (IPPC, 2005). The absorption column comprises of structured or random packing, whereby, the lean solvent stream flows downwards over the packing material and mixes counter–currently with the flue gases. The packing material enhances mass transfer as there is a high surface area which maximises contact between the liquid and the gas.

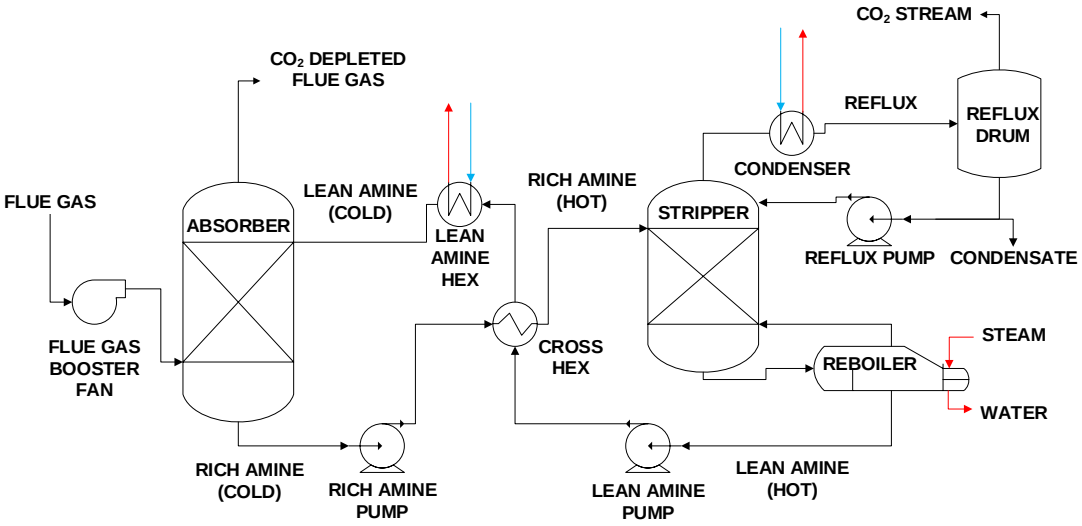

Figure 2.7. Schematic of the amine CO_2 capture process.

Once the aqueous–MEA solvent reaches the bottom of the absorption column, the stream is termed “rich” as it has absorbed CO_2 from the gas phase. The treated flue gases (with a low CO_2 concentration) exit the top of the absorption column and enters a wash column where entrained solvent droplets are removed. This is to ensure that the MEA is not discharged into the atmosphere because of the detrimental impact these emissions have on the environment. The CO_2–rich solvent stream is pumped to the lean/rich heat exchanger and is heated before being sent

to the top of the stripper tower. The rich solvent flows downwards, contacting with the CO_2/steam stream flowing vertically upwards from the reboiler. The reboiler heats the MEA–solvent to approximately 115°C to 120°C, thus, producing a vapour stream acting as a CO_2 stripper (Akram et al., 2015). The vapour stream leaves the top of the stripper column, comprising predominantly of CO_2, steam and small amounts of MEA–solvent. The entrained steam and MEA–solvent droplets are removed by a condenser and refluxed to the stripper column. The residual highly-concentrated CO_2 stream is further purified if necessary, compressed and transported for storage. The hot lean MEA–solvent exits the stripper column where it is pumped via the lean/rich heat exchanger for heat recovery and subject to additional cooling to ~40°C prior to entering the absorber column.

The overall performance of CO_2 capture plants which use MEA solvent is well known, however, the key limitation of this process for gas fired systems is the specific reboiler duty, which requires ~4 MJ/kg CO_2 captured (Li et al., 2011a). This results in a reduction in the CCGT power plant efficiency by ~11 percentage points (DOE/NETL, 2015). The reason why such a reduction occurs is due to the much greater flue gas flowrates that comprise of low CO_2 concentrations ~4 vol%. Furthermore, because of the higher flue gas O_2 concentrations in CCGT power plants, this can affect the energy penalty due to issues associated with oxidative solvent degradation. Thermal degradation is more prominent at temperatures above 120°C or at elevated stripper pressures, when using MEA. However, depending on the process conditions, operating at higher temperature and pressures may be undesirable under S-EGR conditions.

This oxidative and thermal degradation have the potential to lead to greater economic and energy costs when coupling CCS to gas-fired systems (DOE/NETL, 2015). To overcome these issues, research is focused on optimising the post-combustion CO_2 capture plant performance. There are a number of pilot and demonstration plants and two full-scale plants globally which have investigated CO_2 capture mainly from coal fired systems. Boundary Dam, which is located in Saskatchewan, Canada, has the capacity to capture 1 Mt CO_2/year from a 139 MW thermal coal fired power plant using the Shell Cansolv Process with a 90% capture efficiency (Stéphenne, 2014). More recently, Petra Nova in the USA became the largest operational CCS facility to capture 1.4 Mt CO_2/year from a CO_2 capture plant (90% capture efficiency) using an amine KS-1 solvent produced by Mitsubishi Heavy Industries (NRG Energy, 2017). The CO_2 flue gas treated in Petra Nova is from a 240 MW thermal coal-fired power station (NRG Energy, 2017). The majority

of CO_2 capture plants treats flue gases from coal fired power plants, although a small number of facilities that exist which treat flue gases from gas fired systems. In Norway, the CO_2 Technology Centre Mongstad has the capability to capture 20 kt CO_2 / year from the flue gas generated in a combined heat and power combustion facility (Brigman et al., 2014; de Cazenove et al., 2016) burning natural gas. Furthermore, Sulzer in Switzerland has developed a pilot scale plant which treats a flue gas up to ~4 vol% CO_2 (150 kg/h flue gas flowrate) from a gas fired burner (Notz et al., 2012; Tait et al., 2016). The SINTEF facility, situated in Norway, captures CO_2 (flue gas CO_2 concentration up to ~9 vol%) from a 380 kW propane combustor with a flue gas flowrate of up to 50 kg/h (SINTEF, 2018). In the UK, the PACT Research Centre incorporates an amine capture plant which has the capacity to capture up to 1 tonne of CO_2 per day from flue gases produced from either natural gas, coal or biomass combustion (PACT, 2018). The Turbec T100 mGT at PACT produces flue gas CO_2 concentrations of ~1.7 vol% at full load conditions when combusting natural gas. However, work by Best et al. (2016) has simulated EGR increasing the CO_2 concentration to ~6.3 vol% by injecting CO_2 into the micro gas turbine. In addition, an onsite synthetic gas mixing skid allows a range of CO_2 concentrations to be investigated by injection directly into the CO_2 slip stream (Akram et al., 2016). Despite the advancement of post combustion CO_2 capture plants, there are still requirements to optimise the process for gas-CCS. Notably, these include optimising plant performance under flexible operation, decreasing energy and financial costs, the advancement of novel solvents and making process improvements.

2.6.2 Process optimisation

There are currently a range of options being considered to enhance the post-combustion CO_2 capture plant performance including absorber optimisation (e.g. rotating packing beds), heat integration and incorporating heat pumps into the process (Gao et al., 2016; Le Moullec et al., 2014; Yu et al., 2016). The use of rotating packed bed columns are suggested as a different option for CO_2 scrubbing compared to that of traditional absorber columns (Gao et al., 2016; Joel et al., 2014). In rotating packed beds, the centrifugal forces rotate the fluids inside at high velocities where the solvent and flue gas flow inwardly and outwardly, respectively, either in single or combined configurations (parallel or series) (Gao et al., 2016; Joel et al., 2014). In a recent study which investigated the performance of two rotating packed beds in series, the regeneration energy decreased by ~10% due to the augmented rich solvent loading, where the CO_2 flue gas concentration was ~10

vol% (Yu et al., 2016). Furthermore, absorber intercooling is proposed as an option to reduce the energy requirements of this process by decreasing the liquid solvent temperature to aid the higher driving force needed for absorption and increasing the rich solvent loading (Amrollahi et al., 2011). To achieve this, single or multiple solvent cooling stages are applied to the absorber column where a fraction of the solvent is cooled and returned to the absorber. The results of Knudsen et al. (2011) indicate that the absorber intercooling in the bottom section of the absorber has a negligible impact for optimised post combustion CO_2 capture systems using MEA. Interestingly, when using alternative solvents to MEA, the reboiler duty decreased from 3.10 MJ/kg CO_2 at an intercooling temperature of 60°C to 2.90 MJ/kg CO_2 at an intercooling temperature of 25°C. At the same intercooling temperature, the reboiler duty remained about 3.55 MJ/kg CO_2 when using MEA as the solvent. Knudsen et al. (2011) note that the reboiler duty when using MEA solvent is independent to the applied intercooling temperature. The results of Li et al. (2016) illustrate very similar conclusions when using MEA, the reboiler duty decreased from 3.60 MJ/kg CO_2 to 3.55 MJ/kg CO_2 when using intercooling. Despite the negligible influence on reboiler duty, the absorber intercooling process resulted in the absorber column height decreasing by 25% (Li et al., 2016). This is because of the increased driving force at lower temperatures, and thus allowing for a reduced packing height (Le Moullec et al., 2014). Another process optimisation suggested is rich solvent recycling which involves removing a proportion of the solvent at the bottom of the absorber and reintroducing it at the top (Baburao and Schuber, 2011; Gal et al., 2008; Le Moullec et al., 2014). By doing this, the contact time between the CO_2 and solvent is increased, hence, the CO_2 loading is augmented with a small volume of solvent (Le Moullec et al., 2014). To optimise the benefits of this process, multi staged introduction of the rich solvent is proposed to amplify the overall absorption capacity (Le Moullec et al., 2014). However, this is at the determent of larger absorber column heights and diameters (Le Moullec et al., 2014). Another option is to cool the solution and re-introduce it to the absorber top to promote acid gas removal and lower solvent emissions due to the lower temperature (Le Moullec et al., 2014). This process has been developed by Alstom for ammonia and this indicates a 5% reduction in the overall energy penalty and a 7% increase in rich solvent loading (Baburao and Schuber, 2011). Additional approaches for process optimisation include inter-heated absorbers (Aroonwilas and Veawab, 2007), split flow arrangements (Iijima et al., 2011), double loop absorber and stripper configurations (Towler et al., 1997) and flue gas compression and expansion (Kishimoto et al., 2011). In addition to the above mentioned absorption

enhancement options, heat integration between different process streams in the CO_2 capture plant are suggested to further decrease the reboiler duty and limit the heat losses throughout the system (Le Moullec et al., 2014). These options include rich solvent splitting, preheating, and flashing, parallel economizer arrangement, inter heated and heat integrated strippers (Le Moullec et al., 2014). In the rich solvent splitting process, the rich solvent is split into two flows; one is preheated and the other is kept cool where the reboiler duty has been shown to decrease by up to ~12% (Cousins et al., 2011a, 2011b; Le Moullec et al., 2014; Le Moullec and Kanniche, 2011; Oyenekan and Rochelle, 2007). The method of rich solvent preheating increases the rich solvent temperature to beyond that of the economizer via heat transfer between the hot (lean) and cold (rich) solvent, and this leads to an energy penalty saving of up to ~12% in terms of reboiler duty (Ahn et al., 2013; Iijima et al., 2011; Le Moullec et al., 2014). The application of rich solvent flashing flashes the rich solvent that promotes CO_2 liberation and cooling of the remaining rich liquid solvent with small decreases in reboiler duty (~1.5%) (Iijima et al., 2011; Le Moullec et al., 2014; Le Moullec and Kanniche, 2011). The promotion of heat recovery between the incoming and outgoing stripper and reboiler streams is realised by rich or lean solvent splitting that flow through two or more heat exchangers in parallel economizer configurations. This could lead to large reductions in parasitic losses by up to ~18% for MEA systems (Cousins et al., 2011b, 2011a; Gelowitz et al., 2008; Le Moullec et al., 2014). Inter heated stripper arrangements involve reheating using a heat exchanger of a partially lean solvent which is taken from the central stripper section and then re-introduced (Le Moullec et al., 2014). In this process, the reboiler duty is reported to reduce up to ~13% (Iijima et al., 2011; Le Moullec et al., 2014). However, the process simulation work by Oyenekan and Rochelle (2006) demonstrates heat integrated stripper arrangements can reduce stripper work by ~17% (Le Moullec et al., 2014).

2.6.3 Solvent development

The development of alternative solvents is another topic of focus in the literature. This is because MEA typically has high reboiler duties, low absorption capacity and poor thermal stability and corrosion issues (Damartzis et al., 2016; Diego et al., 2017a; Øi and Kvam, 2014). The reboiler duty is these systems which use MEA for gas-CCS is ~3.5-4 MJ/kg CO_2 for highly optimised plants (Øi and Kvam, 2014). At temperatures above 110°C thermal degradation of MEA increases, where, Davis and Rochelle (2009) highlight a 6% weekly degradation rate at reboiler temperature ~135°C. Furthermore, flue gases with increased O_2 content, such as those from

natural gas combustion, also promote oxidative degradation which further enhances operational costs (Supap et al., 2006). Overcoming these issues has led to the development of alternative solvents including cyclic, hindered and ether amines, and non-amine based solvents such as amino acids, phase change solvents and ionic liquids to optimise CO_2 capture plant performance (Dowson et al., 2016; Du et al., 2016; Gurkan et al., 2010; Pinto et al., 2014). The encouraging findings of the application of new solvents in CO_2 capture processes indicates that kinetics, solubility, mass transfer and regeneration energy can be optimised in comparison to MEA (Mandal and Bandyopadhyay, 2006; Samanta and Bandyopadhyay, 2009; Sema et al., 2012). Commercially available solvents such as the Cansolv amine, Praxair MEA-MDEA and Fluor's Econamine have been suggested to provide advantages compared to the utilisation of MEA on its own (IEAGHG, 2009a; Reddy and Gilmartin, 2008). For example the Cansolv amine process which treats flues gas from either natural gas and coal requires ~40% less energy for solvent regeneration and the Praxair MEA-MDEA process has illustrated reboiler duties of ~3 MJ/kg CO_2, whilst Fluor's Econamine FG process has been optimised for flue gases from gas fired combustion systems (IEAGHG, 2009a; Reddy and Gilmartin, 2008). In work by Zhang et al. (2015) they identified dimethylaminoethanol (DMAE) and 2-Amino-2-methyl-1-propanol (AMP) based solvents are potentially more suitable for gas-CCS because the cyclic CO_2 capacity of these solvents is approximately two times greater than that of MEA.

Even though there is significant research in solvent development for post combustion CO_2 capture plants, there are limited solvents specifically designed for gas fired systems. Therefore, new solvents should consider the technical limitations of the flue gases from gas fired systems, notably, due to the concentrations of gaseous emission species such as O_2, CO and NOx (Diego et al., 2017a; Zarogiannis et al., 2016).

2.6.4 Operational flexibility

A key challenge of integrating post-combustion CO_2 capture plants with CCGT power stations is the ability to operate dynamically under flexible CCGT operation. This is to accommodate for the variation in electricity demand, hence load changes, as well as fuel flexibility (IEAGHG, 2012a). Recent studies have focused on flexible operating scenarios of capture plants coupled with CCGTs to help address these challenges (e.g. Burnard, 2017; Ceccarelli et al., 2014; Mechleri and Mac Dowell, 2015; Sharifzadeh and Shah, 2018; Tait et al., 2018). In addition to the contribution of these studies, further understanding of post combustion CO_2 capture plant

dynamic operation is required, especially optimisation. This is to decrease overall economic costs and maintain stable plant operation under these scenarios. A range of options have been proposed to augment the power output from CCGT power plants with ACP during peak demand periods (IEAGHG, 2012b). This includes partial operation (turning down) or shut down of the ACP for a specific time period to produce extra power (IEAGHG, 2012b). Also rich solvent storage has been proposed for subsequent regeneration during off-peak periods (IEAGHG, 2012b). The rich solvent storage process allows for a constant CO_2 supply to the subsequent transport and storage processes, thus, avoiding irregularities in the CO_2 flowrates (IEAGHG, 2012b). During the peak load operating periods, integrated CCGT's with ACP's might also offer enhanced performance, because the ACP can be switched off or only partially operated (IEAGHG, 2012b). This would allow flexible operation during peak demand periods which would offer increased revenues for the power generator, but at the expense of increased CO_2 emissions (IEAGHG, 2012b). To resolve this issue, it has been suggested that the installation of an additional boiler (auxiliary boiler) to provide steam for the desorber would assist in overcoming this problem (Ceccarelli et al., 2014). Furthermore, the implementation of state-of-the-art integrated options, such as flexible steam withdrawal using a low-pressure steam turbine during load following operation, would offer operational flexibility in CCGT+ACP systems. (Sanchez Fernandez et al., 2016). Another issue of coupling ACP's to CCGTs is the quick start up sequence of the gas turbines compared to the steam generating units (e.g. steam turbine and HRSG) (IEAGHG, 2012b). This means that the CO_2 from the flue gas can be absorbed, however, any steam from the other units will not be available quickly during start up (IEAGHG, 2012b). Not capturing the CO_2 and discharging these emissions to the atmosphere would overcome this. The release of these emissions could be minimised by ACP plant modifications (Ceccarelli et al., 2014). As mentioned above, using an additional boiler to provide steam may alleviate the above-mentioned issue of incorporating solvent storage capabilities to the ACP. This implementation would only offer limited advantages at the expense of increasing economic and legislative costs (Dowell and Shah, 2014). The research and development for flexible operation are ongoing, where investigating real-time solvent loading measurements for dynamic operations would be beneficial (Tait et al., 2018, 2016). This includes modelling predictive control, as reported by Mechleri and Mac Dowell (2015).

2.6.5 Economics

An economic analysis and performance of post-combustion CO_2 capture plants is reliant on how these plants are operated, for example, solvent concentration, liquid to gas ratio, flue gas CO_2 content, scale and stripper operating pressure, among other factors (Abu-Zahra et al., 2007). In this context, the widely reported parameters used for economic assessments is the COE and COA. CCGT's coupled with amine based CO_2 capture are estimated to have COE values of ~$70-84/MWh and COA values of $54-64 tonne of CO_2 avoided in 2011 dollars depending on which turbine configuration is used (DOE/NETL, 2013b). Depending on the upstream combustion process and whether novel configurations such as S-EGR are used then the economic performance may improve and therefore this requires further investigation for gas-CCS applications. In terms of S-EGR, limited studies have investigated the full-scale economic performance of CCGT power plants coupled with this technology. Hence, developing an economic model investigating this to advance gas-CCS further is needed.

2.7 Chapter conclusions

This chapter has critically reviewed the literature associated with gas-CCS, specifically focusing on humidified gas turbines, supplementary firing, EGR, S-EGR and the advancement of amine-based CO_2 capture processes. The likely benefits of CCS are widely acknowledged within the literature; however, decreasing the costs associated with this technology is essential. Furthermore, advancing the research and development into the proposed configurations evaluated in this chapter would make these options more developed and attractive for commercial deployment.

In addition, the development of policies, reducing the risk to stakeholders, creating a CCS market based economy and sharing knowledge to make gas-CCS an attractive mitigation strategy is fundamental. In order to implement gas-CCS, increased flue gas CO_2 concentrations are beneficial to make the post-combustion CO_2 capture plant commercially attractive to operate. As evaluated in this chapter, a number of process configurations are proposed, however, the technological readiness levels (TRL) are at various stages for example S-EGR is at TRL6 to TRL7, which means at prototype development to pilot plant development. Therefore, more research is needed prior to scaling-up these options to demonstrate operational functionality and performance at the commercial scale (TRL9).

The flexible operation of CCGT plants will likely be more prominent going forward and therefore, optimising the dynamic performance of the downstream CO_2 capture

plant is critical. The process optimisation, solvent development and flexible operation of the ACP show the advances made on this topic, with this technology currently operating commercially. Knowledge transfer from and between these commercial sites and decreasing the financial constraints will be essential going forward. The various process configurations evaluated in this chapter aims to assist in reducing costs and optimising gas-CCS configurations. Humid air gas turbine configurations are not economically viable and the techno-economic limitations of steam-injected turbines make these options currently unattractive for gas-CCS. The application of supplementary firing for gas-CCS requires additional research in terms of the economics and flexibility. Both EGR and S-EGR provide promising options for integration into gas-CCS systems. There have been a number of works investigating the EGR process, where this has only been analysed experimentally at pilot scale. A number of modelling studies demonstrate the potential of this process for commercial systems, thus, conducting testing at both demonstration and commercial scale, with the potential modification of combustors for the lower oxygen concentration being also needed. S-EGR has only become more prominent recently with limited works investigating this configuration. A selection of modelling studies have shown that S-EGR may have the potential to be competitive with the above-mentioned processes depending on the membrane costs and performance, however, further research is required. Specifically, this includes the experimental investigation of S-EGR on the performance of gas turbines and the post-combustion CO_2 capture plant at pilot scale before being scaled-up to demonstration and commercial scales if promising results are predicted. This would require the understanding of the gas turbine compressor, turbine and combustion performance at part and full load operation. The need to evaluate the CO_2 capture plant performance under S-EGR with detailed focus on the specific reboiler duty, absorber and stripper temperature profiles, solvent loadings and liquid-to-gas ratio, with an economic analysis of S-EGR integrated with a CCGT+PCC plant is required. Therefore, the subsequent chapters in this thesis will address these gaps in the knowledge to contribute towards the development of S-EGR in gas-CCS systems.

3 Theoretical overview of gas turbines, membranes and amine-based CO_2 capture

3.1 Introduction

This chapter presents a technical overview of gas turbines, followed by a review of the key thermodynamic equations related to simple and regenerative cycles. The chapter then outlines the key membrane principles associated with CO_2 separation. This is included as it is important to understand the fundamentals associated with membranes which will assist in further understanding of S-EGR processes. Subsequently, a review of the chemistry associated with alkanolamines (amines) and the reaction kinetics in relation to their chemical reaction with CO_2 are presented. This succinct theoretical chapter aims to inform the reader of the fundamentals associated with gas turbines, membranes and amines, respectively, in relation to CCS. This chapter forms the basis for understanding the subsequent experimental results chapters associated with simulated S-EGR in gas turbines and amine CO_2 capture plants.

3.2 Gas turbines

3.2.1 Technical overview

A number of gas turbines are currently available for use in a wide range of applications, broadly categorised by manufacturers as aero-derivative, heavy-duty, industrial, light–industrial and micro gas turbines (mGT's) (Giampaolo, 2014). Aero-derivative gas turbines evolved from the aviation industry, designed to be compact, light-weight, very efficient and provide high cycle flexibilities (Boyce, 2002). These turbines generally comprise a gas generator, free-power turbine, low pressure compressor and high pressure compressor with a power output of up to 100 MW, used in different industries, e.g. marine, oil and gas sectors (Boyce, 2002). Heavy-duty gas turbines have been in use since the early 1950's, designed specifically for land operation with high power outputs (>100 MW) and good electrical efficiency (>30%), which characteristically include multi–stage axial–flow compressors and are used for large–scale power generation (Giampaolo, 2014). Industrial and light-industrial gas turbines have similar designs (split–shaft) to heavy–duty turbines with power outputs ranging from 0.50 MW to 15 MW and electrical efficiencies up to 38%

(Boyce, 2011). Micro gas turbines operate at high speed (up to 100,000 rpm) and are highly efficient machines (electrical efficiency ~30%) which can generate up to 500 kW using similar design principles to conventional turbines (Giampaolo, 2014). The major components of a micro-gas turbine system include a compressor (centrifugal or axial), combustor and turbine.

CCGT power plants utilise gas turbines as the topping cycle (Brayton Cycle) and steam turbines as the bottoming cycle (Rankine Cycle) to produce electrical power (Boyce, 2010). The waste heat from the gas turbine is used to produce steam in the Rankine Cycle. The isobaric processes occurring in both cycles accept and reject this heat (Boyce, 2010). A HRSG recovers heat from the flue gases of the gas turbine to produce steam which drives a steam turbine to create additional electrical power. Economisers, evaporators and superheaters are the main components of an HRSG, configured to different steam pressure levels, e.g. single, dual or triple pressure boilers (Boyce, 2011). The superheater increases the temperature of the wet saturated steam to generate dry saturated steam, which is used to drive a steam turbine to produce electrical power. The pinch point and approach point are two parameters that affect steam production in an HRSG. The pinch point can be defined as the temperature difference between the saturated steam and gas exiting the evaporator, usually in the range of 8-22°C (Boyce, 2010). The approach point is the difference between the saturation temperature of the steam and feed water inlet temperature to the evaporator, generally considered to be from 5.5-11°C (Boyce, 2011; Ganapathy, 1996). These variables can affect the operational performance and size of an HRSG, for example, lower pinch points allow greater heat recovery, however, this increases the size of equipment required (Ganapathy, 1996). The combination of a gas and steam turbine results in higher electrical efficiencies of 50% to 60% compared to open cycle gas turbine systems (35% to 40%) (Boyce, 2010).

3.2.2 Gas turbine cycles

3.2.2.1 Simple cycle

The principal operating cycle characteristics of a gas turbine is the Brayton Cycle. In its ideal form, the Brayton Cycle includes compression (isentropic), combustion (isobaric), expansion (isentropic) and heat rejection (isobaric) as illustrated in Figure 3.1 (p. 39) (Boyce, 2010). Process 1 to 2 indicates compression, 2 to 3 denotes combustion, 3 to 4 represents the expansion and 4 to 1 signifies heat rejection.

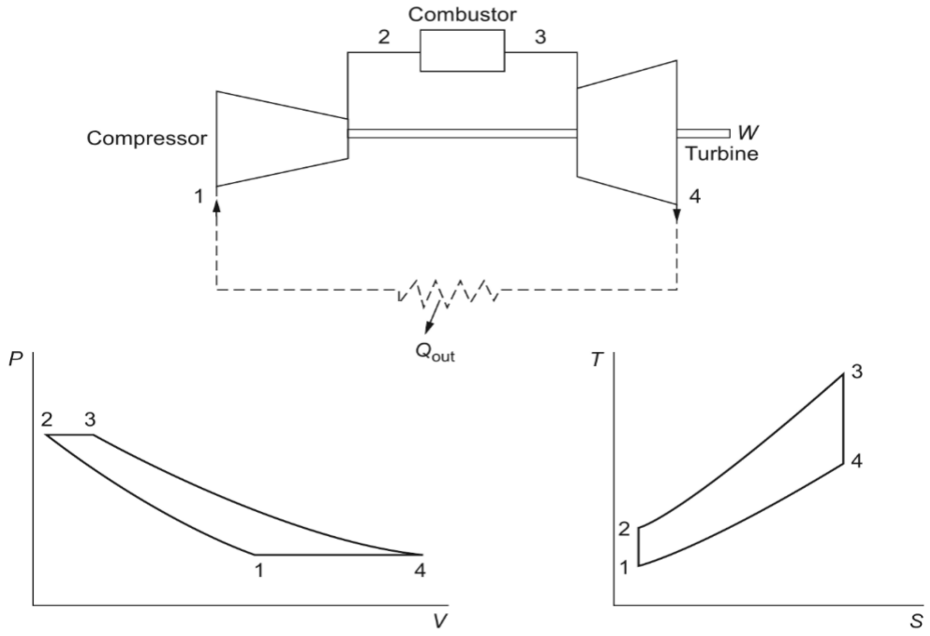

Figure 3.1. Schematic of the air standard Brayton Cycle

(Boyce, 2010).

The first law of thermodynamics mathematically represents the operating principals of a gas turbine and is given by the following equations (the following relationships assume kinetic and potential energy are negligible and steady state exists) (Boyce, 2011). The following equations which are fundamental to understanding the Brayton Cycle are provided to provide a basis of knowledge for how air fired GT systems work. The compressor work is determined from:

$$W_c = \dot{m}_a(h_2 - h_1) \quad \textbf{(3.1)}$$

where $\dot{m}_a$ is the air mass flowrate and h_1 and h_2 is the enthalpy of the fluid between the compressor inlet h_1 and outlet h_2. The enthalpy change can be determined from the relationship of the specific heat capacity and the temperature difference across the compressor. The turbine work is determined by the following relationship:

$$W_t = \dot{m}_t(h_3 - h_4) \quad \textbf{(3.2)}$$

where $\dot{m}_t$ is the total mass flowrate (air + fuel), and h_3 and h_4 are the turbine inlet and outlet enthalpies respectively. The heat added to the system is determined from:

$$Q_{2,3} = \dot{m}_f . LHV_{fuel} = (\dot{m}_a + \dot{m}_f).h_3 - \dot{m}_a.h_2 \quad \textbf{(3.3)}$$

where $\dot{m}_f$ is fuel mass flowrate and LHV_{fuel} is the lower heating value of the fuel, respectively. Hence, the system efficiency is determined from the relationship between output and input, thus, the power output and heat added to the combustor (input) is given by:

$$\eta = \frac{W_t - W_c}{\dot{m}_f . LHV_{fuel}} = \frac{c_p(T_3 - T_4) - c_p(T_2 - T_1)}{c_p(T_3 - T_2)} \quad \textbf{(3.4)}$$

where T_1 to T_4 are the respective temperatures at compressor inlet, combustor inlet, turbine inlet and turbine outlet and c_p is the specific heat capacity of the working fluid at constant pressure. The isentropic relationship for either the compressor or turbine can be determined from the pressure ratio and the isentropic coefficient (Boyce, 2002; Sonntag, 1998), which is determined from:

$$\frac{T_2}{T_1} = \frac{T_3}{T_4} = \left(\frac{P_2}{P_1}\right)^{\frac{\gamma-1}{\gamma}} \quad \textbf{(3.5)}$$

$$r = \frac{P_2}{P_1} = \frac{P_3}{P_4} \quad \textbf{(3.6)}$$

where $P_1$to P_4 is the pressure at the compressor inlet, combustor inlet, turbine inlet and turbine outlet, r is the pressure ratio and γ is the isentropic coefficient. The isentropic coefficient is given by:

$$\gamma = \frac{c_p}{c_v} \quad \textbf{(3.7)}$$

where c_p and c_v are the specific heats at constant pressure and volume, respectively. Implementing the above equations allows the cycle efficiency to be determined from equation 3.8.

$$\eta = 1 - \left(\frac{1}{r}\right)^{\frac{\gamma-1}{\gamma}} \quad \textbf{(3.8)}$$

The cycle efficiency will be dependent on the pressure ratio and the working fluid. Hence, as the isentropic coefficient increases, due to changes in the working fluid associated with the combustion kinetics, the cycle efficiency increases. This relationship is also the same at larger pressure ratios, hence, higher efficiency.

Therefore, to determine the specific power output of the cycle, the following non-dimensional equation is used:

$$\frac{W}{c_p T_1} = \alpha \left(1 - \left(\frac{1}{r}\right)^{\frac{\gamma-1}{\gamma}}\right) - \left(r^{\frac{\gamma-1}{\gamma}} - 1\right) \quad \textbf{(3.9)}$$

where α is the ratio between the combustor outlet and inlet temperature.

3.2.2.2 Regenerative cycle

In a simple cycle, the exhaust gas temperature is higher than the air temperature leaving the compressor, usually lost to the atmosphere (Boyce, 2011). This heat loss is recovered using a recuperator or regenerator (heat exchanger) that uses the heat from the flue gas to pre-heat the compressed air prior to entering the combustion chamber, as illustrated in Figure 3.2 (Boyce, 2011). The mGT used for the experimental campaigns in Chapter 4 and 5 is a combined heat and power unit, which is a regenerative cycle.

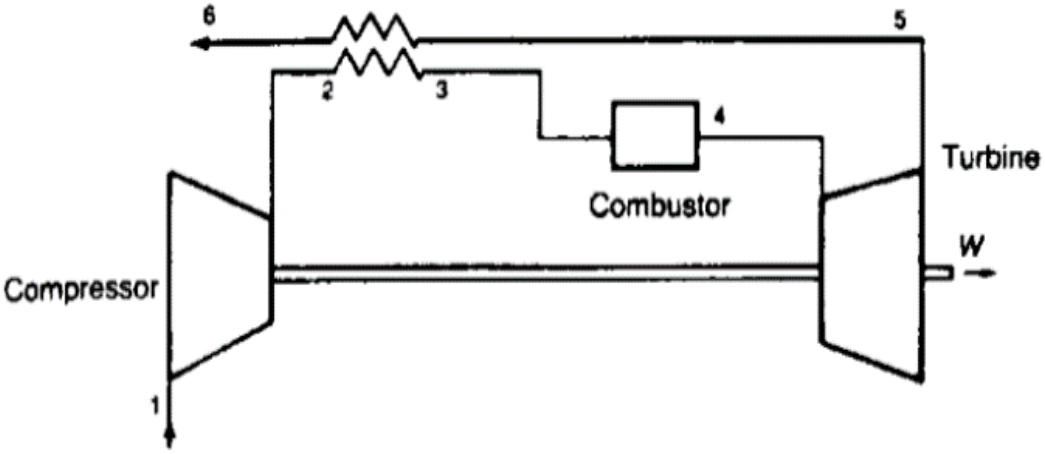

Figure 3.2. Schematic of the regenerative gas turbine cycle

(Boyce, 2011).

As indicated by Boyce (2002) and Saravanamuttoo et al. (2009) the regenerative gas turbine cycle efficiency is determined from:

$$\eta = \frac{c_p(T_4 - T_5) - c_p(T_2 - T_1)}{c_p(T_4 - T_3)} \quad \textbf{(3.10)}$$

where T_1 to T_5 is the cycle temperatures at the compressor inlet (T_1), compressor outlet (T_2), recuperator air-side outlet (T_3), combustor outlet (T_4) and turbine outlet (T_5). Assuming perfect heat transfer across the heat exchanger, it is considered that

the turbine and recuperator air-side outlet temperatures are equal. Therefore, incorporating the pressure and temperature isentropic relationship the cycle efficiency can be determined from:

$$\eta = 1 - \left(\frac{r^{\frac{\gamma-1}{\gamma}}}{\alpha} \right) \quad \textbf{(3.11)}$$

As shown in the above relationship the temperature ratio is associated with the cycle efficiency. In addition, as the pressure ratio reduces the cycle efficiency increases, hence, the cycle efficiency will increase with the maximum gas turbine temperature. The ideal Carnot efficiency can, therefore, be applied, expressed by:

$$\eta = 1 - 1\alpha \quad \textbf{(3.12)}$$

where the pressure ratio limiting value is 1 and the cycle efficiency is associated with the temperature ratio relationship (Saravanamuttoo et al., 2009). The recuperators used in these cycles are often designed with effectiveness above 0.9. However, this is dependent on the specific heat capacity of the working fluid on the air and flue gas sides of the heat exchanger, respectively. To determine the effectiveness (ε) the following relationship is used:

$$\varepsilon = \frac{T_3 - T_2}{T_5 - T_2} \quad \textbf{(3.13)}$$

3.3 Membranes

Membrane separation technologies are one of the alternatives being considered for CO_2 capture. Research and development of semi-permeable membrane systems throughout the 1950's, 1960's and 1970's led to the commercialisation of high-flux interfacial reverse osmosis membranes, patented by John Cadotte in 1979 (Seoane et al., 2015). In the 1980's, Perma (Air Products) commercialised gas separation membranes, e.g. polysulfone hollow-fiber membrane, and subsidiaries of WR Grace, Honeywell UOP and Cameron developed one of the first membrane systems for the natural gas processing industry (Baker and Lokhandwala, 2008; Kao et al., 1989; Qiu et al., 1989; Seoane et al., 2015). The "*anisotropic cellulose acetate membrane*" system was developed to separate CO_2 from natural gas using the Loeb-Sourirajan method (Baker and Lokhandwala, 2008). Since 1998, membrane research has advanced with novel membrane systems, e.g. polyimide, perfluoropolymer and poly(4-methyl-1-pentene) membranes, being developed, resulting in greater membrane performance and competition for industrial gas

processing (Baker and Lokhandwala, 2008). This industry typically uses hollow–fibre or flat sheet membranes with the increased use of composite membrane systems (Seoane et al., 2015). There are several membrane technologies currently available for this industry, however, the viability of using membranes for carbon capture technologies pose a number of technical challenges including membrane stability, wetting, material longevity and operability issues (González-Salazar, 2015). A number of researchers are investigating membranes for PCC systems, typically for coal-fired power stations with limited works investigating membranes for gas-CCS (e.g. Merkel et al., 2013; Turi et al., 2017; Voleno et al., 2014). In Merkel et al. (2013) work, they use a Polaris membrane for S-EGR in gas fired systems, where research and development is ongoing to optimise this membrane for gas-CCS applications. This selective membrane accounts for the transfer of CO_2, N_2, H_2O, O_2 and Ar, from the feed and the permeate streams, which is based on the membrane principles outlined in section 3.3.1. The expressions within section 3.3.1 are important because they provide the fundamental background to appreciate the mass transfer phenomena occurring in S-EGR systems (Diego et al., 2018; Merkel et al., 2013; Turi et al., 2017; Voleno et al., 2014). The subsequent research chapters in this thesis investigate S-EGR. The S-EGR process incorporates membrane technology, hence, as this research focuses on S-EGR, understanding how membranes work is important.

3.3.1 Membrane principles

Gas separation via membranes is traditionally a physical process where the feed stream containing different gas compounds flows along one side of the membrane. The permeating gas molecules, e.g. CO_2 in this case, diffuse through the membrane barrier due to the concentration gradient and exits as the permeate stream (Incropera et al., 2007; Khalilpour et al., 2015). The remaining gas compounds exit as the retentate stream as illustrated in Figure 3.3 (Khalilpour et al., 2015).

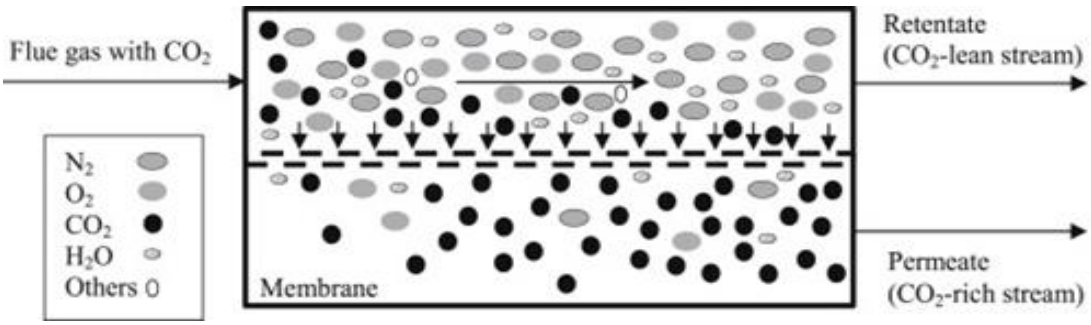

Figure 3.3. Schematic of the CO_2 separation process using membranes

(Khalilpour et al., 2015).

The permeation process, where diffusion occurs, depends on the membrane material used for the specific process, e.g. S-EGR. For example, the solution-diffusion mechanism governs the transport principals in polymeric membranes, whereas, adsorption, diffusion, and molecular sieving govern the transport process in membranes with distinct pores, e.g. zeolites (Seoane et al., 2015). The membrane permeance and selectivity are also important parameters to consider when determining which membrane material to use (Khalilpour et al., 2015). A flux solution-diffusion mechanism, according to Fick's first law of diffusion, represents the transport phenomena illustrated by Figure 3.3, which is expressed as follows (Incropera et al., 2007; Tyrrell, 1964):

$$J_i = -D_i \frac{\partial c}{\partial x} \tag{3.14}$$

where J_i is the gas flux through membrane (cm^3 (STP) / cm^2.s), D_i is the diffusion coefficient (cm^2/s), ∂c is the concentration gradient over the membrane (mol / cm^3) and ∂x is the position represented by length (cm). The above equation can be applied to membranes, assuming the diffusion flow is at steady state conditions, where ∂x changes to l, and ∂c is represented by $c_{i,f}$ and $c_{i,p}$ expressed by as follows (George and Thomas, 2001):

$$J_i = \frac{D_i(c_{i,f} - c_{i,p})}{l} \tag{3.15}$$

where $c_{i,f}$ is the feed concentration (mol / cm^3), $c_{i,p}$ is the permeate concentration (mol / cm^3) and l is the membrane thickness (cm). Henry's law is a linear relationship of gas solubility in a liquid at equilibrium being directly proportional to the gas partial pressure, namely (Rosenberg and Peticolas, 2004):

$$c_i = S_i . p_i \tag{3.16}$$

where c_i is the concentration (mol / cm^3), S_i is the solubility coefficient (cm^3 (STP) / cm^3.cmHg) and p_i is the partial pressure (mmHg). The combination of equations (3.16) and (3.17) allows the membrane permeability to be determined where the diffusion (D_i) and solubility coefficient (S_i) can be expressed by the permeability (P_i), namely (Baker and Lokhandwala, 2008):

$$J_i = \frac{P_i(p_{i,f} - p_{i,p})}{l} \tag{3.17}$$

where P_i is the permeability (cm^3 (STP) . cm / cm^2 . s . cmHg), $p_{i,f}$ is the feed partial pressure (mmHg) and $p_{i,p}$ is the permeate partial pressure (mmHg). The ratio of $p_{i,f}$ to $p_{i,p}$ can be defined as the driving force (Seoane et al., 2015) and the membrane selectivity can be determined by the permeability ratio ($\alpha_{f,p}$) defined as follows (Baker and Lokhandwala, 2008):

$$\alpha_{f,p} = \frac{p_{i,f}}{p_{i,p}} = \frac{(D_{i,f}/D_{i,p})}{(S_{i,f}/S_{i,p})} \quad \textbf{(3.18)}$$

where $D_{i,f}/D_{i,p}$ is the diffusion coefficient ratio at feed and permeate and $S_{i,f}/S_{i,p}$ is the solubility coefficient ratio at the feed and permeate.

3.4 Amine scrubbing

Chemical absorption is a well–known process used in many industries where amine absorption has been used for CO_2 removal since the 1930's (MacDowell et al., 2010). There are three classifications of amines including primary, e.g. monoethanolamine (MEA), secondary, e.g. diethanolamine (DEA) and tertiary, e.g. methyldiethanolamine (MDEA), which are widely investigated in the literature for CCS systems (Kohl and Nielsen, 1997). These basic organic compounds which are derived from ammonia are categorised as primary, secondary or tertiary amines, depending on the quantity of hydrogen atoms attached to the nitrogen atoms, are typically represented by RNH_2, R_2NH and R_3N, where R can be the alkyl or aryl group (Morrison, 1992). The primary and secondary amines form carbamate from the quick chemical reaction with CO_2, which are sterically hindered compounds (primary amine fixed to tertiary carbon atom or secondary amine fixed on secondary or tertiary carbon atom) (Morrison, 1992). Primary and secondary amines are governed by the formation of carbamate and bicarbonate expressed in equations (3.19) and (3.21), respectively:

$$CO_2 + 2R_1R_2NH \rightleftharpoons \left[R_1R_2NH_2^+\right]\left[R_1R_2NCOO^-\right] \quad \textbf{(3.19)}$$

$$CO_2 + H_2O + R_1R_2NH \rightleftharpoons \left[R_1R_2NH_2^+\right]\left[HCO_3^-\right] \quad \textbf{(3.20)}$$

Tertiary amines catalyse the hydration of CO_2 instead of directly reacting with this species expressed as:

$$CO_2 + H_2O + R_1R_2R_3N \rightleftharpoons \left[R_1R_2R_3NH^+\right]\left[HCO_3^-\right] \quad \textbf{(3.21)}$$

This leads to increased carbamate production related to the heat of absorption from this reaction, hence, greater solvent regeneration penalties (Vaidya and Kenig, 2007). However, in tertiary amines (non-sterically hindered compounds) the absence of H_2, combined to N_2, prevents the carbamate reaction occurring (Vaidya and Kenig, 2007). Tertiary amines form bicarbonate from the CO_2 hydrolysis reaction (see section 3.4.1.3) where the heat of absorption in this reaction is smaller than the carbamate reaction in primary and secondary amines (Vaidya and Kenig, 2007). Sterically and non-sterically hindered compounds influence the chemical bonds associated with the hydrolysis reaction, whereby, at higher CO_2 concentrations in the liquid phase this reaction becomes crucial for non-sterically hindered compounds (Chakma et al., 1995; Nielsen et al., 2012).

The methyl group which exists with sterically hindered compounds weakens the carbamate chemical bond and favours bicarbonate formation, thus, influencing the CO_2/amine loading capacity (Nielsen et al., 2012). The bulky alkyl attached to the amino group, which is associated with hindered compounds, affects the stability of the carbamate. The stability of carbamate (equations 3.19 and 3.20) is dependent on whether the amines are hindered or non-hindered e.g. bulky or not bulky. Non–hindered amines are not bulky favouring carbamate formation (equation 3.20), which means the theoretical capacity is 0.5 moles of CO_2 per one mole of amine (Gouedard et al., 2014; Nielsen et al., 2012). However, in tertiary amines (equation 3.21) this reaction involves non-hindered amines that lead to unstable carbamate formation. This carbamate instability affects the reaction with CO_2, thus allowing a theoretical capacity of one mole of CO_2 to be absorbed per one mole of amine. The stable carbamate formation reaction (equation 3.19) in primary and secondary amines is a thermodynamic limitation for CO_2 absorption and desorption, as the capacity of this hindered amine is lower than the non-hindered amines (equation 3.21), e.g. tertiary amines (Nielsen et al., 2012). Sterically hindered compounds can also influence amine thermal stability in CO_2 capture systems, whereas, tertiary amines are often combined with primary or secondary amines to decrease solvent regeneration costs due to the lower heat of reaction during bicarbonate formation (Gouedard et al., 2014, 2012).

The typical MEA concentration used in post-combustion CO_2 capture systems is 30 wt% MEA and 70 wt% H_2O. However, this concentration will vary depending on the operating requirements of the plant. For example, higher concentrations of MEA are suggested to optimise the CO_2 absorption capacity and decrease the solvent flowrate which has possible economic and energy benefits, however, corrosion

issues might be more prominent (Abu-Zahra et al., 2007; Fytianos et al., 2016). Chapter 5 of this thesis evaluates the experimental performance of a pilot scale CO_2 capture plant using a 40 wt% MEA concentration.

3.4.1 Amine chemistry

The degree at which electrolytes dissociate is dictated by chemical equilibrium, where, partial electrolyte dissociation is associated with weak species such as CO_2 (acid) and MEA (organic base) (Austgen et al., 1989). In aqueous solutions the partial ionisation or dissociation of CO_2 and MEA occurs, where the acid gas, e.g. CO_2, is absorbed in the aqueous solution, e.g. MEA represented by RNH_2 below. The ionisation reaction of water and dissociation of CO_2 dissolved via carbonic acid is governed by (Aboudheir et al., 2003):

$$CO_2 + H_2O \overset{k_1}{\leftrightarrow} OH^- + H^- \quad \textbf{(3.22)}$$

$$CO_2 + H_2O \overset{k_{H_2O},k_2}{\longleftrightarrow} HCO_3^- + H^+ \quad \textbf{(3.23)}$$

The formation and dissociation of bicarbonate is given by (Aboudheir et al., 2003):

$$CO_2 + OH^- \overset{k_{OH^-}}{\longleftrightarrow} HCO_3^- \quad \textbf{(3.24)}$$

$$HCO_3^- + H_2O \overset{k_{HCO_3^-},k_3}{\longleftrightarrow} CO_3^- + H_3O^+ \quad \textbf{(3.25)}$$

The carbamate reaction and the reversible hydrolysis reaction to form bicarbonate is expressed from (Aboudheir et al., 2003):

$$CO_2 + RNH_2 + B \overset{k_4,k_{-4},k_4}{\longleftrightarrow} RNH_2^+COO^- + BH^+ \quad \textbf{(3.26)}$$

$$RNHCOO^- + H_2O \overset{k_6}{\leftrightarrow} RNH_2 + HCO_3^- \quad \textbf{(3.27)}$$

where $RNH_2^+COO^-$ is MEA and B is the base usually represented by $H_2O, RNH_2\ or\ OH^-$. The following equation represents the pronation reaction of MEA given by (Aboudheir et al., 2003):

$$RNH_2 + H_3O^+ \overset{k_{RHN_2}^{"},k_9,k_5}{\longleftrightarrow} RNH_3^+ + H_2O \quad \textbf{(3.28)}$$

3.4.1.1 Zwitterion mechanism

The Zwitterion mechanism is a two-step process initially suggested by Caplow (1968) and subsequently reinvestigated by Danckwerts (1979) where the reversible

reaction of CO_2 with either primary or secondary amines forms Zwitterion that is unstable as expressed by:

$$CO_2 + RNH_2 \overset{k_1, k_{-1}}{\longleftrightarrow} RNH_2^+COO^- \quad \textbf{(3.29)}$$

The reversible reaction allows Zwitterion to revert to CO_2 and amine, or de-pronation occurs by a base which exists allowing carbamate formation given by (Caplow, 1968; Crooks and Donnellan, 1989; Danckwerts, 1979; Glasscock et al., 1991):

$$RNH_2^+COO^- + B \overset{k_B, k_{-B}}{\longleftrightarrow} BH^+ + RNHCOO^- \quad \textbf{(3.30)}$$

The combination of the above chemical reactions leads to the carbamate formation as shown in equation 3.26.

3.4.1.2 Termolecular mechanism

The termolecular mechanism was initially suggested by Crooks and Donnellan, (1989) which infers the CO_2/MEA reaction occurs concurrently in a single-step reaction, where the initial product is a loosely bound encounter complex instead of a Zwitterion, determined from:

$$RNH_2 \ldots B + CO_2 \leftrightarrow RNHCOO^- + BH^+ \quad \textbf{(3.31)}$$

The loosely bound encounter complex is broken down forming the initial reactants, e.g. CO_2, MEA and the base, however, a partial amount reacts with H_2O and MEA which leads to the formation of ionic products (Vaidya and Kenig, 2007).

3.4.1.3 Base-catalysed hydration mechanism

The mechanism was first devised by Donaldson and Nguyen, (1980) who noted that tertiary amines (represented by R_3H) are unable to react with CO_2 directly. Hence, tertiary amines are associated with base-catalysed hydration mechanism, which is given by:

$$R_3H + H_2O + CO_2 \overset{k'}{\rightarrow} R_3N^+H + HCO_3^- \quad \textbf{(3.32)}$$

Chapter 5 investigates the performance of a pilot scale CO_2 capture plant using amines under S-EGR conditions. The above mechanisms are of fundamental importance to understand the principal chemical reactions occurring under these conditions.

3.5 Chapter conclusions

The chapter initially evaluates the technical background associated with gas turbines, where the principle thermodynamic equations are also discussed. These thermodynamic principles associated with the simple and regenerative cycle are of fundamental importance in the understanding of the micro gas turbine (mGT) cycle and its performance. The subsequent chapter of this thesis assesses the experimental performance of the Turbec T100 mGT under S-EGR conditions. The membrane principles presented here define the governing equations for the diffusion mechanism, which is important in the understanding of the basis of S-EGR configurations, which is evaluated in this thesis. The final section of this chapter presents an overview of amine scrubbing with the subsections discussing the theoretical reaction mechanisms associated with primary, secondary and tertiary amines. In chapter 5 of this thesis the influence of S-EGR on the performance of a pilot scale post-combustion CO_2 capture plant using 40 wt% MEA is evaluated. The fundamental chemical reactions presented in this chapter provides essential knowledge to understand the reaction kinetics associated with the CO_2 capture process. Chapter 4 and 5 investigate the performance of the mGT and post-combustion CO_2 capture plant (using amines) under S-EGR conditions at pilot-scale. Therefore, the principles covered in this chapter form the basis of understanding for S-EGR configurations in the combustion and the CO_2 capture phase of the process.

4 Experimental investigation of the impacts of selective exhaust gas recirculation on a micro gas turbine

4.1 Introduction

This work evaluates the influence of selective CO_2 recirculation conditions on the performance of a Turbec T100 Series 3 mGT at the Pilot-scale Advanced CO_2 Capture Technology (PACT) core facilities located in Sheffield, UK (PACT, 2018). CO_2-enhanced conditions characteristic of S-EGR processes are simulated in the mGT by injecting CO_2 into the compressor inlet and mixing with the combustion air. Several experimental tests have been performed over the 60-100 kW_e operating envelope to compare baseline conditions to CO_2 injection rates of up to 300 kg/h (up to 9.4 vol% CO_2 in the oxidiser stream) to mimic a range of S-EGR scenarios. Flue gas CO_2 concentrations up to 10.1 vol.% have been tested, which represent more than a six times increase in the CO_2 content of the flue gas, similar to what is expected in S-EGR systems (e.g. Diego et al., 2018, 2017b; Herraiz et al., 2018; Merkel et al., 2013). Impacts on the operational performance of the mGT have been analysed, together with the resulting CO, UHC and NOx emission trends under S-EGR simulated conditions. The novelty of this work includes the appraisal of mGT performance in terms of compressor, turbine and combustion performance at part and full load operation under these S-EGR conditions.

4.2 Experimental methodology

4.2.1 Turbec T100 micro gas turbine system

The PACT facilities located in Sheffield, UK are a national centre for research and development into carbon capture and clean power generation (PACT, 2018). Several core facilities are available, including two Turbec T100 combined power and heat mGT's, Series 1 and 3 models. The Series 3 model that is used for the baseline and simulated S-EGR experimental campaigns in this work has a maximum 100 kW_e electrical power output and 165 kW_{th} thermal power output. The electrical and overall efficiencies are 30% and 80%, respectively, with a recuperator and exhaust gas heat exchanger increasing the total efficiency of the system (Turbec, 2009). The mGT scheme, illustrated in Figure 4.1 (p.51), shows the electrical generator, the radial centrifugal compressor and the radial turbine are

mounted on a single shaft, with a maximum turbine speed of 70,000 rpm (Turbec, 2009). The ambient air entering the mGT passes through a coarse pre-filter and internal fine filter before separating into two flows, the primary flow (combustion air) and secondary flow (ventilation air). The combustion air entering the compressor, is compressed to a maximum pressure ratio of ~4.5:1 at nominal conditions. Subsequently, the pressurised air enters the recuperator and is pre-heated with hot exhaust gases prior to entering the combustion chamber. The pre-heated combustion air is mixed with the natural gas which is burnt in the combustion chamber. The flame is swirl-stabilised, with a non-premixed pilot flame used to further enhance flame stability. The fuel-lean pre-mixed combustion chamber ensures low CO, NOx and UHC emissions (Turbec, 2009).

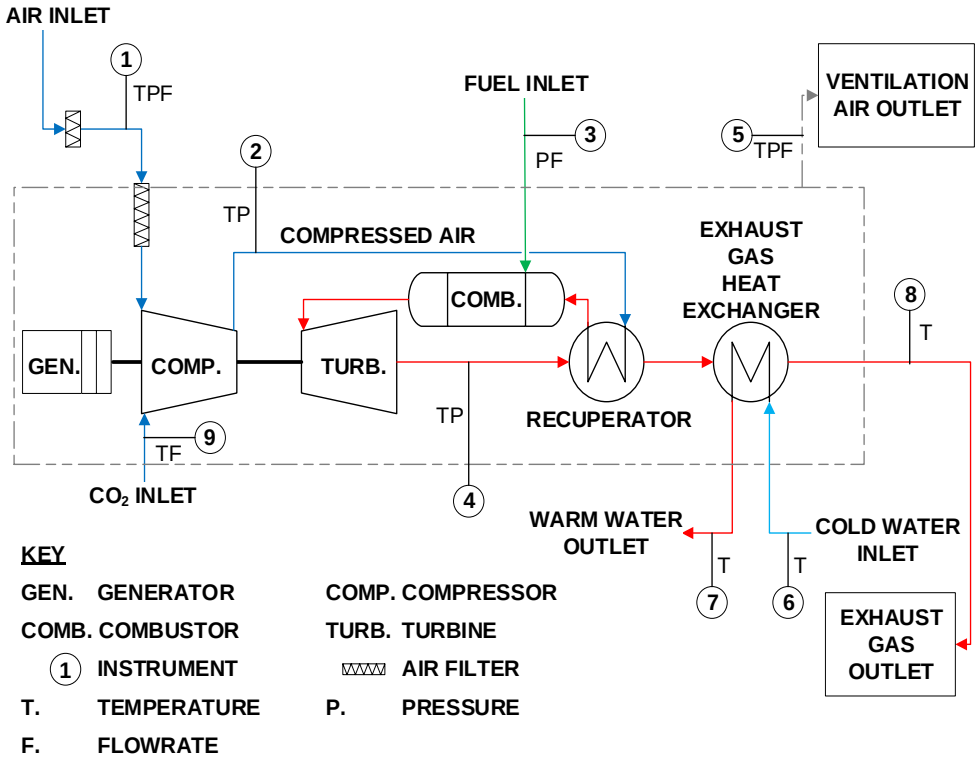

Figure 4.1. Schematic of the key turbine components and the instrumentation locations for the Turbec T100 Series 3 mGT.

The exhaust gases leave the combustion chamber at ~950°C (turbine inlet temperature at nominal conditions) and expand through the turbine, driving the compressor and generator (Turbec, 2009). The mGT control system keeps the turbine outlet temperature (TOT) constant at ~645°C thus changing the air and fuel flowrate depending on the set power output and ambient conditions in each test.

The exhaust gases leaving the turbine are used to pre-heat the combustion air in the recuperator, which works with an effectiveness close to 90% (Hohloch et al.,

2010). The remaining thermal energy contained in the gas stream entering the exhaust gas heat exchanger (at ~270°C at nominal conditions) can be used to heat up a water stream. The exhaust gases leaving the exhaust gas heat exchanger at ~70°C (nominal conditions) are then discharged either to the onsite capture plant (see Chapter 5) or to the atmosphere.

4.2.2 mGT data collection and monitoring

The mGT uses the Turbec remote monitor and control (RMC) system to monitor various operational parameters of the turbine, for example, the rotational speed. The RMC system uses a web browser, e.g. Internet Explorer, that allows the mGT operator to start, stop and control various parameters of the mGT (Turbec, 2006). The mGT uses the FPserver and FirstOp software supplied by the manufacturer to display and record parameters defined by the operator. The parameters recorded during the baseline and CO_2 enhancement tests and the calculated maximum standard deviation error for each parameter are shown in Table 4.1. The data presented in Table 4.1 has been collected from baseline and CO_2 enhancement tests. Each test was conducted for a minimum period of 15 minutes and recording data every second. In total, a minimum of seven baseline tests were performed per condition (40-100 kW_e) and a minimum of two tests per condition for the CO_2 tests (60-100 kW_e). For each test the calculated standard deviation and standard error was calculated.

Table 4.1. mGT standard deviation errors.

		Maximum standard deviation	
Parameter	**Unit**	**Baseline (±)**	**CO_2 enhancement (±)**
Air inlet temperature	°C	0.15	0.48
Turbine outlet temperature	°C	0.19	1.24
Turbine shaft rotational speed	rpm	60.56	102.42
Exhaust gas outlet temperature	°C	2.02	2.13
Actual active power	kW_e	0.30	0.72

Appendix A.5 provides the standard error values for the experimental results.

4.2.3 LabVIEW and additional instrumentation

The mGT has been fitted with additional instrumentation to complement existing parameters measured by the RMC system. The thermocouples and pressure transmitters were calibrated on site, in addition to the manufacturer's own calibration

certificates. A multiple channel National Instruments data acquisition system receives the electrical signals from each device and transfers this information to the LabVIEW software. The LabVIEW software processes the signal data from the data acquisition system and automatically records the data measurements every second. Figure 4.1, see section 4.2.1 (p. 51), illustrates the additional instrumentation locations for the mGT. The additional instrumentation installed measures the temperature, pressure and flowrate as identified in Table 4.2. These parameters were selected because they allowed for the most comprehensive data collection within the limits of the system to analyse the performance of S-EGR at pilot scale in gas turbines. The calculated maximum standard deviation for each parameter measured in Table 4.2 is shown in Table 4.3 for the baseline and CO_2 enhancement tests. The accuracy of each instrument is as per the manufacturer's guidance, which is quoted as a percentage of the reading error.

Table 4.2 Additional instrumentation accuracy.

ID number	Parameter	Type	Unit	Accuracy
S3–TC2	Compressor outlet temperature	RTD PT100	°C	±0.03°C at 0°C to ±0.08°C at 100°C
S3–TC9	Compressor / CO_2 inlet temperature	K-type thermocouple	°C	±2.2°C from -40°C to 333°C
S3–PT1	Air inlet pressure	Rosemount 2051T	bar(g)	±0.065%
S3–PT2	Compressor outlet pressure	Rosemount 2051T	bar(g)	±0.065%
S3–PT4	FG diffusion zone pressure	Rosemount 2051T	bar(g)	±0.065%
S3–FR3	Fuel inlet flowrate	Common S.A. Quantometer CPT-0	m^3/h	±0.36% at 40m^3/h - ±0.63% at 25 m^3/h

Table 4.3. Additional instrumentation standard deviation errors.

		Maximum standard deviation	
Parameter	**Unit**	**Baseline (±)**	**CO_2 enhancement (±)**
Compressor / CO_2 inlet temperature	°C	0.130	0.370
Compressor outlet temperature	°C	0.990	1.290
Air inlet pressure	bar(g)	0.002	0.007
Compressor outlet pressure	bar(g)	0.010	0.050
FG diffusion zone pressure	bar(g)	0.005	0.005

As indicated in Table 4.2 the fuel flowrate is measured by a Quantometer flow meter. The natural gas flowrate readings are taken manually and therefore this introduces human error in addition to the accuracy variations outlined in Table 4.2. Hence, the data for the fuel flowrate values will vary slightly. The fuel flowmeter records the volumetric flowrate at every 0.1 m^3 to two decimal places. The fuel mass flowrate is a function of the fuel density where the fuel temperature and pressure are assumed to be at standard conditions as stated by National Grid (2017), which is 15°C and 101325 Pa. The equation which identifies how the density of the fuel is determined from the ideal gas law equation, is given by:

$$\rho_f = \frac{MW.P}{R.T} \quad \textbf{(4.1)}$$

where ρ_f is the density of the fuel (kg/m^3), MW is the molecular weight (kg/mol), P is pressure (Pa), R is the ideal gas constant (8.314 m^3 Pa K^{-1} mol^{-1}) and T is the temperature (K). To determine the moles of O_2, CO_2 and H_2O consumed/produced per mole of fuel burnt, stoichiometric calculations are performed considering the natural gas composition and assuming complete combustion. The air inlet mass flowrate can be calculated by performing a CO_2 balance using the CO_2 contained in the flue gas (see Appendix A.1). This is calculated assuming complete combustion of the natural gas (see Table 4.5, p. 60) for the test conditions investigated and the experimental measurements of the CO_2, O_2 and H_2O concentrations in the exhaust gas which are measured using Fourier Transform Infrared (FTIR) spectroscopy and the Servomex gas analysers; gas analysis is discussed further in section 4.2.5.

4.2.4 CO_2 injection system

The mGT was modified to incorporate a CO_2 injection system into the compressor inlet to simulate S-EGR processes. Figures 4.2 and 4.3 (p. 55) illustrate the CO_2 injection system within the compressor inlet, which was designed to supply CO_2 from an external cryogenic storage tank supplied by BOC. The CO_2 flows through an external evaporator and trim heater to ensure that the CO_2 enters the gas mixing skid at a temperature above 10°C. The gas mixing skid that is located inside the PACT facility controls the CO_2 flowrate via two supply lines using Siemens Coriolis mass flow meters and pneumatically actuated flow control valves. The flowrate is measured and recorded at the skid via the Supervisory Control and Data Acquisition (SCADA) system. The CO_2 distribution system to the mGT from the gas mixing skid was designed by the author of this thesis, in accordance with Pressure Systems Safety Regulations 2000 (HSE, 2014).

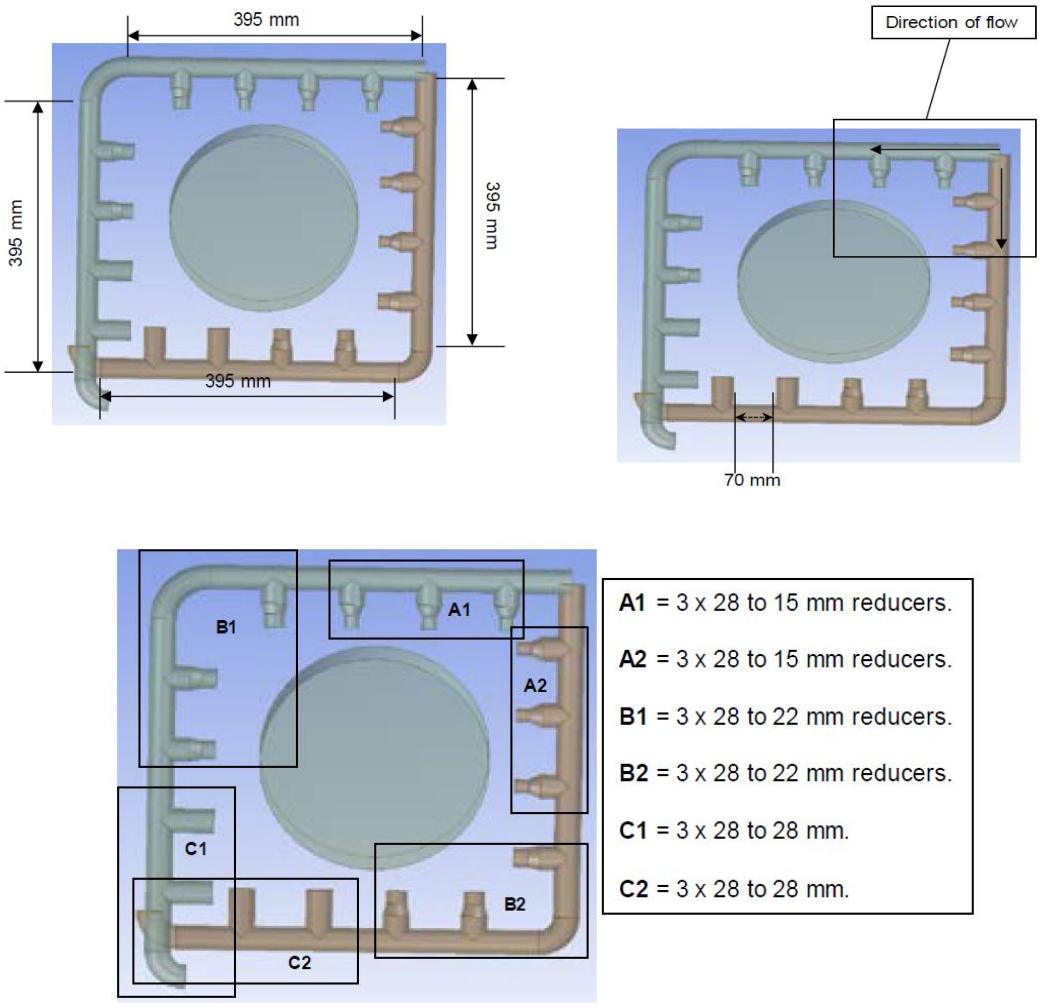

Figure 4.2. Design of the CO_2 injection system inside the compressor inlet.

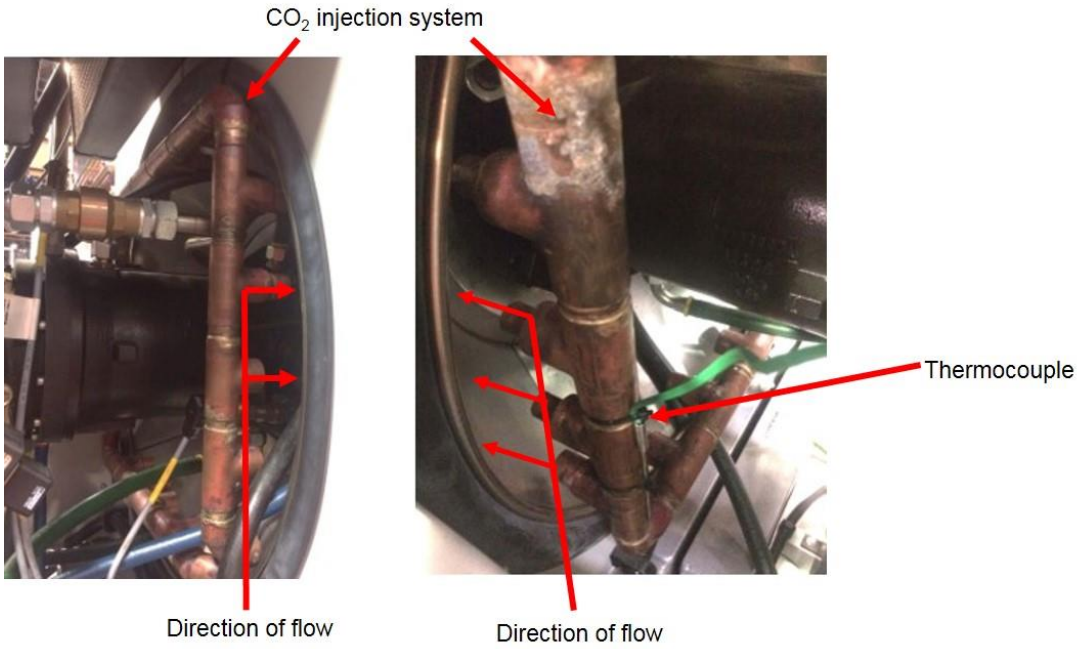

Figure 4.3. The installed CO_2 injection system inside the compressor inlet.

The system pressure was checked at regular intervals to establish any leaks. This was to ensure the safe delivery of CO_2 downstream of the gas mixing skid into the mGT compressor inlet. The two CO_2 supply lines are each designed to deliver a flowrate of 150 kg/h, thus allowing a maximum CO_2 flowrate of 300 kg/h into the system. The CO_2 injection system inside the compressor inlet was designed and modelled to ensure an equal distribution of CO_2 and mixing with the combustion air.

To record temperature variation at the point of CO_2 delivery, a K-type thermocouple was installed as illustrated in Figure 4.3 (p. 55), see the green wire in the second photograph, and shown in Table 4.3 (p. 53). The calculated maximum standard deviation for the CO_2 flowrate during the CO_2 enhancement experimental campaign was ±2.21 kg/h. The standard deviation was calculated for each CO_2 test and the maximum standard deviation determined as the maximum deviation of all tests collectively.

4.2.5 Gas analysers

The Gasmet® FTIR DX4000 uses Fourier Transform Infrared (FTIR) spectroscopy to measure the infrared absorption spectra of different gas compounds. As each gas species absorbs different quantities of infrared radiation at different wavelengths, the Gasmet® FTIR DX4000 can simultaneously analyse up to 50 different gas species within a short response time (<120 seconds) (Gasmet, 2016). The technique of infrared spectroscopy investigates how molecular vibrations interact with electromagnetic fields along an infrared spectrum (Gasmet, 2010). This method sends infrared radiation through a molecule at a certain frequency and establishes what proportion of the incident radiation is absorbed at a particular energy, thus, allowing an infrared spectrum to be determined (Gasmet, 2010). The frequency shown in an infrared spectrum corresponds to the photon energy relationship with the molecular vibrations of a molecule. The infrared regions along an electromagnetic spectrum are categorised as near infrared (12500 to 4000 cm^{-1}), mid infrared (4500 to 400 cm^{-1}) and far infrared (400 to 12.5 cm^{-1}) (Gasmet, 2010).

FTIR spectroscopy emits a light source e.g. infrared radiation, through a Michelson interferometer and a beamsplitter as illustrated by Figure 4.4 (p. 57) (Gasmet, 2010). The beamsplitter reflects half the infrared beam to the moving mirror and the other half reflects from a stationary mirror. These infrared beams reflect back to the beamsplitter, and then are transferred via a parabolic mirror to the detector. The detector determines the interferogram from the interference pattern, where this

information is sent to the computer generating the spectrum via the manufacturers software e.g. Calcmet (Gasmet, 2010).

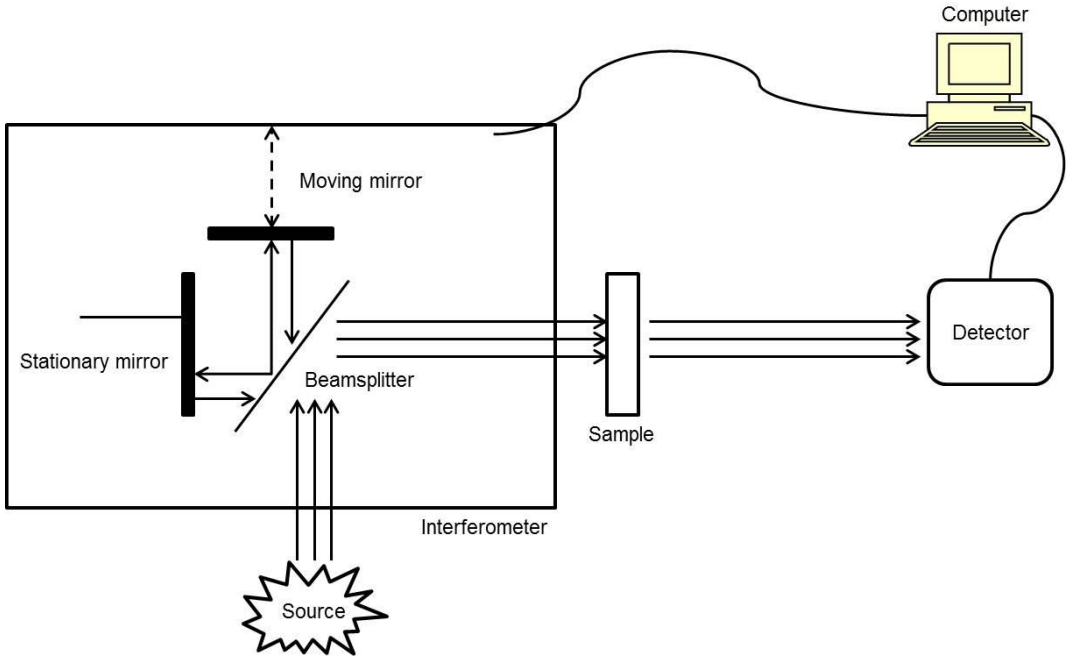

Figure 4.4. Schematic of the FTIR spectroscopy process.

Gasmet heated sampling lines transfer flue gas samples into a portable gas conditioning system and into the Gasmet FTIR DX4000. The heated filter and valve located within the sampling cell are heated to 180ºC, ensuring that the Gasmet portable sampling unit can measure wet, corrosive and undiluted gas streams prior to automatically transferring the gas sample to the Gasmet FTIR DX4000. The heated sampling lines that are operated at 180ºC have an important role by ensuring the gas samples remain in the gas phase and inhibit condensation from water soluble gas species e.g. SO_2. Calcmet is the software used in conjunction with the Gasmet gas analysers that records, collects and analyses the FTIR spectra and concentrations of the sample gas composition.

Prior to recording data, system calibration is required each time before measuring commences which is fed with zero grade N_2 for ~30 minutes during warm up. The operator purges the unit for 60 seconds with N_2 (zero grade) supplied by BOC, which flows from a gas cylinder via a BOC regulator and polytetrafluoroethylene (PTFE) tubing. Once purged the unit measures and displays the background spectrum, scanning 10 times per second for a period of three minutes, providing the operator with background values, which are checked against previous readings to ensure consistency. Once the background measurements are complete, the operator performs a zero check, recording the values and checking these readings

are at or near zero (Gasmet, 2010). If the new background and zero check values are significantly different (±0.2%) to previous readings, the operator can complete a secondary background and zero check. Before the start of each test, the background and zero checks are performed to ensure consistency. During FTIR operation the unit records the residual value, which specifies the maximum residual value in the absorbance spectra that remains. The closer this value is to zero the greater the accuracy of the result (Gasmet, 2010). The maximum standard deviation for each gas species considered in the results section recorded during both experimental campaigns is highlighted in Table 4.4.

Table 4.4. Emission standard deviation errors.

		Maximum standard deviation	
Species	**Unit**	**Baseline (±)**	**CO_2 enhancement (±)**
CO_2	vol%.	0.014	0.074
H_2O	vol%.	0.153	0.039
CO	ppm	3.746	20.485
NOx	ppm	1.266	1.496
CH_4	ppm	1.811	7.157
C_2H_6	ppm	1.222	0.687

During the CO_2 enhancement tests, the CO_2 concentrations reported by the FTIR were checked against known CO_2 concentrations supplied from a BOC gas cylinder. These certified values were 4.835 and 14.85 vol%. It was found that the CO_2 readings had drifted from its calibration values. The reported CO_2 concentrations presented in this work are corrected to account for the drift values reported by the FTIR. The correction equation for the FITR is given by:

$$\frac{x - 0.00157}{1.1192} \tag{4.2}$$

where x is the original reported CO_2 concentration in vol% (wet basis).

Two Servomex 5200 gas analysers are used for measuring O_2 and CO_2 concentrations in the exhaust gas and ventilation air outlet. These analysers use paramagnetic transducers which generate a strong magnetic field. They contain two suspended rotating glass spheres filled with N_2, diverged by a fixed mirror. A light beam reflects from the mirror onto two photocells, whereby, the O_2 attracted to the magnetic field displaces the suspended spheres, leading to rotation that generates

a signal. As the O_2 concentration increases, sphere displacement becomes greater. The feedback system detecting the generated signal creates a current that is passed through a wire fixed to the suspension. This leads to the motor effect that keeps the suspension in place. Converting the current creates an O_2 measurement due to its direct proportionality to the sample gas O_2 concentration. Figure 4.5 illustrates the paramagnetic process.

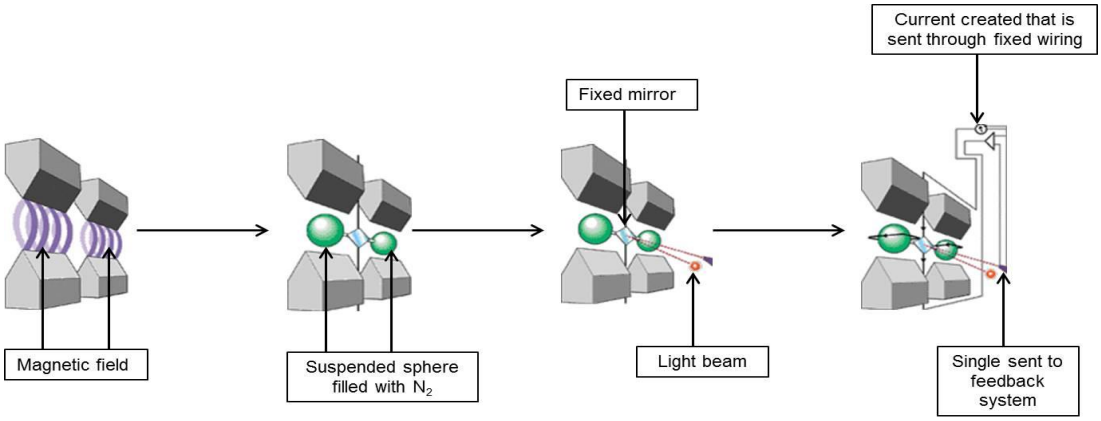

Figure 4.5. Schematic of the paramagnetic process.

Infrared transducers focus an infrared light source through a sample cell where CO_2 flows continuously and the concentration is measured. Two optical filters attached to a rotating disc allow the alternative transmission of infrared light. This single double wave beam process allows CO_2 molecules and atoms to absorb infrared light at a specific wavelength via the measuring filter, whereas, the reference filter, has infrared light transmitted through it at a wavelength unaffected by inert gases e.g. N_2. An infrared detector providing a gas concentration measurement, measures the difference in the absorbance variance, recorded by the operator

The Servomex analysers require calibration prior to measuring sample gases to limit measurement errors. One analyser measures the exhaust gas O_2 concentration and CO_2 and the second analyser is used to monitor O_2 and CO_2 concentrations in the ventilation outlet. The Servomex has an accuracy of ±0.1% and ±2.0% for O_2 and CO_2 reading, respectively (Servomex, 2008). To be consistent with industrial standards all the flue gas emissions values from the mGT experiments are reported in dry concentration as per ISO11042 (ISO, 1996) determined from:

$$\varphi_{i,dry} = \varphi_{i,wet} \cdot \left(\frac{100}{100 - vol\ \%_{\cdot H2O}} \right) \quad \textbf{(4.3)}$$

where $\varphi_{i,wet}$ is the wet gas species concentration and $vol\ \%_{\cdot H2O}$ is the water vapour content recorded in the flue gas. Moreover, NOx emissions are usually reported

corrected to 15% O_2. However, ElKady et al. (2009) suggests reporting mass specific NOx emissions based on net power output under CO_2-enhanced conditions. These authors suggest that representing NOx emission values corrected to 15% O_2 under CO_2-enhanced conditions may be misleading, as the oxygen content at combustor outlet is naturally reduced (potentially the inlet O_2 concentration could be as low as ~16 vol%) in these cases due to the partial replacement of the combustion air with the recirculated stream. As a result, correcting emissions to 15% O_2 could lead to an artificial reduction in the values of NOx emission (ElKady et al., 2009). Therefore, NOx emissions reported here are presented using the NOx emissions index, based on grams per kilowatt hour.

The NOx emission index is determined from:

$$EINOx = \frac{NO_x . 10^{-6} . MW . n_{FG} . 3600}{P_e} \quad \textbf{(4.4)}$$

where $EINOx$ is the NO_x emissions index in g/kWh, NO_x is the reported volumetric FTIR concentration in ppmv on a dry basis, MW is the molecular weight in g/mol, n_{FG} is the molar flue gas flowrate in mol/s and P_e is the net power output in kW. The gas samples were collected using the FTIR as described in the gas analyser section above.

4.2.6 Natural gas composition and performance calculations

The natural gas composition of the fuel was requested from National Grid at the end of each test day, as the experimental facilities do not have the capabilities to perform on-site natural gas composition measurements. The dry higher heating value (HHV) of the fuel supplied by National Grid to the UK ranges from 37.5 MJ/m^3 to 43.0 MJ/m^3 at standard conditions (National Grid, 2017). The normalised natural gas composition of the fuel supplied to the experimental facilities during the baseline and CO_2 testing campaigns are provided in Table 4.5.

Table 4.5. Average natural gas composition and higher heating value.

	Natural gas composition – normalised (mol. %)								HHV
Test campaign	**N_2**	**CO_2**	**CH_4**	**C_2H_6**	**C_3H_8**	**C_4H_{10}**	**C_5H_{12}**	**C_6H_{14}**	**(MJ/m^3)**
Baseline	1.08	1.31	90.76	5.04	1.26	0.39	0.09	0.06	39.56
CO_2 enhancement	0.94	1.46	91.09	4.74	1.18	0.40	0.10	0.08	39.46
% diff.	13.0	11.5	0.4	6.0	6.3	2.6	11.1	33.3	0.25

The mGT electrical efficiency is determined as a function of net electrical power output and fuel heat consumption as:

$$\eta_{el} = \frac{kW_e}{Q_{f1}} \cdot 100 \quad \textbf{(4.5)}$$

where η_{el} is the electrical efficiency (%), kW_e is the net electrical power output, Q_{f1} is the thermal input associated with fuel combustion (kW_{th}).

4.2.7 Experimental campaigns

Standard operating procedures (SOPs) for the experimental campaigns were developed to ensure each test followed the same method. This included the development of two separate SOPs, for normal mGT operation and S-EGR mGT operation. This ensured the correct procedure was followed for each test allowing for consistency between tests conducted over multiple testing days. Prior to starting any tests, it was ensured that the mGT was at steady state conditions and the turbine outlet temperature (TOT) was ~645°C, with the actual power output reaching the user-defined set point, the exhaust gas emission levels constant and the CO_2 flowrate stable. The start-up sequence for the mGT is typically ~2 hours. In this time, the mGT operator (author of this thesis) calibrated all analysers, monitored all the parameters and troubleshooted any technical errors during start up and throughout the experiments. This root-cause analysis and problem solving required the author of this thesis to find solutions which we not immediately identified, which led to delays in completing testing. All experiments were conducted for a minimum of 15 minutes per test as per ISO gas turbine acceptance tests (ISO, 2009).

A preliminary reference test campaign (40-100 kW_e) without CO_2 injection was conducted prior to any mGT modifications (additional instrumentation + CO_2 injection system). This was used to confirm that these changes did not affect the normal functioning and performance of the mGT. The author of this thesis researched, procured and tested the best available instrumentation (within the limits of the mGT) for investigation S-EGR at pilot scale. Subsequently, the performance of the mGT through a 60-100 kW_e operating envelope was initially assessed without CO_2 injection (baseline conditions) to provide a reference for comparison and characterise the performance of the mGT as a function of the ambient temperature conditions. Then, CO_2-enhancement experiments were carried out by injecting different quantities of CO_2 (up to 300 kg/h, corresponding to up to 10.1 vol% in the flue gas) into the compressor inlet, thus replacing some of the combustion air, to simulate a range of S-EGR scenarios at power outputs of 60-100 kW_e. Tests at

power outputs below 60 kW_e were not considered as the mGT is far from its design conditions and its steady-state performance was compromised due to the high emission levels of CO and UHC, and the TOT not achieving 645°C (see Appendix A.2).

The mGT can operate as low as 40 kW_e, however, the performance is significantly inhibited. At the lower power outputs (<60 kW_e) the limits of the FTIR analyser readings for CO and UHC were at maximum. This means that testing at power outputs below 60 kW_e for the S-EGR tests would provide inaccurate readings as CO and UHC emissions are anticipated to increase beyond the maximum analyser value, hence the residual error value would also become greater. Moreover, experiments at 90 kW_e with a CO_2 injection rate of 300 kg/h are omitted in the test matrix in Table 4.6 due to a malfunctioning of the fuel booster which prevented further tests. The test conditions for the baseline and CO_2 enhancement experiments are summarised in Table 4.6.

Table 4.6. Test conditions investigated for the baseline and CO_2 enhancement experiments.

	Set power output (kW)				
CO_2 injection rate (kg/h)	60	70	80	90	100
0	❖	❖	❖	❖	❖
100	❖	❖	❖	❖	❖
150	❖	❖	❖	❖	❖
200	❖	❖	❖	❖	❖
250	❖	❖	❖	❖	❖
300	❖	❖	❖		❖

4.3 Results and discussion

The CO_2 concentrations recorded in the flue gas throughout the baseline and S-EGR tests are presented in Figure 4.6 (p. 63). For the baseline, the reference flue gas concentration of CO_2 increases from 1.4 to 1.7 vol% when increasing the power output from 60 to 100 kW_e. This is associated with the amount of excess air and the air-fuel ratio, which are higher at part load conditions (see figures in Appendix A.3). The simulated S-EGR conditions tested in this work augmented the CO_2 concentrations in the flue gas from 1.7 to 8.4 vol% (0-300 kg/h CO_2) at 100 kW_e and from 1.4 to 10.1 vol% (0-300 kg/h CO_2) at 60 kW_e. This represents a ~400% and ~600% increase at 100 and 60 kW_e, respectively, at maximum CO_2 addition compared to the baseline conditions. These are in the range of the expected changes in S-EGR systems based on the literature review, which suggested CO_2

concentrations in the flue gas ~18-26 vol% (depending on which S-EGR configuration is used) in CCGT plants. The key objective of this study is to investigate the effects of these S-EGR conditions on the mGT performance. For this purpose, the impacts on electrical efficiency, turbine rotational speed and compressor discharge temperature are analysed, as well as the NOx, CO and UHC emissions. Standard error bars are displayed on all the figures, however, as the standard error is relatively small, these are not always visible on the graphs. Appendix A.5 provides tables with the standard error information.

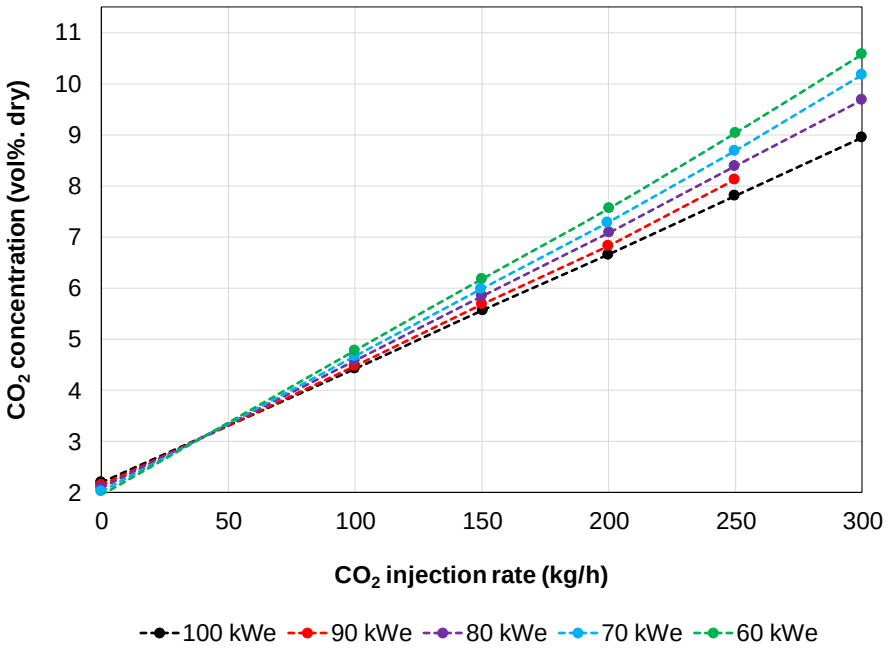

Figure 4.6. Flue gas CO_2 concentrations for the baseline and S-EGR CO_2 injection cases across the 60-100 kW_e operating envelope.

4.3.1 Influence of S-EGR on the mGT performance

Figure 4.7 (a)-(e) illustrates the effects of S-EGR on the mGT electrical efficiency and rotational speed at power outputs of 60-100 kW_e for all cases, showing the air temperature at the compressor inlet for each test. This is compared to the baseline values calculated at the average air temperature in the S-EGR cases using the baseline results obtained, which characterise the mGT performance at different air inlet temperatures for each power output. Lower values of the electrical efficiency are obtained at decreasing power outputs, as expected (Turbec, 2009). The electrical efficiency of the mGT slightly decreases with CO_2 injection, which has a higher heat capacity than air for the mGT cycle temperatures. This causes a decrease in the gas temperature at the combustor outlet and thus, at the turbine inlet, leading to a reduction in the power output (Best et al., 2016; Nikpey et al.,

2014). Throughout the tests the power output remained stable and the heat capacity of CO_2 leads to the abovementioned effects. This performance is seen for all power outputs, with reductions in the electrical efficiency of between ~4 and 8% when compared with the reference case with no CO_2 injection.

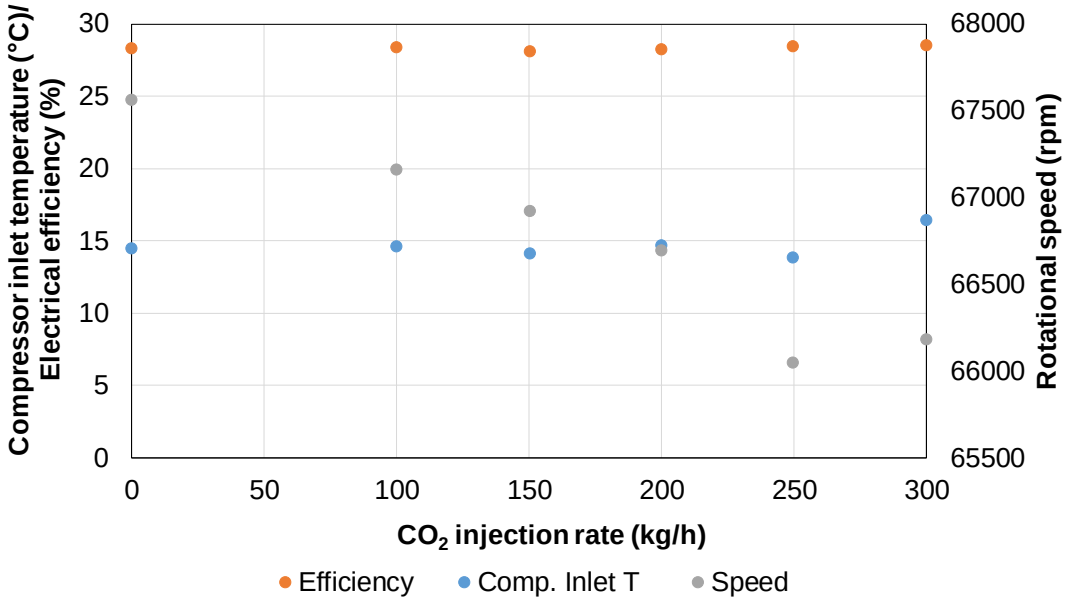

(a)

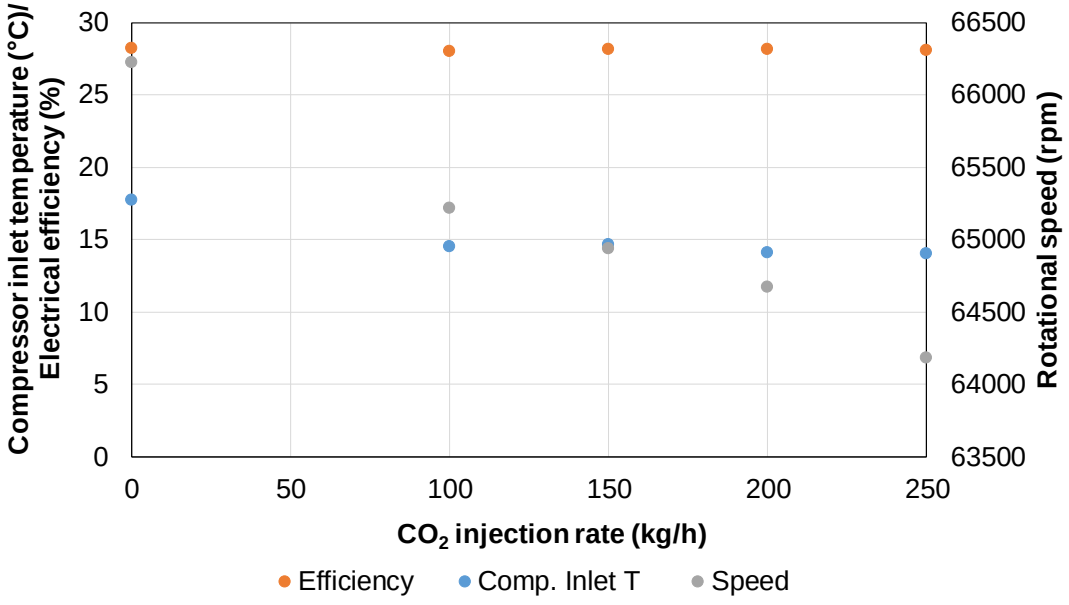

(b)

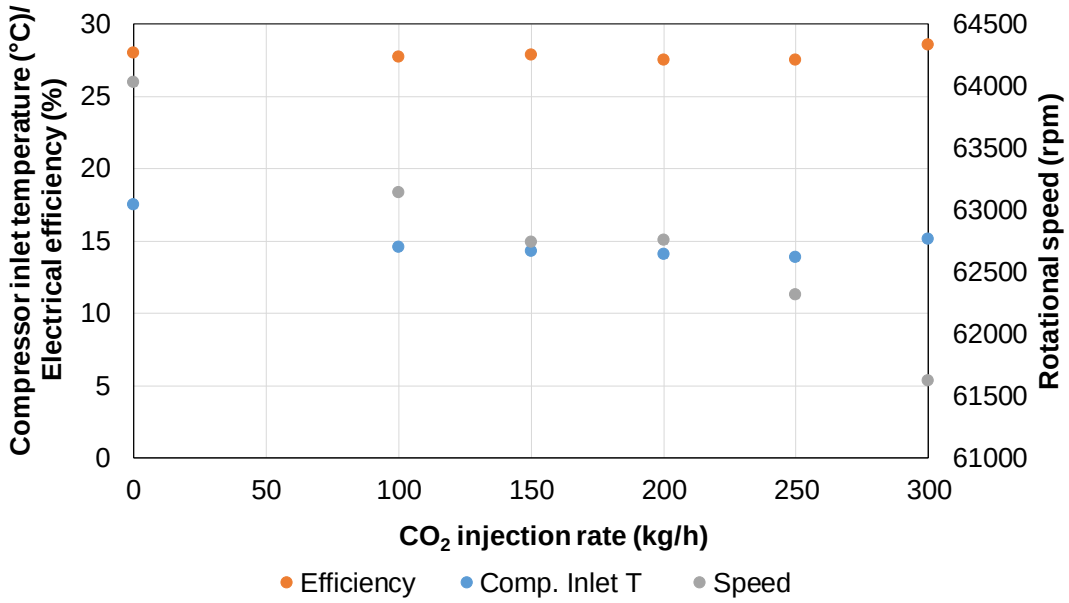
Compressor inlet temperature (°C)/
Electrical efficiency (%)
Rotational speed (rpm)
30
25
20
15
10
5
0
64500
64000
63500
63000
62500
62000
61500
61000
0
50
100
150
200
250
300
CO2 injection rate (kg/h)
Efficiency
Comp. Inlet T
Speed

(c)

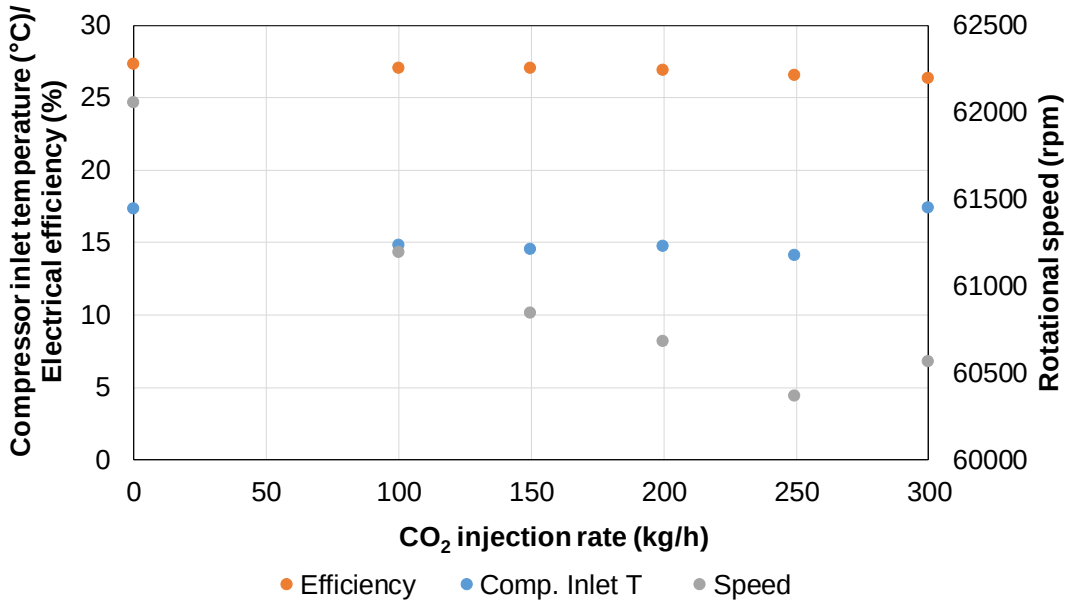
Compressor inlet temperature (°C)/
Electrical efficiency (%)
Rotational speed (rpm)
30
25
20
15
10
5
0
62500
62000
61500
61000
60500
60000
0
50
100
150
200
250
300
CO2 injection rate (kg/h)
Efficiency
Comp. Inlet T
Speed

(d)

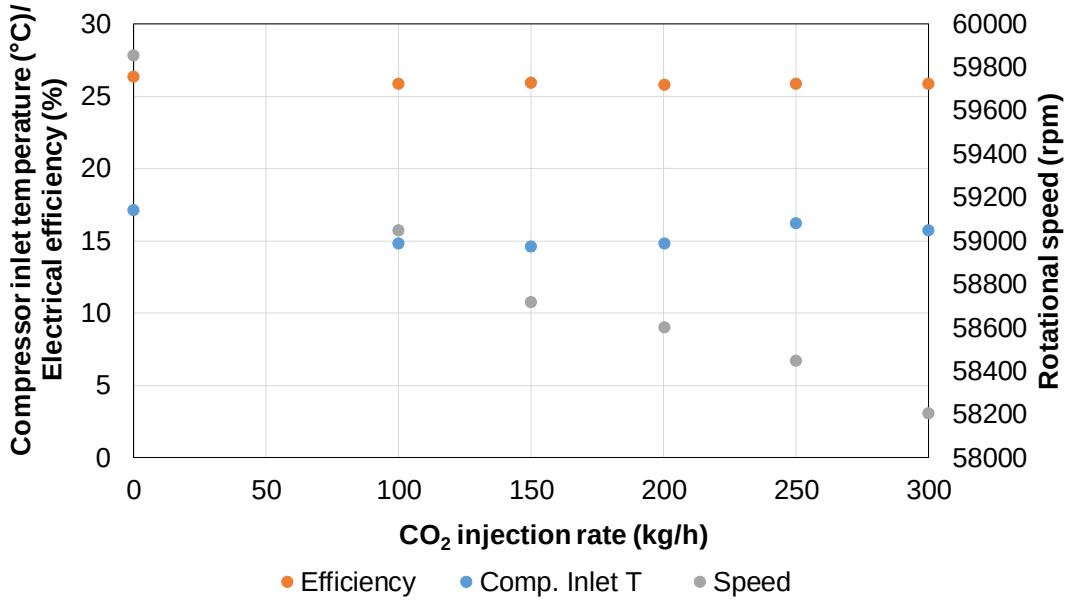

(e)

Figure 4.7. Influence of different S-EGR CO_2 injection rates on the compressor inlet temperature, electrical efficiency and rotational speed at (a) 100 kW_e, (b) 90 kW_e, (c) 80 kW_e, (d) 70 kW_e and (e) 60 kW_e.

The impacts of S-EGR conditions on the rotational speed of the mGT are also illustrated in Figure 4.7 (a)-(e). As expected, this variable decreases with reducing electrical power output, as it is a function of the volumetric gas flowrates required at each condition. Focusing on the CO_2 injection cases, the turbine rotational speed shows a decreasing trend when the CO_2 injection rate increases, with values ranging from 650 to 1400 rpm lower for the baseline compared to the higher CO_2 injection rates at power outputs of 60 and 100 kW_e respectively (see Figure 4.7 (a) and (e)). This is a result of a change in the properties of the working fluid due to the addition of CO_2, which is denser than the air. The mGT adjusts the amount of fuel and air required to achieve the desired power output under each set of experimental conditions. As discussed above, a fraction of the air flow is replaced by CO_2 in the S-EGR tests. Therefore, a similar mass flowrate passing through the turbine is equivalent to a lower volumetric air+CO_2 flowrate to deliver the desired power output, thus reducing the turbine rotational speed. This trend is seen for all power outputs, with greater speed reductions observed with increasing CO_2 injection rates. Similar trends have been reported by Mansouri Majoumerd et al. (2014) and Best et al. (2016), who both indicate rotational speed reduces with increasing CO_2 content in the oxidiser when testing lower CO_2 enhancement levels typical of EGR.

Small deviations from this trend are usually due to changes in the air temperature during the experiments, as seen in the 100 kW_e case with a CO_2 injection rate of 300 kg/h. The air density decreases when the temperature rises, and therefore the compressor rotates at higher speeds to maintain a similar mass flow of air through the turbine and thus deliver the same power output. This leads to an increase in the compressor work to generate the required electrical power output, which in turn leads to a slightly higher heat input and air demand. This is associated with increased rotational speeds in the mGT that offset the expected speed reductions due to the S-EGR conditions in this case. The mGT has not been programmed to operate under S-EGR conditions. Due to the changes in working fluid properties, the compressor and turbine maps would require reprogramming to account for these changes and therefore this is also a possible reason why these small variations are observed.

Throughout the baseline and simulated S-EGR tests, the compressor discharge pressure seldom changed for a specified power output; with the values ranging from 3.4-4.3 bara at 60-100 kW_e, respectively. Similar unchanged performance is reported by the modelling study of Herraiz et al. (2018), who found that the pressure ratio is not significantly affected under S-EGR operation. Moreover, the effect of S-EGR conditions on the compressor discharge temperature is shown in Figure 4.8 (p. 68) for the different CO_2 injection rates. As can be observed, this temperature increases with the power output, due to the higher-pressure ratios achieved. The addition of CO_2 which is mixed with the combustion air, changes the working fluid entering the compressor which has a lower specific heat capacity ratio due to the effect of CO_2. This results in a narrower temperature change for compression at a given pressure ratio (Best et al., 2016; Herraiz et al., 2018; Sander et al., 2011). Therefore, it is expected that the compressor outlet temperature decreases with increasing CO_2 injection rates for the same power output. However, the expected variation in the heat capacity ratio under S-EGR conditions is small, reducing by around 1-2% at the compressor inlet (Herraiz, 2016; Herraiz et al., 2018). Therefore, large changes in the compressor discharge temperature due to this effect were not expected in the CO_2 injection tests, as seen in Figure 4.8 (p. 68).

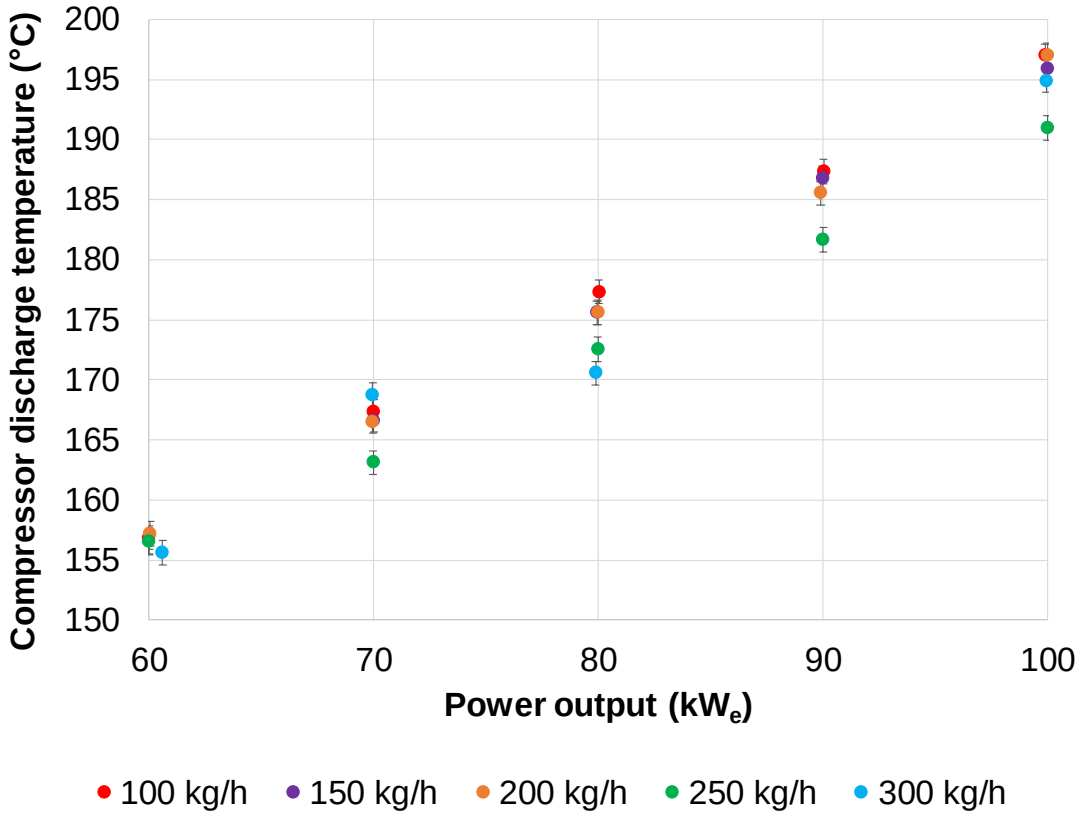

Figure 4.8. Influence of different S-EGR CO_2 injection rates on the compressor discharge temperature across the 60-100 kW_e operating envelope.

This figure shows there is a slight decrease in the temperature at the outlet of the compressor when increasing the CO_2 injection rate at 80 and 90 kW_e power outputs, as expected (7 and 6°C, respectively, between the minimum and the maximum CO_2 injection rate). However, no clear trend is seen for the other power outputs. This is because the compressor outlet temperature is more influenced by the air inlet temperature, which varies slightly between experiments, thus concealing the effect of a marginal reduction in the heat capacity ratio.

4.3.2 Influence of S-EGR on emission performance: NOx, CO and UHC

As discussed above, S-EGR operation changes the properties of the working fluid and reduces the O_2 concentration in the oxidiser that enters the combustor, which is affecting combustion efficiency and emissions performance (ElKady et al., 2009; Marsh et al., 2017, 2016). The calculated O_2 concentration at the compressor inlet for the tests included in this work is shown in Figure 4.9 (p. 69) across the 60-100 kW_e operating envelope. As can be seen, the O_2 concentration of the air+CO_2 mixture at the compressor inlet and at the inlet of the combustion chamber, ranged from 19.2 to 19.8 vol% for the maximum CO_2 injection rates tested in the mGT

across all power outputs which is an acceptable MOC. The reduced O_2 concentrations in the oxidiser together with the increased CO_2 content, impact the combustion performance. As discussed in section 2.5 of the literature review, reductions in the laminar flame speed and changes in the velocity field have been reported under CO_2-enhanced conditions because CO_2 dilutes the combustion mixture and the specific heat capacity changes due to this, thereby decreasing the flame temperature and the burning velocity (De Santis et al., 2016; Hinton and Stone, 2014). As a result, combustion efficiency reduces and the emission performance of the mGT is modified as depicted in Figures 4.10 to 4.12.

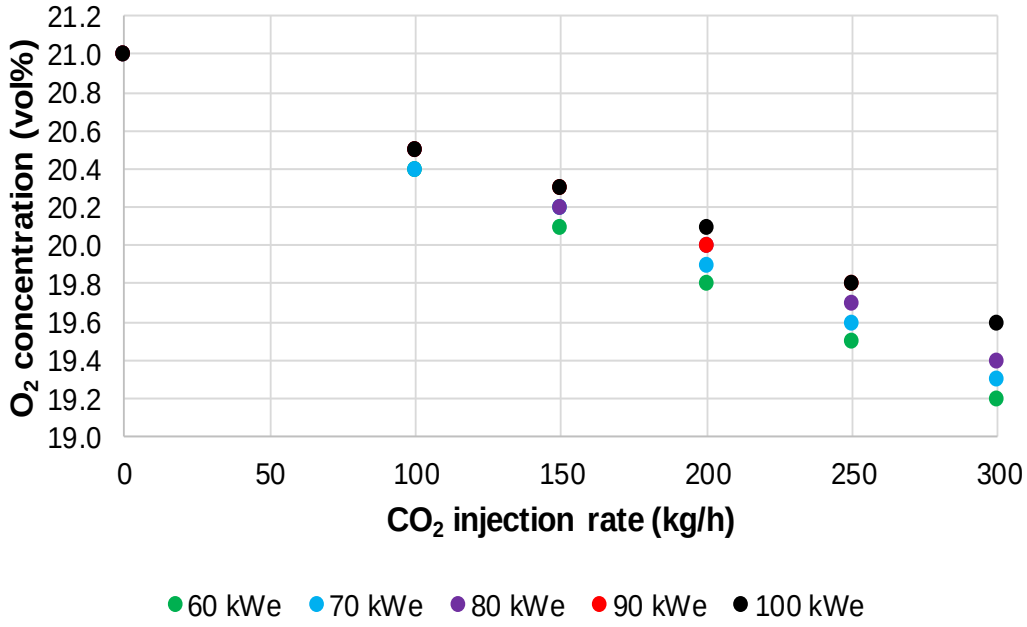

Figure 4.9. Influence of different S-EGR CO_2 injection rates on the compressor discharge temperature across the 60-100 kW_e operating envelope.

The measured NOx emissions in the baseline and S-EGR cases are shown in Figure 4.10, given by the emission index as per equation (4.4) (p.60) (ElKady et al. 2009). In general, as the net electrical power output decreases, the NOx emissions also decrease for both baseline and S-EGR conditions. This can be explained on the basis that the mGT operates under lean premixed combustion conditions where the formation of thermal NOx is associated with the Zeldovich mechanism (Seliger et al., 2015). The mGT NOx emissions are then mainly related to the combustion temperature which decreases at part load due to the higher air-fuel ratio (see Appendix A.3) in these cases and lead to lower thermal NOx values (De Santis et al., 2016; Seliger et al., 2015).

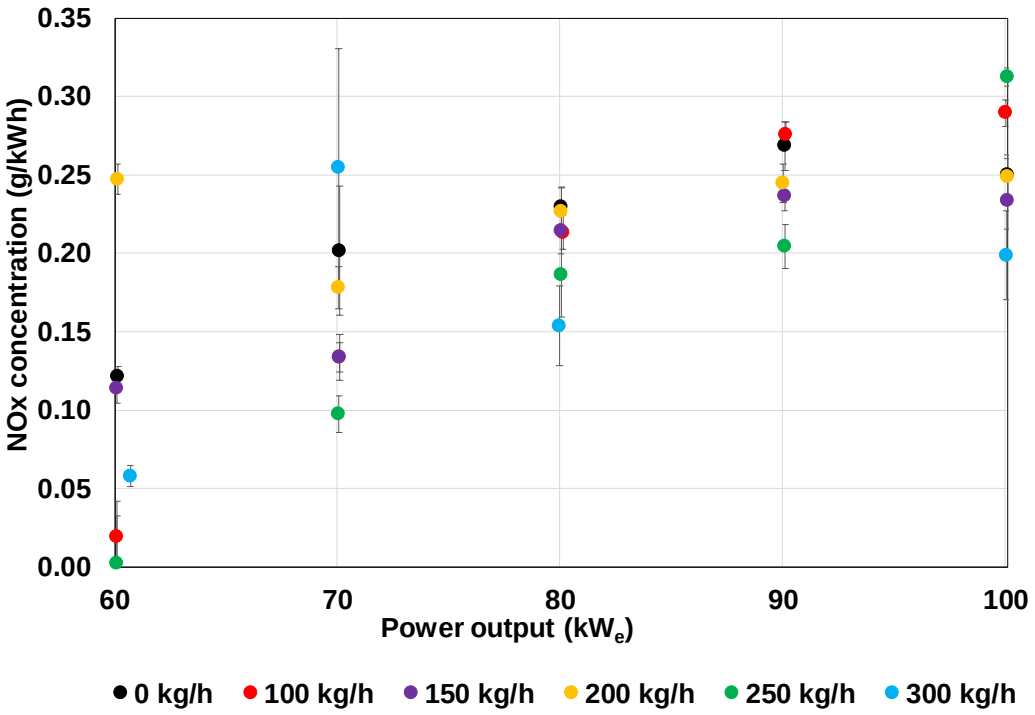

Figure 4.10. Influence of the different S-EGR CO_2 injection rates on flue gas NOx concentrations across the 60-100 kW_e operating envelope.

This represents ~61% reduction from 0.31 (100 kW_e) to 0.12 (60 kW_e) g/kWh for the baseline tests. Despite some dispersion in Figure 4.10, the influence of S-EGR on NOx emissions also demonstrates an overall reduction with increasing CO_2 injection rate compared to the baseline tests across the operating envelope tested. Similarly to the baseline cases, the reason for NOx emissions reductions with increasing CO_2 injection rates is due to slower flame speeds and greater radiative heat losses (De Santis et al., 2016; Lee et al., 2013; Marsh et al., 2017). This is caused by the change in the properties of the working fluid under CO_2-enhanced conditions, which lead to a reduction in the flame temperature and therefore lower thermal NOx production (De Santis et al., 2016; Lee et al., 2013; Marsh et al., 2017). It could therefore be expected that NOx emissions reduce with increasing CO_2 injection rates, however, there is no clear trend for the S-EGR cases shown in Figure 4.10. A possible reason why there is no obvious trend is likely due to the very lean flame conditions under normal operation without enhance CO_2 conditions. In Figure 4.10 the NOx concentrations are not corrected to 15% O_2 as the NOx emission index calculation (Eq. 4.4, p. 60) is used to calculate NOx emissions. Correcting NOx emissions to 15% O_2 could lead to an artificial reduction in the values of NOx emissions.

Measured CO and UHC emissions are illustrated in Figures 4.11 and 4.12 across all power outputs tested. As can be seen in Figure 4.11, CO emissions for the baseline tests increase from 2 ppmv at nominal conditions (100 kW_e) to 96 ppmv at lower loads (60 kW_e). CO concentrations in the flue gas increased from 2 ppmv (baseline) to 24 ppmv when injecting 300 kg/h CO_2 at 100 kW_e, and from 96 ppmv (baseline) to 516 ppmv at 60 kW_e with a 300 kg/h CO_2 injection rate.

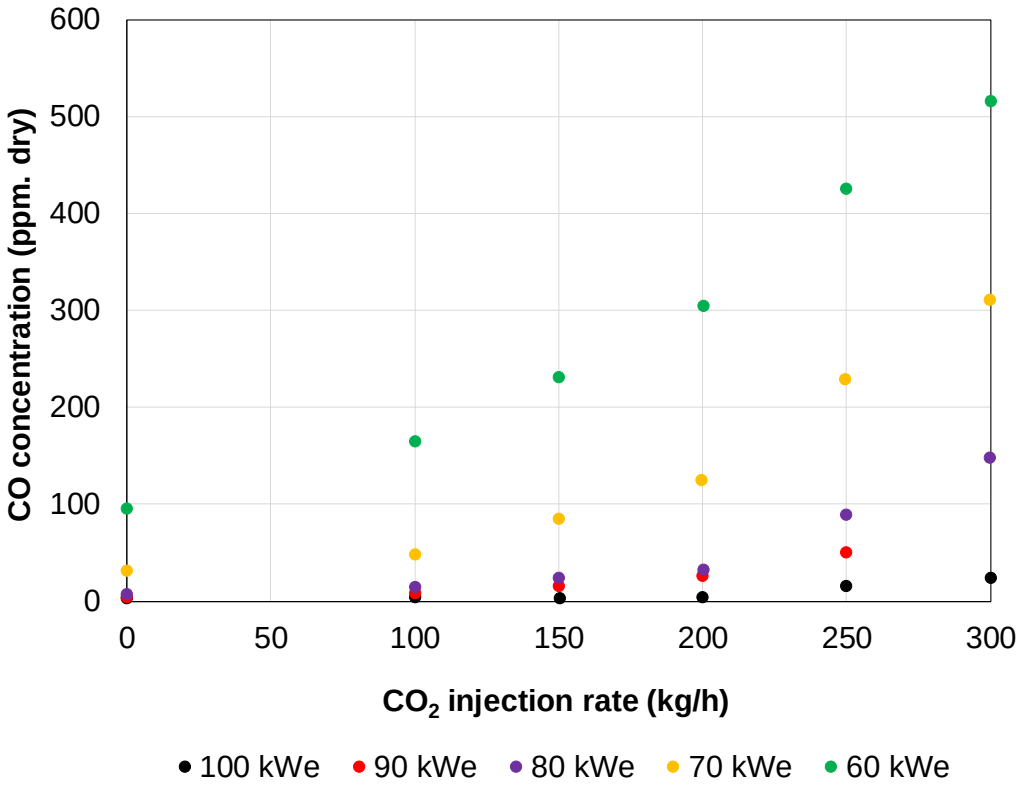

Figure 4.11. Influence of the different S-EGR CO_2 injection rates on flue gas CO concentrations across the 60-100 kW_e operating envelope.

Similarly, UHC emissions (CH_4 and C_2H_6) also experience a sharp increase when the mGT is operated at low power outputs, being close to zero at 100 kW_e and rising to 7 ppmv at 60 kW_e for the baseline (Figure 4.12, p. 71). Other UHC's recorded during the experiments included hexane, propane and ethylene, however, these emissions were negligible and within the FTIR error uncertainty. The increase in the recorded CO and UHC emissions at part load conditions can be associated with incomplete combustion due to poor fuel and air mixing, insufficient flame stability and lower combustion temperatures (Lefebvre and Ballal, 2010; Seliger et al., 2015). The $CO + OH \rightarrow CO_2 + H$ reaction rate is thus reduced which leads to increased CO emissions (Seliger et al., 2015).

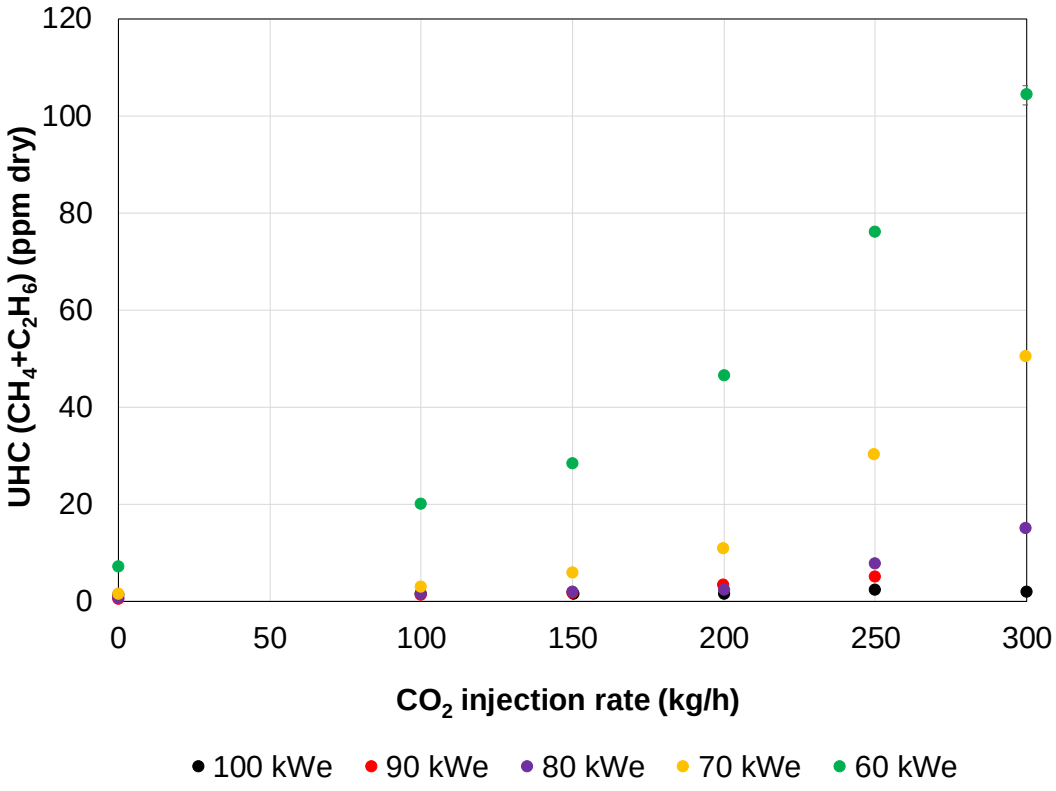

Figure 4.12. Influence of the different S-EGR CO_2 injection rates on flue gas UHC concentrations across the 60-100 kW_e operating envelope.

CO_2 thermal dissociation might also be considered as a possible reason for the increases in CO emissions outlined above. This typically occurs at flame temperatures above 1500°C (Evulet et al., 2009). De Santis et al. (2016) calculated that the maximum adiabatic flame temperature in a Turbec T100 combustor under EGR to be 2200°C which suggests that CO_2 thermal dissociation could potentially be occurring under simulated S-EGR. This might be unlikely as Marsh et al. (2017) indicated that increased CO emissions are likely to be associated with incomplete combustion instead of CO_2 dissociation, due to the reduction in temperatures, mixing and flame speeds as considered above. At part load operation, higher residence times of the exhaust gases inside the combustor would be required to ensure complete combustion and minimise CO emissions, as shown in the study by Zanger et al. (2013) using a Turbec T100 mGT.

These effects become more prominent with increasing CO_2 injections at each power output as discussed above, especially at lower power outputs, leading to increased emissions as shown in Figures 4.11 and 4.12. The reported levels of UHC presented in Figure 4.12 also follow a similar trend, supporting the incomplete combustion effects mentioned above. The UHC emissions remain at values lower

than 2-3 ppmv for all CO_2 injection cases when the nominal power output (100 kW_e) is set. However, they substantially increase under S-EGR conditions at lower power outputs, rising from 7 ppmv (baseline) to 104 ppmv (300 kg/h CO_2 injection rate) at 60 kW_e. These results show the emissions performance of the mGT varies slightly under S-EGR simulated conditions when it operates at the designed nominal power output (100 kW_e) with limited changes at nearby power outputs such as 80-90 kW_e. This is affected by increases in the CO_2 content of the oxidiser at lower power outputs. These large increases in emissions at the lowest power outputs, are substantially higher than those reported under EGR conditions (Best et al., 2016), indicate that the compressor and turbine maps require reprogramming to operate under S-EGR conditions. Reprogramming the engine to operate under S-EGR will allow the gas turbine to maintain enough heat throughput for gas turbines operating under S-EGR scenarios to ensure appropriate full and part-load emission performance.

4.4 Chapter conclusions

A pilot-scale experimental study investigating the performance of a Turbec T100 Series 3 mGT under simulated S-EGR conditions has been conducted. The mGT has been modified to incorporate a CO_2 delivery system to investigate a range of conditions characteristic of S-EGR. The conditions tested led to a maximum increase in the flue gas CO_2 concentrations of ~400% and ~600% at 100 and 60 kW_e, respectively, similar to what is expected in S-EGR systems. The experimental results indicate that the electrical efficiency marginally decreases by ~8 to 4% under S-EGR conditions compared to the baseline values without CO_2 injection, due to the modified heat capacity of the working fluid which leads to reductions in the turbine inlet temperature. The mGT rotational speed decreased by 650 to 1400 rpm under S-EGR conditions compared to the baseline. This is attributed to the higher density of the working fluid. However, variations in compressor discharge pressure were negligible throughout the CO_2 enhancement tests. The compressor discharge temperature showed a slightly decreasing trend in the S-EGR scenarios.

The O_2 concentration decreased with increasing CO_2 injection rates, impacting the mGT combustion and emission performance. The NOx emissions show a generally decreasing trend under the simulated S-EGR conditions due to the effect that the lower associated combustion temperatures have on thermal NOx formation. The emissions of CO and UHC increased under S-EGR conditions due to incomplete combustion mostly at lower power outputs. Nonetheless, the increases in such

emissions at higher power outputs are limited. The experimental results demonstrate a stable mGT operation across the operating envelope considered.

The increased CO_2 concentrations reported here could offer potential economic and energy savings for the downstream CO_2 capture plant. The emission performance results indicate that modifications to the design of the combustion chamber might be needed for gas turbines operating under S-EGR scenarios to ensure appropriate emission performance especially at part loads.

5 Experimental investigation of the impacts of selective exhaust gas recirculation on an amine CO_2 capture plant

5.1 Introduction

This work evaluates the influence of selective CO_2 recirculation conditions on the performance of a solvent based CO_2 capture plant (herein referred to as the (ACP) at the PACT core facilities located in Sheffield, UK (PACT, 2018). This chapter evaluates two experimental campaigns under S-EGR conditions using flue gas CO_2 concentrations representing those recorded in the mGT at 80 kW_e in the preceding chapter. The flue gas CO_2 concentration at this power output for CO_2 injection rates of 150-300 kg/h is ~5.3-9.2 vol% (dry basis), respectively. To the author's knowledge, no works have experimentally investigated the influence of S-EGR on amine CO_2 capture plant performance using 40 wt% MEA at pilot scale. This is important because it will provide key information about operating the ACP under S-EGR which can be used to assist in the development of gas-CCS and for knowledge transfer. Akram et al. (2016) investigated the performance for EGR at CO_2 concentrations up to ~10 vol% using 30 wt% MEA solvent. In addition, recent modelling studies have investigated commercial scale CCGT's coupled with parallel, series or hybrid S-EGR configurations (Diego et al., 2018, 2017b; Herraiz et al., 2018). Therefore, this work aims to analyse the ACP performance under conditions representing S-EGR.

5.2 Experimental methodology

5.2.1 Amine capture plant

The ACP illustrated in Figure 5.1 (p. 76) and 5.2 (p. 78), is designed to capture 1 tonne per day of CO_2 using 30 wt% MEA solvent, based on coal combustion (Akram et al., 2016). This study uses 40 wt% MEA solvent with Sulzer Mellapak CC3 structured packing in the absorber and desorber. The 40 wt% MEA solvent was chosen because of the limited number of studies which use this concentration and the potential reductions in the energy penalty it could lead to. This packing is used as it has been specifically designed for post-combustion CO_2 capture processes

(Menon and Duss, 2010). Structured packing is also used due to the lower economic costs and ease of installation compared to random packing (Rousseau, 1987). The packing height and diameter are 6.5 m and 0.3 m in both columns, respectively. The ACP has the capability to treat flue gases from a range of combustion processes including the Turbec T100 S3 mGT. The flue gas flowrate exiting the mGT system is typically 0.80 kg/s at ISO conditions (100 kW_e) (Turbec, 2009). The ACP (Figure 5.1) is designed to operate at lower flue gas flowrates (~250 Nm^3/h / ~320 kg/h).

Figure 5.1. Photograph of the pilot-scale post-combustion CO_2 capture plant.

This means that the combined operation (mGT+ACP) requires a proportion of the mGT flue gas to be taken from a slipstream. Typically, under ISO conditions the CO_2 concentration of the mGT flue gas is ~1.7 vol% (dry basis) at full load. In order for successful ACP operation, the flue gas stream entering the absorber should be at least 4-5 vol%. To augment the CO_2 flue gas concentration a synthetic gas-mixing skid is used. This system mixes ambient air and CO_2 from a cryogenic tank to achieve the desired CO_2 concentration to represent the conditions to be investigated. The gas mixing controls the flow of synthetic gas via Siemens Coriolis mass flow meters and pneumatically actuated flow control valves. The flowrate is measured and recorded at the skid via the SCADA system. Operating under synthetic flue gas conditions is limiting because the flue gas contains a negligible water vapour or emission species such as CO and UHC similar to the flue gas conditions under mGT+S-EGR operation. The mGT has been modified to investigate a range of conditions characterising S-EGR as illustrated in chapter 4. Due to a technical fault associated with a damaged fuel booster, combining experiments sequentially (mGT+ACP) was not possible. Therefore, the ACP experiments were conducted using the synthetic gas-mixing skid to represent S-

EGR conditions investigated in the previous chapter at part load operation, thus mixing CO_2 and air. The mGT flue gas CO_2 concentrations at 80 kW_e and the synthetic gas skid concentrations are presented in Table 5.1.

Table 5.1. CO_2 concentrations.

	CO_2 concentration (vol%, dry)			
mGT	5.3	6.6	7.9	9.2
Synthetic skid	5.2	6.5	7.5	9.0

As illustrated in Figure 5.2 (p. 78), the booster fan drives the synthetic flue gas stream into the absorber which flows upwards and comes into contact with the counter-current lean liquid solvent flowing downwards. The ACP investigated here is a scaled down version of a commercial scale ACP. The CO_2 free flue gas exits the absorber entering the water wash column which eradicates entrained solvent droplets prior to being discharged to the atmosphere (Akram et al., 2016). However, small MEA concentrations might also be discharged to the atmosphere. The water used in the water wash column is recirculated to continue the process. In addition, water losses are experienced due to the lower synthetic flue gas water content which subsequently increases MEA concentration by 2-3 wt% per day, hence, the water levels are topped up (Tait et al., 2018). The rich solvent stream descends through the desorber contacting with the rising CO_2+H_2O stream exiting the reboiler. The rich solvent stream is heated up by the pressurised hot water which promotes CO_2 liberation. The gaseous CO_2 rich+H_2O stream flowing out of the desorber is condensed to eliminate entrained water and MEA droplets. Subsequently, excess condensate is removed via a reflux drum into the desorber and the gaseous CO_2 rich stream is released to the atmosphere. The lean solvent stream leaves the reboiler, flowing through the lean solvent pump, cooler and activated carbon filter prior to re-entering the absorber column. The cooler lowers the temperature of the lean solvent flowrate temperature and the activated carbon filter removes solvent degradation products (Akram et al., 2016). The thermal input to the reboiler at PACT is supplied using pressurised hot water instead of steam. To allow for comprehensive data collection, the ACP has been modified with instrumentation, including thermocouples, pressure transmitters and flow meters. These devices were installed prior to conducting the experiments in this chapter for previous experimental research. As these devices were installed prior to conducting this research, it was not possible to determine the instrument error as per the manufacturer's guidance. Therefore, the standard error has been used to determine the error and accuracy of the results presented (see Appendix A.5).

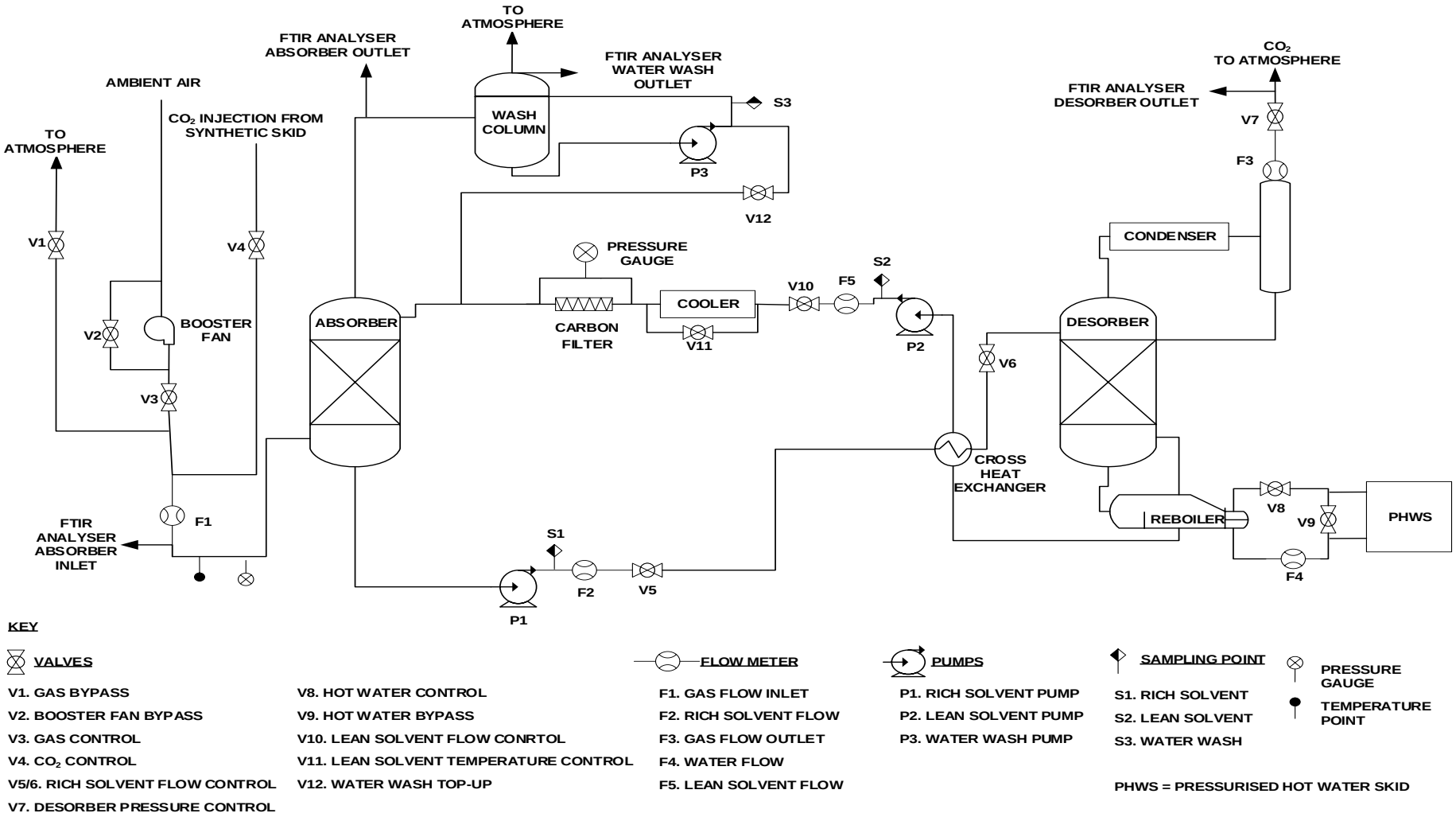

Figure 5.2. Schematic of the ACP.

5.2.1.1 Test campaign 1: Varying the CO_2 concentration

In this experimental campaign, conditions characteristic of simulated S-EGR are investigated to determine the impact on ACP performance. The synthetic flue gas CO_2 concentrations ranged from 5.2-9.0 vol% (dry basis). These concentrations were selected to represent part load operation (80 kW_e) of the mGT under S-EGR conditions, investigated in the previous chapter. The reason why S-EGR conditions at 80 kW_e were selected is because flexible part load gas turbine and ACP operation is anticipated to become more important in the future energy scenarios. Hence, it is important to understand the behaviour of the ACP under S-EGR conditions under part load mGT operation (see Chapter 4 for mGT performance). Depending on which S-EGR configuration is used, the S-EGR ratio, the CO_2 concentration sent to the ACP, the CO_2 capture efficiency and selective membrane CO_2 transfer efficiency will vary. As no membrane system was used in this work, this is difficult to quantify the solvent flowrate was changed to achieve ~90% CO_2 capture efficiency in each experiment and the pressurised hot water inlet temperature was fixed at ~126°C and pressure of 1.5 bara. The pressurised hot water is used to in the reboiler main body to transfer heat to the rich solvent to strip CO_2. The experimental parameters for test campaign 1, including the calculated maximum standard deviation for the results are presented in Table 5.2. The rich solvent flowrate was varied to control the absorber and desorber levels to ensure stable ACP operation. Appendix A.5 presents the standard error values for the experimental tests.

Table 5.2. Test campaign 1 experimental conditions.

Parameter	Unit	Max. STDev (±)	Test 1	Test 2	Test 3	Test 4
Synthetic CO_2 conc. (dry basis)	vol%	0.9	5.2	6.5	7.6	9.0
Synthetic flue gas flowrate	Nm^3/h	7.2	170.1	171.8	171.0	173.2
Flue gas inlet temperature	°C	0.5	41.7	39.3	39.6	39.6
Flue gas outlet temperature	°C	0.6	48.1	49.2	42.5	41.2
Flue gas inlet pressure	bara	0	1.04	1.04	1.05	1.05
Flue gas outlet pressure	bara	0	1.04	1.04	1.05	1.05
Lean solvent flowrate	kg/h	59.1	476.5	578.8	859.2	990.9
Lean solvent temperature	°C	0.6	40.2	40.1	39.9	39.9
Rich solvent flowrate	kg/h	114.	480.9	601.8	898.6	1020.7
PHW flowrate	m^3/h	0.3	11.4	11.4	11.4	11.3
PHW inlet temperature	°C	1.7	125.7	125.6	125.6	125.6
PHW outlet temperature	°C	0.8	122.7	122.4	121.5	121.3
Cold approach temperature	°C	-	26.6	27.4	27.4	26.9
Hot approach temperature	°C	-	26.0	27.0	27.1	26.6

5.2.1.2 Test campaign 2: Varying the hot water inlet temperature

In this experimental campaign, the influence of a fixed solvent flowrate and varied pressurised hot water inlet temperatures (124-127°C) on the ACP performance under simulated S-EGR was investigated. The reason for investigating varying hot water inlet temperature was to determine if there is an optimal reboiler temperature using 40 wt% MEA and fixed ~9.0 vol% (dry basis) flue gas CO_2 concentration. The highest CO_2 concentration was selected to represent the augmented CO_2 flue gas streams expected in S-EGR configurations. Operating at different reboiler temperatures might be beneficial depending on which process configuration and solvent concentration are used for amine-based CO_2 capture. The experimental parameters for test campaign 2 including the calculated maximum standard deviation are presented in Table 5.3. Test 4 from test campaign 1 was used as the baseline where the solvent flowrate is fixed at ~990 kg/h. This fixed flowrate is used because for the baseline test, this represents a 90% CO_2 capture efficiency. As the reboiler temperature varies at a fixed solvent flowrate, the CO_2 capture efficiency will change.

Table 5.3. Test campaign 2 experimental conditions.

Parameter	Unit	Max. STDev (±)	Baseline	Test 2	Test 3	Test 4
PHW inlet temperature	°C	1.6	125.6	126.8	124.7	123.7
Synthetic CO_2 conc. (dry basis)	vol%	0.5	9.0	9.0	9.0	9.0
Synthetic flue gas flowrate	Nm^3/h	17.9	173.2	169.7	170.0	166.6
Flue gas inlet temperature	°C	0.6	39.6	40.9	40.6	40.8
Flue gas outlet temperature	°C	0.6	41.2	41.4	41.8	41.6
Flue gas inlet pressure	bara	0	1.05	1.04	1.05	1.05
Flue gas outlet pressure	bara	0	1.05	1.04	1.05	1.05
Lean solvent flowrate	kg/h	59.4	990.9	947.6	981.9	985.8
Lean solvent temperature	°C	0.6	39.9	40.0	40.1	40.1
Rich solvent flowrate	kg/h	114.0	1020.7	1011.7	1001.6	1021.9
PHW flowrate	m^3/h	0.3	11.3	11.1	11.1	11.1
PHW outlet temperature	°C	0.8	121.3	122.2	120.5	119.5
Cold approach temperature	°C	-	26.9	26.9	26.7	27.1
Hot approach temperature	°C	-	26.6	26.5	26.3	26.7

5.2.2 Data collection and system monitoring

The ACP uses the Programmable Logic Controller (PLC) system to monitor and control various operational parameters, for example, solvent flowrate and desorber pressure. The PLC system allows the plant operator to start, stop and control several parameters of the ACP. The desorber pressure was set at 0.5 ±0.02 barg (~1.5 bara) throughout the experiments using the proportional integral derivative (PID) control. The rich and lean solvent flowrates are also controlled via the PLC using the control valves to achieve the desired flowrate for each experiment. In addition to the PLC system, additional instrumentation has been installed onto the ACP. This includes monitoring for temperatures, pressures and flowrates which are recorded through LabVIEW. Tables 5.2 and 5.3 illustrate the recorded parameters and calculated maximum standard deviation. The PLC data is recorded every 20 seconds and LabVIEW data is recorded every second. The absorber and desorber have been instrumented to allow for the temperature profile across the columns to be determined as shown in Tables 5.4 and 5.5, respectively. The thermocouple numbers are located from the bottom to the top of the columns with the first measurement points at the absorber flue gas entry point and desorber bottom, respectively. Appendix A.5 provides the standard error data for the absorber and desorber thermocouples of each experiment.

Table 5.4. Absorber thermocouple locations and maximum standard error.

No.	Height (m) at flue gas entry to the absorber	TC no.	Test campaign 1	Test campaign 2
			Max. Standard Error (±°C)	
1	0.6	T121	0.022	0.013
2	1.2	T124	0.032	0.018
3	1.9	T127	0.040	0.018
4	2.6	T130	0.042	0.021
5	3.3	T133	-	-
6	4.0	T136	0.034	0.026
7	4.7	T139	0.034	0.034
8	5.4	T142	-	-
9	6.0	T145	0.030	0.041
10	6.7	T148	0.065	0.035

Table 5.5. Desorber thermocouple locations and maximum standard error.

No.	Height (m) at the bottom of the desorber	TC no.	Test campaign 1	Test campaign 2
			Max. Standard Error (±°C)	
1	0.4	T308	0.058	0.036
2	1.3	T317	0.051	0.056
3	2.2	T316	0.057	0.032
4	3.0	T321	-	-
5	3.9	T309	-	-
6	4.8	T312	0.055	0.020
7	5.7	T311	-	-
8	7.1	T310	-	-
9	7.6	T307	0.088	0.020

5.2.3 Gas analysers

The gaseous emissions are recorded online using a Gasmet FTIR DX4000 gas analyser over four different locations: the absorber inlet, absorber outlet, water wash column outlet and desorber outlet, as illustrated in Figure 5.2 (p. 78). Sampling across each of the FTIR locations was performed throughout the experiments with average measurement times of: absorber inlet and outlet ~30 minutes, water wash outlet ~4 minutes and desorber outlet ~5 minutes. Due to a technical issue recording at the wash column and desorber outlet, it was not possible to assess the data for Test 1 (5.2 vol% CO_2) in the first experimental campaign at these locations.

5.2.4 Solvent sampling and titration

The solvent loading is the ratio between the moles of CO_2 and moles of MEA. Lean solvent loading is defined when the MEA solvent is desorbed of CO_2 (typically when exiting the stripper and entering the top of the absorber). The rich solvent loading is when the MEA solvent is loaded with CO_2 after exiting the absorber. Rich and lean solvent samples were taken manually at the end of each test (see sampling point locations in Figure 5.2) for each experiment to determine rich and lean loadings. Water wash samples were also taken to monitor MEA levels transferred to the wash column from the flue gas. The samples were analysed using a Mettler Toledo T90 automatic titrator. To determine the CO_2 loading of the samples, 50 ml of methanol is loaded into the analyser port of the titrator where the pH level is increased to ~11.2 by adding 0.5M sodium hydroxide (NaOH) from the titrator pumps. A pipette

is used to add ~1 ml of the collected solvent sample into the methanol and titrated with NaOH to a pH of ~11.2. MEA concentrations are determined by adding ~50 ml of deionised water into a beaker and ~1 ml of the collected sample and titrating this with 0.2M hydrochloric acid (HCL) to a ~4.8 pH. Tait et al. (2018) identified that the measurement uncertainty for this procedure to be ±3.2%.

5.2.5 Iron measurements

A HACH Pocket Colorimeter II was used to measure the iron content of the solvent samples at the end of each test day. This was to determine the rate of solvent degradation due to the effects of oxidative degradation. To determine the iron content the sample cell is filled with 10 ml of rich solvent taken from the sampling point on the ACP, see Figure 5.2, which is mixed with FerroVer Iron Reagent Powder Pillow for a period of three minutes (HACH, 2014). During the mixing period, a blank sample is also prepared, where 10 ml of solvent is added to a vile. Once the three minute period expires the blank sample cell is cleaned and added to the HACH Pocket Colorimeter II cell holder and zeroed. Subsequently, the sample mixed with the reagent powder is measured using the colorimeter to determine the iron content in mg/L.

5.2.6 ACP performance calculations

The ACP performance is determined in terms of CO_2 capture rate and specific reboiler duty. The CO_2 capture rate $(CO_{2,CR})$ is determined from (Akram et al., 2016):

$$CO_{2,CR}\ (kg/h) = \left(nCO_{2Abs_{in}} - nCO_{2Abs_{out}}\right).MWCO_2/1000 \quad \textbf{(5.1)}$$

where $nCO_{2Abs_{in}}$ and $nCO_{2Abs_{out}}$ is the CO_2 molar flowrate entering and leaving the absorber in mol/h and $MWCO_2$ is the CO_2 molecular weight.

The reboiler duty (RD) is calculated from (Akram et al., 2016):

$$RD\ (kJ/h) = PHW_f.cp.(\Delta T) \quad \textbf{(5.2)}$$

where PHW_f is the pressurised hot water flowrate in kg/h, cp is the specific heat capacity of water in kJ/kg K and ΔT is the temperature difference between the pressurised hot water inlet and outlet temperature in K. The specific reboiler duty is calculated from (Akram et al., 2016):

$$Specific\ reboiler\ duty\ (MJ/kg) = \left(\frac{RD}{CO_{2,CR}}\right)/1000 \quad \textbf{(5.3)}$$

5.3 Results and discussion

The experimental results from both experimental campaigns are summarised in Appendix A.4. In both experimental campaigns, the solvent concentration was thought to be 40 wt% MEA, however, the measured concentrations were up to 6.8 and 9% lower for experimental campaigns 1 and 2, respectively.

In the work by Akram et al. (2016) they identified that the rich and lean solvent concentrations varied above or below the 30 wt% MEA investigated. These authors also attribute this to either evaporation losses or solvent degradation. Experimental work by Tait et al. (2018) at the PACT facilities used a 30 wt% MEA concentration and also observed varying amine concentration of 28-35%. These authors note that the synthetic flue gas mixture is unsaturated which means that the H_2O content is ~1 vol%, leading to water losses in the absorber flue gas outlet stream (Tait et al., 2018).

In addition to the water losses resulting in varying solvent concentration, solvent degradation is a possible reason for the lower solvent concentrations reported in the results presented in Appendix A.4. In the literature, thermal and oxidative degradation of MEA in CO_2 capture plants is widely reported (e.g. Bedell, 2009; Chi and Rochelle, 2002; Davis and Rochelle, 2009; Du et al., 2016; Fredriksen and Jens, 2013; Gouedard et al., 2012; Sexton and Rochelle, 2011). Oxidative degradation typically occurs in the absorber where the flue gas O_2 concentration is the greatest. For example, in CCGT's with ACP the flue gas O_2 concentrations are ~12 vol% (IEAGHG, 2012a). However, this concentration is likely to reduce under S-EGR operation as shown in the following modelling studies. Diego et al. (2018, 2017b) investigated parallel and hybrid S-EGR configurations at commercial scale, where the flue gas O_2 concentration reduced to 11.3 and 7.1 vol%, respectively. Herraiz et al. (2018) also showed O_2 concentrations in the flue gas stream varied from ~10-11 vol% and 9 vol% for series and parallel S-EGR, respectively. The flue gas O_2 concentrations at 80 kW_e under S-EGR for the mGT experiments ranged from 16.7-17.4 vol% (dry basis) and ~19 vol% under standard operation. The higher O_2 concentrations in the mGT experiments are because of the much higher excess air requirements than in commercial scale gas turbines, but still shows reduced O_2 concentrations sent to the ACP under S-EGR. The synthetic flue gas O_2 concentration sent to the absorber remained around 17 vol% throughout the experimental campaigns, representing similar concentrations to the mGT tests.

Oxidative degradation occurs due to MEA solvent disintegration which is catalysed in the presence of dissolved metal ions such as iron via electron abstraction mechanisms (Bedell, 2009; Chi and Rochelle, 2002; Fredriksen and Jens, 2013; Goff and Rochelle, 2004; Gouedard et al., 2012; Sexton and Rochelle, 2011). The electron abstraction mechanism uses a free radical, for example Fe^{3+}, which eradicates an electron from N_2 in the amine group (Goff and Rochelle, 2004; Gouedard et al., 2012). The resulting amine radical is transferred (de-protonated) to form an imine radical, which leads to aldehyde and ammonia formation due to its reaction with H_2O (Goff and Rochelle, 2004; Gouedard et al., 2012). The main MEA degradation product is NH_3, with subsequent degradation products being aldehydes (Goff and Rochelle, 2004; Gouedard et al., 2012). In the presence of O_2, these products will form carboxylic acids due to the oxidization mechanism. The production of these acids leads to corrosion and fouling issues, which ultimately leads to increased operating costs. Furthermore, NH_3 formation is greater at higher MEA concentrations and the rate of degradation is linked to the solvent temperature and metal ion concentrations (Chi and Rochelle, 2002; Goff and Rochelle, 2004). As the lean solvent temperature remained at ~40°C for all the experiments, the effect of temperature on oxidative degradation will be the same, thus, oxidative degradation is likely due to the metal ion concentrations. The iron content was measured at the end of each test day, where the iron concentration increased from 9.16 mg/L (test day 1), 14.4 mg/L (test day 2) to 15.64 mg/L (test day 3), representing a 71% increase over the three day testing campaign. As noted above, the presence of dissolved metal ions leads to oxidative solvent degradation, hence, it is likely that this has contributed to lower solvent concentrations. Chi and Rochelle (2002) also noted that NH_3 formation increases with increasing O_2 concentration. The O_2 and NH_3 concentrations reported in Tables 5.6 and 5.7 show this trend which also supports that oxidative solvent degradation has led to reduced solvent concentrations.

Thermal solvent degradation typically occurs in the stripper and reboiler due to higher temperatures (Davis and Rochelle, 2009). Thermal degradation is also caused by operating at elevated stripper pressures, although this has been shown to reduce stripper energy requirements (Oyenekan and Rochelle, 2007, 2006). However, operating at higher stripper temperatures and pressures promotes thermal solvent degradation which is associated with carbamate polymerization (Davis and Rochelle, 2009; Polderman et al., 1955; Yazvikova, 1975). The thermal degradation products formed from carbamate polymerization include 2-oxazolidone,

dihydroxyethylurea, 1-(2-hydroxyethyl)-2-imidazolidone (HEIA) and N-(2-hydroxyethyl)-ethylenediamine (HEEDA) (Davis and Rochelle, 2009). The formation of these four species is associated with the stripper temperature, CO_2 loading and solvent concentration (Davis and Rochelle, 2009). In this work, the reboiler pressure remained constant for all the experiments at ~1.5 bara whereas the pressurised hot water inlet temperature was kept either constant (126°C) or varied (124-127°C). As the solvent concentration used was 40 wt% MEA, this means that the boiling point is higher compared to using a 30 wt% MEA solvent, as well as the reboiler temperature which will augment the rate of thermal degradation. Davis and Rochelle's (2009) also indicated this and demonstrated that ~67% of thermal degradation arises in the reboiler sump and ~33% develops in the stripper packing. These authors also show that the loss of MEA solvent increases by up to 7 times with a 20°C rise in stripper temperature from 108-128°C (Davis and Rochelle, 2009). Furthermore, the higher CO_2 concentrations considered here will lead to increased CO_2 loadings. This has also been shown to increase the thermal degradation rate (Davis and Rochelle, 2009). Hence, due to the elevated pressurised hot water temperatures considered in this work, thermal degradation can also be attributed to the lower solvent concentrations reported in Appendix A.4. In optimised S-EGR configerations, thermal degdration in the downstream capture plant is not anticpated to be of major concern. The results presented here idicates that operating the stripper at lower temperature reduces the rate of thermal degdradation. Hence, for optimised S-EGR systems, the reboiler duty will be lower ~3-4 MJ/kg and the stripper temperature will be operating at the optimal temperature for amine based scrubbing ~120°C.

5.3.1 Influence of S-EGR on the solvent loadings

The impact of increased flue gas CO_2 concentrations on the rich and lean CO_2 loadings is presented in Figure 5.3 (p. 87); as the CO_2 concentration increases both the lean and rich loadings also increase. The rich loadings increased from 0.378 to 0.399 mol CO_2/mol MEA and lean loadings increased from 0.262 to 0.319 mol CO_2/mol MEA at CO_2 concentrations in the absorber inlet gas of 5.2 and 9.0 vol%, respectively. This represents a 5.6 and 21.8% increase for the rich and lean loadings. As noted in chapter 3, the theoretical maximum of CO_2 loading is 0.5 mol CO_2/mol MEA (Gouedard et al., 2014; Nielsen et al., 2012). Thus, the cyclic capacity is important to understand the solvent loading characteristics. This can be defined as the difference between the CO_2 loading for the gas to liquid equilibrium for absorption and regeneration (Fan et al., 2016). The mass transfer of CO_2 from

the gas to liquid phase is related to the interfacial area, mass transfer coefficients and the driving force in the absorber column (Notz et al., 2012). The driving force in the absorber is linked to the distance between the operating and equilibrium lines and the CO_2 mass transfer profile which is influenced by the absorption reaction kinetics (Notz et al., 2012).

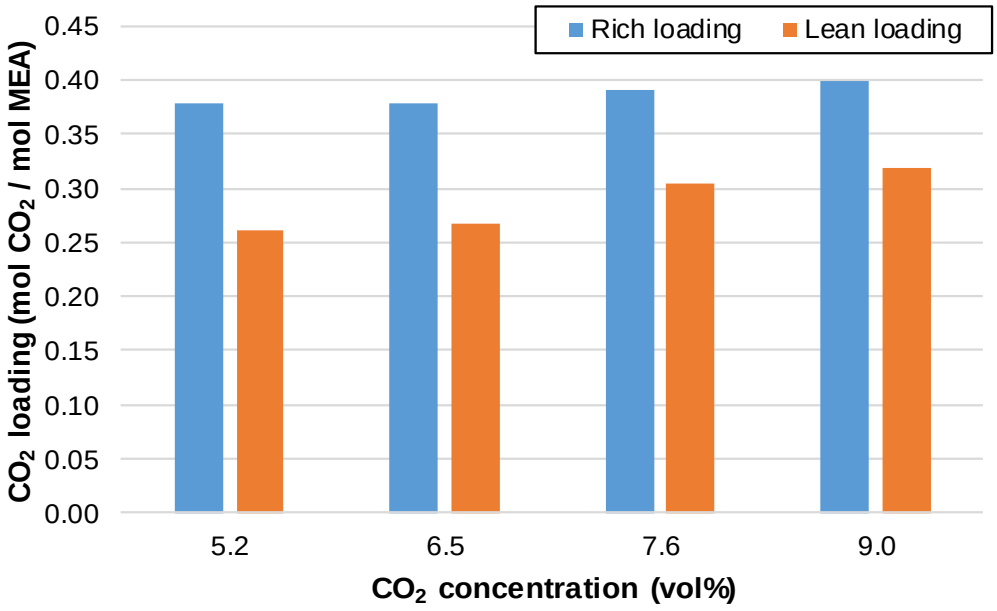

Figure 5.3. Influence of increasing CO_2 concentration on rich and lean solvent loading.

At higher CO_2 concentrations, the driving force increases at a constant interfacial area and the reaction rate of bicarbonate and carbamate formation is faster (Notz et al., 2012). The mass transfer coefficients (gas phase driving force and mass transfer) also increases with higher CO_2 concentrations (Wu et al., 2017). Furthermore, higher MEA concentrations will have more molecules available to react with CO_2, leading to improved mass transfer (Wu et al., 2017). Abu-Zahra et al. (2007) process modelling and economic study investigated the influence of different MEA concentrations including 40 wt% MEA from coal-fired power generation with ~13 vol% CO_2 (wet basis). The results from this study indicate that the optimal lean and rich solvent loading for 40 wt% MEA is ~0.30 and ~0.47 mol CO_2/mol MEA. Brigman et al. (2014) experimental study investigated the ACP performance using of 30 and 40 wt% MEA when treating flue gases from a combined heat and power plant with typical CO_2 flue gas concentrations of ~3.5 vol%. Their finding suggests that lean solvent loading ranged from ~0.2-0.30 mol CO_2/mol MEA. Akram et al. (2016) also investigated 30 wt% MEA under similar operating conditions considered in this work. These authors also highlighted that both rich and lean solvent loadings increased with higher CO_2 concentrations. They

reported lean and rich solvent loadings of 0.163-0.204 and 0.388-0.443 mol CO_2/mol MEA at flue gas CO_2 concentrations of 5.5-9.9 vol%. The difference in the results presented here and those of Akram et al. (2016) are attributed to the variances in the liquid to gas ratio, MEA concentration and also the stripper operating conditions. Despite this, the solvent rich and lean loadings presented in this work at varying CO_2 concentrations are in reasonable agreement with published work. The impact of varying the reboiler temperature at 9.0 vol% CO_2 concentration is shown in Figure 5.4. The results demonstrate that both rich and lean solvent loadings increased with decreasing pressurised hot water inlet temperature. The lean and rich solvent loadings were 0.277 and 0.373 mol CO_2/mol MEA at a pressurised hot water inlet temperature of ~127°C. However, by reducing the pressurised hot water inlet temperature to ~124°C, the lean and rich solvent loadings increase by 24 and 11%, respectively, to 0.344 and 0.414 mol CO_2/mol MEA. This is because at higher reboiler temperature the regeneration of the solvent increases with increasing temperature as shown in Figure 5.4. At a lower reboiler temperature, lower solvent regeneration is expected which leads to higher rich and lean loadings.

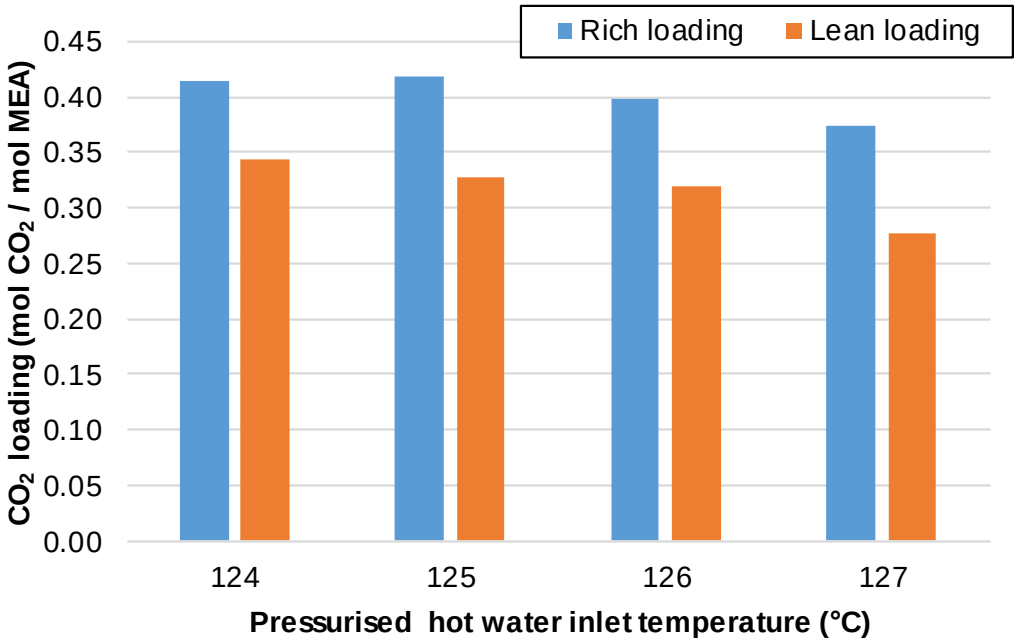

Figure 5.4. Influence of increasing pressurised hot water inlet temperature on rich and lean solvent loading at constant CO_2 concentration of 9.0 vol%.

5.3.2 Influence of S-EGR on liquid to gas ratio

As shown in results presented in Appendix A.4, the liquid to gas ratio increases with higher flue gas CO_2 concentrations, with this increasing by ~100% from 2.12 kg/kg at 5.2 vol% CO_2 to 4.25 kg/kg at 9.0 vol% CO_2. This large increase is due to the quantity of solvent needed to captured the CO_2 at higher concentrations to maintain a 90% CO_2 capture efficiency. The lean solvent flowrate increased from 477 kg/h (5.2 vol% CO_2) to 991 kg/h (9.0 vol% CO_2) which equates to a 108% increase. Hence, to achieve the desired CO_2 capture efficiency, the solvent flowrate is changed, which means changes in the rich and lean loadings. As the CO_2 concentration increases, the difference between the rich and lean solvent loading is reduced as indicated in the results (Appendix A.4). The liquid to gas ratio for the second experimental campaign remained ~4.3 kg/kg for all the tests as the solvent and flue gas flowrates were kept constant.

5.3.3 Influence of S-EGR on absorber and desorber performance

Figures 5.5 and 5.6 present the temperature profile across the absorber for both experimental campaigns. The overall trend presented in Figure 5.5 indicates that as the flue gas CO_2 concentration increases the temperature profile increases. As the MEA / CO_2 reaction is exothermic then this is what is expected (Akram et al., 2016).

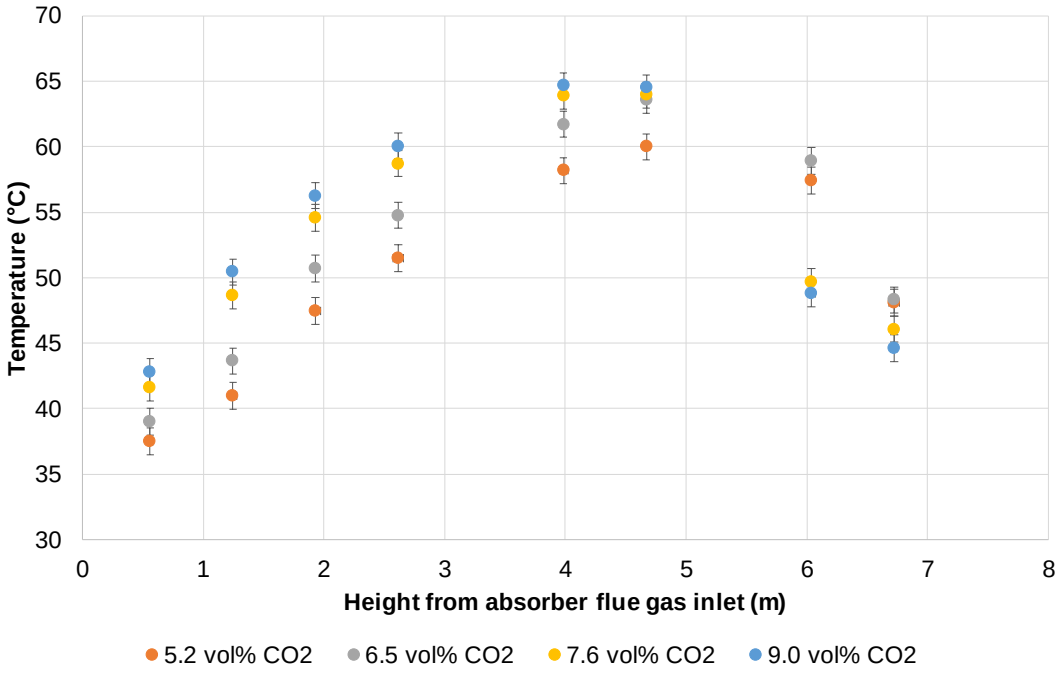

Figure 5.5. Influence of increasing the CO_2 concentration on the absorber temperature profile.

The results indicate for all the varying CO_2 concentrations considered in Figure 5.5, the maximum reaction point occurs at 4.7 m which suggests that most of the CO_2 absorption is occurring in the upper section of the absorber column. Akram et al. (2016) also demonstrate this trend, suggesting that the maximum driving force is within the top section of the absorber and this promotes optimal mass transfer. The reaction kinetics occurring in the liquid phase promotes CO_2 mass transfer, hence, greater bicarbonate and carbamate production occurring in the liquid phase with higher CO_2 concentrations (Notz et al., 2012). Furthermore, this increased CO_2 concentration and higher temperature will lead to an increase the kinetics of the reaction mechanisms, promoting this mass transfer (Notz et al., 2012). Herraiz et al.'s (2018) modelling work investigating both series and parallel S-EGR configurations also indicates that the temperature bulge at its maximum point occurs within the top section of the absorber. At this maximum temperature point, the absorption enthalpy released for the rate of CO_2 absorption decreases because the equilibrium curve moves toward the reagents (Akram et al., 2016). As shown in Figure 5.5, the temperature profile for the 7.6 and 9.0 vol% CO_2 concentration, demonstrates a lower overall temperature profile compared to the other CO_2 concentrations. The reason for this is likely associated with the different CO_2 mass transfer profiles and the rate of flue gas cooling for these concentrations. The maximum temperature point remains at a height of 4.7 m as per the other CO_2 concentrations considered in experimental campaign 1. In Figure 5.6 (p. 91), the trend clearly indicates that the temperature profile decreases with lower pressurised hot water inlet temperatures where the maximum temperature point is at a height of 4 m. At lower CO_2 inlet concentrations with the same CO_2 capture efficiency, smaller amounts of CO_2 are captured because less heat is released due to absorption and the lower temperature inlet in the absorber. As indicated in the results (see Appendix A.4), the lean loadings decrease with the increasing pressurised hot water inlet temperature. This means there is more solvent available to react with CO_2 in the flue gas. The temperature profile is also proportional to the difference in solvent loadings, with a greater difference in loading leading to an increase in the temperature profile due to the rate of the exothermic reaction occurring in the absorber (Heischkamp et al., 2011).

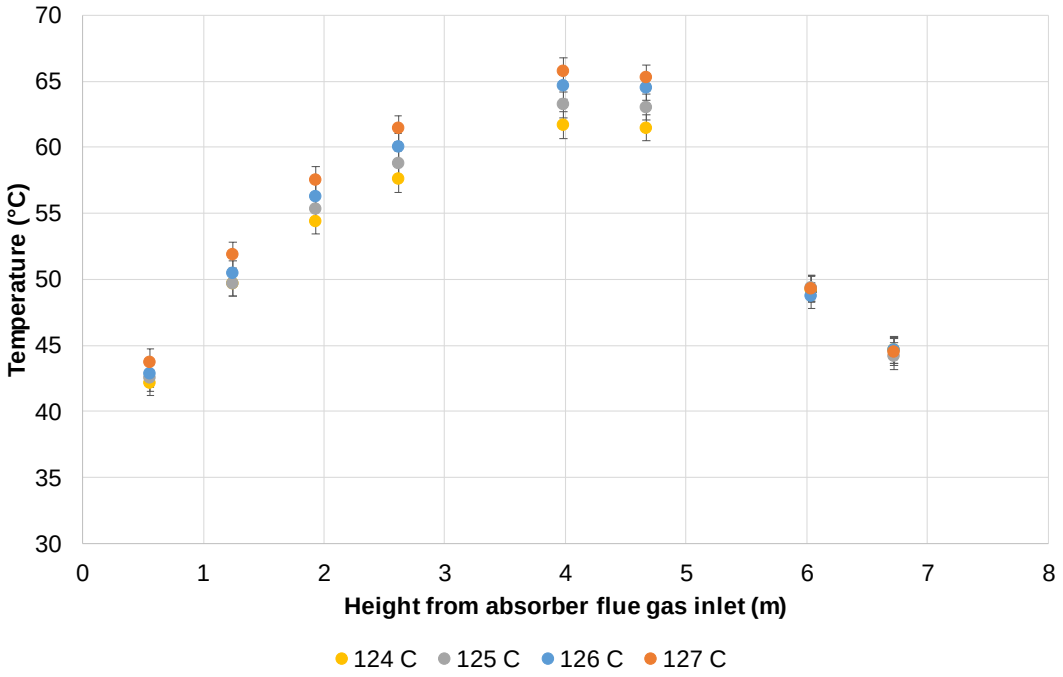

Figure 5.6. Influence of increasing the pressurised hot water inlet temperature on absorber temperature profile at constant CO_2 concentration of 9.0 vol%.

Figures 5.7 and 5.8 present the temperature profile across the desorber for both experimental campaigns. As shown in these figures, the temperatures decrease with increasing CO_2 concentrations and decreasing pressurised hot water inlet temperatures, respectively. In both of the temperature profile figures, the maximum temperature point is at the first measurement point at a height of ~0.4 m. This suggests that the rich solvent stream receives the largest proportion of steam energy at the bottom of the desorber column where the desorption enthalpy and sensible heat is the greatest (Notz et al., 2012). The vapour stream provides the energy required for CO_2 desorption, and heats up the solvent for this to occur. At a higher solvent flowrate the energy needed to heat up the solvent will also increase (Notz et al., 2012). Reducing the pressurised hot water inlet temperature from 127°C to 124°C lowers the maximum measured temperature point (0.4 m) by ~7% from 119°C to 111°C. Theoretically, the specific reboiler duty should decrease because of the lower energy input, however, as shown in Appendix A.4, this is not the case and is discussed in the subsequent section. The desorption enthalpy and energy required to generate steam are the two key factors which influence the overall energy requirement for solvent regeneration in the stripper (Notz et al., 2012).

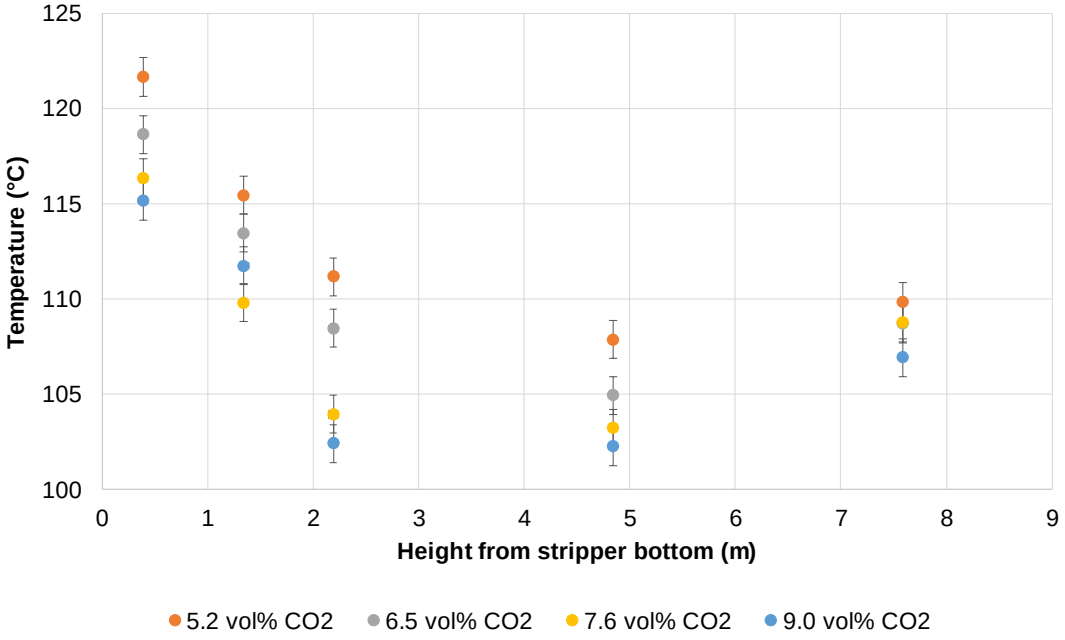

Figure 5.7. Influence of increasing the CO_2 concentration on the desorber temperature profile.

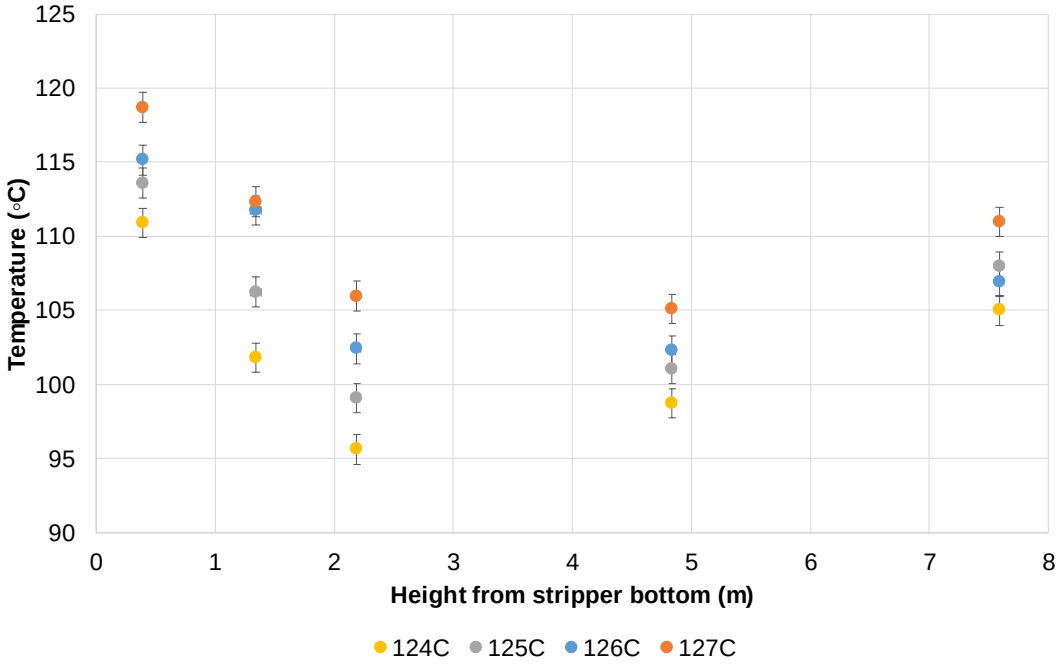

Figure 5.8. Influence of increasing the pressurised hot water inlet temperature on desorber temperature profile at constant CO_2 concentration of 9.0 vol%.

The pressurised hot water inlet temperatures will have a greater influence on the desorber energy requirements as indicated by Notz et al. (2012) and Kim and Svendsen (2007). The pilot plant used for these experimental campaigns has not been specially designed for S-EGR configurations, therefore plant optimisation to

accommodate for S-EGR would improve the absorber performance. This plant was originally designed for coal-fired flue gases, hence, flue gas CO_2 concentrations of 12-13 vol%. To optimise the ACP, the new plant would need to consider the CO_2 concentrations in full scale S-EGR systems for gas-CCS. In recent modelling studies, depending on the S-EGR configurations used, the flue gas flowrate is greatly reduced which means that the size of the absorber column could be smaller.

5.3.4 Influence of S-EGR on specific reboiler duty

The specific reboiler duty decreased by ~18% from 8.9 to 7.3 MJ/kg CO_2 with increasing CO_2 concentration of 5.2 to 9.0 vol%. Akram et al. (2016) showed that the specific reboiler duty reduced by ~25% from 7.1 to 5.3 MJ/kg with CO_2 concentration increasing from 5.5 to 9.9 vol%. The reason for the differences in Akram et al.'s (2016) work compared to this study is due to the different MEA concentrations used (40 wt% instead of 30 wt%). This means that the boiling point is higher for the 40 wt% MEA considered here, and more energy is required to liberate CO_2 at a 90% capture efficiency. The pressurised hot water inlet temperatures for experimental campaign 1 was ~126°C as opposed to ~121°C used in the study by Akram et al. (2016). In addition, the pressurised hot water flowrate used in this study is 50-53% higher than that of Akram et al. (2016), which is also due to the higher MEA concentration, and the boiling point being higher with increased MEA concentration.

As shown in Appendix A.4 the specific reboiler duty increases from 7.6 MJ/kg CO_2 (6.5 vol%) to 8.2 MJ/kg CO_2 (7.6 vol%). This is also the case for experimental campaign 2 (Appendix A.4), where the specific reboiler duty increases from 7.3 to 8 MJ/kg CO_2 at pressurised hot water inlet temperature of 125 and 124 °C, respectively. This is due to the lower MEA solvent concentrations at these test conditions indicating higher water content and increased solvent degradation, which means the energy requirement for solvent regeneration is greater. Akram et al. (2016) also demonstrates this and note that the specific heat capacity of water is greater than MEA, and more energy is required to heat up the solvent to desorb CO_2. The results indicate that overall, the specific reboiler duty tends to fall with larger solvent loadings, however, the influence of the pressurised hot water inlet temperature demonstrates a similar trend for specific reboiler duty. This is except for the 124°C test because of the reasons mentioned above regarding solvent concentration, though, the differences in the loadings increases with reduced temperature. This indicates that operating at lower temperatures at a constant liquid to gas ratio and CO_2 concentration would be beneficial for reduced specific reboiler

duty, albeit at the expense of a lower overall CO_2 capture efficiency. Nevertheless, depending on which S-EGR configuration is used the CO_2 capture efficiency is typically lower for series S-EGR by ~30-58% (Herraiz et al., 2018; Merkel et al., 2013).

Li et al. (2013) has shown that if the energy input to the reboiler is lower, less solvent is regenerated which leads to higher loadings at increased solvent flowrates at the same CO_2 capture efficiency. Furthermore, at lower liquid to gas ratios the residence times increase influencing the specific reboiler duty (Akram et al., 2016). The degree of regeneration is a function of the percentage difference between the lean and rich solvent loadings. The thermal decomposition of carbamate and bicarbonate liberates CO_2 from the rich solvent, hence, the amount of CO_2 which is stripped in the desorber (Akram et al., 2016; Fan et al., 2016). In Appendix A.4, the degree of regeneration reduces from ~31 to ~20% with increasing CO_2 concentrations. The increases in solvent loadings with higher CO_2 concentrations influences the regeneration energy. A higher lean loadings indicates less solvent has been regenerated which consumes less energy. Since the lean loading is higher, more solvent is required to capture the same amount of CO_2, which increases the reboiler demand to heat up the solvent. Therefore, as the lean loading increases a smaller quantity of steam is required which means that the specific reboiler reduces (Akram et al., 2016). The degree of regeneration also reduces (~26-17%) as the pressurised hot water inlet temperature is decreased (Appendix A.4).

The degree of regeneration for all the tests considered in this work is relatively low in comparison to other authors who have conducted experimental investigations at the PACT facilitates (e.g. Akram et al., 2016; Tait et al., 2018). These lower regeneration ratios are likely because of the higher energy demand requirements (desorption and evaporation) for using 40 wt% MEA instead of 30 wt% MEA. Fan et al. (2016) also indicates that at lower regeneration ratios only partial carbamate decomposition is occurring, which mean selecting the optimal solvent concentration is important for effective CO_2 capture that is also applicable to S-EGR.

5.4 Chapter conclusions

This study has investigated the ACP performance under S-EGR conditions at pilot-scale. Two experimental campaigns were conducted at the PACT Research Centre, which evaluated the influence of increasing CO_2 concentrations (~5.2-9.0 vol%) and

varying pressurised hot water inlet temperatures (124-127°C) on the ACP performance under S-EGR conditions.

The results indicate that the solvent concentrations in both experimental campaigns were up to 7 and 9% lower than the 40 wt% MEA expected due to solvent degradation. This leads to a reduction in the CO_2 capture efficiency from 91 to 78% at pressurised hot water inlet temperatures of 127 and 124°C, respectively. This is possibly due to evaporative losses, however, thermal and oxidative degradation is more likely. Throughout the experimental campaigns, the flue gas O_2 concentration remained ~17 vol%. At higher O_2 concentrations, oxidative degradation is more prominent due to the higher ion concentrations. In this work, the ion concentrations increase by 71% from 9.16 to 15.64 mg/L due to oxidative degradation. Furthermore, NH_3 is the principal MEA degradation product that increases with higher O_2 concentration, which is also demonstrated in the results. However, in commercial CCGT plants coupled with S-EGR configurations, the O_2 concentrations will be lower (~7-11 vol% O_2) and oxidative degradation should be less problematic (Diego et al., 2018, 2017b; Herraiz et al., 2018).

The 40 wt% MEA which is used in this work, means that the reboiler temperature is higher for CO_2 dissociation. Thermal degradation is also suggested as a reason for lower solvent concentrations. The lean and rich solvent loadings increased by 5.6 and 21.8% under S-EGR with higher CO_2 concentrations. The impact of decreasing the pressurised hot water inlet temperature showed that the lean and rich solvent loadings increase by 24 and 11%, respectively. To maintain a 90% CO_2 capture efficiency in experimental campaign 1, the liquid to gas ratio increased from 2.12 kg/kg to 4.42 kg/kg with higher CO_2 concentrations.

The absorber temperature profile increased with increasing CO_2 concentrations, with most CO_2 absorption occurring within the top section of the absorber. This has also been shown in modelling studies investigating parallel and series S-EGR configurations (Herraiz et al., 2018). To decrease temperatures in the and favour CO_2 capture in the reactor, absorber intercooling could be investigated in S-EGR systems. As the pressurised hot water inlet temperature is reduced, the absorber temperature profile follows the same trend associated with the differences in solvent loadings. The desorber temperature profile reduces with increasing CO_2 concentrations and decreasing pressurised hot water inlet temperatures, respectively. In terms of the specific reboiler duty, this decreased by 21% as the CO_2 concentration increases, though reducing the pressurised hot water inlet temperature (i.e., decreasing the reboiler temperature) indicated similar specific

reboiler duties. Hence, operating at lower temperatures in the reboiler with consistent liquid to gas ratios and CO_2 concentrations would be more cost-effective, but at the detriment of a reduced CO_2 capture efficiency. Operating under S-EGR conditions is beneficial in terms of lowering reboiler duty and improving loadings. In a highly optimised plant specifically designed for S-EGR, the packing height for the absorber would reduce, further decreasing costs. However, more work is required to consider solvents tolerant to high O_2 concentrations. This combined with developing a demonstration plant specifically for S-EGR is required.

6 Economic analysis of selective exhaust gas recirculation in CCGT power plants

6.1 Introduction

This chapter evaluates the economic performance of parallel and hybrid S-EGR configurations of CCGT power plants coupled with an ACP. The parallel S-EGR economic study investigates four cases which includes a CCGT power plant with an ACP (reference plant case (a)), with an ACP (validated ACP case (b)), with an ACP and EGR (EGR case (c)) and with an ACP and parallel S-EGR (parallel case (d)). The hybrid S-EGR economic study investigates five cases which includes a CCGT power plant with an ACP (ACP case (e)), with an ACP and EGR (EGR case (d)), with an ACP and hybrid S-EGR (S-EGR 2200, with a membrane CO_2 permeance of 2200 gpu (g)). The remaining two cases consider greater membrane CO_2 permeances of 5000 gpu (S-EGR 5000 (h)) and 10000 gpu (S-EGR 10000 (i)). The economic studies use the capital cost scaling methodology developed the US Department of Energy (DOE) and National Energy Technology Laboratory (NETL) to scale the costs associated with the configurations investigated in relation to a reference plant (DOE/NETL, 2013c). The reference plant is an CCGT power plant that includes two GE 7FA.05 gas turbines, two HRSG and a steam turbine and ACP (DOE/NETL, 2013b). The CCGT power plants in all the cases investigated in both the economic studies incorporate the same gas turbines, HRSG and steam turbine as the reference plant. The scaling parameters which are used to perform the economic studies have been taken from the modelling results presented in the published work associated with this chapter (Diego et al., 2018, 2017b). Following the economic analysis of both S-EGR configurations, a sensitivity analysis is performed to identify economic opportunities associated with these schemes.

6.2 Economic analysis methodology

The economic studies use the capital cost scaling methodology developed by DOE/NETL (2013b) to investigate the economic performance of the cases b-d (first economic study including parallel S-EGR) and cases e-i (second economic study including hybrid S-EGR). The process schematics and descriptions for the parallel and hybrid S-EGR configurations are presented previously, in section 2.5 (Figures 2.5 and 2.6), and are not reproduced here. The capital costs for the reference ACP are taken from the values reported by DOE / NETL in Case 1B 7FA.05 (DOE/NETL,

2013b). The capital costs for the EGR system are obtained from Case 1C 7FA.05 in the DOE/NETL report to scale the costs for the S-EGR schemes (DOE/NETL, 2013b). Figure 6.1 illustrates how the economic model works.

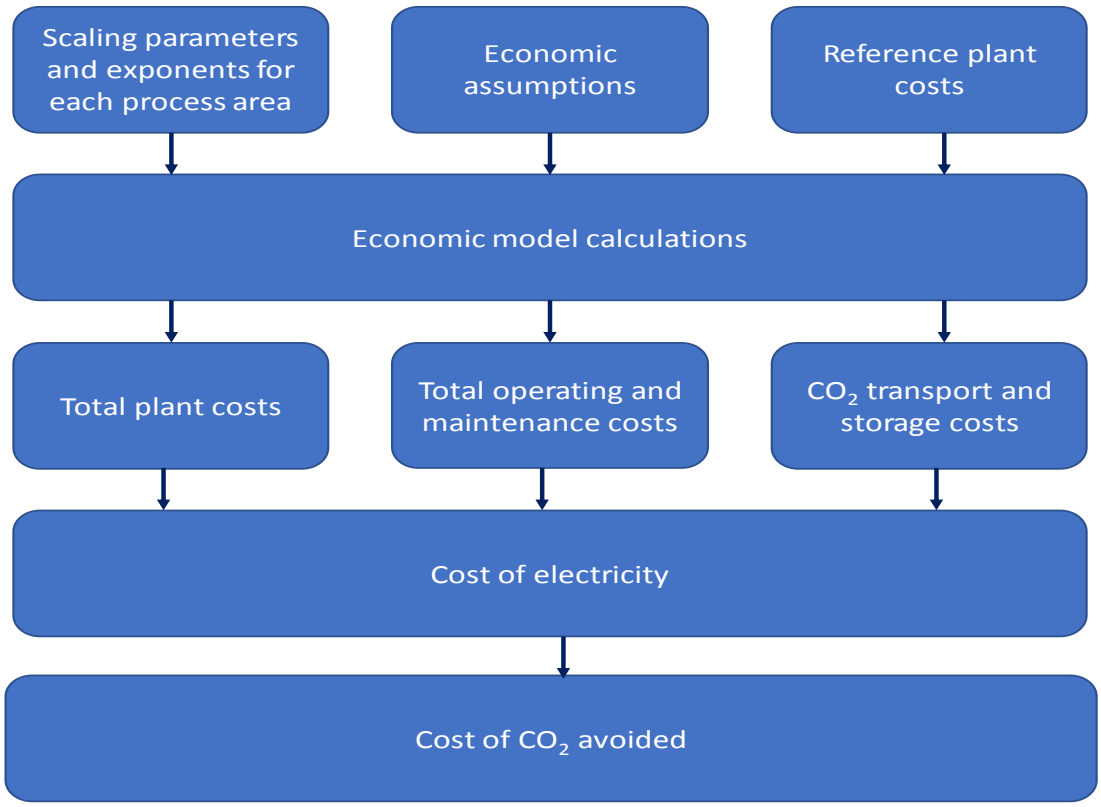

Figure 6.1. Schematic of the economic model.

The methodology adopted in this study uses the cost of electricity (COE) and cost of CO_2 avoided (COA) to determine the economic performance of cases a-d (first economic study including parallel S-EGR) and cases e-i (second economic study including hybrid S-EGR) The COE ($/MWh) is determined by (DOE/NETL, 2013b; IPPC, 2005):

$$COE = \frac{TOC.CCF + FOM}{CF.8760.MW} + VOM + HR.FC + T\&SC \quad \textbf{(6.1)}$$

where TOC is the total overnight costs in US$, fixed ($FOM$) and variable ($VOM$) operating and maintenance costs are expressed in $/yr and $/MWh. The capital charge factor and capacity factor are represented by CCF and CF, respectively. The net power output (MW), heat rate of the plant (HR) and fuel cost (FC) are reported in MW_e, MJ/MWh and $/MJ. The transport and storage costs ($T\&SC$) are expressed in $/tonne CO_2. The COA ($/tonne CO_2 avoided) can be expressed by (DOE/NETL, 2013b; IPPC, 2005):

$$\mathrm{COA} = (COE_{CCS} - COE_{REF}) \,/\, (EMS_{REF} - EMS_{CCS}) \quad \textbf{(6.2)}$$

where COE_{CCS}, COE_{REF}, EMS_{REF} and EMS_{CCS} are the cost of electricity with and without CO_2 capture, and the CO_2 emission rate in kg CO_2/MWh$_e$ with and without CO_2 capture, respectively.

The total overnight costs in equation (6.1) include the total plant costs and other overnight costs. Cases a-d (first economic study including parallel S-EGR) uses the total plant cost for each process area to scale costs for the configurations considered. These include the reference, ACP, EGR and parallel configurations. However, the second economic study was conducted subsequently, and it was decided to create a more robust economic approach when determining the TOC. The scaled costs for the configuration investigated in the cases e-i (second economic study including hybrid S-EGR), are from the bare erected costs (BEC), the engineering, procurement and construction (EPC) services cost and the process and project contingencies (DOE/NETL, 2015, 2013b, 2013c, 2010).

The fixed and variable operating and maintenance costs used in equation (6.1) include the costs for annual operating and maintenance labour, administrative and support labour, taxes and insurance, maintenance materials, membrane replacement and consumables. The membrane module costs over a five-year lifetime period is assumed to be \$50 per m^2 as reported in the published literature (Baker et al., 2017; Ho et al., 2008; Merkel et al., 2013; Turi et al., 2017; Voleno et al., 2014; Zhai and Rubin, 2013). The value for membrane replacement costs is widely reported (\$10 m^2 per year), however, it is important to note that membrane systems for gas-CCS are still currently under research and development, which means that this cost is still uncertain. The scaling parameters and exponents which are used in this work to determine the scaled costs for the corresponding process areas for the configurations investigated (cases b-i), are presented in Table 6.1 (p. 100). The economic studies use the scaled costs (SC) equation to determine the variations in scale associated with each configuration investigated. This is calculated from (DOE/NETL, 2013c):

$$\mathrm{SC} = \mathrm{RC}.(SP/RP)^{EXP} \quad \textbf{(6.3)}$$

where RC, SP, RP and EXP are the reference cost, scaling parameter, reference parameter and scaling exponent, respectively.

Table 6.1. Scaling parameter and exponents.

Process area	Scaling parameter	Scaling exponent
Feed water system	High pressure water flowrate	0.72
Natural gas pipeline	Fuel gas flowrate	0.07
Natural gas misc.	Fuel gas flowrate	0.76
EGR system	EGR flowrate	0.70
Amine capture plant (absorption)	Flue gas flowrate	0.61
Amine capture plant (desorber)	Rich solvent flowrate	0.61
CO_2 compression and drying	CO_2 flowrate	0.77
HRSG and additional components	HRSG duty	0.70
Steam turbine	Steam turbine power	0.80
Cooling water system	Cooling tower duty	0.71

The scaling parameters and exponents are taken from the quality guidelines developed by DOE/NETL (2013b). The absorption and desorption scaling parameters are taken to be the flue gas and rich solvent flowrates. The ACP cost is split into absorber and desorber costs. This is to take into account that the absorber changes size with S-EGR, whereas the desorber remains approximately the same. This means that the absorption process area includes the costs for the direct contact cooler, blower and absorber column. The desorption process area incorporates the costs of the circulation pumps, heat exchangers, desorber column and reboiler. To determine the split of the ACP costs the IECM V9.2.1 software was used to determine this (Carnegie Mellon University, 2017). The absorption and desorption sections represent 65% and 35% of the reference costs for these process areas, respectively. As both the S-EGR configurations will have a reduced absorber size due to a lower flue gas flowrate compared to the other configurations investigated in this work, this approach makes the results more accurate. In respect of the desorption section, a negligible effect on the column size is anticipated due to the same amount of CO_2 captured and thus, released in the desorber, as in the reference plant.

6.2.1 Economic assumptions for the first economic study

The economic assumptions used to perform the first economic study are presented in Table 6.2 (p. 101). In order to determine the membrane costs, the area has been estimated using a similar methodology as outlined by Voleno et al. (2014). This approach splits the membrane into 10 sections of the same size where perfect

separation of CO_2 is assumed with a CO_2 permeance of 2200 gpu (Merkel et al., 2013; Voleno et al., 2014). To calculate the membrane cost the following expression is used (Merkel et al., 2013; Zhai and Rubin, 2013):

$$\text{Membrane area} = A_M . C_{SKID} \quad \textbf{(6.4)}$$

where A_M and C_{SKID} are the membrane area and skid cost ($50 per m^2 in this case) (Merkel et al., 2013; Zhai and Rubin, 2013).

Table 6.2. Economic assumptions for the first economic study.

Capacity factor (CF) [a]	85.0 %
Capital charge factor (CCF) with CCS [a]	0.11
COE_{REF} [a]	57.1 $/MWh$_e$
EMS_{REF} [a]	354 kg CO_2/MWh$_e$
CO_2 transport and storage over 100 km [a]	10 $/tonne
Natural gas price [a]	5.8 $/GJ
Plant operating period [a]	30 Years
Membrane installed skid cost [b]	50 $/$m^2$
Membrane module lifetime [c]	5 Years
Total as spent cost (TASC) multiplier [a]	1.078
Cost year [a]	2011
Labour rate [a]	51.6 $/h
Labour per shift [a]	6.3
Shifts per day [a]	3
Preproduction costs [a]	6 months operating labour 1 month maintenance materials cost 1 month non-fuel consumables 25% of 1 month fuel cost 2% of total plant cost (TPC)
Inventory capital [a]	2 months non-fuel consumables Spare parts (0.5% TPC)
Other [a]	Initial cost for chemicals (0.002% TPC) [b] Land Other owners costs (15%TPC) Financing costs (2.7% TPC)
Fixed O&M costs [a]	Annual operating labour (AOL) Annual maintenance labour (AMC) (40% of Variable O&M costs)[d] Administrative and support labour (25% of AOL+AMC) Tax and insurance (2% TPC)
Variable O&M costs	Maintenance material cost (1.1% TPC) [a] Non-fuel consumables cost (0.6% TPC) [a] Membrane replacement cost (10 $/$m^2$yr)

[a] Economic assumptions from reference (DOE/NETL, 2013b).
[b] Membrane skid cost from references (Merkel et al., 2013; Zhai and Rubin, 2013).
[c] Membrane lifetime from reference (Zhai and Rubin, 2013).
[d] Economic assumption from reference (IEAGHG, 2009b).

6.2.2 Economic assumptions for the second economic study

The economic assumptions used to perform the economic analysis for the hybrid S-EGR configuration are presented in Table 6.3. In the process simulation work related to this study (Diego et al., 2018), a programming code was developed to model the hybrid membrane system where the membrane included 20 sections of equal area using a similar approach to Voleno et al. (2014).

Table 6.3. Economic assumptions for the second economic study.

	Capital charge factor with CCS[(a)]	0.111
	Capacity factor – CF (%)	85
	Financial cost year	2011
	Fuel cost ($/GJ) [(a)]	5.8
	Transport and storage cost ($/$t_{CO2}$) [(a)]	10
TPC	Cost of installed membrane skid ($/$m^2$) [(b)]	50
	Cost of accessory electric plant, instrumentation and control, improvements to site and buildings and structures (% of process equipment BEC) [(c)]	20
	EPC cost (% of BEC) [(c)]	8
	Project contingency (% of TPC)[(d)]	13
	Process contingency [(e)]	
	Amine capture plant (% of BEC_{ACP})[(f)]	20
	CO_2 selective membrane (% of BEC_{mb}) [(f)]	20
	Pre-production costs[(a)]	
	No. of months of all labour	6
	No. of months of maintenance materials costs at 100%CF	1
	No. of months of non-fuel consumables at 100%CF	1
	Percentage of 1 month fuel cost at 100% CF (%)	25
	Miscellaneous (% of TPC)	2
	Inventory capital costs[(a)]	
	No. of days of consumables at 100% CF	60
	Spare parts (% of TPC)	0.5
	Others[(a)]	
	Initial cost for chemicals ($/kW)	2.5
	Land costs (M$)	0.3
	Other owner's costs (% of TPC)	15
	Financing costs (% of TPC)	2.7
FOM[(a)]	Cost of labour ($/h)	51.6
	No. of shifts per day	3
	No. of operators per shift (operating and maintenance)	6.3
	Administrative and support labour costs (% of O&M labour costs)	25
	Taxes and insurance (% of TPC)	2
VOM	Maintenance material cost (% of TPC) [(c)]	1.1
	Membrane lifetime (yr) [(g)]	5
	Membrane replacement cost ($/$m^2$) [(g)]	10
	Consumables cost ($/kW) [(c)]	0.001

[(a)] Economic assumptions from reference (DOE/NETL, 2013b).
[(b)] Economic assumptions from references (Baker et al., 2017; Ho et al., 2008; Merkel et al., 2013; Turi et al., 2017; Voleno et al., 2014; Zhai and Rubin, 2013).
[(c)] Calculated values from reference (DOE/NETL, 2013b).
[(d)] Economic assumption from reference (DOE/NETL, 2015).
[(f)] Economic assumption from reference (Zhai and Rubin, 2013).
[(g)] Economic assumption from reference (DOE/NETL, 2013c).

6.2.3 Uncertainty of the capital cost scaling methodology

This high-level cost evaluation uses can represent up to 30% uncertainty in the results presented (DOE/NETL, 2015, 2013b, 2013c). In order to ensure the results are accurate and representative, the methodology used (DOE/NETL, 2013c) has been validated against the CCGT configurations evaluated by DOE/NETL (2013b). Consequently, the calculation procedure used to performance the economic analysis is this work is determined to be accurate and repeatable.

In the first economic study, the validation of the ACP against the reference plant is shown in the results, which demonstrates a 1% difference in the total overnight costs. However, the variation in the COE and COA between these two cases can be attributed to the 94 MW_e difference in the net power output shown in the modelling results by Diego et al. (2017). The reason for the difference in the COE and COA values is because of the type of solvent used in the CO_2 capture plant. In the reference plant an advanced solvent is used and in the ACP case 30 wt% MEA is used which leads to a greater energy penalty (DOE/NETL, 2013b). The second economic study has also been validated against the CCGT plant with an ACP. The results presented for the total overnight costs, COE and COA represent up to 2% difference.

6.3 Results and discussion

6.3.1 Results of the first economic study

The results of the high-level cost evaluation conducted for the first economic study is presented in Table 6.4 (p. 103), where the costs are confined to the respective process areas as per the reference case (DOE/NETL, 2013b). As shown in Table 6.4, the results indicate that for the EGR and S-EGR configurations considered, the total overnight costs decrease and increase by 4% and 2%, respectively, compared to the ACP case. The reason for these variations is due to S-EGR membrane costs and the reduced capital costs associated with the CO_2 amine capture system in the EGR and S-EGR configurations. The capital costs of the amine capture plant demonstrate a decrease of 16% and 22% for the EGR and S-EGR cases in comparison to the ACP case. These large reductions are mainly associated with the decreased costs of the absorber, direct contact cooler and blower in the EGR and S-EGR cases because of the reduced flue gas flowrates treated in the ACP. However, the costs associated with the heat exchangers, circulation pumps, stripper and reboiler remain similar for all cases despite a slight reduction in the stripper column size. As a fraction of the flue gases is returned to the compressor inlet in

both the EGR and S-EGR cases, the quantity of flue gases treated in the absorber reduce, hence, the absorber size decreases which lowers the capital costs of this unit.

Table 6.4. Results of the first economic study

		Reference plant [a]	ACP	EGR	Parallel S-EGR
	Process area			**$M**	
1	Feed water system and natural gas pipeline	55.8	56.0	56.7	57.3
2	EGR system [b]	-	-	21.5	26.5
3	CO_2 removal system[c]	313.1	311.2	260.0	242.4
4	Gas turbine system	134.0	134.0	134.0	134.0
5	HRSG system	55.5	54.9	55.5	56.1
6	Steam turbine system	66.9	63.6	65.6	66.7
7	Cooling water system	26.2	20.9	21.9	22.2
8	Parallel membrane system	-	-	-	49.9
9	Accessory electric plant, instrumentation & control, improvements to site, buildings & structures (14% TPC)	107.1	105.3	101.2	107.7
	Total plant cost (TPC)	**758.7**	**746.0**	**716.5**	**762.9**
10	Preproduction costs	26.4	25.9	25.3	26.2
11	Inventory capital and initial chemical cost	5.8	5.9	5.6	6.0
12	Land costs	0.3	0.3	0.3	0.3
13	Other owners cost (15% TPC)	113.8	111.9	107.5	114.4
14	Financing costs (2.7% TPC)	20.5	20.1	19.3	20.6
	Total overnight cost (TOC)	**925.5**	**910.1**	**874.5**	**930.4**
	Total as spent cost (TASC)	**997.7**	**981.0**	**942.7**	**1003.0**
15	Total FOM	25.7	22.6	21.8	27.7
16	Total VOM	12.9	12.7	12.2	22.4
17	Total fuel cost	190.5	190.5	190.5	190.5
	Total O&M cost	**229.1**	**225.8**	**224.5**	**240.5**
	CO_2 transport and storage cost ($/MWh)	**3.7**	**3.7**	**3.7**	**3.8**

[a] Values from reference (DOE/NETL, 2013b).

[b] This includes the EGR blowers, cooler and cooler pumps (DOE/NETL, 2013b).

[c] This includes the cost of the amine capture plant and of the CO_2 compression and drying system (DOE/NETL, 2013b).

In the economic methodology, the scaling parameter for the CO_2 removal system absorption section is the flue gas flowrate which is used to determine these costs. Despite these benefits for this S-EGR case, the membrane system used for the parallel S-EGR configuration increases the total plant costs by 6% from M$716 (EGR) to M$763 (S-EGR). Due to the higher total plant costs and frequency of replacing the membrane in the S-EGR configuration, the operating and

maintenance costs also demonstrate a 7% increase. The COE and COA for the cases considered here are presented in Figure 6.2.

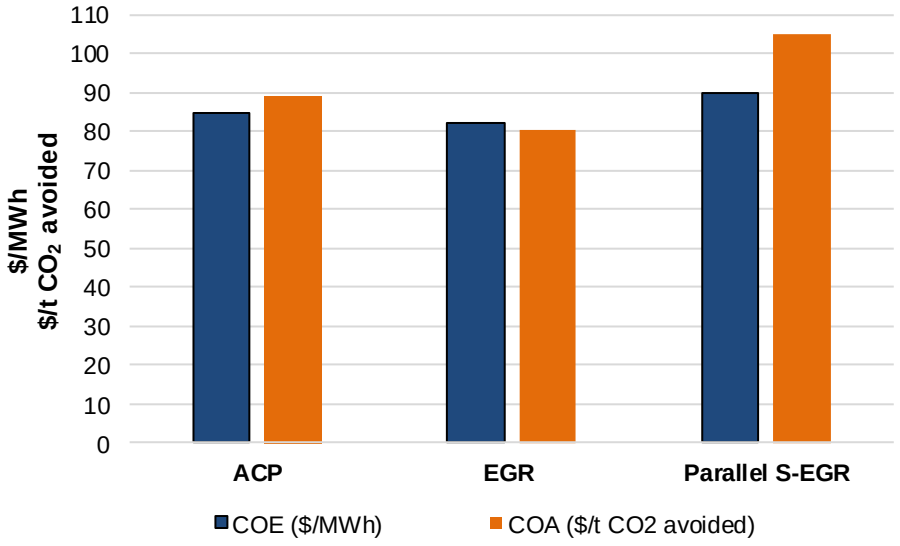

Figure 6.2. COE and COA for the reference ACP, ACP, EGR and parallel S-EGR configurations.

As shown in Figure 6.2, the COE for the EGR case decreases by 3% from \$85 to \$82.4 per MWh in comparison to the ACP case. In the S-EGR case, the COE increases by 6% to \$90.0 per MWh. The COA for the EGR case also reduces by 10% in comparison to the ACP case to \$80.4 per tonne CO_2 avoided, whereas, for the S-EGR configuration this increases by 18% to \$105.1 per tonne CO_2 avoided. These increases are due to the higher capital, fixed and operating costs associated with the S-EGR membrane system.

6.3.1.1 Sensitivity analysis for the first economic study

The use of membranes for post-combustion CO_2 capture are still in their infancy and the technical and economic performance associated with these systems can be improved. Currently, a membrane module reference cost of \$50/m^2 is widely reported in the literature (Ho et al., 2008; Merkel et al., 2013; Voleno et al., 2014; Zhai and Rubin, 2013). Despite the higher economic costs for the parallel S-EGR system compared to the ACP and EGR cases, the anticipated technical improvements to membrane systems will be beneficial for optimising the parallel S-EGR configuration. Furthermore, the pressure drop across the membrane, which is 0.1 bar (~ 10%) in this work, is associated with the auxiliary energy consumption. This leads to a reduction in the total net power output leading to higher COE and COA for the parallel S-EGR configuration evaluated here. As discussed previously, the lower flue gas flowrate and enhanced CO_2 concentration in S-EGR

configurations will be beneficial in reducing the costs associated with the amine capture plant. Assessing the benefit of enhanced CO_2 flue gas streams is difficult to determine in an economic evaluation.

Therefore, to quantify the effects of improved membrane performance in terms of COE and COA, a sensitivity analysis is performed. This sensitivity analysis considers seven scenarios (1-7) that evaluate different membrane pressure drops and the costs associated with the membrane and CO_2 removal systems, as shown in Table 6.5.

Table 6.5. Sensitivity analysis scenarios.

Parameter	Scenario						
	1	**2**	**3**	**4**	**5**	**6**	**7**
Membrane (Fraction)	1	0.5	0.25	1	1	0.5	0.25
ACP S-EGR (Fraction)	1	1	1	0.8	0.8	0.8	0.8
Pressure drop across the membrane (bar)	0.1	0.1	0.1	0.1	0.05	0.05	0.05

The scenarios consider a membrane which is a fraction of the cost considered with respect to that of the membrane cost illustrated in Table 6.4 (i.e., 0.25 means the membrane cost is assumed to be 25% of \$50 m^2). The amine capture plant cost also consider costs between 100 and 80% of the reference cost to account for the reduced absorber size expected in S-EGR systems. In addition, membrane pressure drops of 0.1 to 0.05 bar (10-5% DP) are also considered, which only influence the auxiliary energy consumption of the plant and thus, the COE and COA. In Figures 6.3(a) and (b), the influence of varying membrane cost, pressure difference and CO_2 removal system cost are presented in relation to the COE and COA compared to the ACP and EGR cases. As illustrated in Figures 6.3(a) for scenario 7, a reduction in the COE by up to 3.4% and 0.3% in comparison to the ACP and EGR cases may be possible the most favourable scenario. Furthermore, in Figure 6.3(b) the COA also reduces for scenario 7 by 10.4% and 0.8% in comparison to the ACP and EGR cases. The sensitivity analysis results show that a combined decrease in the pressure difference, membrane cost and CO_2 removal system influences the COE and COA where scenario 6 and 7 would make S-EGR competitive with the ACP. This sensitivity analysis demonstrates that any improvements to the parallel S-EGR configuration would be beneficial to make this system more competitive to both ACP and EGR in gas-CCS applications.

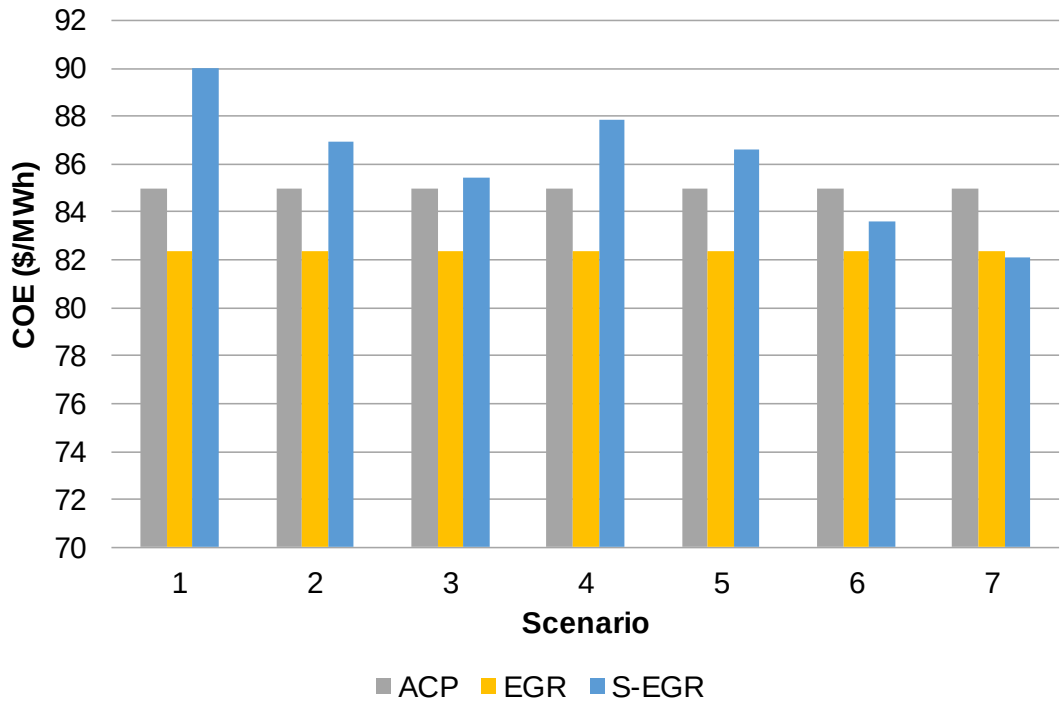

(a)

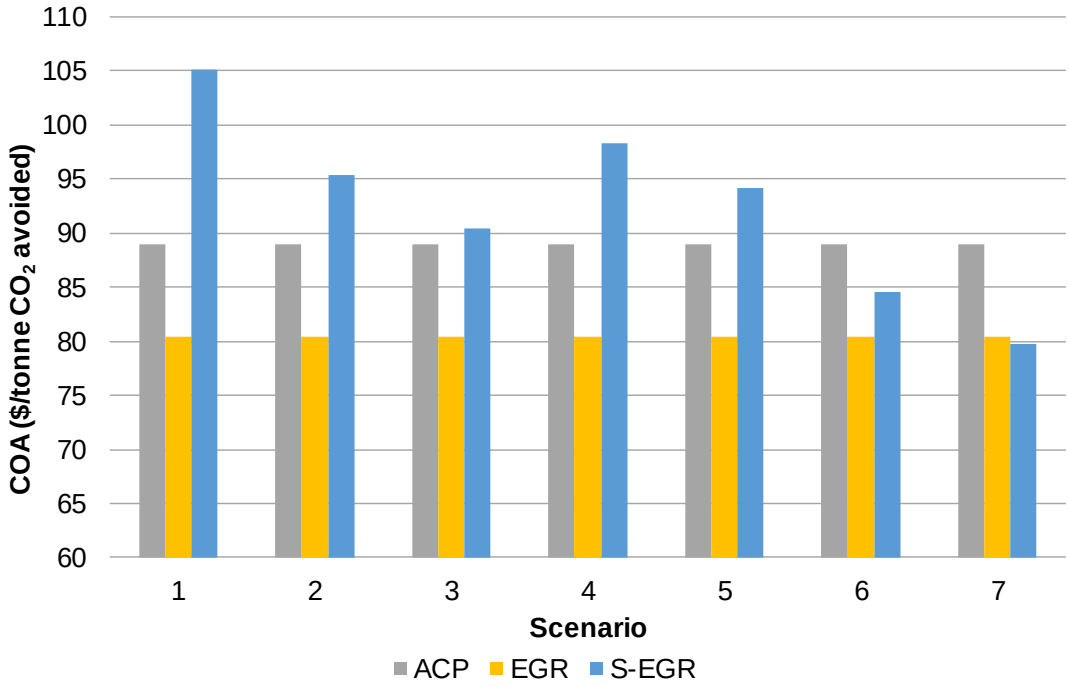

(b)

Figure 6.3. Sensitivity analysis on the (a) COE and (b) COA for different sensitivity analysis scenarios.

6.3.2 Results of the second economic study

The results of the economic evaluation for the three different hybrid S-EGR configurations are presented in Table 6.6. These three cases consider membrane CO_2 permeances of 2200, 5000 and 10000 gpu with a pressure drop across the membrane of 5%. These three cases are compared against the ACP and EGR cases. The results demonstrate that the amine capture plant capital costs decrease due to the smaller flue gas flowrate being treated, hence, the absorber size is more compact. A reduction of up to 40% and 27% in absorber size, is realised with the hybrid S-EGR configuration compared to the ACP and EGR cases. However, due to the size and associated equipment (e.g. blowers) of the membrane system, the capital costs of the hybrid S-EGR system increases the total overnight costs compared to the ACP and EGR scenarios by up to 26% and 30%, respectively.

Table 6.6. Results of the second economic analysis.

	Unit	**S-EGR**			**ACP**	**EGR**
Membrane CO_2 permeance	gpu	2200	5000	10000		
Equipment area			**M$**			
Feed water unit and natural gas pipeline		47.9	47.9	47.9	44.7	45.3
Gas turbine system		112.4	112.4	112.4	112.4	112.4
Stream turbine system		59.6	59.6	59.6	52.9	54.9
HRSG system		48.7	48.7	48.7	45.8	46.5
Cooling water system		23.6	23.6	23.6	18.4	20.4
Amine capture plant		105.5	105.5	105.5	176.7	144.3
Membrane system		145.2	63.9	31.9	-	-
S-EGR equipment		31.0	31.0	31.0	-	
EGR equipment		-	-	-	-	16.5
CO_2 compression and drying		28.4	28.4	28.4	28.4	28.4
Accessory electric plant etc.		120.4	104.2	97.8	95.8	93.7
BEC	M$	722.7	625.1	586.8	575.0	562.3
EPC	M$	57.8	50.0	46.9	46.0	45.0
Project and process contingency	M$	174.3	139.8	126.3	133.4	123.9
TPC	M$	954.7	814.9	760.0	754.4	731.2
TOC	**M$**	**1161.4**	**993.2**	**927.2**	**920.4**	**892.5**

By considering increasing membrane CO_2 permeances, the membrane area decreases, hence the total overnight costs reduce. Increasing the permeance from 2200 to either 5000 or 10000 gpu decreases the total overnight costs by 14% and 20%, respectively. As with the parallel S-EGR configuration discussed previously, the COE and COA are the economic indicators used to compare these

configurations. The COE and COA for all the scenarios considered in Table 6.6 are presented in Figure 6.4. The key factors that influence the COE are the total overnight costss. The equipment costs influencing the total overnight costs largely incorporates variable operating and maintenance costs as shown in Table 6.3 (p. 102). The fixed operating and maintenance cost also contribute to the total overnight costs. The total operating and maintenance costs per year ranged from $50m (for a 2200 gpu membrane) to $40m (for 10000 gpu), whereas for the ACP and EGR configurations these costs reduced to M$39 and M$38. The values for the ACP and EGR cases are lower because no membrane system is required as per the hybrid S-EGR cases.

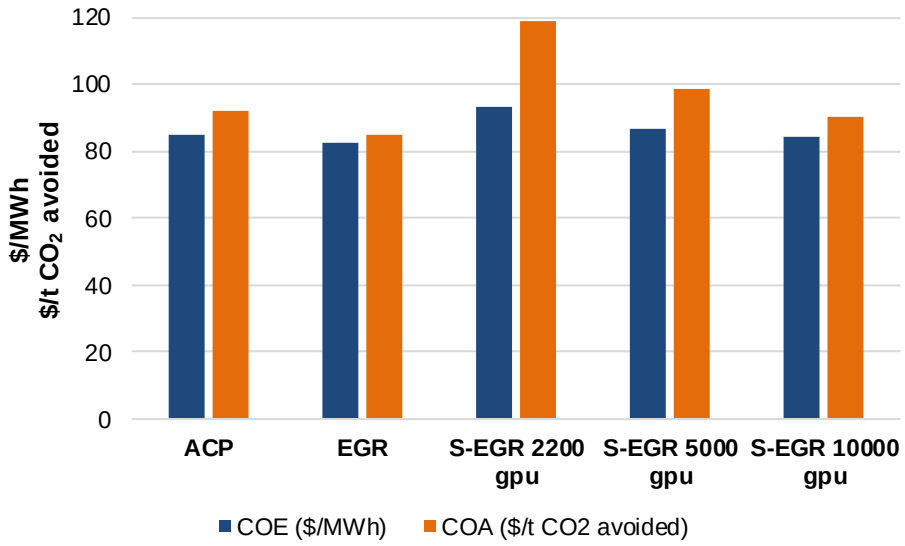

Figure 6.4. COE and COA for the reference, ACP, EGR and hybrid S-EGR configurations.

As illustrated in Figure 6.4, the COE and COA for the ACP and EGR configurations are $84.7 and $82.7 per MWh and $92.1 and $85.1 per tonne of CO_2 avoided, respectively. In comparison, the COE for the S-EGR cases with CO_2 permeances of 2200, 5000 and 10,000 gpu decrease from $93.0, $86.8 and $84.3 per MWh, representing a 9.3% reduction overall. Considering the same S-EGR cases, the COA also reduces by 23.7% from $118.6 (2200 gpu) to $90.5 (10000 gpu) per tonne of CO_2 avoided. These economic savings demonstrate the effect of membrane permeance on the COE and COA, which suggests that the advancement of membrane technology to accommodate higher permeances is required to develop the hybrid S-EGR configuration for gas-CCS.

6.3.2.1 Sensitivity analysis for the second economic study

The research and development of membranes for CCS and S-EGR configurations is ongoing, hence, it is expected that the economic performance of S-EGR configurations is likely to improve whilst uncertainties are investigated. For example, the majority of studies use the membrane skid cost of \$50 per m^2 where the membrane operates under pressure/vacuum conditions (Baker et al., 2017; Diego et al., 2018, 2017b; Ho et al., 2008; Merkel et al., 2013; Turi et al., 2017; Voleno et al., 2014; Zhai and Rubin, 2013). The advancement of membrane technology would likely reduce the costs associated with the skid costs. The sensitivity analysis presented here considers the influence of varying the membrane skid cost (\$10-50 per m^2) and the pressure drop across the membrane (2.5, 5.0 and 10%) for the three hybrid S-EGR configurations at membrane CO_2 permeances of 2200, 5000 and 10000 gpu, respectively. These are compared to the ACP and EGR cases in terms of COE and COA as shown in Figures 6.5-6.7.

Membrane ΔP of 2.5 %

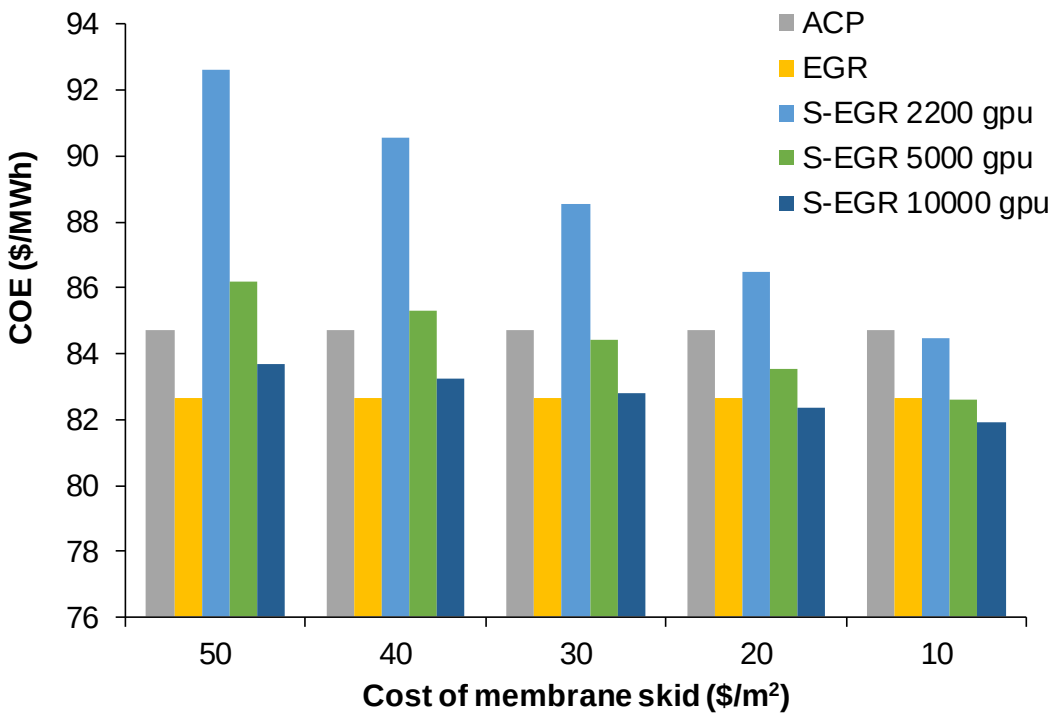

(a)

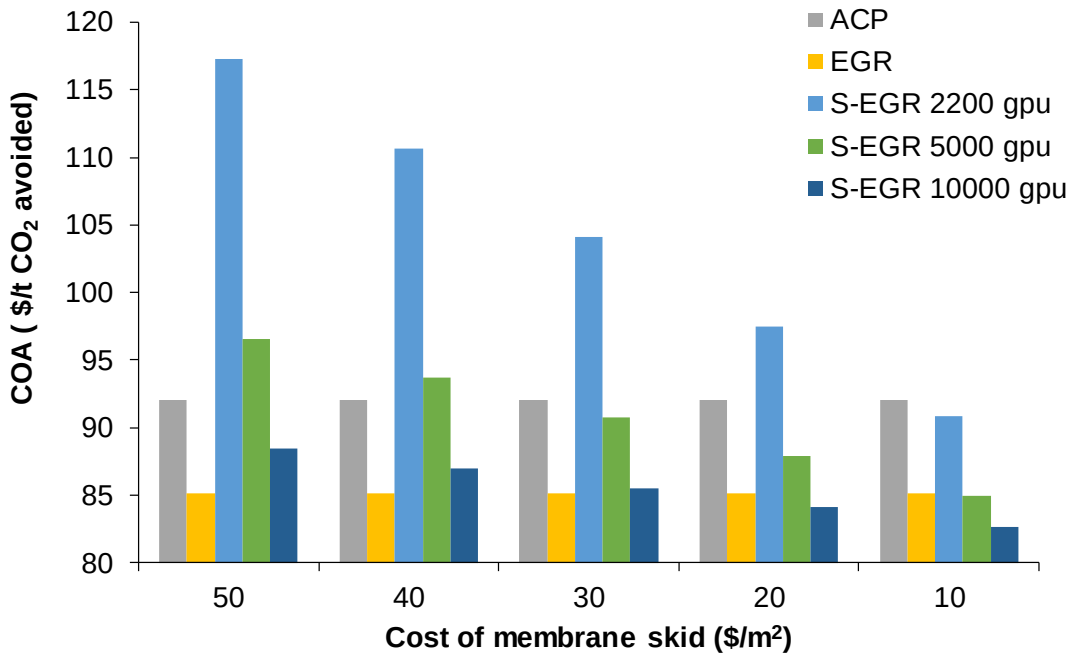

(b)

Figure 6.5. (a) COE and (b) COA for the ACP, EGR and hybrid S-EGR configurations at a pressure drop of 2.5%.

Membrane ΔP of 5 %

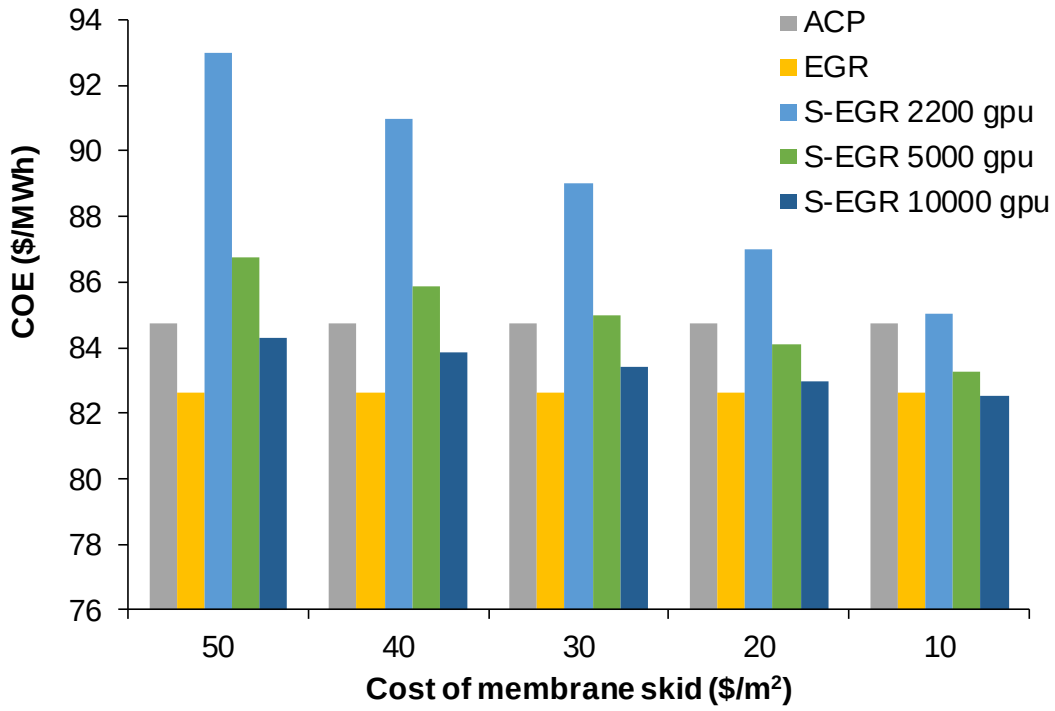

(a)

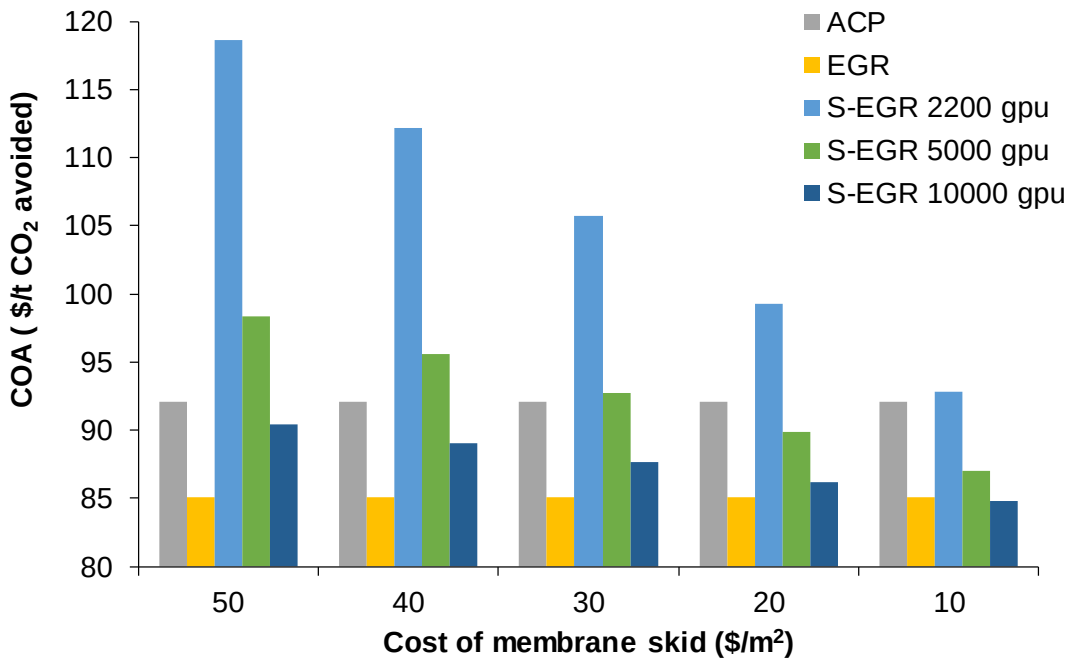

(b)

Figure 6.6. (a) COE and (b) COA for the ACP, EGR and hybrid S-EGR configurations at a pressure drop of 5%.

Membrane ΔP of 10 %

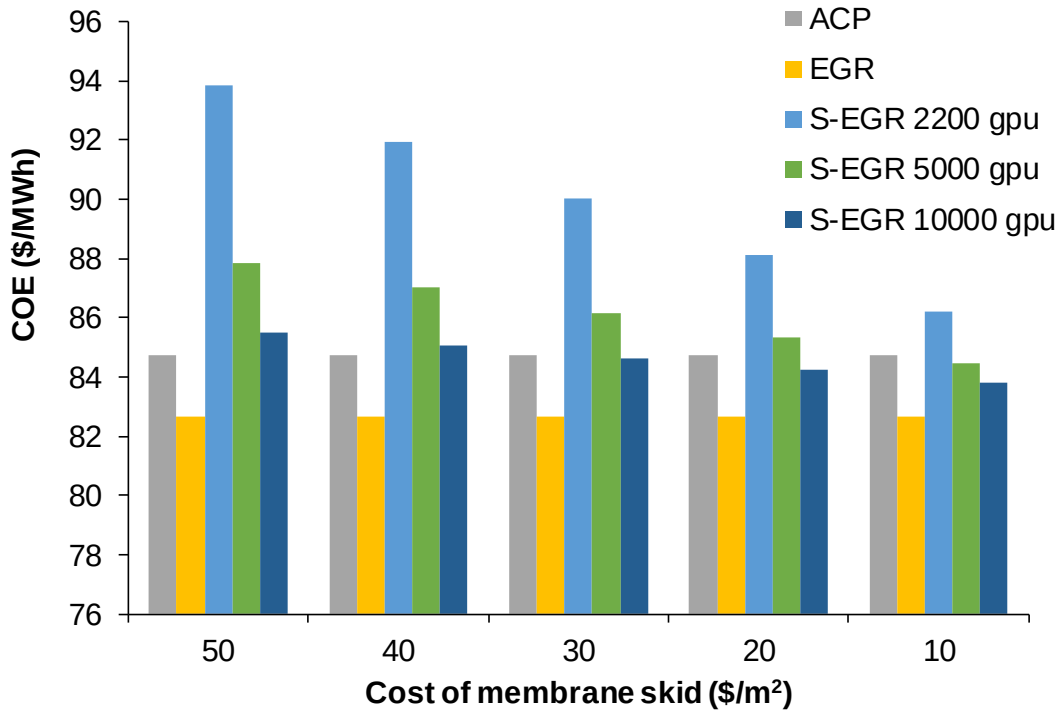

(a)

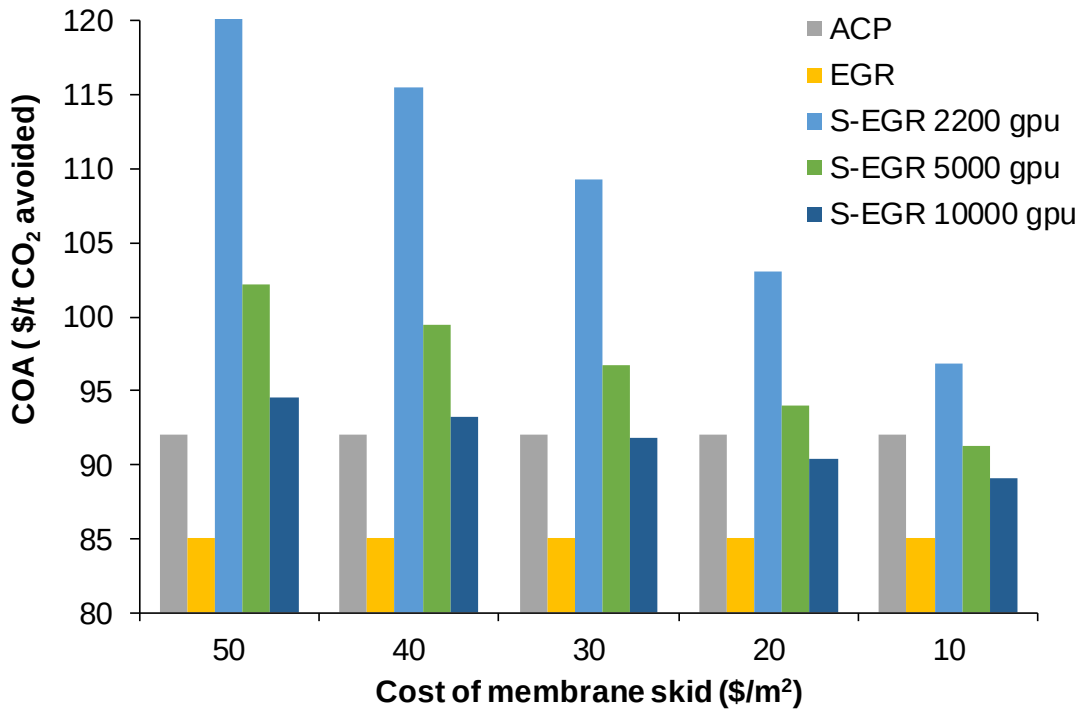

(b)

Figure 6.7. (a) COE and (b) COA for the ACP, EGR and hybrid S-EGR configurations at a pressure drop of 10%.

The application of S-EGR does not seem to be competitive with the reference values considered against the ACP and EGR case. To make the hybrid S-EGR configuration an attractive option for gas-CCS applications, increases in the permeance and reduction in the membrane cost are needed to make it competitive. The results shown in Figures 6.5 to 6.7 illustrate the large cost savings which could be achieved for hybrid S-EGR configurations if continued efforts are made to lower membrane skid costs. In all the figures, the COE and COA is the lowest when considering the 10000 gpu membrane CO_2 permeance, as expected. For example, in Figure 6.6, where the pressure drop across the membrane is 5%, the COE and COA is consistently lower than the ACP configuration when varying membrane skid costs between \$10-50 per m^2. However, to make the hybrid S-EGR configuration competitive with respect to EGR, further improvements would be required. This is shown in Figure 6.5, where the pressure drop and membrane skid costs are reduced to 2.5% and \$20 per m^2, respectively, for a 10000 gpu membrane CO_2 permeance. The COE and COA when considering this scenario decreases to \$82.4 per MWh and \$84.1 per tonne of CO_2 avoided. This is a reduction of 0.4% and 1.2% compared to the COE and COA for the EGR case at \$82.6 per MWh and \$85.1 per tonne of CO_2 avoided, respectively. The results presented in Figures 6.5 and 6.7, demonstrate the potential cost reduction targets when considering improvements to

the hybrid S-EGR configuration with respect to ACP or EGR, thus, making it competitive for gas-CCS.

6.4 Chapter conclusions

This chapter evaluates the economic performance of parallel and hybrid S-EGR configurations coupled to CCGT power plants. The results of the first economic study illustrates that the total overnight cost for the parallel S-EGR case increases by 2% to M$930, compared to the ACP case where these costs are M$910. In the EGR case the total overnight costs reduce by 4% to M$875 and the capital costs for both the EGR and parallel S-EGR configurations reduce by 16% and 22%, respectively compared to the ACP case. Despite the benefits of the reduced absorber capital costs for the parallel S-EGR configuration, the total plant cost increases by 6% to M$763 compared to the EGR case where the total plant cost is M$716. Operating and maintenance costs increased by 7% in the parallel S-EGR configuration because of higher membrane replacement and total plant costs. The COE and COA for the parallel S-EGR configuration are $90 per MWh and $105 per tonne of CO_2 avoided, respectively. This represents a 6% and 18% increase compared to the ACP case which is attributed to the high costs associated with the parallel S-EGR system. The sensitivity analysis of the parallel S-EGR configuration illustrates that the COE and COA can be decreased to $82 per MWh and $80 per tonne of CO_2 avoided, with a combined reduction in the cost of the membrane and CO_2 capture system, and operating at a smaller pressure difference.

The results of the second economic study demonstrates that the capital costs of the CO_2 capture amine system, when considering hybrid S-EGR, decreases by 40% and 27% from M$177 and M$144 for the ACP and EGR cases to M$106 for hybrid S-EGR. However, the large membrane areas for the three hybrid S-EGR configurations considered, with CO_2 permeances of 2200, 5000 and 10000 gpu, lead to greater total overnight costs compared to the EGR and ACP cases. The total overnight costs increase by 26, 8 and 1% compared to the ACP case, whereas, these costs rise further by 30, 11 and 4% compared to EGR case. The COE and COA for the three hybrid S-EGR cases ranged from $93-84 per MWh and $91-119 per tonne of CO_2 avoided at CO_2 permeances of 10000, 5000 and 2200 gpu. These reductions demonstrated that the hybrid S-EGR configuration may be competitive with the ACP or EGR cases. Although this is dependent on the permeance, pressure drop and membrane cost. The sensitivity analysis of the hybrid S-EGR configurations illustrates that the COE and COA could decreased to $82 per MWh

and \$83 per tonne of CO_2 avoided, with a combined reduction in the cost of the membrane, increased CO_2 permeance and operating with a membrane system that lead to a smaller pressure difference.

7 Conclusions, recommendations and future work

7.1 Introduction

S-EGR has been proposed to overcome the issues associated with EGR where parallel, series and hybrid configurations are currently being investigated. Initial work identifies that the CO_2 concentration can be increased up to ~26% operating at 14 vol% O_2 concentrations, although combustor modifications would be required (Turi et al., 2017). Limited experimental work has been conducted at bench scale, with pilot scale experimental work investigating gas turbine and CO_2 capture plant performance lacking in the literature. The optimisation of amine based CO_2 capture is the focus of many studies to decrease the economic and energy costs associated with these systems. The key issue for gas-CCS is flexible operation, increasing CO_2 concentrations and operating at pilot and demonstration scale to facilitate knowledge transfer and reduce the risks for all stakeholders.

7.2 Pilot-scale operation of gas turbines with S-EGR

Operating the mGT under conditions representative of S-EGR significantly increased the flue gas CO_2 concentration to 8.4 vol% and 10.1 vol% at 60 and 100 kW_e, representing a ~400 and 600% increase compared to the baseline. In CCGT plants with S-EGR, CO_2 concentrations have been increased to ~18-26 vol% from ~4 vol%, representing a ~350-550% increase (Diego et al., 2018; Herraiz et al., 2018; Merkel et al., 2013). The results presented in this work are within a similar range to that of S-EGR systems investigated in the literature. The increase in CO_2 concentrations is associated with the changes to the working fluid properties which influences the excess air and air fuel ratio. The excess air decreased and the air fuel ratio increased with increasing CO_2 injection rate. Under the S-EGR conditions investigated a marginal decrease in the O_2 concentration at the compressor inlet from 21.0 to 19.2 vol% was observed. This is expected because of the modified working fluid due to the CO_2 injection. The reduced O_2 values at the compressor inlet are similar to those reported in the literature investigating commercial scale S-EGR systems (16-20 vol% O_2 depending on which S-EGR configuration is used). This would indicate that operating under S-EGR is beneficial compared to EGR, where at the maximum EGR ratio, O_2 levels are 16 vol% and the maximum CO_2

concentration ~6.5 vol%. Hence, the implementation of S-EGR for gas-CCS would maintain the O_2 levels at the MOC whilst significantly increasing the flue gas CO_2 concentration. Furthermore, implementing S-EGR will reduce the volumetric flue gas flowrate (with high CO_2 concentrations) treated in the downstream CO_2 capture system which will be beneficial in terms of cost and energy penalty savings. The mGT operational performance under conditions characteristic of S-EGR indicate that the efficiency and rotational speed are impacted with increasing CO_2 injection rates. The electrical efficiency decreased by ~4-8% with increasing CO_2 injection rate compared to the baseline with no CO_2 injection. The reason for this reduction is due to the larger heat capacity of CO_2, which leads to a marginal decrease in the power output, hence the mGT increases the amount of fuel required which leads to a decrease in the electrical efficiency. The rotational speed decreased by 650-1400 rpm with increasing CO_2 injection rate. This was caused by the addition of CO_2 to the working fluid which replaced a proportion of the ambient air; because CO_2 is denser than air, the rotational speed reduced though the mass flowrate remained the same. At higher ambient air temperatures the density of air reduces, which means the compressor will rotate faster to deliver a similar air flowrate to provide the desired electrical power output. Due to the variation in ambient air temperatures throughout the experiments this will also influence any deviations illustrated in the S-EGR tests. The compressor inlet temperature remained at a similar temperature for all tests, however, depending the ambient air temperature, this will have a marginal impact on the rotational speed and efficiency. The compressor outlet pressure is not significantly affected operating the mGT under S-EGR. This is also demonstrated in work by Herraiz et al. (2018). The compressor outlet temperature showed slight reductions with CO_2 injection at 80 and 90 kW_e, however, at the other power outputs, no clear trend was seen, although a slight decrease is attributed to the varying ambient air temperature rather than the CO_2 injection rate. This is because the heat capacity ratio under S-EGR conditions reduces by ~1-2% at the compressor inlet, therefore, significant reductions are not expected. The NOx emissions for S-EGR tests investigated showed an overall decrease with increasing CO_2 injection rates due to lower flame temperatures. This is a key benefit of operating under S-ERG, because as emission regulations become stricter, operators will need to adhere to these. The application of S-EGR will help mitigate these emissions and meeting emission targets whilst the deployment of gas-CCS can be realised. Emissions of CO and UHC increased due to the reduction of O_2 and incomplete combustion under S-EGR. However, this is more prevalent at part loads and operating at 80-100% load, these emission levels are at acceptable

levels. The results presented indicate the effectiveness of applying S-EGR to mGT configurations at part and full load operation. Further investigation on larger turbines is needed to determine what modifications are required for commercial applications implementing S-EGR.

7.2.1 Novelty and original contribution to knowledge

The novelty and original contribution to knowledge of chapter 4 includes:

- The influence of S-EGR on the mGT performance at pilot scale, which includes:
    - the effect on the mGT rotational speed, electrical efficiency, and compressor performance at 60-100 kW_e at CO_2 injection rates up to 300 kg/h which equates to CO_2 enriched air up to 9.4 vol% CO_2 and 19.2 vol% O_2 in the oxidiser stream; and
    - the effect on the mGT emission performance in terms of NOx, CO, UHC, CO_2 and O_2.

7.2.2 Recommendations and future work

The system used in this work was designed to mimic a range of conditions which represented S-EGR. To further advance the development of S-EGR at pilot scale the following recommendations and future work should be considered:

- Modify the current system to include a membrane which can be tested at pilot scale. This would require the modification of the turbine exhaust system where a slip-steam of the exhaust is diverted through a membrane system. Depending on the resources available a number of options could be investigated including:

    - Install a membrane system at PACT where a slip steam of the exhaust gases under S-EGR operation with CO_2 injection are sent through the membrane and the membrane performance is evaluated.
    - Complete redesign of the entire system to represent actual S-EGR configurations.
    - Modify the mGT combustor to include thermocouples and a high-resolution camera to allow for flame temperature measurements and flame profiles to be investigated under S-EGR at pilot scale.

In addition to the above, the following should also be investigated:

- Development of process simulation models which incorporate modified compressor and turbine maps under S-EGR for the full operational range of the turbine. This would allow for the validation and optimisation of process models and further understating of the turbine performance; and
- Combustor modelling of the Turbec T100 and commercial combustors under S-EGR conditions using CFD and CHEMKIN. Developing combustor models will allow for an in depth understanding of what modifications are required to deploy S-EGR commercially.

Modifying the mGT to incorporate an exhaust gas flowmeter and new fuel flow meter would also improve the accuracy of the results further. A SKI SDF Flow Sensor was purchased after significant research, which allows for accurate readings of the flue gas flowrate, temperature, and pressure. However, due to time constraints this was not installed during the experimental work. To accommodate this flowmeter, new fabricated exhaust ducting would be required. The design for the new flue gas ducting is shown in Figure 7.1, which has been integrated into ANSYS® R17.2 Academic computational fluid dynamics (CFD) software. This was to determine any issues associated with total pressure, temperature, and velocity along the new ducting. The CFD analysis showed no issues associated with this design.

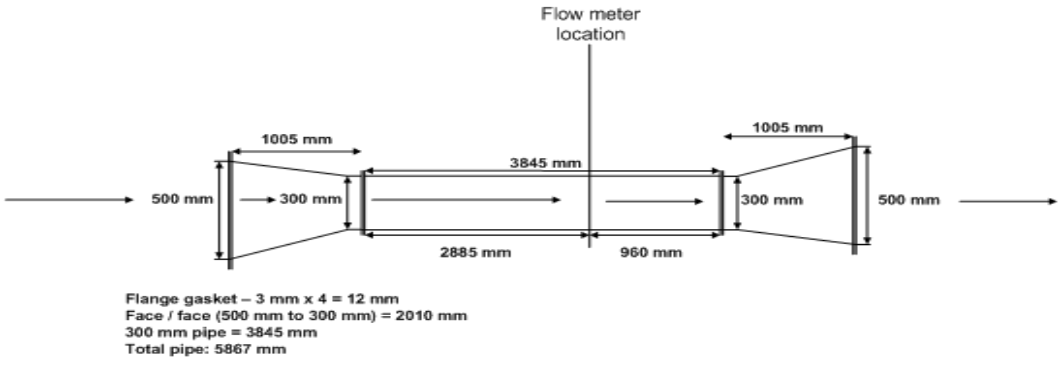

Figure 7.1. Design for new flue gas ducting at PACT.

7.3 Pilot-scale operation of ACP with S-EGR

The results indicate that solvent degradation reduces the solvent concentration, which reduces the CO_2 capture efficiency under conditions characteristic of S-EGR. This is evident when the pressurised hot water temperature was reduced to from 127-124°C where the CO_2 capture efficiency decreased from 91 to 78% at a flue gas CO_2 concentration of 9.0 vol%. Thermal and oxidative degradation are the reason why the solvent concentration decreased by up to 9%. Operating with higher O_2 concentrations will promote the rate of oxidative degradation and this is demonstrated by the 71% increase in iron concentrations over the S-EGR experimental campaign. In full scale S-EGR, the O_2 concentration in the flue gases treated by the CO_2 capture plant will be lower, typically ~7-11 vol%, which means, oxidative degradation should be less problematic (Diego et al., 2018, 2017b; Herraiz et al., 2018). Operating the ACP with higher MEA concentrations (40 wt% instead of 30 wt%) means that the reboiler temperature was higher to free the CO_2. The results suggest that the rate of thermal degradation increases because of the higher temperature, thus lower solvent concentrations. Increasing the concentration of CO_2 in the flue gas under S-EGR, illustrated that both lean and rich loading increased up to 6% and 22%. Furthermore, operating at lower reboiler temperatures promoted this increase further by 24% and 11% for the lean and rich loadings at 124°C. The liquid to gas ratio increased with higher CO_2 concentrations by ~100%, however, in commercial S-EGR systems, this will be dependent on the S-EGR configuration used. Optimising S-EGR systems to minimise the increase in liquid to gas ratio with higher CO_2 concentrations will be important to curtail any increase in economic and energy costs. The S-EGR experiments illustrated that CO_2 absorption occurred within the top section of the absorber column, and the temperature profile increased at higher CO_2 concentrations. In commercial S-EGR systems this has also been shown, e.g. Herraiz et al., 2018. To overcome this, optimising the ACP to accommodate intercooling would be advantageous and would further advance S-EGR for gas-CCS. The results demonstrate that operating the ACP under S-EGR at lower reboiler temperatures also decreased the absorber temperature profile, therefore, selecting the correct solvent and concentration for S-EGR systems is important. The stripper temperature profile showed that it is beneficial to operate at higher CO_2 concentrations and lower pressurised hot water temperatures, as the temperature profile decreased. This suggests that the energy required to separate CO_2 decreases under these conditions which will be more cost effective, however, the CO_2 capture efficiency may also reduce. Depending on which S-EGR system is

used, the CO_2 capture efficiency is lower ~30-58% (Herraiz et al., 2018; Merkel et al., 2013), therefore, this will be specific to each S-EGR system.

7.3.1 Novelty and original contribution to knowledge

The novelty and original contribution to knowledge of chapter 5 includes:

- The influence of S-EGR on the ACP performance at pilot scale, which includes:
    - the impact on specific reboiler duty, absorber and desorber performance, CO_2 capture efficiency, rich and lean solvent loadings, liquid to gas ratio, and thermal and oxidative degradation.

7.3.2 Recommendations and future work

The experimental campaigns evaluated in chapter 5 investigated the ACP performance under S-EGR conditions. However, to further advance the development of S-EGR at pilot scale the following recommendations and future work should be considered:

- Operate the mGT sequentially with the ACP under S-EGR to investigate the performance with specific attention focusing on degradation products and amine emissions.
- Validation of process simulation models representing the S-EGR experimental results at 40 wt% MEA considered in this work. This will allow for different scenarios to be investigated including using 30 wt% MEA.
- Investigate the dynamic performance of the ACP under S-EGR. This would include operating the mGT at 100 kW_e with a CO_2 injection rate of 300 kg/h aiming for a capture rate of 90% until steady state has been achieved. At steady state, progressively decreasing the flue gas flowrate, solvent recirculation rate and hot water flowrate over 4 hours. After 4 hours return the plant to initial operating conditions until steady state has been achieved. This experimental campaign would be to represent load following at times of peak electricity demand.

In addition to the above, the following should also be considered to optimise and improve the ACP:

- Redesign of the absorber to include absorber intercooling;
- Testing alternative solvents specifically designed for gas-CCS; and
- Redesign of the plant to incorporate the gas turbine, a CO_2 selective membrane system, and ACP to represent S-EGR.

7.4 Economics

The parallel S-EGR configurations demonstrates that the COE ranged from \$82.1 to \$90.0 per MWh and the COA from \$79.1 to \$105.1 per tonne of CO_2 avoided, depending on the improvements to membrane performance (e.g. varying pressure drop and skid cost) and reduction in amine capture plant costs.

The hybrid S-EGR configuration, which applies the benefits of both the parallel and series S-EGR schemes, has also been evaluated in terms of its economic performance. The results indicate that a balance between the lower amine capture plant costs and net efficiency with the higher operating and maintenance costs of the hybrid membrane system needs to be considered.

A number of scenarios were considered by appraising different skid costs, membrane permeances and pressure drops across the membrane. The COE and COA ranged \$81.9–93.9/MWh and \$82.7–121.9 per tonne of CO_2 avoided, respectively. The S-EGR scenario with a CO_2 membrane permeance of 2200 gpu and selectivity of 50 was shown to have a greater COE and COA than the ACP and EGR cases due to the large membrane system costs. The sensitivity analysis demonstrated that the hybrid S-EGR configuration has the potential to be competitive with respect to the ACP and EGR configurations.

The results of both economic studies illustrate that continued research and development of membrane systems for gas-CCS is required. This should focus on improving membrane CO_2 permeance, decreasing the pressure drop across the membrane and reducing the membrane skid costs. The overall analysis indicates that S-EGR configurations offer economic advantages, which would make them attractive for gas-CCS, however, further development is needed before these systems can be operated at commercial scale.

7.4.1 Novelty and original contribution to knowledge

The novelty and original contribution to knowledge of chapter 6 includes:

- Economic and sensitivity analysis of parallel and hybrid S-EGR configurations in CCGT power plants.

7.4.2 Recommendations and future work

The parallel and hybrid economic studies presented in chapter 6 identify that further research and development on reducing membrane costs and improving performance is required to make S-EGR more attractive for gas-CCS. Therefore, the following recommendations and future work should be considered:

- Perform a techno-economic study which considers the flexible operation of CCGT plants which incorporates hybrid, parallel or series S-EGR configurations.
- The development of costing methodology for S-EGR systems. This could include the development of a detailed economic model which allows the user to consider a range of future energy scenarios and perform sensitivity analysis for a number of options.
- The development of S-EGR membranes which can accommodate higher CO_2 permeances, reduced pressure ratios and consider different materials which maybe more cost effective for gas-CCS.

7.5 Overall conclusions and the future of gas-CCS

The thesis has experimentally analysed the performance of a gas turbine and ACP under conditions characteristic of S-EGR at pilot scale. Furthermore, the economic evaluation of parallel and hybrid S-EGR configurations coupled to CCGT power plants has been performed. The novelty and original contribution to knowledge of the work conducted as part of this thesis has added to the development of gas-CCS. This is evident through knowledge transfer by the findings of this work being published in peer review journal papers and presented at conferences.

This research demonstrates that the application of S-EGR at pilot-scale works effectively by increasing the CO_2 concentration in the flue gas. Furthermore, that economic costs of the downstream capture plant are significantly reduced by the application of S-EGR. However, the development and commercial deployment of gas-CCS is dependent on the correct conditions being established to facilitate and drive the commercial deployment at the correct pace, in which our climate change

targets and future energy scenarios can be achieved. The barriers, which are limiting the development and deployment of gas-CCS, include policy, legal and regulatory frameworks, and establishing specific sites for storage. The continue determination to mitigate the impacts of climate change is evident such as the Paris Agreement. However, the predicated increase of natural gas in our energy systems going forward means that fossil fuels will continue to have a role in our energy mix. In the future, gas-CCS will be needed to mitigate the CO_2 emissions from CCGT power plants. The policy, legal and regulatory frameworks, which are needed to create a CCS market-based economy and de-risk the investment of this mitigation option, are lacking from nations climate change mitigation strategies. The development of these frameworks, in addition to stakeholder and public consultation is required. Furthermore, educating society about CCS, emphasising the importance, and why it is required to protect the future of our climate is essential to developing the social acceptance of this mitigation strategy. The deployment of gas-CCS is of critical important for countries that are heavily reliant on fossil fuels such as the UK, China and Brazil. Therefore, energy decarbonisation and the implementation of gas-CCS will be essential to limit the potential negative consequences of climate change on the economic, environmental and social prosperity of nations around the world. To do this, nations who are leaders in gas-CCS, e.g. the UK, US, Canada, Norway and Australia, must lead by example, in actually developing, deploying and operating gas-CCS. This will promote gas-CCS, and de-risk the CCS model which will contribute to establishing a CCS market based economy. Despite the knowledge growing significantly, the actual deployment of CCS is decelerating and we all need to play a pivotal part in reducing emissions and ensure real investments are made to make gas-CCS a reality.

8 References

Abdallah, H., Harvey, S., 2001. Thermodynamic analysis of chemically recuperated gas turbines. Int. J. Therm. Sci. 40, 372–384. https://doi.org/10.1016/S1290-0729(01)01225-X.

Aboudheir, A., Tontiwachwuthikul, P., Chakma, A., Idem, R., 2003. Kinetics of the reactive absorption of carbon dioxide in high CO_2 -loaded, concentrated aqueous monoethanolamine solutions. Chem. Eng. Sci. 58, 5195–5210. https://doi.org/10.1016/j.ces.2003.08.014.

Abu-Zahra, M.R.M., Niederer, J.P.M., Feron, P.H.M., Versteeg, G.F., 2007. CO_2 capture from power plants. Int. J. Greenh. Gas Control 1, 135–142. https://doi.org/10.1016/S1750-5836(07)00032-1.

Adolf Meyer, B.B., 1939. The Combustion Gas Turbine: Its History, Development and Prospects. Inst. Mech. Eng. 141, 197–222.

Ahn, H., Luberti, M., Liu, Z., Brandani, S., 2013. Process configuration studies of the amine capture process for coal-fired power plants. Int. J. Greenh. Gas Control 16, 29–40. https://doi.org/10.1016/j.ijggc.2013.03.002.

Akram, M., Ali, U., Best, T., Blakey, S., Finney, K.N., Pourkashanian, M., 2016. Performance evaluation of PACT Pilot-plant for CO_2 capture from gas turbines with Exhaust Gas Recycle. Int. J. Greenh. Gas Control 47, 137–150. https://doi.org/10.1016/j.ijggc.2016.01.047.

Akram, M., Blakey, S., Pourkashanian, M., 2015. Influence of Gas Turbine Exhaust CO_2 Concentration on the Performance of Post Combustion Carbon Capture Plant, in: Volume 3: Coal, Biomass and Alternative Fuels; Cycle Innovations; Electric Power; Industrial and Cogeneration. ASME, p. V003T08A005. https://doi.org/10.1115/GT2015-42454.

Ali, U., Hughes, K.J., Ingham, D.B., Ma, L., Pourkashanian, M., 2017. Effect of the CO_2 enhancement on the performance of a micro gas turbine with a pilot-scale CO_2 capture plant. Chem. Eng. Res. Des. 117, 11–23. https://doi.org/10.1016/j.cherd.2016.10.001.

Amrollahi, Z., Ertesvåg, I.S., Bolland, O., 2011. Optimized process configurations of post-combustion CO_2 capture for natural-gas-fired power plant—Exergy analysis. Int. J. Greenh. Gas Control 5, 1393–1405. https://doi.org/10.1016/J.IJGGC.2011.09.004.

Arias, B., Diego, M.E., Méndez, A., Alonso, M., Abanades, J.C., 2018. Calcium looping performance under extreme oxy-fuel combustion conditions in the calciner. Fuel 222, 711–717. https://doi.org/10.1016/j.fuel.2018.02.163.

Arndt, D., Blunden, J., Willett, K., 2015. State of the climate in 2014. Bull. Amer. Meteorol. Soc. 96, S1–+.

Aroonwilas, A., Veawab, A., 2007. Heat recovery gas absorption process. US7906087B2.

Arrieta, F.R.P., Lora, E.E.S., 2005. Influence of ambient temperature on combined-cycle power-plant performance. Appl. Energy 80, 261–272. https://doi.org/10.1016/j.apenergy.2004.04.007.

Austgen, D.M., Rochelle, G.T., Peng, X., Chen, C.C., 1989. Model of vapor-liquid equilibria for aqueous acid gas-alkanolamine systems using the electrolyte-NRTL equation. Ind. Eng. Chem. Res. 28, 1060–1073. https://doi.org/10.1021/ie00091a028.

Baburao, B., Schuber, C., 2011. Advanced intercooling and recycling in CO2 absorption. WO2011066042A1.

Baker, R.W., Freeman, B., Kniep, J., Wei, X., Merkel, T., 2017. CO_2 capture from natural gas power plants using selective exhaust gas recycle membrane designs. Int. J. Greenh. Gas Control 66, 35–47. https://doi.org/10.1016/j.ijggc.2017.08.016.

Baker, R.W., Lokhandwala, K., 2008. Natural Gas Processing with Membranes: An Overview. Ind. Eng. Chem. Res. 47, 2109–2121. https://doi.org/10.1021/ie071083w.

Bedell, S.A., 2009. Oxidative degradation mechanisms for amines in flue gas capture. Energy Procedia 1, 771–778. https://doi.org/10.1016/j.egypro.2009.01.102BEIS, 2019. UK greenhouse gas emissions: annual data. [Online]. Avaialble from: https://data.gov.uk/dataset/9a1e58e5-d1b6-457d-a414-335ca546d52c/uk-greenhouse-gas-emissions-annual-data [Accessed: 18.03.2019].

BEIS, 2017. The Clean Growth Strategy Leading the way to a low carbon future.

Best, T., Finney, K.N., Ingham, D.B., Pourkashanian, M., 2016. Impact of CO_2-enriched combustion air on micro-gas turbine performance for carbon capture. Energy 115, 1138–1147. https://doi.org/10.1016/j.energy.2016.09.075.

Bhattacharya, A., Datta, A., 2013. Effects of supplementary biomass firing on the performance of combined cycle power generation: A comparison between NGCC and IGCC plants. Biomass and Bioenergy 54, 239–249. https://doi.org/10.1016/j.biombioe.2013.04.008.

Biliyok, C., Canepa, R., Hanak, D.P., 2015. Investigation of Alternative Strategies for Integrating Post-combustion CO_2 Capture to a Natural Gas Combined Cycle Power Plant. Energy & Fuels 29, 4624–4633. https://doi.org/10.1021/acs.energyfuels.5b00811.

Biliyok, C., Yeung, H., 2013. Evaluation of natural gas combined cycle power plant for post-combustion CO_2 capture integration. Int. J. Greenh. Gas Control 19, 396–405. https://doi.org/10.1016/j.ijggc.2013.10.003.

Black, S., Szuhánszki, J., Pranzitelli, A., Ma, L., Stanger, P.J., Ingham, D.B., Pourkashanian, M., 2013. Effects of firing coal and biomass under oxy-fuel conditions in a power plant boiler using CFD modelling. Fuel 113, 780–786. https://doi.org/10.1016/j.fuel.2013.03.075.

Bolland, O., Mathieu, P., 1998. Comparison of two CO_2 removal options in combined cycle power plants. Energy Convers. Manag. 39, 1653–1663. https://doi.org/10.1016/S0196-8904(98)00078-8.

Bolland, O., Sæther, S., 1992. New concepts for natural gas fired power plants which simplify the recovery of carbon dioxide. Energy Convers. Manag. 33, 467–475. https://doi.org/10.1016/0196-8904(92)90045-X.

Boot-Handford, M.E., Abanades, J.C., Anthony, E.J., Blunt, M.J., Brandani, S., MacDowell, N., Fernández, J.R., Ferrari, M.-C., Gross, R., Hallett, J.P., Haszeldine, R.S., Heptonstall, P., Lyngfelt, A., Makuch, Z., Mangano, E., Porter, R.T.J., Pourkashanian, M., Rochelle, G.T., Shah, N., Yao, J.G., Fennell, P.S., 2014. Carbon capture and storage update. Energy Environ. Sci. 7, 130. https://doi.org/10.1039/c3ee42350f.

Bowman, J., 1990. The greenhouse effect. Land use policy 7, 101–108. https://doi.org/10.1016/0264-8377(90)90002-G.

Boyce, M.P., 2011. Combined Cycle Power Plant, in: Rao, K.R. (Ed.), Energy and Power Generation Handbook: Established and Emerging Technologies. ASME, New York, pp. 27-1 to 27-29.

Boyce, M.P., 2010. Handbook for cogeneration and combined cycle power plants, 2nd ed. ed. ASME Press, New York.

Boyce, M.P., 2002. Gas Turbine Engineering Handbook, 2nd ed. Butterworth-Heinemann, Oxford.

BP, 2018. BP statistical review of world energy.

Brigman, N., Shah, M.I., Falk-Pedersen, O., Cents, T., Smith, V., De Cazenove, T., Morken, A.K., Hvidsten, O.A., Chhaganlal, M., Feste, J.K., Lombardo, G., Bade, O.M., Knudsen, J., Subramoney, S.C., Fostås, B.F., de Koeijer, G., Hamborg, E.S., 2014. Results of Amine Plant Operations from 30 wt% and 40 wt% Aqueous MEA Testing at the CO_2 Technology Centre Mongstad. Energy Procedia 63, 6012–6022.

Burnard, K., 2017. Operational flexibility of power plants with CO_2 capture 3 rd International CCS Symposium for a Low-Carbon Society. Tokyo, Japan.

Can-Gülen, S., 2015. Étude on Gas Turbine Combined Cycle Power Plant—Next 20 Years. J. Eng. Gas Turbines Power 138, 051701. https://doi.org/10.1115/1.4031477.

Caplow, M., 1968. Kinetics of carbamate formation and breakdown. J. Am. Chem. Soc. 90, 6795–6803. https://doi.org/10.1021/ja01026a041.

Carapellucci, R., Giordano, L., Vaccarelli, M., 2015. Studying heat integration options for steam-gas power plants retrofitted with CO_2 post-combustion capture. Energy 85, 594–608. https://doi.org/10.1016/j.energy.2015.03.071.

Carapellucci, R., Milazzo, A., 2007. Repowering combined cycle power plants by a modified STIG configuration. Energy Convers. Manag. 48, 1590–1600. https://doi.org/10.1016/j.enconman.2006.11.024.

Carnegie Mellon University, 2017. Integrated Environmental Control Model.

Ceccarelli, N., van Leeuwen, M., Wolf, T., van Leeuwen, P., van der Vaart, R., Maas, W., Ramos, A., 2014. Flexibility of Low- CO_2 Gas Power Plants: Integration of the CO_2 Capture Unit with CCGT Operation. Energy Procedia 63, 1703–1726. https://doi.org/10.1016/j.egypro.2014.11.179

Chakma, A., Mehrotra, A.K., Nielsen, B., 1995. Comparison of chemical solvents for mitigating CO_2 emissions from coal-fired power plants. Heat Recover. Syst. CHP 15, 231–240. https://doi.org/10.1016/0890-4332(95)90030-6.

Chi, S., Rochelle, G.T., 2002. Oxidative Degradation of Monoethanolamine. Ind. Eng. Chem. Res. 41, 4178–4186. https://doi.org/10.1021/ie010697cChiesa, P., 2012. Novel cycles: humid air cycle systems, in: Rao, A.D. (Ed.), Combined Cycle Systems for Near-Zero Emission Power Generation. Elsevier, pp. 162–185. https://doi.org/10.1533/9780857096180.162.

Chiesa, P., Campanari, S., Manzolini, G., 2011. CO_2 cryogenic separation from combined cycles integrated with molten carbonate fuel cells. Int. J. Hydrogen Energy 36, 10355–10365. https://doi.org/10.1016/j.ijhydene.2010.09.068.

Committee on Climate Change (CCC), 2015. Sectoral scenarios for the Fifth Carbon Budget. [Online]. Available from: https://www.theccc.org.uk/wp-content/uploads/2015/11/Sectoral-scenarios-for-the-fifth-carbon-budget-Committee-on-Climate-Change.pdf [Accessed on 18.03.2019].

Cousins, A., Wardhaugh, L., Feron, P., 2011a. Preliminary analysis of process flow sheet modifications for energy efficient CO_2 capture from flue gases using chemical absorption. Chem. Eng. Res. Des. 89, 1237–1251. https://doi.org/10.1016/j.cherd.2011.02.008.

Cousins, A., Wardhaugh, L., Feron, P., 2011b. A survey of process flow sheet modifications for energy efficient CO_2 capture from flue gases using chemical absorption. Int. J. Greenh. Gas Control 5, 605–619. https://doi.org/10.1016/j.ijggc.2011.01.002.

Crooks, J.E., Donnellan, J.P., 1989. Kinetics and mechanism of the reaction between carbon dioxide and amines in aqueous solution. J. Chem. Soc. Perkin Trans. 2 331. https://doi.org/10.1039/p29890000331.

Cuéllar-Franca, R.M., Azapagic, A., 2015. Carbon capture, storage and utilisation technologies: A critical analysis and comparison of their life cycle environmental impacts. J. CO_2 Util. 9, 82–102. https://doi.org/10.1016/j.jcou.2014.12.001.

Damartzis, T., Papadopoulos, A.I., Seferlis, P., 2016. Process flowsheet design optimization for various amine-based solvents in post-combustion CO_2 capture plants. J. Clean. Prod. 111, 204–216. https://doi.org/10.1016/j.jclepro.2015.04.129.

Danckwerts, P.V., 1979. The reaction of CO_2 with ethanolamines. Chem. Eng. Sci. 34, 443–446. https://doi.org/10.1016/0009-2509(79)85087-3

Darabkhani, H.G., Jurado, N., Prpich, G., Oakey, J.E., Wagland, S.T., Anthony, E.J., 2018. Design, process simulation and construction of a 100 kW pilot-scale CO_2 membrane rig: Improving in situ CO_2 capture using selective exhaust gas recirculation (S-EGR). J. Nat. Gas Sci. Eng. 50, 128–138. https://doi.org/10.1016/J.JNGSE.2017.09.012

Datta, A., Mondal, S., Gupta, S.D., 2008. Perspectives for the direct firing of biomass as a supplementary fuel in combined cycle power plants. Int. J. Energy Res. 32, 1241–1257. https://doi.org/10.1002/er.1421Davis, L.B. and Black, S.H., 2000. Dry Low NOx Combustion Systems for GE Heavy-Duty Gas Turbines. *GE Power Systems*, GER-3568G.

Davis, J., Rochelle, G., 2009. Thermal degradation of monoethanolamine at stripper conditions. Energy Procedia 1, 327–333. https://doi.org/10.1016/j.egypro.2009.01.045

de Cazenove, T., Bouma, R.H.B., Goetheer, E.L.V., van Os, P.J., Hamborg, E.S., 2016. Aerosol Measurement Technique: Demonstration at CO_2 Technology Centre Mongstad. Energy Procedia 86, 160–170. https://doi.org/10.1016/j.egypro.2016.01.017.

Department of Energy and Climate Change and The Rt Hon Amber Rudd MP, 2015. Amber Rudd's speech on a new direction for UK energy policy. Available at: https://www.gov.uk/government/speeches/amber-rudds-speech-on-a-new-direction-foruk-energy-policy.

De Santis, A., Ingham, D.B., Ma, L., Pourkashanian, M., 2016. CFD analysis of exhaust gas recirculation in a micro gas turbine combustor for CO_2 capture. Fuel 173, 146–154. https://doi.org/10.1016/j.fuel.2016.01.063.

Diego, M.E., Akram, M., Bellas, J.-M., Finney, K.N., Pourkashanian, M., 2017a. Making gas-CCS a commercial reality: The challenges of scaling up. Greenh. Gases Sci. Technol. 7, 778–801. https://doi.org/10.1002/ghg.1695.

Diego, M.E., Bellas, J.-M., Pourkashanian, M., 2018. Techno-economic analysis of a hybrid CO_2 capture system for natural gas combined cycles with selective exhaust gas recirculation. Appl. Energy 215, 778–791. https://doi.org/10.1016/j.apenergy.2018.02.066.

Diego, M.E., Bellas, J.-M., Pourkashanian, M., 2017b. Process Analysis of Selective Exhaust Gas Recirculation for CO_2 Capture in Natural Gas Combined Cycle Power Plants Using Amines. J. Eng. Gas Turbines Power 139, 121701. https://doi.org/10.1115/1.4037323.

Dimitriou, I., García-Gutiérrez, P., Elder, R.H., Cuéllar-Franca, R.M., Azapagic, A., Allen, R.W.K., 2015. Carbon dioxide utilisation for production of transport fuels: process and economic analysis. Energy Environ. Sci. 8, 1775–1789. https://doi.org/10.1039/C4EE04117H.

Ditaranto, M., Hals, J., Bjorge, T., 2009. Investigation on the in-flame NO reburning in turbine exhaust gas. Proc. Combust. Inst. 32 II, 2659–2666. https://doi.org/10.1016/j.proci.2008.07.002.

DOE/NETL, 2015. Cost and Performance Baseline for Fossil Energy Plants Volume 1a: Bituminous Coal (PC) and Natural Gas to Electricity Revision 3. USA. https://doi.org/DOE/NETL-2015/1723.

DOE/NETL, 2013a. DOE/NETL Advanced Carbon Dioxide Capture R & D Program : Technology Update.

DOE/NETL, 2013b. Current and Future Technologies for Natural Gas Combined Cycle (NGCC) Power Plants. Pittsburgh, USA. https://doi.org/DOE/NETL-341/061013.

DOE/NETL, 2013c. Quality Guidelines for Energy System Studies Capital: Capital Cost Scaling Methodology. Pittsburgh, PA. https://doi.org/DOE/NETL-341/013113.

DOE/NETL, 2010. Carbon Capture Approaches for Natural Gas Combined Cycle Systems. Revision 2. https://doi.org/DOE/NETL-2011/1470.

Donaldson, T.L., Nguyen, Y.N., 1980. Carbon Dioxide Reaction Kinetics and Transport in Aqueous Amine Membranes. Ind. Eng. Chem. Fundam. 19, 260–266. https://doi.org/10.1021/i160075a005.

Dowell, N. Mac, Shah, N., 2014. Optimisation of Post-combustion CO_2 Capture for Flexible Operation. Energy Procedia 63, 1525–1535. https://doi.org/10.1016/j.egypro.2014.11.162.

Dowson, G.R.M.R.M., Reed, D.G.G., Bellas, J.-M., Charalambous, C., Styring, P., 2016. Fast and selective separation of carbon dioxide from dilute streams by pressure swing adsorption using solid ionic liquids. Faraday Discuss. 00, 1–17. https://doi.org/10.1039/C6FD00035E.

Du, Y., Wang, Y., Rochelle, G.T., 2016. Thermal degradation of novel piperazine-based amine blends for CO_2 capture. Int. J. Greenh. Gas Control 49, 239–249. https://doi.org/10.1016/j.ijggc.2016.03.010.

ElKady, A.M., Evulet, A., Brand, A., Ursin, T.P., Lynghjem, A., 2009. Application of Exhaust Gas Recirculation in a DLN F-Class Combustion System for Postcombustion Carbon Capture. J. Eng. Gas Turbines Power 131, 034505. https://doi.org/10.1115/1.2982158EBTF, 2011. European best practice guidelines for assessment of CO_2 capture technologies.

Energy Technologies Institute, 2015. *Carbon capture and storage: Building the UK carbon capture and storage sector by 2030 - Scenarios and actions*, Available at: http://www.eti.co.uk/wp-content/uploads/2015/03/CCS-Building-the-UK-carboncapture-and-storage-sector-by-2013.pdf.

ETI (Energy Technologies Institute), 2016. *Reducing the cost of CCS developments in capture plant technology*.

European Commission, 2014. *A policy framework for climate and energy in the period from 2020 to 2030*.

European Commission, 2012. *A Roadmap for moving to a competitive low carbon economy in 2050*.

European Environment Agency (EEA), 2018. GHG emissions by sector in the EU-28, 1990-2016. [Online]. Available from: https://www.eea.europa.eu/data-and-maps/daviz/ghg-emissions-by-sector-in#tab-chart_1 [Accessed on 18.03.2019].

Evulet, A.T., ELKady, A.M., Branda, A.R., Chinn, D., 2009. On the Performance and Operability of GE's Dry Low NOx Combustors utilizing Exhaust Gas Recirculation for PostCombustion Carbon Capture. Energy Procedia 1, 3809–3816. https://doi.org/10.1016/j.egypro.2009.02.182.

Fan, W., Liu, Y., Wang, K., 2016. Detailed experimental study on the performance of Monoethanolamine, Diethanolamine, and Diethylenetriamine at absorption/regeneration conditions. J. Clean. Prod. 125, 296–308. https://doi.org/10.1016/j.jclepro.2016.03.144.

Figueroa, J.D., Fout, T., Plasynski, S., McIlvried, H., Srivastava, R.D., 2008. Advances in CO_2 capture technology-The U.S. Department of Energy's Carbon Sequestration Program. Int. J. Greenh. Gas Control 2, 9–20. https://doi.org/10.1016/S1750-5836(07)00094-1.

Finkenrath, M., Bartlett, M., Hoffmann, S.M.-N., Dlgamber, N., Joshl, 2011. Method and system for reducing CO_2 emissions in a combustion stream. US Patent 7,966,829 B2.

Fredriksen, S.B., Jens, K.J., 2013. Oxidative degradation of aqueous amine solutions of MEA, AMP, MDEA, Pz: A review. Energy Procedia 37, 1770–1777. https://doi.org/10.1016/j.egypro.2013.06.053.

Fytianos, G., Ucar, S., Grimstvedt, A., Hyldbakk, A., Svendsen, H.F., Knuutila, H.K., 2016. Corrosion and degradation in MEA based post-combustion CO_2 capture. Int. J. Greenh. Gas Control 46, 48–56. https://doi.org/10.1016/j.ijggc.2015.12.028.

Gabrielsson, R., Torisson, T., 2003. Research and development for turbo machinery-based electric generation in a sustainable energy system.

Gal, E., Bade, O.M., Laslo, D.J., Kozak, F.Z., Muraskin, D.J., Dopatka, J., 2008. Multi-stage CO_2 removal system and method for processing a flue gas stream. US20090101012A1.

Gallo, W.L.R., 1997. A comparison between the hat cycle and other gas-turbine based cycles: Efficiency, specific power and water consumption. Energy Convers. Manag. 38, 1595–1604. https://doi.org/10.1016/S0196-8904(96)00220-8.

Ganapathy, V., 1996. Heat-recovery steam generators: Understand the basics. Chem. Eng. Prog. 92, 32–45.

Gao, X.-Y., Liu, L., Hu, M.-L., Xiang, Y., Chu, G.-W., Zou, H.-K., Sun, B.-C., Chen, J.-F., 2016. Numerical simulation for mass transfer characteristics of CO_2 capture in a rotating packed bed. Chem. Eng. Process. Process Intensif. 109, 68–79. https://doi.org/10.1016/j.cep.2016.08.015.

Gasmet, 2016. DX4000 FTIR gas analyzer Multicomponent FTIR Gas Analyzer - V.1.9 [WWW Document]. URL http://www.gasmet.com/images/tiedostot/product-downloads/gasmet_dx4000_technical_data_v1.9.pdf (accessed 9.30.16).

Gasmet, 2010. Calcmet for Windows: User manual, 11.11. ed. Gasmet Technologies Oy, Helsinki, Finland.

Gelowitz, D., Tontiwachwuthikul, P., Idem, R., 2008. Method and absorbent composition for recovering a gaseous component from a gas stream. US20100229723A1.

George, S.C., Thomas, S., 2001. Transport phenomena through polymeric systems. Prog. Polym. Sci. 26, 985–1017. https://doi.org/10.1016/S0079-6700(00)00036-8.

Ghazikhani, M., Passandideh-Fard, M., Mousavi, M., 2011. Two new high-performance cycles for gas turbine with air bottoming. Energy 36, 294–304. https://doi.org/10.1016/j.energy.2010.10.040.

Giampaolo, T., 2014. Gas Turbine Handbook: Principles and Practice, 5th ed. Fairmont Press, Lilburn.

Glasscock, D.A., Critchfield, J.E., Rochelle, G.T., 1991. CO_2 absorption/desorption in mixtures of methyldiethanolamine with monoethanolamine or diethanolamine. Chem. Eng. Sci. 46, 2829–2845. https://doi.org/10.1016/0009-2509(91)85152-N.

Global CCS Institute (GCCSI), 2015. The global status of CCS. , pp.1–12.

Gnanapragasam, N. V., Reddy, B. V., Rosen, M.A., 2009. Optimum conditions for a natural gas combined cycle power generation system based on available oxygen when using biomass as supplementary fuel. Energy 34, 816–826. https://doi.org/10.1016/j.energy.2009.03.006.

Goff, G.S., Rochelle, G.T., 2004. Monoethanolamine Degradation: O_2 Mass Transfer Effects under CO_2 Capture Conditions. Ind. Eng. Chem. Res. 43, 6400–6408. https://doi.org/10.1021/ie0400245.

González-Salazar, M.A., 2015. Recent developments in carbon dioxide capture technologies for gas turbine power generation. Int. J. Greenh. Gas Control 34, 106–116. https://doi.org/10.1016/j.ijggc.2014.12.007.

González Díaz, A., Sánchez Fernández, E., Gibbins, J., Lucquiaud, M., 2016. Sequential supplementary firing in natural gas combined cycle with carbon capture: A technology option for Mexico for low-carbon electricity generation and CO_2 enhanced oil recovery. Int. J. Greenh. Gas Control 51, 330–345. https://doi.org/10.1016/j.ijggc.2016.06.007.

Gouedard, C., Picq, D., Launay, F., Carrette, P.L., 2012. Amine degradation in CO_2 capture. I. A review. Int. J. Greenh. Gas Control 10, 244–270. https://doi.org/10.1016/j.ijggc.2012.06.015.

Gouedard, C., Rey, A., Cuzuel, V., Brunet, J., Delfort, B., Picq, D., Dugay, J., Vial, J., Pichon, V., Launay, F., Assam, L., Ponthus, J., Carrette, P.L., 2014. Amine degradation in CO_2 capture. 3. New degradation products of MEA in liquid phase: Amides and nitrogenous heterocycles. Int. J. Greenh. Gas Control 29, 61–69. https://doi.org/10.1016/j.ijggc.2014.07.013.

Gurkan, B.E., de la Fuente, J.C., Mindrup, E.M., Ficke, L.E., Goodrich, B.F., Price, E.A., Schneider, W.F., Brennecke, J.F., 2010. Equimolar CO_2 Absorption by Anion-Functionalized Ionic Liquids. J. Am. Chem. Soc. 132, 2116–2117. https://doi.org/10.1021/ja909305t.

HACH, 2014. Iron, Total, FerroVer® Method 8008 , Powder Pillows or AccuVac® Ampuls, Pocket Colorimeter II [WWW Document]. https://doi.org/DOC316.53.01458.

Hamborg, E.S. et al., 2014. Results from MEA testing at the CO_2 technology centre mongstad. Part II: Verification of baseline results. *Energy Procedia*, 63, pp.5994–6011. Available at: http://dx.doi.org/10.1016/j.egypro.2014.11.634.

Hansen, J., Ruedy, R., Sato, M., Lo, K., 2010. Global Surface Temperature Change. Rev. Geophys. 48, RG4004. https://doi.org/10.1029/2010RG000345

Heischkamp, E., Varlik, M., Korkmaz, Ö., Oeljeklaus, G., Görner, K., 2011. Analysis of operating conditions of a flue gas scrubbing process for CO_2 separation in a coal-fired power plant. Energy Procedia 4, 1377–1384. https://doi.org/10.1016/j.egypro.2011.02.002.

Heppenstall, T., 1998. Advanced gas turbine cycles for power generation: a critical review. Appl. Therm. Eng. 18, 837–846. https://doi.org/10.1016/S1359-4311(97)00116-6.

Herraiz, L., 2016. Selective Exhaust Gas Recirculation in Combined Cycle Gas Turbine Power Plants with Post-combustion Carbon Capture. Ph.D. Thesis. The University of Edinburgh. https://doi.org/10.1146/annurev.bioeng.4.020702.153427.

Herraiz, L., Fernández, E.S., Palfi, E., Lucquiaud, M., 2018. Selective exhaust gas recirculation in combined cycle gas turbine power plants with post-combustion CO_2 capture. Int. J. Greenh. Gas Control 71, 303–321. https://doi.org/10.1016/J.IJGGC.2018.01.017.

Hinton, N., Stone, R., 2014. Laminar burning velocity measurements of methane and carbon dioxide mixtures (biogas) over wide ranging temperatures and pressures. Fuel 116, 743–750. https://doi.org/10.1016/J.FUEL.2013.08.069.

Ho, M.T., Allinson, G.W., Wiley, D.E., 2008. Reducing the Cost of CO_2 Capture from Flue Gases Using Membrane Technology. Ind. Eng. Chem. Res. 47, 1562–1568. https://doi.org/10.1021/ie070541y.

Hohloch, M., Zanger, J., Widenhorn, A., Aigner, M., 2010. Experimental Characterization of a Micro Gas Turbine Test Rig, in: Volume 3: Controls, Diagnostics and Instrumentation; Cycle Innovations; Marine. ASME, pp. 671–681. https://doi.org/10.1115/GT2010-22799.

Horlock, J.H., 2003. Advanced gas turbine cycles. Pergamon, Oxford, UK.

HSE, 2014. Pressure Systems Safety Regulations 2000. Approved Code of Practice and guidance on Regulations.

Hu, Y., Ahn, H., 2017. Process integration of a Calcium-looping process with a natural gas combined cycle power plant for CO_2 capture and its improvement by exhaust gas recirculation. Appl. Energy 187, 480–488. https://doi.org/10.1016/j.apenergy.2016.11.014.

Huang, B., Banzon, V.F., Freeman, E., Lawrimore, J., Liu, W., Peterson, T.C., Smith, T.M., Thorne, P.W., Woodruff, S.D., Zhang, H.-M., 2015. Extended Reconstructed Sea Surface Temperature Version 4 (ERSST.v4). Part I: Upgrades and Intercomparisons. J. Clim. 28, 911–930. https://doi.org/10.1175/JCLI-D-14-00006.1.

Hunt, R.J., 2011. The History of the Industrial Gas Turbine (Part 1 The First Fifty Years 1940-1990). Indep. Tech. Forum Power Gener. 582–2, 1–48.

IEA, 2017a. CO_2 Emissions from Fuel Combustion 2017 - Highlights. Paris, France.

IEA, 2017b. World Energy Outlook 2017. Paris, France. https://doi.org/10.1016/0301-4215(73)90024-4.

IEA, 2013. Technology roadmap - Carbon capture and Storage, Technology Roadmap. Paris, France. https://doi.org/10.1007/SpringerReference_7300

IEAGHG, 2012a. CO_2 Capture at Gas Fired Power Plant: 2012/8. Cheltenham, UK.

IEAGHG, 2012b. Operating Flexibility of Power Plants with CCS.

IEAGHG, 2009a. Evaluation of novel post-combustion CO_2 capture solvents: Technical study. Cheltenham, UK. https://doi.org/2009/14.

IEAGHG, 2009b. Criteria for Technical and Economic Assessment of Plants With Low CO_2 Emissions. Cheltenham, UK. https://doi.org/2009/TR3.

Iijima, M., Yonekawa, T., Mimura, T., Yagi, Y., 2011. CO_2 recovery system and method. US20110120315A1.

Incropera, F.P., DeWitt, D.P., Bergman, T.L., Lavine, A.S., 2007. Fundamentals of heat and mass transfer., 6th ed. ed. John Wiley & Son Inc., New Jersey, USA.

IPCC, 2014. Climate Change 2014: Synthesis Report. Contribution of Working Groups I, II and III to the Fifth Assessment Report of the Intergovernmental Panel on Climate Change. IPPC, Geneva (Switzerland).

IPCC, 2001. Climate Change 2001: The Scientific Basis. Contribution of Working Group I to the Third Assessment Report of the Intergovernmental Panel on Climate Change. Cambridge University Press, Cambridge.

IPPC, 2007. FAQ 1.3 Figure 1 - AR4 WGI Chapter 1: Historical Overview of Climate Change Science [WWW Document]. Clim. Chang. 2007 Work. Gr. I Phys. Sci. Basis. URL https://www.ipcc.ch/publications_and_data/ar4/wg1/en/faq-1-3-figure-1.html (accessed 1.4.16).

IPPC, 2005. IPCC Special Report on Carbon Dioxide Capture and Storage. Prepared by Working Group III of the Intergovernmental Panel on Climate Change. Cambridge University Press, Cambridge, United Kingdom and New York, NY, USA.

ISO, 2009. Gas turbines — Acceptance tests. International Organization for Standardization, Switzerland.

ISO, 1996. Gas Turbines- Exhaust gas emission - Part 1: Measurement and evaluation: ISO11042-1. London.

Janssens-Maenhout, G., Crippa, M., Guizzardi, D., Muntean, M., Schaaf, E., Dentener, F., Bergamaschi, P., Pagliari, V., Olivier, J.G.J., Peters, J.A.H.W., van Aardenne, J.A., Monni, S., Doering, U., Petrescu, A.M.R., 2017. EDGAR v4.3.2 Global Atlas of the three major Greenhouse Gas Emissions for the period 1970-2012. Earth Syst. Sci. Data Discuss. 1–55. https://doi.org/10.5194/essd-2017-79.

Joel, A.S., Wang, M., Ramshaw, C., Oko, E., 2014. Process analysis of intensified absorber for post-combustion CO_2 capture through modelling and simulation. Int. J. Greenh. Gas Control 21, 91–100. https://doi.org/10.1016/j.ijggc.2013.12.005.

Jonsson, M., Yan, J., 2005. Humidified gas turbines—a review of proposed and implemented cycles. Energy 30, 1013–1078. https://doi.org/10.1016/j.energy.2004.08.005.

Kao, Y.K., Qiu, M.M., Hwang, S.T., 1989. Critical evaluations of two membrane gas-permeator designs: continuous membrane column and two strippers in series. Ind. Eng. Chem. Res. 28, 1514–1520. https://doi.org/10.1021/ie00094a014.

Karmellos, M., Kopidou, D., Diakoulaki, D., 2016. A decomposition analysis of the driving factors of CO_2 (Carbon dioxide) emissions from the power sector in the European Union countries. Energy 94, 680–692. https://doi.org/10.1016/j.energy.2015.10.145.

Khalilpour, R., Mumford, K., Zhai, H., Abbas, A., Stevens, G., Rubin, E.S., 2015. Membrane-based carbon capture from flue gas: a review. J. Clean. Prod. 103, 286–300. https://doi.org/10.1016/j.jclepro.2014.10.050.

Kim, I., Svendsen, H.F., 2007. Heat of Absorption of Carbon Dioxide (CO_2) in Monoethanolamine (MEA) and 2-(Aminoethyl)ethanolamine (AEEA) Solutions. Ind. Eng. Chem. Res. 46, 5803–5809. https://doi.org/10.1021/ie0616489.

Kishimoto, A., Kansha, Y., Fushimi, C., Tsutsumi, A., 2011. Exergy Recuperative CO_2 Gas Separation in Post-Combustion Capture. Ind. Eng. Chem. Res. 50, 10128–10135. https://doi.org/10.1021/ie200852b.

Knudsen, J.N., Andersen, J., Jensen, J.N., Biede, O., 2011. Evaluation of process upgrades and novel solvents for the post combustion CO_2 capture process in pilot-scale. Energy Procedia 4, 1558–1565. https://doi.org/10.1016/j.egypro.2011.02.025.

Kohl, A.L., Nielsen, R.B., 1997. Gas purification. Gulf Publishing, Houston, Texas, USA.

Koornneef, J., Ramírez, A., Turkenburg, W., Faaij, A., 2012. The environmental impact and risk assessment of CO_2 capture, transport and storage - An evaluation of the knowledge base. Prog. Energy Combust. Sci. 38, 62–86. https://doi.org/10.1016/j.pecs.2011.05.002.

Le Moullec, Y., Kanniche, M., 2011. Screening of flowsheet modifications for an efficient monoethanolamine (MEA) based post-combustion CO_2 capture. Int. J. Greenh. Gas Control 5, 727–740. https://doi.org/10.1016/j.ijggc.2011.03.004.

Le Moullec, Y., Neveux, T., Al Azki, A., Chikukwa, A., Hoff, K.A., 2014. Process modifications for solvent-based post-combustion CO_2 capture. Int. J. Greenh. Gas Control 31, 96–112. https://doi.org/10.1016/j.ijggc.2014.09.024.

Lee, K., Kim, H., Park, P., Yang, S., Ko, Y., 2013. CO_2 radiation heat loss effects on NOx emissions and combustion instabilities in lean premixed flames. Fuel 106, 682–689. https://doi.org/10.1016/J.FUEL.2012.12.048.

Lefebvre, A.H. (Arthur H., Ballal, D.R., 2010. Gas turbine combustion : alternative fuels and emissions. Taylor & Francis.

Li, H., Ditaranto, M., Berstad, D., 2011a. Technologies for increasing CO2 concentration in exhaust gas from natural gas-fired power production with post-combustion, amine-based CO_2 capture. Energy 36, 1124–1133. https://doi.org/10.1016/j.energy.2010.11.037.

Li, H., Ditaranto, M., Yan, J., 2012. Carbon capture with low energy penalty: Supplementary fired natural gas combined cycles. Appl. Energy 97, 164–169.

Li, H., Flores, S., Hu, Y., Yan, J., 2009. Simulation and Optimization of Evaporative Gas Turbine with Chemical Absorption for Carbon Dioxide Capture. Int. J. Green Energy 6, 527–539. https://doi.org/10.1080/15435070903231393.

Li, H., Haugen, G., Ditaranto, M., Berstad, D., Jordal, K., 2011b. Impacts of exhaust gas recirculation (EGR) on the natural gas combined cycle integrated with chemical absorption CO_2 capture technology. Energy Procedia 4, 1411–1418. https://doi.org/10.1016/j.egypro.2011.02.006.

Li, K., Leigh, W., Feron, P., Yu, H., Tade, M., 2016. Systematic study of aqueous monoethanolamine (MEA)-based CO_2 capture process: Techno-economic assessment of the MEA process and its improvements. Appl. Energy 165, 648–659. https://doi.org/10.1016/j.apenergy.2015.12.109.

Li, X., Wang, S., Chen, C., 2013. Experimental Study of Energy Requirement of CO_2 Desorption from Rich Solvent. Energy Procedia 37, 1836–1843. https://doi.org/10.1016/j.egypro.2013.06.063.

LSE, 2015. HM Government Statement Re Carbon Capture, Storage - RNS - London Stock Exchange [WWW Document]. URL http://www.londonstockexchange.com/exchange/news/market-news/market-news-detail/other/12597443.html (accessed 4.18.16).

Lugo-Leyte, R., Zamora-Mata, J.M., Toledo-Velzquez, M., Salazar-Pereyra, M., Torres-Aldaco, A., 2010. Methodology to determine the appropriate amount of excess air for the operation of a gas turbine in a wet environment. Energy 35, 550–555. https://doi.org/10.1016/j.energy.2009.10.023.

MacDowell, N., Florin, N., Buchard, A., Hallett, J., Galindo, A., Jackson, G., Adjiman, C.S., Williams, C.K., Shah, N., Fennell, P., 2010. An overview of CO_2 capture technologies. Energy Environ. Sci. 3, 1645. https://doi.org/10.1039/c004106h

Mandal, B., Bandyopadhyay, S.S., 2006. Simultaneous Absorption of CO_2 and H_2S Into Aqueous Blends of N -Methyldiethanolamine and Diethanolamine. Environ. Sci. Technol. 40, 6076–6084. https://doi.org/10.1021/es0606475.

Manfrida, G., 1999. Opportunities for High-Efficiency Electricity Generation Inclusive of CO_2 Capture. Int.J. Appl. Thermodyn. 2, 165–175.

Mansouri Majoumerd, M., Nikpey Somehsaraei, H., Assadi, M., Breuhaus, P., 2014. Micro gas turbine configurations with carbon capture – Performance assessment using a validated thermodynamic model. Appl. Therm. Eng. 73, 172–184. https://doi.org/10.1016/j.applthermaleng.2014.07.043.

Marsh, R., Giles, A., Runyon, J., Pugh, D., Bowen, P., Morris, S., Valera-Medina, A., Best, T., Finney, K., Pourkashanian, M., 2016. The Future of Gas Turbine Technology 8 th International Gas Turbine Conference 12-13.

Marsh, R., Runyon, J., Giles, A., Morris, S., Pugh, D., Valera-Medina, A., Bowen, P., 2017. Premixed methane oxycombustion in nitrogen and carbon dioxide atmospheres: measurement of operating limits, flame location and emissions. Proceedings of the Combustion Institute. Proc. Combust. Inst. 36, 3949–3958. https://doi.org/10.1016/J.PROCI.2016.06.057.

Martínez, F.R., Martínez, A.R., Velazquez, M.T., Diez, P.Q., Eslava, G.T., Francis, J.A., 2011. Evaluation of the Gas Turbine Inlet Temperature with Relation to the Excess Air. Energy Power Eng. 03, 517–524. https://doi.org/10.4236/epe.2011.34063.

McGlade, C., Pye, S., Watson, J., Bradshaw, M., Ekins, P., 2016. The future role of natural gas in the UK. London.

Mechleri, E.D., Mac Dowell, N., 2015. Controllability analysis of a post-combustion CO_2 capture plant integrated with a coal and natural gas-fired power plant, in: 3rd Post Combustion Capture Conference. 8–11 September 2015. . Boundary Dam, Regina, Saskatchewan, Canada.

Menon, A., Duss, M., 2010. The New Sulzer Mellapak^{TM}CC^{TM} and AYPlus^{TM}DC Structured Packings for Post-Combustion Capture, in: IEAGHG 1st Post Combustion Capture Conference. IEAGHG, Cheltenham, UK, Adu Dhabi, UAE.

Merkel, T.C., Lin, H., Wei, X., Baker, R., 2010. Power plant post-combustion carbon dioxide capture: An opportunity for membranes. J. Memb. Sci. 359, 126–139. https://doi.org/10.1016/j.memsci.2009.10.041.

Merkel, T.C., Wei, X., He, Z., White, L.S., Wijmans, J.G., Baker, R.W., 2013. Selective Exhaust Gas Recycle with Membranes for CO_2 Capture from Natural Gas Combined Cycle Power Plants. Ind. Eng. Chem. Res. 52, 1150–1159. https://doi.org/10.1021/ie302110z.

Mission Innovation, 2017. Mission Innovation – Accelerating the Clean Energy Revolution [WWW Document]. URL http://mission-innovation.net/ (accessed 10.26.17).

MOHAD / CRU, 2017. Met Office Hadley Centre observations datasets [WWW Document]. URL https://www.metoffice.gov.uk/hadobs/ (accessed 7.4.18).

Mondal, M.K., Balsora, H.K., Varshney, P., 2012. Progress and trends in CO_2 capture/separation technologies: A review. Energy 46, 431–441. https://doi.org/10.1016/j.energy.2012.08.006.

Morrison, R.T., 1992. Organic chemistry, 6th ed. ed. London : Prentice-Hall International, 1992, London.

Moss, R.H., Edmonds, J.A., Hibbard, K.A., Manning, M.R., Rose, S.K., van Vuuren, D.P., Carter, T.R., Emori, S., Kainuma, M., Kram, T., Meehl, G.A., Mitchell, J.F.B., Nakicenovic, N., Riahi, K., Smith, S.J., Stouffer, R.J., Thomson, A.M., Weyant, J.P., Wilbanks, T.J., 2010. The next generation of scenarios for climate change research and assessment. Nature 463, 747–756. https://doi.org/10.1038/nature08823.

NASA, 2018. Carbon Dioxide | Vital Signs – Climate Change: Vital Signs of the Planet [WWW Document]. URL https://climate.nasa.gov/vital-signs/carbon-dioxide/ (accessed 7.4.18).

National Grid, 2017. Gas calorific value | National Grid UK [WWW Document]. URL https://www.nationalgrid.com/uk/gas/market-and-operations/calorific-value-cv (accessed 11.29.17).

Nielsen, C.J., Herrmann, H., Weller, C., 2012. Atmospheric chemistry and environmental impact of the use of amines in carbon capture and storage (CCS). Chem. Soc. Rev. 41, 6684. https://doi.org/10.1039/c2cs35059a.

Nikpey, H., Mansouri Majoumerd, M., Assadi, M., Breuhaus, P., 2014. Thermodynamic Analysis of Innovative Micro Gas Turbine Cycles, in: Volume 3A: Coal, Biomass and Alternative Fuels; Cycle Innovations; Electric Power; Industrial and Cogeneration. ASME, p. V03AT07A029. https://doi.org/10.1115/GT2014-26917.

Notz, R., Mangalapally, H.P., Hasse, H., 2012. Post combustion CO_2 capture by reactive absorption: Pilot plant description and results of systematic studies with MEA. Int. J. Greenh. Gas Control 6, 84–112. https://doi.org/10.1016/j.ijggc.2011.11.004.

NRG Energy, 2017. Petra Nova [WWW Document]. URL http://www.nrg.com/generation/projects/petra-nova/ (accessed 12.10.17).

Øi, L.E., Kvam, S.H.P., 2014. Comparison of Energy Consumption for Different CO_2 Absorption Configurations Using Different Simulation Tools. Energy Procedia 63, 1186–1195. https://doi.org/10.1016/j.egypro.2014.11.128.

Oxburgh, 2016. *Lowest cost of decarbonisation for the UK: The critical role of CCS. Report to the Secretary of State for Business, Energy and Industrial Strategy from the Parliamentary Advisory Group on Carbon Capture and Storage (CCS)*.

Oyenekan, B.A., Rochelle, G.T., 2007. Alternative stripper configurations for CO_2 capture by aqueous amines. AIChE J. 53, 3144–3154. https://doi.org/10.1002/aic.11316.

Oyenekan, B.A., Rochelle, G.T., 2006. Energy Performance of Stripper Configurations for CO_2 Capture by Aqueous Amines. Ind. Eng. Chem. Res. 45, 2457–2464. https://doi.org/10.1021/ie050548k.

PACT, 2018. PACT – Pilot-scale Advanced Capture Technology [WWW Document]. URL https://pact.group.shef.ac.uk/ (accessed 8.23.18).

Parsons, E.L., Shelton, W.W., Lyons, J.L., 2002. Advanced Fossil Power Systems Comparison Study: Final Report. USA.

Pedemonte, A.A., Traverso, A., Massardo, A.F., 2008a. Experimental analysis of pressurised humidification tower for humid air gas turbine cycles. Part B: Correlation of experimental data. Appl. Therm. Eng. 28, 1623–1629. https://doi.org/10.1016/j.applthermaleng.2007.10.031.

Pedemonte, A.A., Traverso, A., Massardo, A.F., 2008b. Experimental analysis of pressurised humidification tower for humid air gas turbine cycles. Part A: Experimental campaign. Appl. Therm. Eng. 28, 1711–1725. https://doi.org/10.1016/j.applthermaleng.2007.10.030.

Penning, F.M., de Lange, H.C., 1996. Steam injection: Analysis of a typical application. Appl. Therm. Eng. 16, 115–125. https://doi.org/10.1016/1359-4311(95)00052-F.

Pinto, D.D.D., Knuutila, H., Fytianos, G., Haugen, G., Mejdell, T., Svendsen, H.F., 2014. CO_2 post combustion capture with a phase change solvent. Pilot plant campaign. Int. J. Greenh. Gas Control 31, 153–164. https://doi.org/10.1016/j.ijggc.2014.10.007.

Polderman, L.D., Dillon, C.P., Steele, A.B., 1955. Why monoethanolamine solution breaks down in gas-treating service. Oil Gas J. 52, 180–3.

Poullikkas, A., 2005. An overview of current and future sustainable gas turbine technologies. Renew. Sustain. Energy Rev. 9, 409–443. https://doi.org/10.1016/j.rser.2004.05.009.

Pourkashanian, M., Yapp, L., Williams, A., 1989. The use of oxygen enrichment in combustion technology, in: Proceedings of the Institute of Energy Conference, 5-7 September. Applied Energy Research, Swansea, UK.

Qiu, M.M., Hwang, S.T., Kao, Y.K., 1989. Economic evaluation of gas membrane separator designs. Ind. Eng. Chem. Res. 28, 1670–1677. https://doi.org/10.1021/ie00095a016.

Rao, A., 2014. Evaporative Gas Turbine (EvGT)/Humid Air Turbine (HAT) Cycles, in: Handbook of Clean Energy Systems. John Wiley & Sons, Ltd, Chichester, UK, pp. 1–18. https://doi.org/10.1002/9781118991978.hces141.

Reddy, S., Gilmartin, J., 2008. Fluor's Econamine FG Plus SM Technology for Post-Combustion CO_2 Capture. Amsterdam, Netherlands.

Rhodes, M., 2013. Combined Cycle Power Generation: Head of the H-class. Diesel Gas Turbine Worldw.

Røkke, P.E., Hustad, J.E., 2005. Exhaust Gas Recirculation in Gas Turbines for Reduction of CO_2 Emissions; Combustion Testing with Focus on Stability and Emissions, International Journal of Thermodynamics. https://doi.org/10.5541/ijot.158.

Rosenberg, R.M., Peticolas, W.L., 2004. Henry ' s Law : A Retrospective 81, 1647–1652.

Rousseau, R.W., 1987. Handbook of separation process technology. Wiley, New York.

Russo, G., Prpich, G., Anthony, E.J., Montagnaro, F., Jurado, N., Di Lorenzo, G., Darabkhani, H.G., 2018. Selective-exhaust gas recirculation for CO_2 capture using membrane technology. J. Memb. Sci. 549, 649–659. https://doi.org/10.1016/j.memsci.2017.10.052.

Samanta, A., Bandyopadhyay, S.S., 2009. Absorption of carbon dioxide into aqueous solutions of piperazine activated 2-amino-2-methyl-1-propanol. Chem. Eng. Sci. 64, 1185–1194. https://doi.org/10.1016/j.ces.2008.10.049.

Sanchez Fernandez, E., Sanchez del Rio, M., Chalmers, H., Khakharia, P., Goetheer, E.L.V., Gibbins, J., Lucquiaud, M., 2016. Operational flexibility options in power plants with integrated post-combustion capture. Int. J. Greenh. Gas Control 48, 275–289. https://doi.org/10.1016/j.ijggc.2016.01.027.

Sander, F., Carroni, R., Rofka, S., Benz, E., 2011. Flue Gas Recirculation in a Gas Turbine: Impact on Performance and Operational Behavior, in: Volume 4: Cycle Innovations; Fans and Blowers; Industrial and Cogeneration; Manufacturing Materials and Metallurgy; Marine; Oil and Gas Applications. ASME, pp. 123–132. https://doi.org/10.1115/GT2011-45608.

Saravanamuttoo, H.I.H., Rogers, G.F.C., Cohen, H., Straznicky, P., 2009. Gas turbine theory. Pearson Prentice Hall, Harlow, UK.

SaskPower, 2017. Boundary Dam Carbon Capture Project [WWW Document]. URL http://www.saskpower.com/our-power-future/carbon-capture-and-storage/boundary-dam-carbon-capture-project/ (accessed 12.10.17).

Seliger, H., Huber, A., Aigner, M., 2015. Experimental Investigation of a FLOX®-Based Combustor for a Small-Scale Gas Turbine Based CHP System Under Atmospheric Conditions, in: ASME Turbo Expo 2015: Turbine Technical Conference and Exposition. ASME, Montreal, Quebec, Canada, p. V04BT04A004.

Sema, T., Naami, A., Fu, K., Edali, M., Liu, H., Shi, H., Liang, Z., Idem, R., Tontiwachwuthikul, P., 2012. Comprehensive mass transfer and reaction kinetics studies of CO_2 absorption into aqueous solutions of blended MDEA–MEA. Chem. Eng. J. 209, 501–512. https://doi.org/10.1016/j.cej.2012.08.016.

Seoane, B., Coronas, J., Gascon, I., Benavides, M.E., Karvan, O., Caro, J., Kapteijn, F., Gascon, J., 2015. Metal–organic framework based mixed matrix membranes: a solution for highly efficient CO_2 capture? Chem. Soc. Rev. 44, 2421–2454. https://doi.org/10.1039/C4CS00437J.

Servomex, 2008. Servomex MiniMP (5200) Gas Analyser: Operator Manual, 8th ed. Servomex, Crowborough, East Sussex, UK.

Sexton, A.J., Rochelle, G.T., 2011. Reaction Products from the Oxidative Degradation of Monoethanolamine. Ind. Eng. Chem. Res. 50, 667–673. https://doi.org/10.1021/ie901053s.

Sharifzadeh, M., Shah, N., 2018. MEA-based CO_2 Capture integrated with Natural Gas Combined Cycle or Pulverized Coal Power Plants: Operability and Controllability through Integrated Design and Control. J. Clean. Prod. https://doi.org/10.1016/j.jclepro.2018.09.115.

SINTEF, 2018. CO_2 laboratory, Tiller - SINTEF [WWW Document]. URL https://www.sintef.no/en/all-laboratories/co2-laboratory-tiller/ (accessed 9.28.18).

Sonntag, R.E., 1998. Fundamentals of thermodynamics, 5th ed. ed. New York , New York .

Sreenivasulu, B., Gayatri, D. V., Sreedhar, I., Raghavan, K. V., 2015. A journey into the process and engineering aspects of carbon capture technologies. Renew. Sustain. Energy Rev. 41, 1324–1350. https://doi.org/10.1016/j.rser.2014.09.029.

Stéphenne, K., 2014. Start-up of World's First Commercial Post-combustion Coal Fired CCS Project: Contribution of Shell Cansolv to SaskPower Boundary Dam ICCS Project. Energy Procedia 63, 6106–6110. https://doi.org/10.1016/j.egypro.2014.11.642.

Supap, T., Idem, R., Tontiwachwuthikul, P., Saiwan, C., 2006. The Roles of O_2 and SO_2 in the Degradation of Monoethanolamine during CO_2 Absorption from Industrial Flue Gas Streams, in: 2006 IEEE EIC Climate Change Conference. IEEE, pp. 1–6. https://doi.org/10.1109/EICCCC.2006.277275.

Tait, P., Buschle, B., Ausner, I., Valluri, P., Wehrli, M., Lucquiaud, M., 2016. A pilot-scale study of dynamic response scenarios for the flexible operation of post-combustion CO_2 capture. Int. J. Greenh. Gas Control 48, 216–233. https://doi.org/10.1016/j.ijggc.2015.12.009.

Tait, P., Buschle, B., Milkowski, K., Akram, M., Pourkashanian, M., Lucquiaud, M., 2018. Flexible operation of post-combustion CO_2 capture at pilot scale with demonstration of capture-efficiency control using online solvent measurements. Int. J. Greenh. Gas Control 71, 253–277. https://doi.org/10.1016/j.ijggc.2018.02.023.

Thimsen, D. et al., 2014. Results from MEA testing at the CO_2 Technology Centre Mongstad. Part I: Post-Combustion CO2 capture testing methodology. *Energy Procedia*, 63, pp.5938–5958. Available at: http://linkinghub.elsevier.com/retrieve/pii/S187661021402445X.

Tol, R.J., De Vos, A., 1998. A Bayesian Statistical Analysis of the Enhanced Greenhouse Effect. Clim. Change 38, 87–112. https://doi.org/10.1023/A:1005390515242.

Towler, G.P., Shethna, H.K., Cole, B., Hajdik, B., 1997. Improved absorber-stripper technology for gas sweetening to ultra-low H_2S concentrations, in: Proceedings, Annual Convention - Gas Processors Association. pp. 93–100.

Traverso, A., 2010. Humidification tower for humid air gas turbine cycles: Experimental analysis. Energy 35, 894–901. https://doi.org/10.1016/j.energy.2009.07.021.

Traverso, A., Massardo, A.F., 2002. Thermoeconomic analysis of mixed gas–steam cycles. Appl. Therm. Eng. 22, 1–21. https://doi.org/10.1016/S1359-4311(01)00064-3.

Turbec, 2009. T100 microturbine system: Technical description: T100 natural gas: D14127–03.

Turbec, 2006. Operator's manual: Turbec T100: Series 3: D12430.

Turi, D.M.M., Ho, M., Ferrari, M.C.C., Chiesa, P., Wiley, D.E.E., Romano, M.C.C., 2017. CO_2 capture from natural gas combined cycles by CO_2 selective membranes. Int. J. Greenh. Gas Control 61, 168–183. https://doi.org/https://doi.org/10.1016/j.ijggc.2017.03.022.

Tyrrell, H.J. V., 1964. The Origin and Present Status of Fick ' s Diffusion Law. J. Chem. Educ. 41, 397–400. https://doi.org/10.1021/ed041p397.

UK Gov, 2019. Climate Change Act 2008. [Online]. Available from: https://www.legislation.gov.uk/ukpga/2008/27/contents [Accessed 18.03.2019].

UNFCCC, 2015. Adoption of the Paris Agreement. United Nations Framework Convention on Climate Change (UNFCCC), Paris.

UNFCCC, 2014. National greenhouse gas inventory data for the period 1990–2012. Geneva (Switzerland).

US EPA, C.C.D., 2015. Causes of Climate Change [WWW Document]. URL http://www3.epa.gov/climatechange/science/causes.html (accessed 12.9.15).

Vaidya, P.D., Kenig, E.Y., 2007. CO_2-Alkanolamine Reaction Kinetics: A Review of Recent Studies. Chem. Eng. Technol. 30, 1467–1474. https://doi.org/10.1002/ceat.200700268.

Voleno, A., Romano, M.C., Turi, D.M., Chiesa, P., Ho, M.T., Wiley, D.E., 2014. Post-combustion CO_2 Capture from Natural Gas Combined Cycles by Solvent Supported Membranes. Energy Procedia 63, 7389–7397. https://doi.org/10.1016/j.egypro.2014.11.775.

Wall, T., Liu, Y., Spero, C., Elliott, L., Khare, S., Rathnam, R., Zeenathal, F., Moghtaderi, B., Buhre, B., Sheng, C., Gupta, R., Yamada, T., Makino, K., Yu, J., 2009. An overview on oxyfuel coal combustion—State of the art research and technology development. Chem. Eng. Res. Des. 87, 1003–1016. https://doi.org/10.1016/j.cherd.2009.02.005.

Wang, Y., Li, Y., Weng, S., Su, M., 2007a. Experimental investigation on humidifying performance of counter flow spray saturator for humid air turbine cycle. Energy Convers. Manag. 48, 756–763. https://doi.org/10.1016/j.enconman.2006.09.005.

Wang, Y., Li, Y., Weng, S., Wang, Y., 2007b. Numerical simulation of counter-flow spray saturator for humid air turbine cycle. Energy 32, 852–860. https://doi.org/10.1016/j.energy.2006.05.008.

Wei, C., Zang, S., 2012. Experimental investigation on the off-design performance of a small-sized humid air turbine cycle. ATE 51, 166–176. https://doi.org/10.1016/j.applthermaleng.2012.08.061.

Wu, X., He, M., Yu, Y., Qin, Z., Zhang, Z., 2017. Overall Mass Transfer Coefficient of CO_2 Absorption in a Diameter-varying Spray Tower. Energy Procedia 114, 1665–1670. https://doi.org/10.1016/j.egypro.2017.03.1295.

Yazvikova, N. V, 1975. Mechanism of side reactions during removal of carbon dioxide from gases by treatment with monoethanolamine. Zh. Prikl. Khim.

Yu, C.-H., Chen, M.-T., Chen, H., Tan, C.-S., 2016. Effects of process configurations for combination of rotating packed bed and packed bed on CO_2 capture. Appl. Energy 175, 269–276. https://doi.org/10.1016/j.apenergy.2016.05.044.

Zanger, J., Thomas, M., Manfre, A., 2013. Experimental Investigation of the Influence of Combustor Cooling on the Characteristics of a FLOX©-Based Micro Gas Turbine Combustor, in: Progress in Gas Turbine Performance. InTech. https://doi.org/10.5772/54405.

Zarogiannis, T., Papadopoulos, A.I., Seferlis, P., 2016. Systematic selection of amine mixtures as post-combustion CO_2 capture solvent candidates. J. Clean. Prod. 136, 159–175. https://doi.org/10.1016/j.jclepro.2016.04.110.

Zhai, H., Rubin, E.S., 2013. Techno-Economic Assessment of Polymer Membrane Systems for Postcombustion Carbon Capture at Coal-Fired Power Plants. Environ. Sci. Technol. 47, 3006–3014. https://doi.org/10.1021/es3050604

Zhang, J., Tong, D., Fennell, P.S., Trusler, J.P.M., 2015. Solubility of CO_2 in aqueous amine solutions: A study to select solvents for carbon capture from natural-gas power plant, in: Proceedings of the 4th International Gas Processing Symposium. Elsevier, pp. 1–10. https://doi.org/10.1016/B978-0-444-63461-0.50001-8.

Zhang, W., Magee, J., Singh, H., Ruchti, C., Selby, G., 2012. HRSG development for the future., in: PowerGen Europe 12–14 June 2012. PowerGen Europe, Cologne, Germany.

9 Appendices

9.1 Appendix A.1

To determine the moles of O_2, CO_2, H_2O per mole of fuel, the stoichiometric reactions presented Table 9.1 and the mole fraction of the gas species in the fuel composition have been used.

Table 9.1. Stoichiometric reaction of different natural gas species.

Species	Stoichiometric reaction
Methane (CH_4)	$CH_4 + 2O_2 \rightarrow CO_2 + 2H_2O$
Ethane (C_2H_6)	$C_2H_6 + 3.5O_2 \rightarrow 2CO_2 + 3H_2O$
Propane (C_3H_8)	$C_3H_8 + 5O_2 \rightarrow 3CO_2 + 4H_2O$
Butane (C_4H_{10})	$C_4H_{10} + 6.5O_2 \rightarrow 4CO_2 + 5H_2O$
Pentane (C_5H_{12})	$C_5H_{12} + 8O_2 \rightarrow 5CO_2 + 6H_2O$
Hexane (C_6H_{14})	$C_6H_{14} + 9.5O_2 \rightarrow 6CO_2 + 7H_2O$

The following equation is used to calculate the number of moles of O_2 required and, CO_2 and H_2O produced per mole of fuel, which assumes complete combustion.

$$n = (i_1.X_1) + (i_2.X_2) + (i_3.X_3) + (i_4.4) + (i_5.X_5) + (i_6.X_6) + \ldots \quad \textbf{(9.1)}$$

$$\text{e.g. } n_{O2} = (2O_2.X_{CH4}) + (3.5O_2.X_{C2H6}) + (5O_2.X_{C3H8}) + (6.5O_2.X_{C4H10}) + (8O_2.X_{C5H12}) + (9.5O_2.X_{C6H14}) \quad \textbf{(9.2)}$$

n = Number mole of species per mole of fuel (g/mol).

i_1 = Number of moles.

X_1 = Mole fraction of the gas composition.

The flue gas flowrate (mol/s) is determined from:

$$n_{fg,CO2} = n_{fuel}.n_{CO2} \quad \textbf{(9.3)}$$

$$n_{fg} = n_{fg,CO2} / \left(\frac{vol.\%_{CO2}}{100} \right) \quad \textbf{(9.4)}$$

Where $n_{fg,CO2}$ is the CO_2 flowrate in the flue gas (mol/s), n_{fuel} is the fuel flowrate (mol/s), n_{CO2} is the mole of CO_2 per mole of fuel (g/mol), $vol.\%_{CO2}$ is the CO2 concentration in the FTIR on a dry basis in vol%, and n_{fg} is the flue gas flowrate (mol/s). To determine the molar flowrate of O_2 and H_2O in the flue gas, the total flue gas flowrate is divided by the measured concentrations of O_2 and H_2O in the FTIR. The N_2 is determined from subtracting the CO2, O_2 and H_2O from the total flue gas flowrate. The air flowrate is then determined by dividing the N_2 in mol/s by 0.79 (which corresponds to air containing 79% N_2.

9.2 Appendix A.2

The average TOT, CO and UHC for the 40 and 50 kWe baseline tests are presented in Table 9.2.

Table 9.2. Average TOT, CO and UHC data for the 40 and 50 kW_e baseline tests.

Electrical power output (kW_e)	TOT (°C)	CO (ppmv, dry)	UHC (ppmv, dry)
40	618	827	398
50	645	233	19

9.3 Appendix A.3

Figure 9.1 (a) and (b) presents the air fuel ratio and excess air requirement against increasing CO_2 injection rate across the 60-100 kW_e electrical power output.

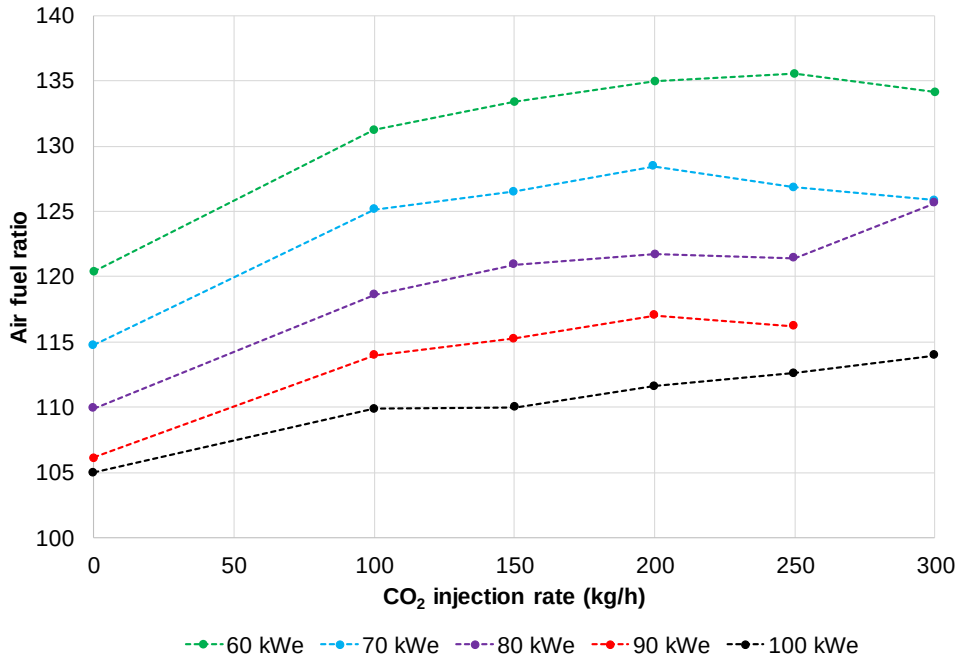

(a)

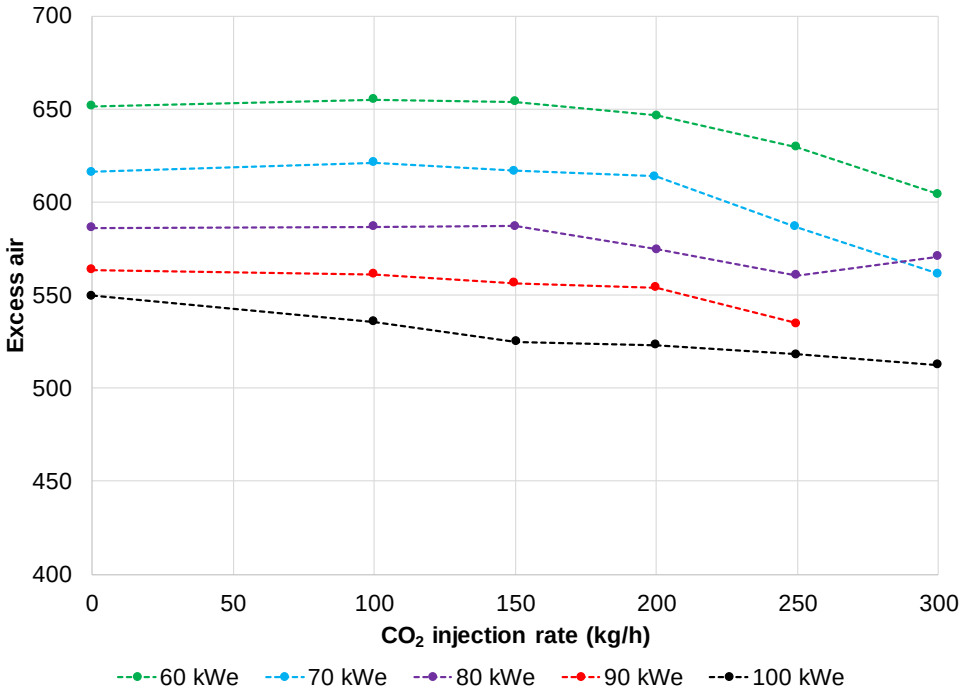

(b)

Figure 9.1. Influence of increasing CO_2 injection rates on (a) the air fuel ratio and (b) excess air at electrical power output of 60-100 kW_e.

9.4 Appendix A.4

Table 9.3. Summary of results for the ACP experimental test campaign 1.

Parameter	Unit	Test 1	Test 2	Test 3	Test 4
CO_2 conc.	***vol%***	***5.2***	***6.5***	***7.6***	***9.0***
CO_2 flowrate absorber inlet	mol/h	391.9	496.6	577.5	697.2
CO_2 flowrate absorber outlet	mol/h	44.5	53.8	64.8	82.0
CO_2 captured	kg/h	15.3	19.5	22.6	27.1
CO_2 capture efficiency	%	89	89	89	88
Lean MEA conc.	wt.%	38.4	38.9	38.3	37.3
Rich MEA conc.	wt.%	38.4	39.0	38.6	37.4
Lean loading	molCO_2/molMEA	0.262	0.267	0.304	0.319
Rich loading	molCO_2/molMEA	0.378	0.379	0.392	0.399
Degree of regeneration	%	30.7	29.6	22.4	20.1
Lean solvent flowrate	kg/h	476.5	578.8	859.2	990.9
Flue gas flowrate	kg/h	224.5	228.3	228.5	233.0
Flue gas temperature at booster fan	°C	24.4	24.9	21.5	20.7
Flue gas temperature at absorber inlet	°C	41.7	39.3	39.6	39.6
Flue gas temperature at wash column outlet	°C	44.1	44.7	38.8	36.3
L/G ratio	kg/kg	2.12	2.54	3.76	4.25
Specific reboiler duty	MJ/kg CO_2	8.9	7.6	8.2	7.3
Flue gas exit out of the absorber					
H_2O	vol%	9.2	9.7	6.9	6.7
O_2	vol%	16.9	16.7	16.7	17.2
MEA	ppmv	40	33	23	28
NH_3	ppmv	99	86	89	107

Table 9.4. Summary of results for the ACP experimental test campaign 2.

Parameter	Unit	Baseline	Test 2	Test 3	Test 4
PHW temperature	*°C*	***125.6***	***126.8***	***124.7***	***123.7***
CO_2 conc.	vol%	9.0	9.0	9.0	9.0
CO_2 flowrate absorber inlet	mol/h	697.2	683.1	684.2	670.4
CO_2 flowrate absorber outlet	mol/h	82.0	59.3	110.8	148.8
CO_2 captured	kg/h	27.1	27.5	25.2	23.0
CO_2 capture efficiency	%	88	91	84	78
Lean MEA conc.	wt.%	37.3	38.0	36.4	36.8
Rich MEA conc.	wt.%	37.4	37.3	36.6	36.9
Lean loading	molCO_2/molMEA	0.319	0.277	0.328	0.344
Rich loading	molCO_2/molMEA	0.399	0.373	0.419	0.414
Degree of regeneration	%	20.1	25.7	21.7	16.9
Lean solvent flowrate	kg/h	990.9	947.6	981.9	985.8
Flue gas flowrate	kg/h	233.0	228.2	228.6	224.0
Flue gas temperature at booster fan	°C	20.7	24.3	23.6	23.9
Flue gas temperature at absorber inlet	°C	39.6	40.9	40.6	40.8
Flue gas temperature at wash column outlet	°C	36.3	35.9	37.9	38.1
L/G ratio	kg/kg	4.25	4.27	4.30	4.30
Specific reboiler duty	MJ/kg CO_2	7.3	7.4	7.3	8.0
Flue gas exit out of the absorber					
H_2O	vol%	6.7	6.7	6.8	6.8
O_2	vol%	17.2	16.8	16.7	16.6
MEA	ppmv	28	20	16	12
NH_3	ppmv	107	89	77	65

9.5 Appendix A.5

Table 9.5. Standard errors for the mGT experimental tests.

Electrical power output (kW_e)	Actual CO_2 flowrate (kg/h)	CO_2 (±vol%)	Compressor inlet temperature (±°C)	Turbine speed (±rpm)	Compressor discharge temperature (±°C)	NOx (±g/kWh)	CO (±ppmv)	$CH_4 + C_2H_6$ (±ppmv)
100	0	0.002	0.002	1.321	0.032	0.006	0.018	0.022
100	100	0.003	0.009	2.026	0.035	0.014	0.036	0.024
100	150	0.005	0.002	1.456	0.031	0.009	0.022	0.025
100	200	0.011	0.002	1.418	0.031	0.010	0.046	0.026
100	250	0.017	0.002	1.535	0.030	0.040	0.118	0.024
100	300	0.012	0.007	2.164	0.036	0.007	0.215	0.030
90	0	0.003	0.008	1.731	0.032	0.041	0.083	0.041
90	100	0.004	0.006	1.844	0.034	0.015	0.038	0.022
90	150	0.005	0.013	2.708	0.043	0.010	0.151	0.164
90	200	0.004	0.015	2.376	0.036	0.014	0.149	0.025
90	250	0.007	0.001	1.544	0.032	0.012	0.237	0.069
80	0	0.003	0.006	1.631	0.033	0.013	0.037	0.027
80	200	0.007	0.009	2.358	0.036	0.016	0.122	0.027
80	100	0.003	0.007	1.598	0.032	0.011	0.167	0.046
80	150	0.005	0.004	1.518	0.034	0.015	0.129	0.028
80	250	0.010	0.002	1.385	0.031	0.027	0.366	0.055
80	300	0.009	0.005	2.239	0.033	0.076	4.137	0.686
70	0	0.004	0.003	1.269	0.032	0.016	0.278	0.032
70	100	0.004	0.015	2.281	0.038	0.008	0.796	0.195
70	150	0.005	0.013	1.928	0.035	0.009	0.297	0.041
70	200	0.007	0.007	1.440	0.033	0.012	0.369	0.064
70	250	0.009	0.002	1.529	0.033	0.014	0.484	0.134
70	300	0.018	0.007	1.742	0.032	0.026	0.786	0.216
60	0	0.002	0.003	1.393	0.032	0.013	0.503	0.086
60	100	0.005	0.008	2.020	0.034	0.009	0.796	0.195
60	150	0.007	0.004	1.640	0.033	0.018	0.476	0.127
60	200	0.009	0.005	1.257	0.032	0.012	0.660	0.211
60	250	0.007	0.007	1.394	0.031	0.006	0.856	0.328
61	300	0.015	0.004	1.331	0.031	0.028	4.822	1.986

Table 9.6. Standard errors for the absorber and desorber temperature profiles.

				Experimental test 1				Experimental test 2			
Absorber				5.2	6.5	7.6	9	126	127	125	124
1	0.6	T121		0.022	0.010	0.004	0.013	0.013	0.004	0.007	0.013
2	1.2	T124		0.032	0.016	0.016	0.018	0.018	0.016	0.018	0.017
3	1.9	T127		0.040	0.017	0.008	0.018	0.018	0.007	0.012	0.014
4	2.6	T130		0.042	0.017	0.009	0.021	0.021	0.006	0.010	0.011
5	3.3	T133	±°C	-	-	-	-	-	-	-	-
6	4.0	T136		0.034	0.020	0.005	0.026	0.026	0.006	0.008	0.009
7	4.7	T139		0.026	0.021	0.007	0.034	0.034	0.008	0.008	0.013
8	5.4	T142		-	-	-	-	-	-	-	-
9	6.0	T145		0.020	0.016	0.026	0.030	0.030	0.020	0.014	0.041
10	6.7	T148		0.042	0.065	0.019	0.027	0.027	0.020	0.025	0.035
Desorber											
1	0.4	T308		0.021	0.058	0.030	0.015	0.015	0.012	0.014	0.036
2	1.3	T317		0.014	0.051	0.040	0.044	0.044	0.015	0.045	0.056
3	2.2	T316		0.017	0.057	0.042	0.032	0.032	0.016	0.026	0.020
4	3.0	T321		-	-	-	-	-	-	-	-
5	3.9	T309	±°C	-	-	-	-	-	-	-	-
6	4.8	T312		0.021	0.055	0.028	0.014	0.014	0.012	0.012	0.020
7	5.7	T311		-	-	-	-	-	-	-	-
8	7.1	T310		-	-	-	-	-	-	-	-
9	7.6	T307		0.075	0.088	0.040	0.019	0.019	0.017	0.018	0.020